LANTHANIDE COMPLEXES OF BULKY HYBRID LIGANDS

by

Claire Jones

A thesis submitted in partial

fulfilment of the requirements for the degree of

Doctor of Philosophy

School of Chemistry

October 2017

Abstract

The synthetic and redox chemistry of lanthanide organometallic complexes has considerably expanded since the discovery of Kagan's reagent in 1977 and divalent ionic complexes are now known for the entire lanthanide series. The synthesis, solid-state structures and reductive chemistry of trivalent and divalent lanthanide complexes with cyclopentadienyl-type ligands is reviewed with a focus on the impact of the ligand on the reducing power of the metal centre. Trimethylsilyl and more recently, phosphine-borane stabilised carbanions have facilitated the isolation of trivalent and divalent lanthanide complexes of alkyl ligands with Ln—C σ-bonds. The synthesis, structures and known reactivity of these compounds is discussed.

In order to probe the impact of alkyl carbanion and cyclopentadienyl coordination on lanthanide complex stability, structure and redox reactivity we have designed a novel set of hybrid ligands that combine these two functional groups into a single dianionic ligand. These ligands are potentially very versatile as the sterics and electronics of both groups in the ligand can be modified. The ligands are viable to support sterically congested trivalent complexes for sterically induced reduction as well as metal based reduction and they are good ligands for heteroleptic complexes because they chelate the metal avoiding ligand redistribution equilibria.

The synthesis and characterisation of a range of trimethylsilyl-, phosphine-borane- and phosphine-stabilised alkyl bromo- and chlorosilane precursors is described: $(Me_3Si)_2CHSiMe_2Br$ [4], $(Me_3Si)\{PMe_2(BH_3)\}CHSiMe_2Cl$ [9], $(Me_3Si)\{P^nPr_2(BH_3)\}CHSiMe_2Cl$ [13], $\{PMe_2(BH_3)\}_2CHSiMe_2Cl$ [23], $\{PMe_2(BH_3)\}\{PPh_2(BH_3)\}CHSiMe_2Cl$ [27], $\{PPh_2(BH_3)\}_2CHSiMe_2Cl$ [31] and $(^nPr_2P)_2CHSiMe_2Cl$ [32].

iii

The results of a computational study using NBO methods to investigate the relative stabilising effect of each of these silyl, phosphine-borane and phosphine carbanion stabilising groups on a model system akin to the alkyl part of the hybrid ligand are described.

Reaction of $(Me_3Si)_2CHSiMe_2Br$ with Li/Na/K Cp/Cp'/Cp^{4Me} followed by aqueous work-up gave the hybrid proligands $\{(CpH)Me_2Si\}(Me_3Si)_2CH$ [5], $\{(Cp'H)Me_2Si\}(Me_3Si)_2CH$ [6] and $\{Cp^{4Me}H)Me_2Si\}(Me_3Si)_2CH$ [7] as mixtures of regioisomers [Cp^{4Me} = 1,2,3,4-Tetramethyl-cyclopentadiene]. Reaction of LiCp^{4Me}/KCp^{4Me} with $(Me_3Si)\{PMe_2(BH_3)\}CHSiMe_2Cl$ and $(Me_3Si)\{P^nPr_2(BH_3)\}CHSiMe_2Cl$ gave the hybrid proligands $(CpH^{4Me}Me_2Si)(Me_3Si)CH\{PMe_2(BH_3)\}$ [10] and $(CpH^{4Me}Me_2Si)(Me_3Si)$-$CH\{P^nPr_2(BH_3)\}$ [14]. The compounds $\{Cp^{4Me}H)Me_2Si\}(Me_3Si)_2CH$, $(CpH^{4Me}Me_2Si)$-$(Me_3Si)CH\{PMe_2(BH_3)\}$ and $(CpH^{4Me}Me_2Si)(Me_3Si)CH\{P^nPr_2(BH_3)\}$ crystallise as solvent-free monomers with very similar molecular conformations. The hybrid pro-ligands exhibit variable moisture sensitivity. Reaction of $(Me_3Si)\{PMe_2(BH_3)\}CHSiMe_2Cl$ with NaCp followed by aqueous work-up and column chromatography of the oily residue obtained gave the siloxane $[(Me_3Si)\{PMe_2(BH_3)\}HCMe_2Si]_2O$ [19] and dicyclopentadiene. Reaction of $(^nPr_2P)_2CHSiMe_2Cl$ with NaCp followed by aqueous work-up using deoxygenated water gave $(^nPr_2P)_2CH_2$ in quantitative yield. The same reaction avoiding the aqueous work-up gave $(CpHMe_2Si)CH(P^nPr_2)_2$ [33].

Hybrid ligands were prepared by metalation of $\{Cp^{4Me}H)Me_2Si\}(Me_3Si)_2CH$, $\{(Cp'H)Me_2Si\}(Me_3Si)_2CH$ and $\{(CpH)Me_2Si\}(Me_3Si)_2CH$ with MeK to give the hemisolvated dipotassium salts $[(CpMe_2Si)(Me_3Si)_2C]K_2(Et_2O)_{0.5}$ [50], $[(Cp^{4Me}Me_2Si)(Me_3Si)_2C]K_2(Et_2O)_{0.5}$ [51] and $[(Cp'Me_2Si)(Me_3Si)_2C]K_2(C_6H_6)_{0.5}$ [52], which decomposed slowly in THF and toluene. $[(Cp^{4Me}Me_2Si)(Me_3Si)_2C]K_2(Et_2O)$ [51.Et2O] was crystallised as an alternative solvate from diethyl ether and the

extended structure consists of chelated [(hybrid ligand)K(Et$_2$O)]$^-$ anionic units linked nose to tail by unsolvated K cations in a non-linear (zig-zag) polymer chain. [(Cp′Me$_2$Si)(Me$_3$Si)2C]K$_2$(C$_6$H$_6$)·C$_6$H$_6$ [**52.C$_6$H$_6$**] also crystallised as a monosolvate from benzene, but with addition uncoordinated solvent present in the structure. There are two distinct types of polymer chain in the structure of [(Cp′Me$_2$Si)(Me$_3$Si)2C]K$_2$(C$_6$H$_6$)·C$_6$H$_6$, one is similar to the chain in [(Cp^{4Me}Me$_2$Si)(Me$_3$Si)$_2$C]K$_2$(Et$_2$O) and in the other half the potassium cations in this chain are coordinated by only a cyclopentadienyl ring and a benzene ring. The remainder of the K cations are sandwiched between a carbanion and cyclopentadienyl ring of different hybrid ligands, as in [(Cp^{4Me}Me$_2$Si)(Me$_3$Si)$_2$C]K$_2$(Et$_2$O). These chains are cross-linked by a short contact between K and the −SiMe$_3$ substituent of the Cp′ ring.

Due to their more acidic alkyl protons metalation of (CpH^{4Me}Me$_2$Si)(Me$_3$Si)CH{PMe$_2$(BH$_3$)}, (CpH^{4Me}Me$_2$Si)(Me$_3$Si)CH{P^{n}Pr$_2$(BH$_3$)} and (CpHMe$_2$Si)CH(P^{n}Pr$_2$)$_2$ could be achieved with BnK in THF. (CpH^{4Me}Me$_2$Si)(Me$_3$Si)CH{PMe$_2$(BH$_3$)} is isoelectronic and isosteric with {Cp^{4Me}H)Me$_2$Si}(Me$_3$Si)$_2$CH. [(Cp^{4Me}Me$_2$Si)(Me$_3$Si){PMe$_2$(BH$_3$)}C]K$_2$(THF) [**53.THF**] crystallises as a solvate from benzene/THF with a 3D polymeric network structure through multiple agostic-type B−H····K contacts. Of the two symmetry inequivalent K cations in the structure the alkyl carbanion interacts directly only with the unsolvated cations and the solvated cations are coordinated through the borane-hydrogens.

Metathesis reactions of [(Cp^{4Me}Me$_2$Si)(Me$_3$Si)$_2$C]K$_2$(Et$_2$O)$_{0.5}$ and [(Cp^{4Me}Me$_2$Si)(Me$_3$Si){PMe$_2$(BH$_3$)}C]K$_2$(THF)$_{0.5}$ with LaI$_3$(THF) and SmI$_3$(THF) in THF gave [(Cp^{4Me}Me$_2$Si)(Me$_3$Si)$_2$C]LaI(THF)$_2$ [**56**] and [(Cp^{4Me}Me$_2$Si)(Me$_3$Si){PMe$_2$(BH$_3$)}C]-SmI(THF)$_2$ [**57**] after extraction into diethyl ether and crystallisation from toluene/THF and diethyl ether respectively. The

hybrid ligand bound successfully to the lanthanide metal cations. [(Cp^{4Me}Me$_2$Si)(Me$_3$Si)$_2$C]LaI(THF)$_2$ is a monomer in the solid-state, chelated by the hybrid ligand forming pseudo-four-membered ring and two coordinating molecules of THF in addition to the iodine anion. A zwitterion structure is adopted by [(Cp^{4Me}Me$_2$Si)(Me$_3$Si){PMe$_2$(BH$_3$)}C]SmI(THF)$_3$ with no contact between the Sm(III) cation and the alkyl carbanion centre. The hybrid ligands have a much larger cone angle and are far more sterically bulky when chelating the lanthanide metal, as in [(Cp^{4Me}Me$_2$Si)(Me$_3$Si)$_2$C]LaI(THF)$_2$.

The metathesis reaction of [(Cp^{4Me}Me$_2$Si)(Me$_3$Si)$_2$C]K$_2$(Et$_2$O)$_{0.5}$ with CaI$_2$ gave [(Cp^{4Me}Me$_2$Si)(Me$_3$Si){PMe$_2$(BH$_3$)}C]Ca(THF)$_2$ **[58]** after extraction and crystallisation from diethyl ether. In this structure the phosphine-borane stabilised carbanion group of the hybrid ligand coordinates the Ca cation through the carbanion centre. Synthesis of the Yb(II) analogue, [(Cp^{4Me}Me$_2$Si)(Me$_3$Si){PMe$_2$(BH$_3$)}C]Yb(THF)$_x$ gave an almost identical NMR spectrum, but could not be crystallised.

Acknowledgements

I would like to thank everybody who has helped me to complete this work. Firstly I would like to thank my Dad, for answering incessant questions before I even became a chemistry undergraduate and cultivating a motivational desire to know, which has been so important in carrying me through this work.

I would like to give grateful thanks to Dr. Keith Izod for all his support and academic guidance in sometimes trying circumstances.

A big thank you to Dr. Corinne Wills and Dr. Paul G. Waddell for their help with NMR characterisation and solid-state structure determination of the compounds synthesised in this work.
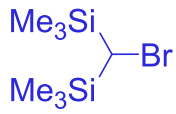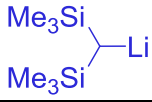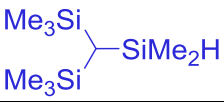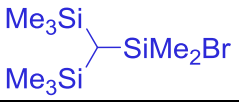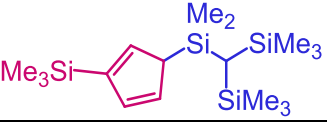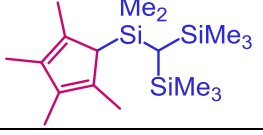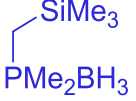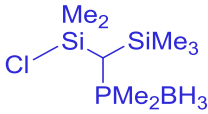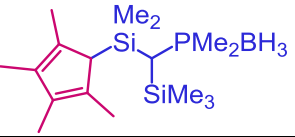
I must thank Peter Evans for being simultaneously the best laboratory colleague and a friend throughout the PhD years and before.

I would like to thank Dr. Ulrich Baisch for the opportunity to develop my understanding and practical skills in the field of crystallography and for supporting my Fulbright Application.
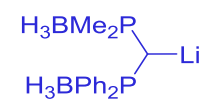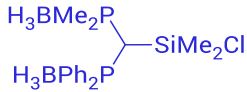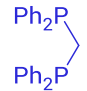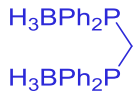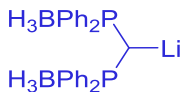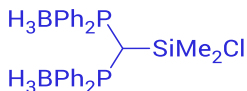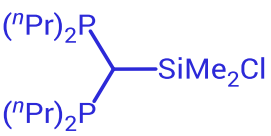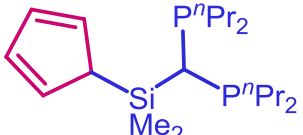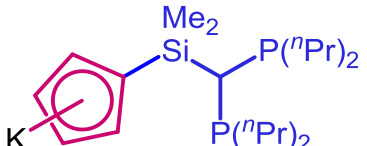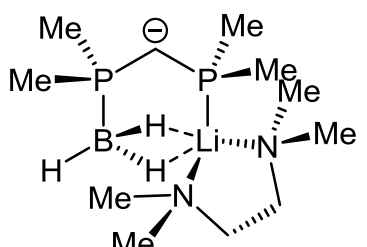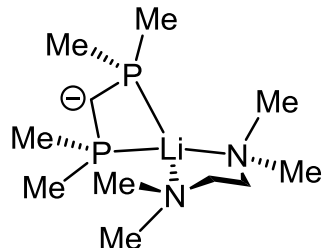
Thank you to The Aizenberg Lab at Harvard University for making my year there so memorable and in particular to Dr. Wim Noorduin and Dr. Nicholas Vogel.
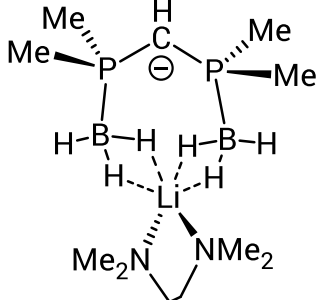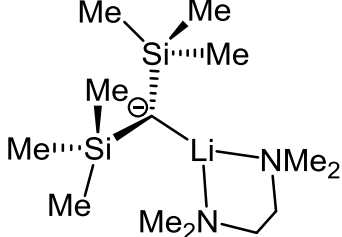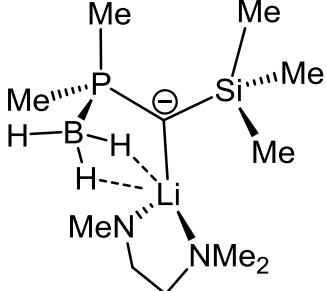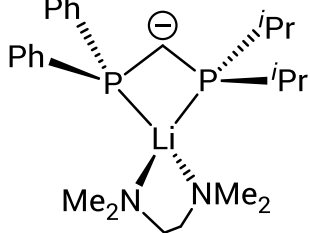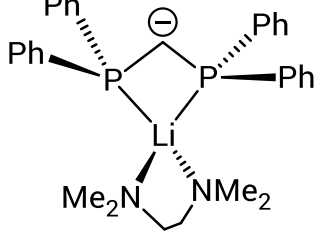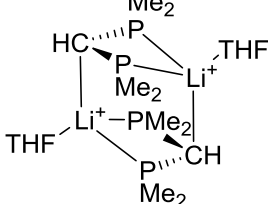
My brothers Dr. Michael Jones and Dr. David Jones are deserving of thanks for their mathematical insights. Finally I would like to give heartfelt thanks to Luke Saunders for being there with me for the final hurdle.
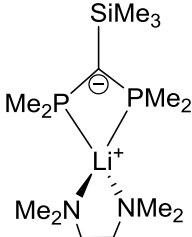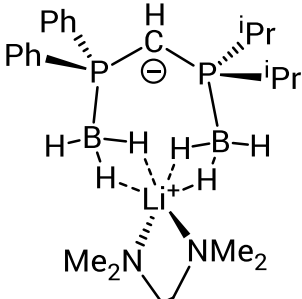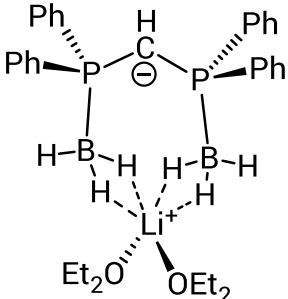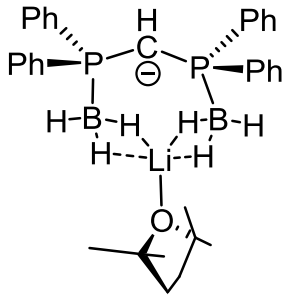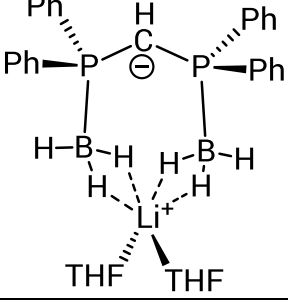
Numerical list of compounds referred to in the main text
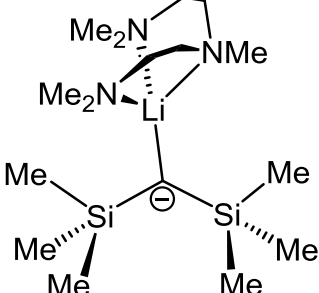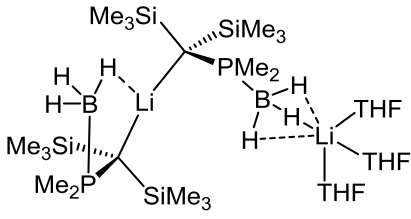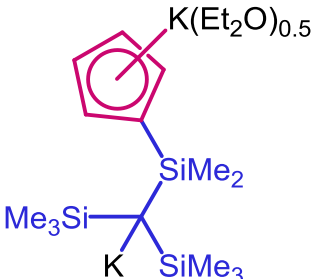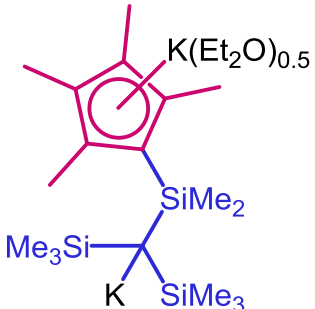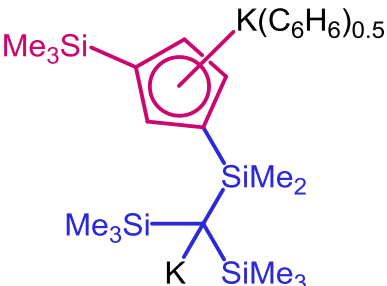
Compound Structure	Compound Formula	Number
	$(Me_3Si)_2CHBr$	**1**
	$\{(Me_3Si)_2CH\}Li$	**2**
	$(Me_2Si)_2(Me_2SiH)CH$	**3**
	$(Me_3Si)_2CHSiMe_2Br$	**4**
	$\{(CpH)Me_2Si\}(Me_3Si)_2CH$	**5**
	$\{(Cp'H)Me_2Si\}(Me_3Si)_2CH$	**6**
	$\{(CpH_4Me)Me_2Si\}(Me_3Si)_2CH$	**7**
	$(Me_3Si)\{PMe_2(BH_3)\}CH_2$	**8**
	$(Me_3Si)\{PMe_2(BH_3)\}CHSiMe_2Cl$	**9**
	$(CpH^{4Me}Me_2Si)(Me_3Si)CH\{PMe_2(BH_3)\}$	**10**
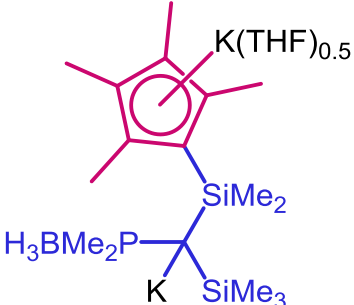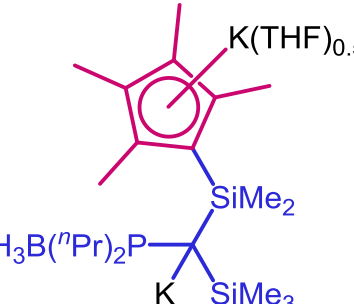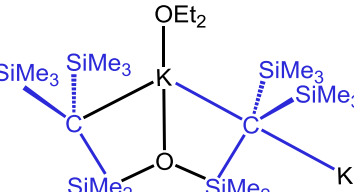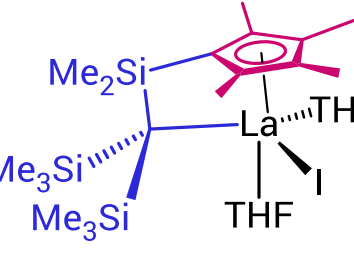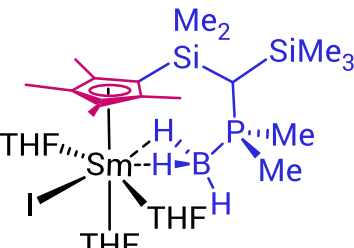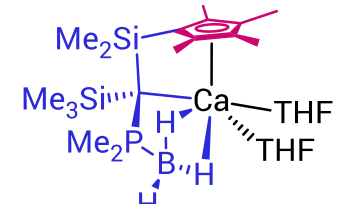
Me(^{n}Pr)$_2$PBH$_3$	Me(^{n}Pr)$_2$PBH$_3$	**11**
SiMe$_3$ / P^{n}Pr$_2$BH$_3$	(Me$_3$Si)CH$_2${P^{n}Pr$_2$(BH$_3$)}	**12**
Me$_2$ Si SiMe$_3$ / Cl / P^{n}Pr$_2$BH$_3$	(Me$_3$Si){P^{n}Pr$_2$(BH$_3$)}CHSiMe$_2$Cl	**13**
Me$_2$ Si P^{n}Pr$_2$BH$_3$ / SiMe$_3$	(CpH^{4Me}Me$_2$Si)(Me$_3$Si)CH{P^{n}Pr$_2$(BH$_3$)}	**14**
PMe$_2$BH$_3$ / Me$_3$Si SiMe$_3$	(Me$_3$Si)$_2${PMe$_2$(BH$_3$)}CH	**15**
SiMe$_3$ / Me$_3$Si SiMe$_3$	(Me$_3$Si)$_3$CH	**16**
Me$_2$ Si PMe$_2$BH$_3$ / Me$_3$Si SiMe$_3$	(CpH^{TMS}Me$_2$Si)(Me$_3$Si)CH{PMe$_2$(BH$_3$)}	**17**
Me$_2$ Si PMe$_2$BH$_3$ / SiMe$_3$	(CpHMe$_2$Si)(Me$_3$Si)CH{PMe$_2$(BH$_3$)}	**18**
Me$_2$ Me$_2$ / Me$_3$Si Si O Si SiMe$_3$ / PMe$_2$BH$_3$ PMe$_2$BH$_3$	[(Me$_3$Si){PMe$_2$(BH$_3$)}HCMe$_2$Si]$_2$O	**19**
Me$_2$P / Me$_2$P	(PMe$_2$)$_2$CH	**20**
H$_3$BMe$_2$P / H$_3$BMe$_2$P	{PMe$_2$(BH$_3$)}$_2$CH	**21**
H$_3$BMe$_2$P Li / H$_3$BMe$_2$P	{PMe$_2$(BH$_3$)}$_2$CHLi	**22**
H$_3$BMe$_2$P SiMe$_2$Cl / H$_3$BMe$_2$P	{PMe$_2$(BH$_3$)}$_2$CHSiMe$_2$Cl	**23**
H$_3$BMe$_2$P / Ph$_2$P	{PMe$_2$(BH$_3$)}{PPh$_2$}CH$_2$	**24**
H$_3$BMe$_2$P / H$_3$BPh$_2$P	{PMe$_2$(BH$_3$)}{PPh$_2$(BH$_3$)}CH$_2$	**25**

x

	{PMe$_2$(BH$_3$)}{PPh$_2$(BH$_3$)}CHLi	**26**
	{PMe$_2$(BH$_3$)}{PPh$_2$(BH$_3$)}CHSiMe$_2$Cl	**27**
	(PPh$_2$)$_2$CH$_2$	**28**
	{PPh$_2$(BH$_3$)}$_2$CH$_2$	**29**
	{PPh$_2$(BH$_3$)}$_2$CHLi	**30**
	{PPh$_2$(BH$_3$)}$_2$CHSiMe$_2$Cl	**31**
	(^{n}Pr$_2$P)$_2$CHSiMe$_2$Cl	**32**
	(CpHMe$_2$Si)CH(P^{n}Pr$_2$)$_2$	**33**
	[(CpMe$_2$Si)CH(P^{n}Pr$_2$)$_2$]K	**34**
	[Me$_2$PCH{P(BH$_3$)Me$_2$}]Li(tmeda)	**35**
	[(Me$_2$P)$_2$CH]Li(tmeda)	**36**

	[{Me$_2$P(BH$_3$)}$_2$CH]Li(tmeda)	**37**
	Li{CH(SiMe$_3$)}(tmeda)	**38**
	[{Me$_2$P(BH$_3$)}CH(SiMe$_3$)]Li(tmeda)	**39**
	[Ph$_2$PCHP^{i}Pr$_2$]Li(tmeda)	**40**
	[(Ph$_2$P)$_2$CH]Li(tmeda)	**41**
	[{(Me$_2$P)$_2$CH}Li(THF)]$_2$	**42**

	[(Me₂P)₂{SiMe₃}C]Li(tmeda)	**43**
	[{Ph₂P(BH₃)}CH{P(BH₃)ⁱPr₂}]Li(tmeda)	**44**
	[{Ph₂P(BH₃)}₂CH]Li(OEt₂)₂	**45**
	[{Ph₂P(BH₃)}₂CH]Li(Me₄THF)₂	**46**
	[{Ph₂P(BH₃)}₂CH]Li(THF)₂	**47**

	Li{CH(SiMe₃)₂}(pmdeta)	**48**
	(THF)₃Li{(Me₃Si)₂CPMe₂(BH₃)}₂Li	**49**
	[(CpMe₂Si)C(Me₃Si)₂]K₂(Et₂O)₀.₅	**50**
	[(Cp⁴ᴹᵉMe₂Si)C(Me₃Si)₂]K₂(Et₂O)₀.₅	**51**
	[(Cp'Me₂Si)C(Me₃Si)₂]K₂(C₆H₆)₀.₅	**52**

	$[(Cp^{4Me}Me_2Si)(Me_3Si)C\{PMe_2(BH_3)\}]K_2(THF)_{0.5}$	**53**
	$[(Cp^{4Me}Me_2Si)(Me_3Si)C\{P^nPr_2(BH_3)\}]K_2(THF)_{0.5}$	**54**
	$[[\{Me_3Si\}_2C(SiMe_2)\}_2O]K_2](OEt_2)$	**55**
	$[(Cp^{4Me}Me_2Si)(Me_3Si)_2C]LaI(THF)_2$	**56**
	$[(Cp^{4Me}Me_2Si)(Me_3Si)C\{PMe_2(BH_3)\}]SmI(THF)_3$	**57**
	$[(Cp^{4Me}Me_2Si)(Me_3Si)C\{PMe_2(BH_3)\}]Ca(THF)_2$	**58**

	$[\{(Cp^{4Me}Me_2Si)PMes^*\}\,SmI(THF)]_2$ $(Mes^* = 2,4,6-{}^tBuC_6H_2)$	**59**
	$[\{(Cp^{4Me}Me_2Si)NMe_2Et\}YCl(THF)]_2$	**60**
	$[\{(Cp^{4Me}Me_2Si)NPh\}ScCl(THF)]_2$	**61**
	$[(Cp^{4Me}Me_2Si)NAr]LaPPh_2(THF)_2$	**62**
	$[\{(Me_3Si)(Me_2MeOSi)C(SiMe_2CH_2)\}_2]LaI(THF)$	**63**
	$[(Me_3Si)_2\{Me_2(MeO)Si\}C]_2LaI(THF)$	**64**

	$[(Me_3Si)_2\{Me_2(Me_2N)Si\}C]_2LaI$	**65**
	$[(Me_3Si)_2\{Me_2P(BH_3)\}C]_2Sm(THF)$	**66a**
	$[(Me_3Si)_2\{Me_2P(BH_3)\}C]_2Sm(THF)_3$	**66b**
	$[(Me_3Si)_2\{Me_2(H_3B)P\}C]_2Ca(THF)_4$	**67**
	$[(Me_3Si)_2\{Me_2(H_3B)P\}C]_2Sr(THF)_5$	**68**
	$[(Me_3Si)_2\{Me_2(H_3B)P\}C]_2Ba(THF)_5$	**69**

	[{PhP(BH₃){CH(SiMe₃)}₂}Ca(OEt₂)]₂	**70**
	[(Me₃Si)₂{Me₂(H₃B)P}C]₂Mg	**71**
	[(Cp⁴ᴹᵉMe₂Si)NR]Ca{N(SiMe₃)₂}(THF)	**72**
	[(Cp⁴ᴹᵉMe₂Si)NPh]Yb(THF)₃	**73**

Table of Contents

Chapter 1 Introduction to organometallic lanthanide chemistry

1.1   The lanthanide elements

The lanthanide metals are the elements from Ce to Lu in the periodic table, and they are also known as rare-earth elements (which also typically includes the group 3 elements Sc, Y and La) or f-block elements. The electronic configurations of the lanthanides (Table 1) and, in particular, the radial contraction of the f-orbitals, govern their chemistry. The f-electrons are poorly shielded, and so these orbitals feel a higher effective nuclear charge pulling them closer to the nucleus as the atomic number increases across the lanthanide series. This contraction of the f-orbitals is responsible for (i) the ionic nature of bonding in lanthanide complexes, (ii) the decrease in size of the lanthanide atoms and of their trivalent and divalent cations with increasing atomic number (Figure 1); this is known as the lanthanide contraction, and (iii) the increase in lewis acidity of the metal cations as their ionic radii contract.

Table 1: Electron configurations of the lanthanide elements

Ce	Pr	Nd	Pm	Sm	Eu	Gd	Tb	Dy	Ho	Er	Tm	Yb	Lu
$4f^15d^16s^2$	$4f^36s^2$	$4f^46s^2$	$4f^56s^2$	$4f^66s^2$	$4f^76s^2$	$4f^75d^16s^2$	$4f^96s^2$	$4f^{10}6s^2$	$4f^{11}6s^2$	$4f^{12}6s^2$	$4f^{13}6s^2$	$4f^{14}6s^2$	$4f^{14}5d^16s^2$

The bonding in compounds of the lanthanide ions is ionic and they are often considered to behave as trivalent versions of the +2 cations Ca^{2+}, Mg^{2+} of the alkaline earth elements.   The ionic nature of the bonding means ligand arrangements are not constrained by orbital geometry.   Ligands can occupy

differing arrangements to maximise the electrostatic interaction with the lanthanide cation and minimise steric and electronic interactions with neighbouring ligands. The lanthanides differ from the transition metals in this lack of predictable geometry for their complexes and also in the types of ligands that can be coordinated to the metal centre. They do not form stable carbonyl complexes where there is multiple synergic bonding character on account of being unable to back-donate electron density from the contracted f-orbitals into the π* orbitals of the CO ligand. Lanthanides also do not form Ln−Ln or metal−metal multiple bonds, which are common in transition metal chemistry where partially filled d-orbitals overlap efficiently, because lanthanide f-orbitals do not extend outside the [Xe] core and cannot overlap with other orbitals. Lanthanides form complexes with anionic ligands and are also extremely oxophilic, meaning they will additionally coordinate donor solvent molecules (THF, Et$_2$O) and must be handled under inert atmosphere conditions to avoid hydrolysis.
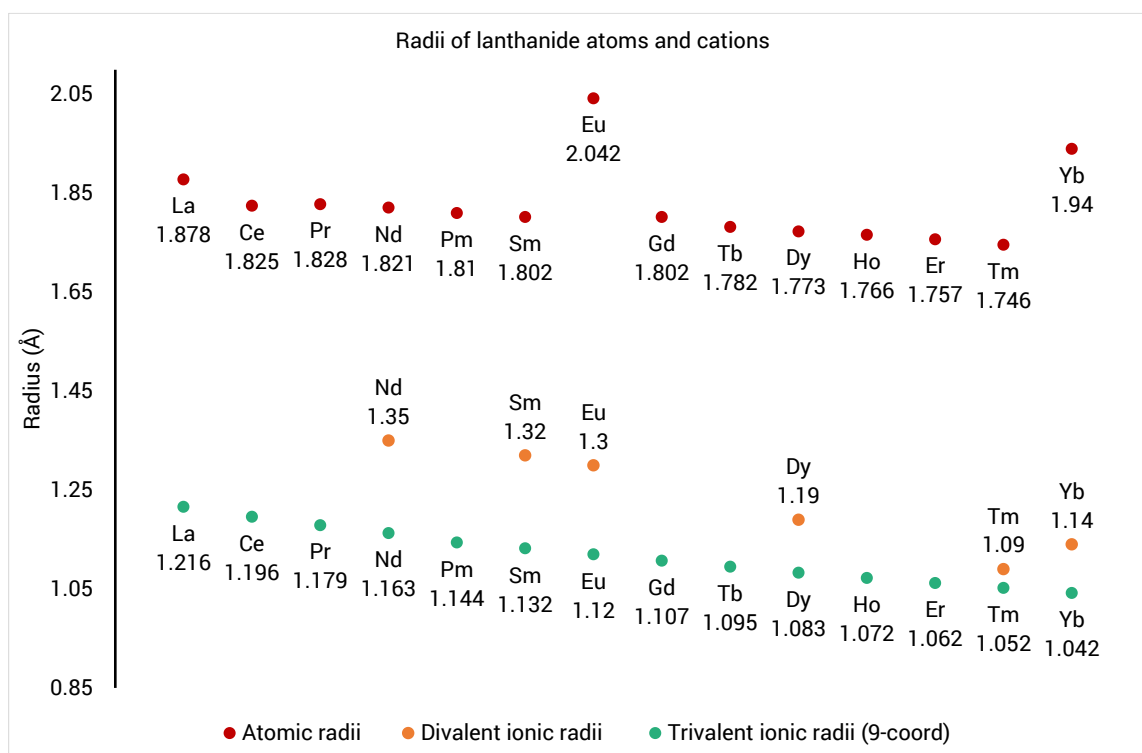
Figure 1. Radii of lanthanide atoms, divalent and trivalent cations

A sequence of lanthanide complexes is rarely uniform in structure or coordination number across the series because the lanthanide contraction means the central metal cation incrementally changes in size. The element at which structural transition in coordination number and/or the geometrical arrangement of the ligands is observed depends on both the cation size and the sterics of the ligand. For the series $Ln(AlMe_4)_3$ the number of methyl groups of each tetraalkylaluminate anion forming contacts of the type: $Ln^{3+}\cdots CH_3-AlMe_3$ depends on the size of the lanthanide cation (Figure 2). From Sm - Lu each of the three coordinating tetraalkylaluminate anions has two methyl groups forming contacts with the lanthanide metal in a planar arrangement and the tetraalkylaluminate ligands can be described as η^2. From Pr − Nd the tetraalkylaluminate anions are still η^2, but are bent so as to occupy more space in the coordination sphere. For La, the largest lanthanide, in addition to distortion from the planar bridging arrangement of one tetraalkylaluminate ligand the third tetraalkylaluminate ligand binds η^3 with three $Ln^{3+}\cdots CH_3-AlMe_3$ contacts with the coordinatively unsaturated lanthanide metal centre.[1] The ligands arrange themselves to achieve steric and electronic saturation of the lanthanide coordination sphere. The lanthanide cations are heavy metal hard lewis acids according to Pearson's HSAB principle.

$Lu(AlMe_4)_3$ $La(AlMe_4)_3$
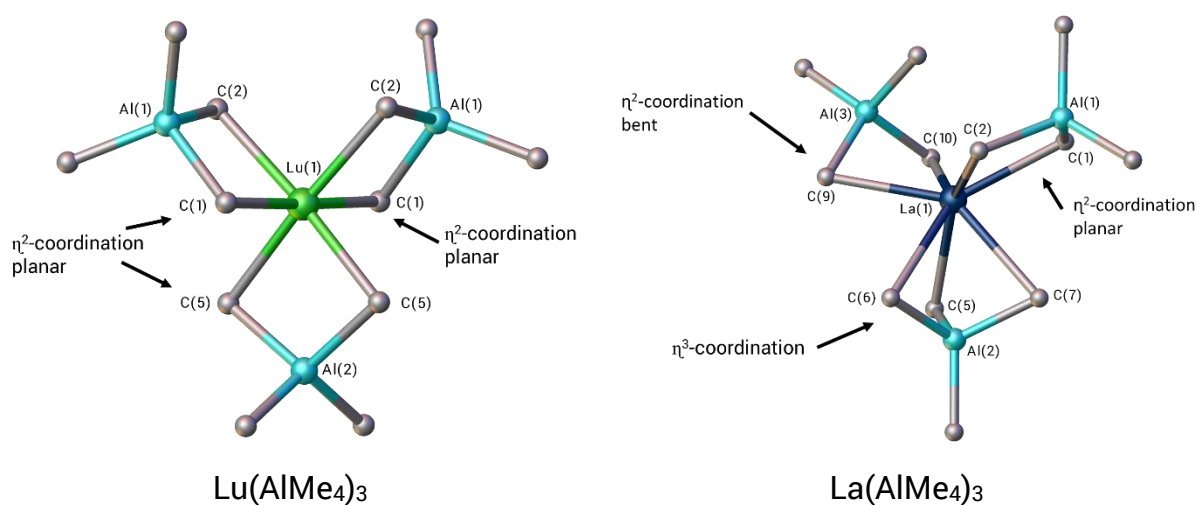
Figure 2. Transition in coordination number and ligand binding mode with increasing lanthanide cation size. Hydrogen atoms omitted for clarity.

In most compounds the lanthanide oxidation state is +3 and there is an energy penalty on going from +3 to +2 which is quantified by the reduction potentials (Figure 3). It is smallest for those lanthanides where the electron configuration is a half-filled or filled set of orbitals. For the purposes of comparison Na in liquid ammonia has a reduction potential of about -1.8 V (vs. NHE).

These high reduction potentials and lewis acidities mean organometallic complexes of the lanthanides, especially the divalent cations, are hard to stabilise, but conversely it also lights the way to the discovery of new and unusual reactions where lanthanide complexes play an important role.
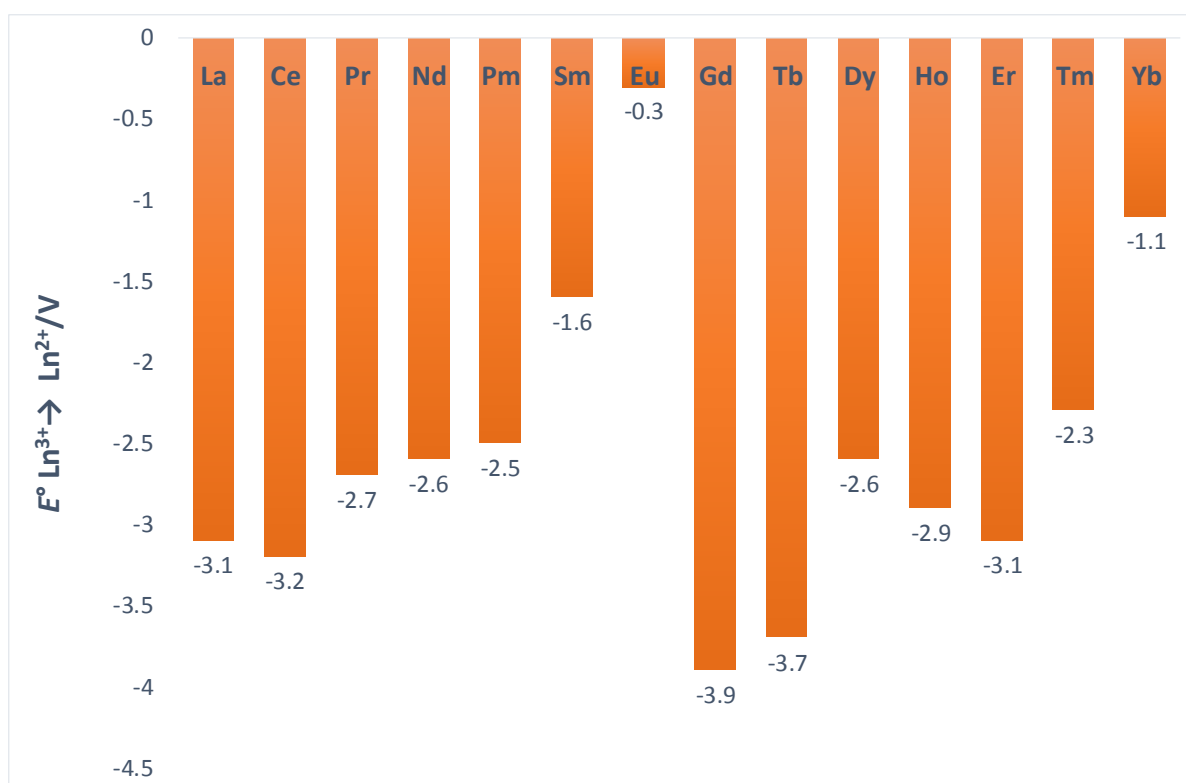
Figure 3. Reduction potentials of the lanthanides (vs. NHE)[2,3]

Some of the lanthanides have very similarly sized cations to the cations of group 2 or group 3 elements (Table 2), and these cations will generally form the same compounds as the lanthanide cation that they substitute. These lanthanide cation analogues have several useful properties: (i) they are diamagnetic, making NMR spectroscopic characterisation of their organometallic compounds straightforward

in comparison to the paramagnetic lanthanide cations, (ii) they are redox inactive, allowing the synthesis and structural evaluation of analogues of divalent lanthanide compounds with equal sized metal cations while avoiding oxidation of the metal centre, and (iii) scandium has a trivalent cation smaller (0.87 Å) than that of Lu^{3+} (0.977 Å), the smallest lanthanide, providing a useful way to 'extend' the decline in size across the series.

Table 2. Pairs of lanthanide cations and their group 2 or group 3 cation analogues. Ionic radii are for 9-coordinate cations

Ln cation	Ionic radius	Cation analogue	Ionic radius
Ho^{3+}	1.072	Y^{3+}	1.075
Yb^{2+}	1.14	Ca^{2+}	1.12
Sm^{2+}, Eu^{2+}	1.32, 1.30	Sr^{2+}	1.31

1.2   Trivalent organolanthanide compounds

1.2.1   Tris(cyclopentadienyl) systems

The development of lanthanide organometallic chemistry involving the coordination of carbanions to the lanthanide metal centre began with the synthesis of lanthanide tris(cyclopentadienyl), $Ln(Cp)_3$ complexes by Birmingham and Wilkinson in 1954.[4] These organolanthanide compounds with three π-bonded, η^5-coordinated cyclopentadienyl anions preceded the synthesis of lanthanide σ-bonded alkyl carbanion, $Ln(CH_2SiMe_3)_3$ and $Ln[CH(SiMe_3)_2]_3$ solvates and ionic 'ate' complexes[5–10] by 20+ years. In the majority of cases the challenge was to find or design and synthesise ligands that were sufficiently sterically bulky to saturate the lanthanide metal coordination sphere. Stabilisation requires sterically bulky anionic ligands but carbanion stability decreases in the order: primary > secondary > tertiary, so 'bulky' alkyl ligands occupying multiple coordination sites were often delocalised, e.g. Cp or allyl ligands.

Tris(cyclopentadienyl) lanthanide compounds can be synthesised by a metathesis reaction between NaCp/KCp and anhydrous $LnCl_3$ or $LnI_3(THF)_x$ at reflux in THF for all of the lanthanides (Scheme 1) with the exception of Eu.[4,11,12] $Eu(Cp)_3$ can be synthesised by the reaction of excess thallous cyclopentadienide with Eu metal in liquid ammonia or pyridine.[13] Solvent-free crystals of these compounds can be obtained by sublimation at ca. 200 - 250 °C under vacuum. Single crystal X-ray diffraction (XRD) data is available for the lanthanides: La,[14,15] Ce,[16] Pr,[17] Ho,[16] Er,[14] Tm,[14] Yb,[18,19] Lu[20] and additionally we have obtained new data for Nd (structure redetermination with new space group). The solid state structures of these homoleptic tris(cyclopentadienyl)lanthanide complexes of the simplest and smallest cyclopentadienyl ring are infinitely polymeric, $[Cp_3Ln]_\infty$, because the lanthanide coordination sphere is unsaturated and lanthanide cations form ionic interactions over distances that exceed the length of chemical bonds (Figure 4).[21,22] The intermolecular interactions connecting the Cp_3Ln molecules in the polymer are η^1- interactions. One cyclopentadienyl ring of each Cp_3Ln unit has an η^5 interaction with one Ln atom and an η^1 interaction with the Ln atom in the neighbouring Cp_3Ln unit. These compounds are only soluble in THF, a good donor solvent, in which they are stable.
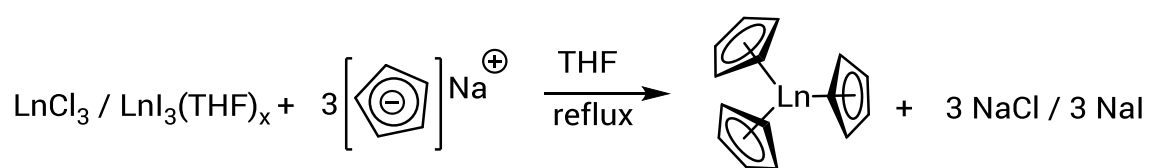
Scheme 1. Synthesis of tris(cyclopentadienyl)lanthanide compounds by metathesis

Increasing the size of the coordinated cyclopentadienyl ligand results in a stepwise reduction in the extent of polymerisation in the solid state, hence tris(methylcyclopentadienyl)lanthanide complexes, $Ln(Cp^{Me})_3$, form tetramers (Figure 4). Solid-state structures have been previously determined for Ce,[23] Nd,[24] and Pr, additionally we have obtained the structure for the Gd compound. The

structure of Yb(MeCp)$_3$ is reported to be monomeric, which is evidence of a transition from a tetrameric structure to a monomeric structure with decreasing ionic radius.[25] However full, detailed crystallographic information is not available in the literature. Solubility is much improved for the tetrameric [Ln(CpMe$_3$)]$_4$ compounds as there are fewer intermolecular interactions to breakdown, so a donor solvent is not needed. Bulkier trimethylsilylcyclopentadienyl rings give monomeric Ln(Cp')$_3$ complexes because the ligands occupy the lanthanide coordination sphere far more fully than unsubstituted cyclopentadienyl ligands; single crystal XRD data are known for Ho, Er and Yb (Figure 4).[26]
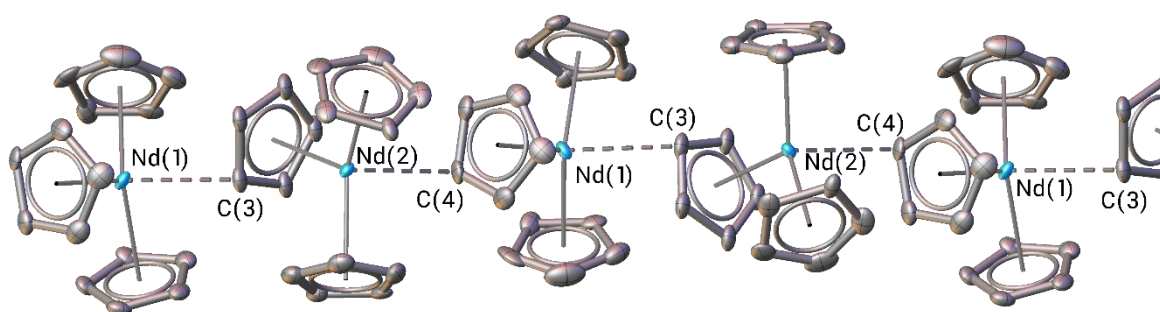
Solid-state polymeric structure of [Cp$_3$Nd]$_\infty$
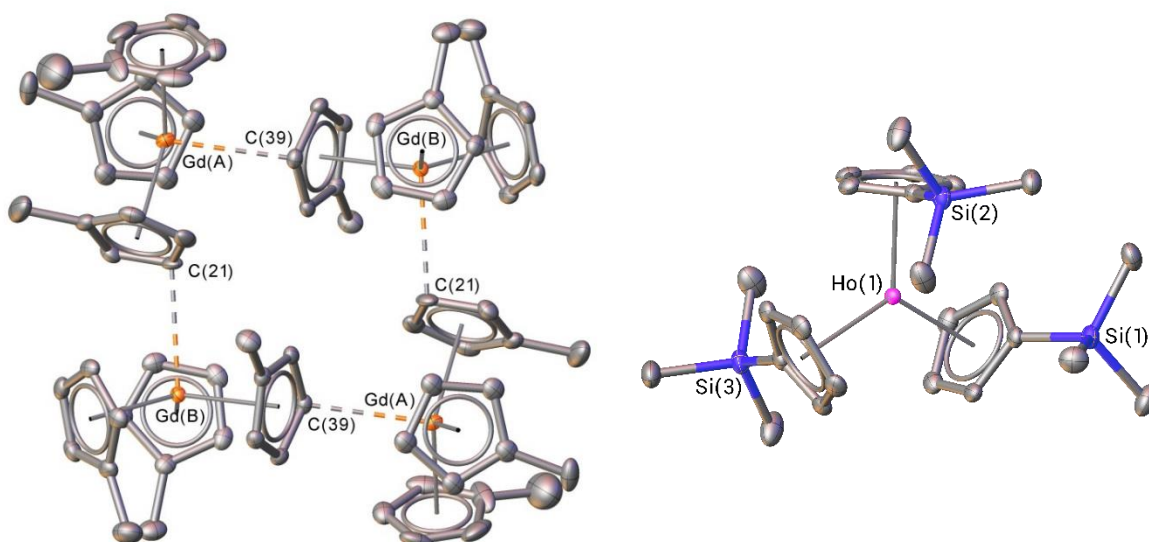
Solid-state tetrameric structure of [Gd(Cp^{Me})$_3$]$_4$

Solid-state monomeric structure of Ho(Cp')$_3$[26]

Figure 4. Structures of tris(cylopentadienyl) lanthanide compounds with progressively more bulky mono-substituted cyclopentadienyl ligands.

A further ligand size increase to pentamethylcyclopentadienyl (Cp*) rings means three ligands cannot be accommodated by cations smaller than Sm^{3+} and for a long time, based on Tolman cone angle data, it was believed that $Sm(Cp*)_3$ was an impossibility. The severe steric strain in the $Sm(Cp*)_3$ complex enables some reduction chemistry, unusual for trivalent lanthanide compounds, called sterically induced reduction (SIR) (see below).

The first synthetic route to $Sm(Cp*)_3$ was discovered by accident in 1991 while investigating the reactivity of divalent $Sm(Cp*)_2$ (which is discussed in section 1.3.1 on divalent bis(cyclopentadienyl) complexes) with cyclooctatetraene (Scheme 2).[27] Crystallographic studies found the $Sm-C(Cp*)$ bond lengths (2.7824(15), 2.8171(16) and 2.910(3) Å, (remaining twelve $Sm-C(Cp*)$ bonds equivalent to one of these by symmetry) and $Sm-$ring centroid distance of 2.55 Å to exceed those of all Sm(III) complexes containing (Cp*) ligands known at the time of the discovery. Trivalent Sm complexes, known today with similar $Sm-$ring centroid distances for (Cp*) ligands include the complex [(Cp*)$_2$Sm(phospholyl)], (phospholyl = *tert*-butylbi-1,1'-phospholyl) and the solvated *ansa*-complex, {Me$_2$Si(C$_5$Me$_4$)$_2$}Sm(Cp*)(THF) with $Sm-$ring centroid (Cp*) distances of 2.553, 2.539 Å and 2.552 Å respectively.[28,29] The complex (C$_5$Me$_4$Et)$_3$Sm of the even more bulky C$_5$Me$_4$Et ligand has a longer $Sm-$ring centroid (C$_5$Me$_4$Et) distance of 2.57 Å which maintains the centroid$-Sm-$centroid angle at 120°.[30]

The long $Sm-$ring centroid distances reduce the Tolman cone angle of the (Cp*) ligand to 120°, whereas in complexes where the bond lengths are shorter it is >120° (Figure 5), for example the complex [(Cp*)$_2$Sm(O$_2$CCH$_2$Ph)]$_2$ has one of the shortest $Sm-$ring centroid (Cp*) distances reported of 2.36 Å for one of the (Cp*) rings (the other is 2.51 Å) and consequently the centroid$-Sm-$centroid angle is 133.5°.[31] Although sterically saturated, the distance between the (Cp*) rings and the metal centre in $Sm(Cp*)_3$ renders the complex electronically unstable. The anionic Cp*

ligands are so far from the metal centre that the electrostatic attraction is weaker than for complexes with shorter metal−ring centroid (Cp*) distances. In addition the steric crowding of the ligands means the coordination mode of a single Cp* ring can change from η^5 to η^1.

Scheme 2
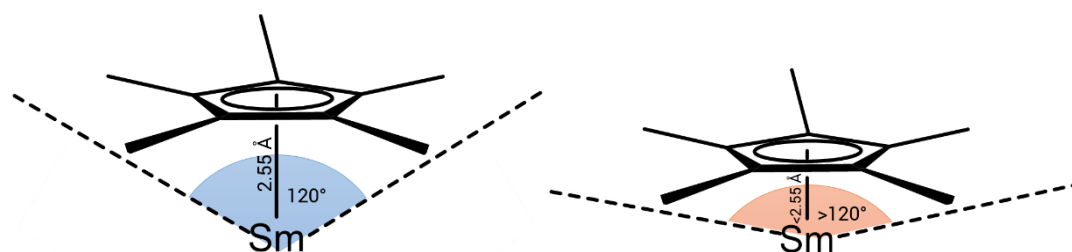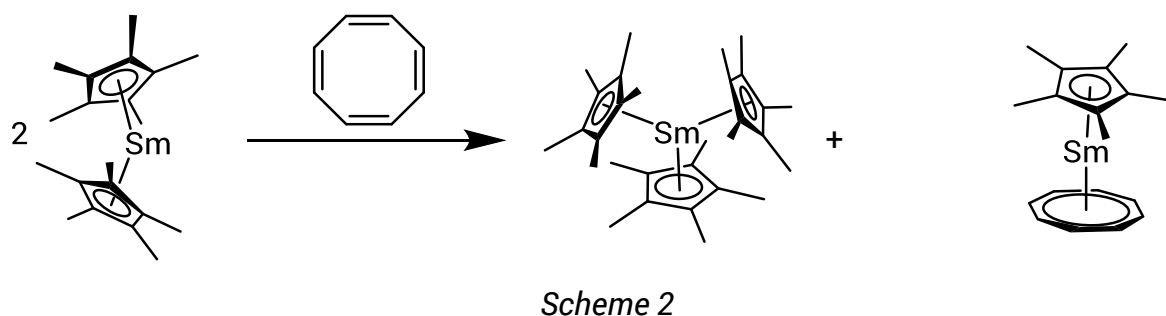
Figure 5. Pictogram depicting the increase in Tolman cone angle for a (Cp) ligand with decreasing Sm−ring centroid distance.*

Tris(pentamethylcylopentadienyl)samarium showed unexpected redox reactivity towards azobenzene, phosphine sulfides and selenides, and cyclooctatetraene. The Sm(Cp*)$_3$ complex reacts as a reductant via the ligand redox couple and not the metal centre. The ligands here are not spectators but are involved in redox chemistry; for example, in the reaction of azobenzene with Sm(Cp*)$_3$ the azide is reduced by one unit and the Cp* ring gains a single electron (Scheme 3). Two Cp* radicals undergo a coupling reaction to give a dimer, but the Sm metal oxidation state is unchanged throughout. This type of lanthanide reduction chemistry is called sterically induced reduction (SIR).
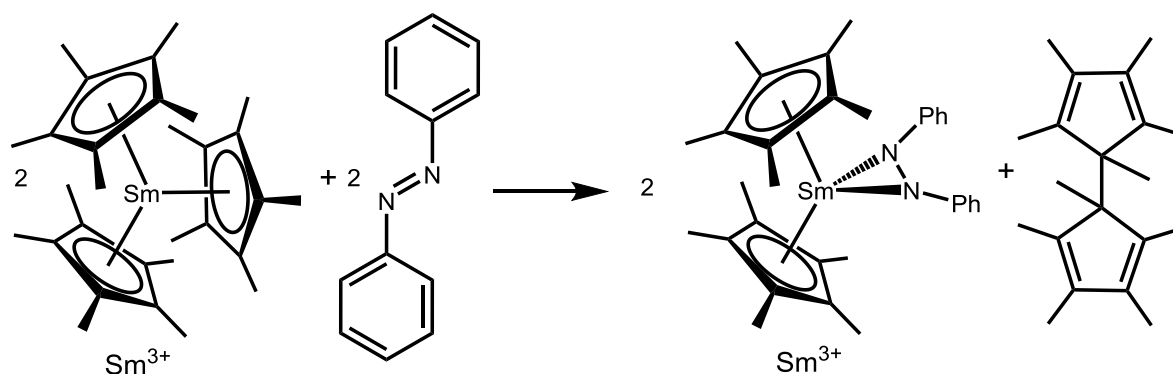
Scheme 3

With access to reductive chemistry using trivalent lanthanide compounds for lanthanides without an accessible +2 oxidation state in mind, steps were taken to find new synthetic routes to sterically crowded $Ln(Cp^*)_3$ complexes that avoided the use of divalent precursors.

The most successful of these new procedures was the synthesis of unsolvated trivalent cations as weakly coordinated ion pairs, $[(Cp^*)_2Ln][BPh_4]$.[32] The first step is preparation of trivalent $(Cp^*)_2Ln(\eta^3\text{-}CH_2CHCH_2)(THF)_n$; a metathesis reaction between $SmCl_3$ and two equivalents of $K(Cp^*)$ in THF gave an 'ate' complex $(Cp^*)_2SmCl_2K(THF)_2$ (Scheme 4).

Reaction of this complex with allyl Grignard CH_2CHCH_2MgCl in toluene appeared to suffer from Schlenk equilibria problems (due to the well documented equilibrium reaction that takes place within Grignard reagents), but the reaction was forced to completion by addition of a small amount of dioxane to polymerise the $MgCl_2$ by-product, causing it to precipitate.

The solvated complex $(Cp^*)_2Ln(\eta^3\text{-}CH_2CHCH_2)(THF)_n$ was isolated, which could then be desolvated by heating under vacuum (10^{-7} Torr) at 70°C for 4 – 20 hours. Protolysis with Et_3NHBPh_4 gives $[(Cp^*)_2Ln][BPh_4]$.
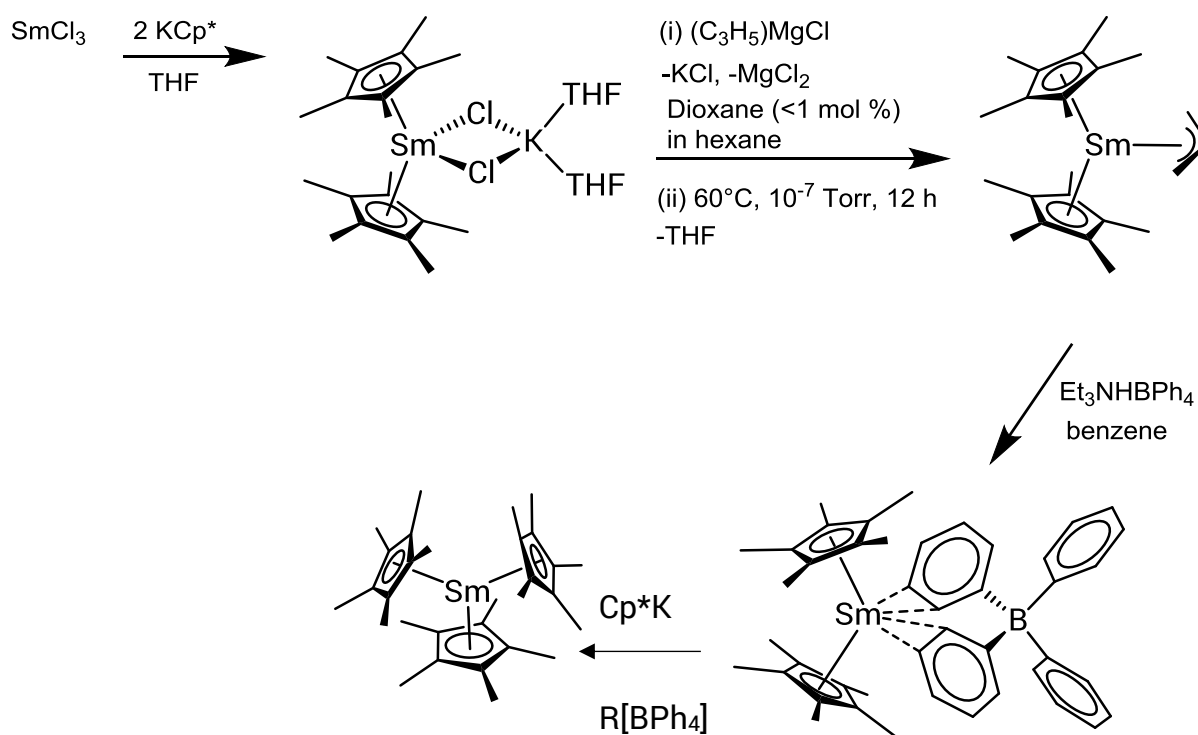
Scheme 4

The [(Cp*)$_2$Ln][BPh$_4$] analogues, (Ln = La − Nd) have been prepared by the method shown in Scheme 4 and salt metathesis reactions of these weakly coordinating ion pairs with K(Cp*) gave Ln(Cp*)$_3$ (although silylated glassware was a prerequisite to obtain the desired product for Ce and Pr). A version of this synthetic pathway has since been used to access the sterically crowded complex Lu(Cp′)$_3$, which is only formed as a minor by-product from the reaction of LuCl$_3$ with three equivalents of KCp′.[33]

Sterically induced reductions proceed via the ligand redox couple (Scheme 5) and the evidence suggests that the more sterically congested the lanthanide metal centre (i.e. the smaller the trivalent cation radius) the more negative the reduction potential of this redox couple.

$$2[C_5Me_5]^- \longrightarrow (C_5Me_5)_2 + 2e^-$$

Scheme 5

The reduction of triphenylphosphine selenide by Sm(Cp*)$_3$ gives a Se^{2-} selenide product, [(Cp*)$_2$Sm]$_2$(μ-Se) and PPh$_3$ (Scheme 6). The same reaction with Nd(Cp*)$_3$ or La(Cp*)$_3$ gives a (Se$_2$)$^{2-}$ perselenide product, [(Cp*)$_2$Sm]$_2$(μ-η^2: η^2-Se$_2$) and PPh$_3$ (Scheme 7).
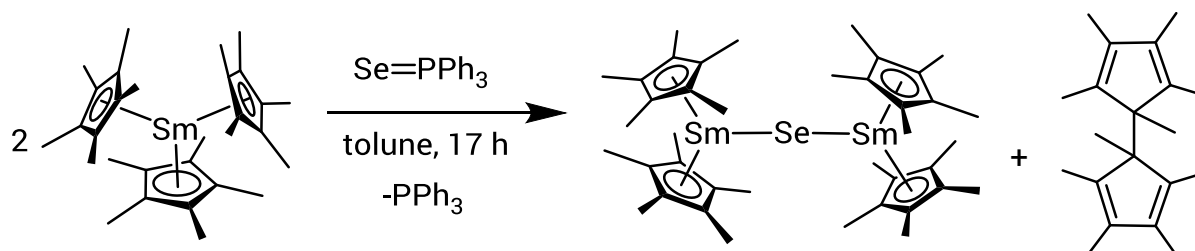
Scheme 6
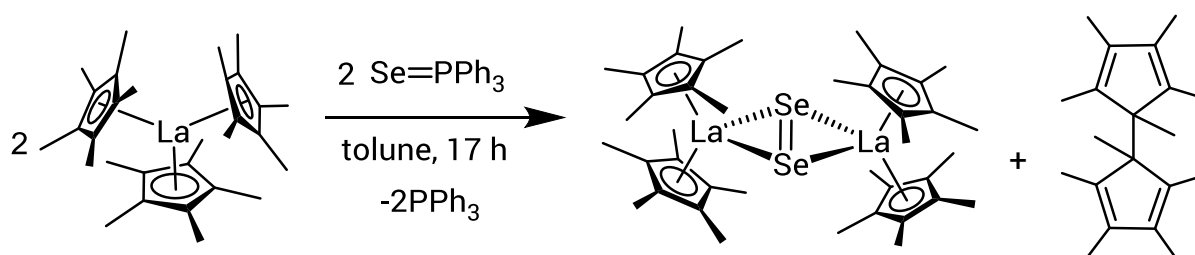
Scheme 7

1.2.2   Tris-alkyls

In recent years neutral [LuMe$_3$]$_\infty$ and [YMe$_3$]$_\infty$ have been prepared from Lu(AlMe$_4$)$_3$ and Y(AlMe$_4$)$_3$, respectively.[22,34] The reaction is a donor-induced cleavage of an Al-Me bond: addition of Et$_2$O to a cold (-35°C) solution of Lu(AlMe$_4$)$_3$ or Y(AlMe$_4$)$_3$ in hexane resulted in the precipitation of [LuMe$_3$]$_\infty$ or [YMe$_3$]$_\infty$. Their infinitely polymeric structure means they are insoluble in all solvents and decompose in donor solvents so no crystal structure of the neutral polymers is known.

Anionic hexamethylated complexes of the form [Li(tmeda)]$_3$[LnMe$_6$] (Ln = Y, La, Pr, Nd, Sm and Gd − Lu) or [Li(dme)]$_3$[LnMe$_6$] (Ln = Ho − Lu) were crystallised from diethyl ether in the 1980s (tmeda = *N,N,N′,N′*-tetramethylethylenediamine, dme = 1, 2-

dimethoxyethane) and the structures of [Li(tmeda)]$_3$[HoMe$_6$] and [Li(dme)]$_3$[LuMe$_6$] were determined by X-ray crystallography. [22,35,36] The series of compounds were synthesised by the addition of six equivalents of MeLi to anhydrous LnCl$_3$ in diethyl ether, at -78°C in the presence of stoichiometric amounts of tmeda or dme (Scheme 8 and Scheme 9). To obtain neutral monomeric lanthanide-alkyl complexes more sterically bulky alkyl carbanions were needed, but this posed synthetic difficulties because carbanion stability usually decreases in the order: primary > secondary > tertiary, primarily due to the destabilising inductive effect of alkyl groups.

LnCl$_3$ + 6 MeLi $\xrightarrow[\text{+ 3 tmeda, - 3 LiCl}]{\text{Et}_2\text{O, -78°C} \longrightarrow \text{rt, 3 hrs}}$

Scheme 8

LnCl$_3$ + 6 MeLi $\xrightarrow[\text{- 3 LiCl}]{\text{Et}_2\text{O/dme, -78°C} \longrightarrow \text{rt, 3 hrs}}$
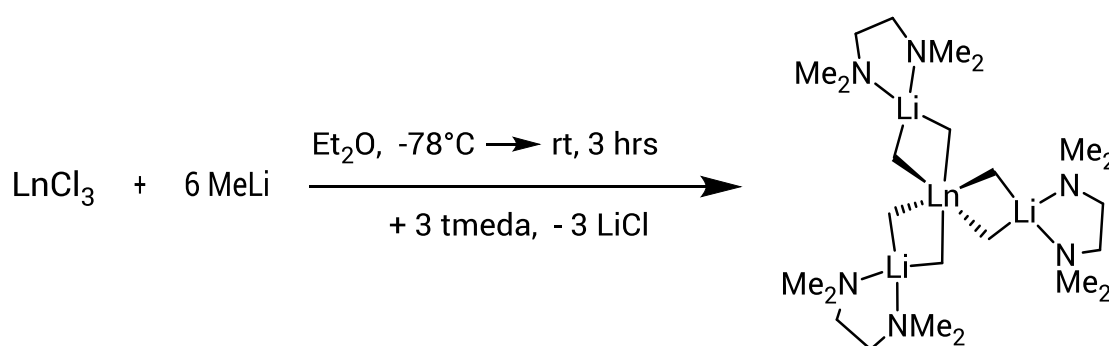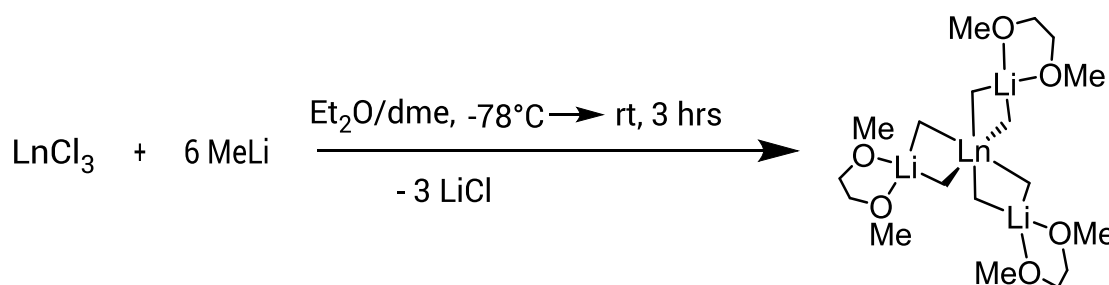
Scheme 9

Trivalent lanthanides can be complexed with neopentyl carbanion ligands[5,22,37] and with alkyl carbanion ligands based on neopentane in which the methyl groups are replaced by charge stabilising Me$_3$Si- or phosphine-borane groups, or protons. Trimethylsilyl- groups stabilise the carbanion centre by negative hyperconjugation into the Si−C σ* antibonding orbitals (see Chapter 3). The more −SiMe$_3$ substituents there are on a carbon centre the more acidic the alkyl proton(s). It follows that (Me$_3$Si)$_3$CH is easier to deprotonate (MeLi, MeK) than (Me$_3$Si)$_2$CH$_2$,

despite the most acidic proton being sterically obstructed.[38,39] The lithium salt $(Me_3Si)_2CHLi$ is made by lithium-halogen exchange as is the even less acidic $Me_3Si CH_2Li$, which is commercially available. Conversion of the organolithiums to the organopotassium compounds can be achieved by stirring in Et_2O with KO^tBu.[40] As the synthesis of lanthanide organometallic compounds has been explored it has become good practise to use an organopotassium salt in metathesis reactions with lanthanide halides because the potassium halide by-products are much less soluble in THF (and other donor solvents) than lithium halides. Precipitation of the potassium halide helps to drive the reaction forward and reduces the likelihood of 'ate' complex formation where, for example a solvated or donor-coordinated lithium cation, $[Li(THF)_4]^+$ or $[Li(donor)]^+$ forms an ion pair with a $[LnR_4]^\ominus$ or $[LnR_3Cl]^\ominus$ anion (Figure 6).[7,41]
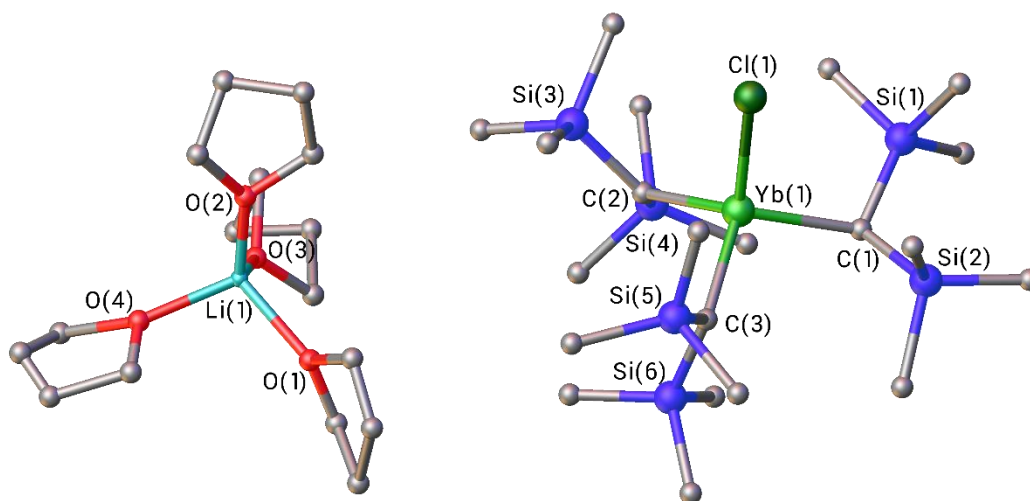
Figure 6. Crystal structure of an 'ate complex': [Li/K(donor)][Ln{(CHSiMe₃)₂}₃Cl]

1.2.2.1   Lanthanide complexes of mono(trimethylsilyl)methyl ligands

Solvated tris(trimethylsilylmethyl)lanthanide complexes, $M(CH_2SiMe_3)_3(THF)_2$, were first reported for the Ho^{3+} lanthanide cation analogue Y^{3+} and the small Sc^{3+} cation by Lappert[5] in 1973 and lanthanide derivatives followed in 1978 for Tb, Er and

Yb.[7,42] Since then these compounds have also been isolated for Lu, Tm and Sm, e.g. Sm(CH$_2$SiMe$_3$)$_3$(THF)$_3$.[6]

These complexes can be synthesised by the addition of exactly three equivalents of LiCH$_2$SiMe$_3$, as a solution in pentane or hexane, to the anhydrous LnCl$_3$ (and a stoichiometric amount of THF) or to the LnCl$_3$(THF)$_x$ adduct as a slurry in equal parts pentane/diethyl ether (Scheme 10). Addition of another equivalent of LiCH$_2$SiMe$_3$ and two or more equivalents of THF gives the ionic 'ate' complexes [Li(THF)$_4$][Ln(CH$_2$SiMe$_3$)$_4$].[7]

The synthesis of Ln(CH$_2$SiMe$_3$)$_3$(THF)$_2$ works best at room temperature indicating a thermodynamic reaction barrier. Once the product is formed it is unstable (hours), and there is a negative correlation between increasing lanthanide cation size and complex stability. To prevent decomposition, reaction times are kept short (3 hours) and the work-up (filtration to remove LiCl, removal of the solvent and extraction) is best performed at low temperatures (0°C).[6] Crystals were grown from pentane at -35°C.

LnCl$_3$ $\xrightarrow{\text{(i) Stoichiometric THF}}$ Ln(CH$_2$SiMe$_3$)$_3$(THF)$_x$ + LiCl

(i) Stoichiometric THF
(ii) 3 LiCH$_2$SiMe$_3$ in pentane

pentane:Et$_2$O, 1:1, rmt $\longrightarrow$ 0°C

(iii) LiCH$_2$SiMe$_3$

2 THF

[Li(THF)$_4$][Ln(CH$_2$SiMe$_3$)$_4$]
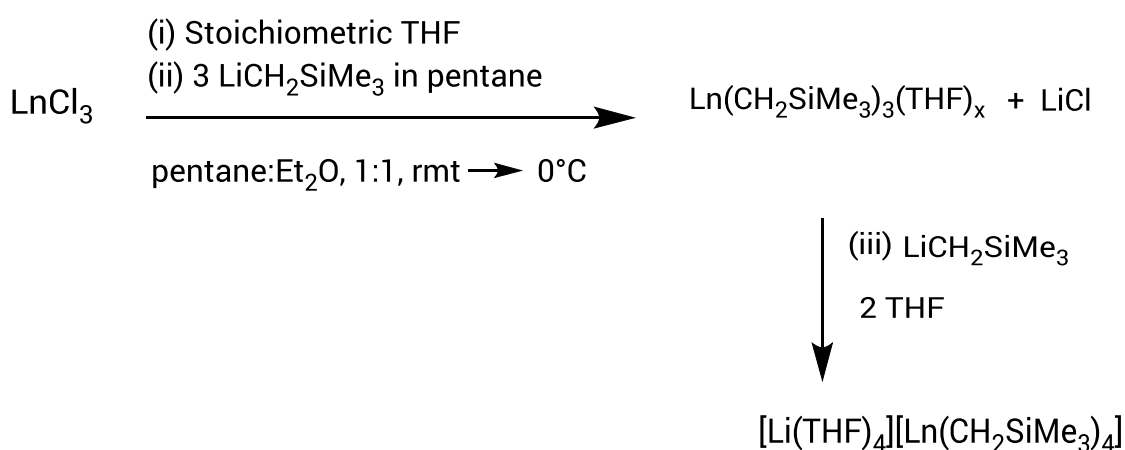
Scheme 10

The complexes Ln(CH$_2$SiMe$_3$)$_3$(THF)$_n$, (Ln = Sm, Er, Yb, Lu) have only recently been structurally characterised by single crystal XRD methods,[6] although the structure of an [Li(THF)$_4$][Ln(CH$_2$SiMe$_3$)$_3$Cl] 'ate' complex (Ln = Yb) was determined earlier.[7]

15

Studies show that there is a structural transition between the Er and Sm complexes; the Lu-Er complexes are trigonal bipyramidal with the three CH_2SiMe_3 ligands in the equatorial positions, whereas the Sm complex (three coordinated THF molecules) is octahedral with a *fac* arrangement of the CH_2SiMe_3 ligands (Figure 7). For CH_2SiMe_3, the smallest of the trimethylsilyl-stabilised carbanions, complexes have not been isolated for lanthanides larger than Sm, presumably because the ligands are not sterically bulky enough to saturate the coordination sphere.[22] The lanthanide contraction is a recurrent theme, and, together with ligand size, controls the structures and reactivity of organolanthanide complexes.
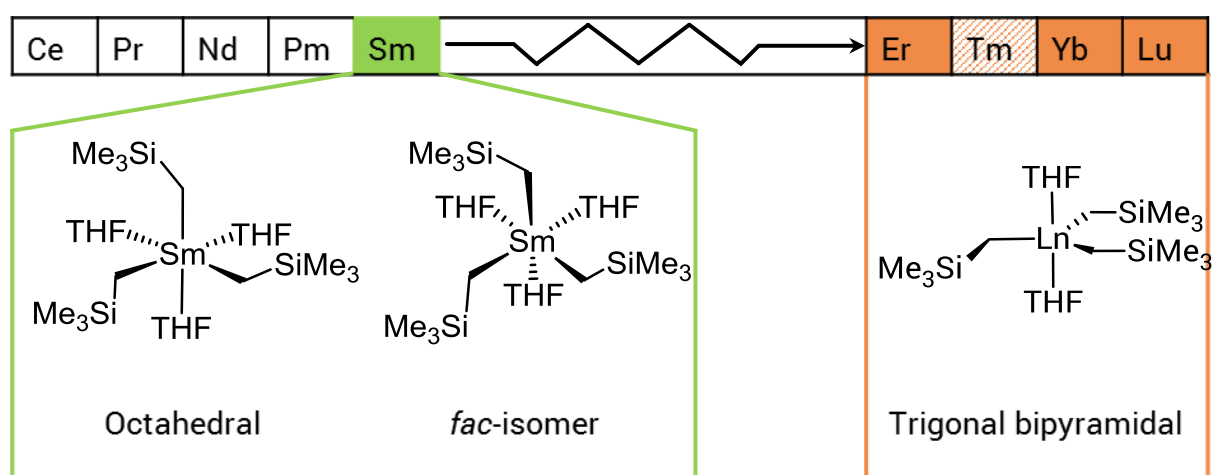
Figure 7. Structural transition for the series of compounds Ln(CH₂SiMe₃)₃(THF)ₙ

1.2.2.2   Lanthanide complexes of bis(trimethylsilyl)methyl ligands

The same salt metathesis reaction between $LnCl_3$ and $LiCH_2SiMe_3$, used to synthesise $M(CH_2SiMe_3)_3(THF)_2$, is not transferable to the synthesis of neutral $Ln\{CH(SiMe_3)_2\}_3$ complexes (with the exception of the smallest group 3 element Sc); instead ionic 'ate' complexes are formed.[6] The workaround of the time was to use a different lanthanide salt, $Ln(OAr^tBu)_3$ (OAr^tBu = 2, 6-di-*tert*-butyl-4-methylphenoxide), because the by-product $LiOAr^tBu$ is bulky and very insoluble in hydrocarbon solvents (the $Ln\{CH(SiMe_3)_2\}_3$ product is soluble) and this helps to

drive the equilibrium towards the desired products (Scheme 11).[22,43] The products Ln{CH(SiMe$_3$)$_2$}$_3$ (Ln = La,[43] Ce,[44] Pr,[45] Nd,[45] Sm,[43], Y[44,46] and Lu[46]) can be isolated as stable, neutral, solvent-free complexes; the ligands are sufficiently sterically bulky that the coordination of donor solvent molecules is not needed to stabilise the complexes.

$$Ln(OAr^tBu)_3 \quad + \quad 3\ LiCH(SiMe_3)_2 \quad \xrightarrow[\text{-3 LiOAr}^t\text{Bu}]{\overset{\text{pentane/hexane}}{\text{rmt}}} \quad Ln\{CH(SiMe_3)_2\}_3$$
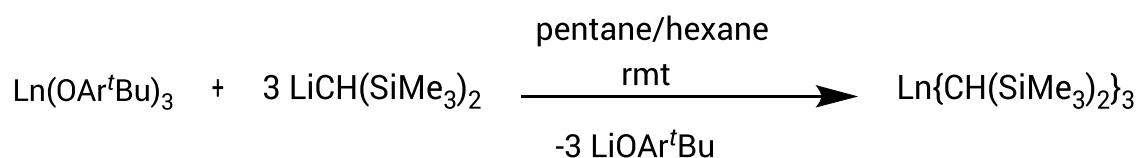
Scheme 11

All determined crystal structures (Ln = La, Ce, Y and Sm) are isomorphous, with the same pyramidal structure adopted across the lanthanide series (Figure 8).[43,47] The bis(trimethylsilyl)methyl ligands each have an agostic-type contact with the lanthanide metal centre, i.e. Ln$^{\delta+}$···$^{\delta-}$Me−Si, which further saturates the lanthanide coordination sphere.[22] These three Ln$^{\delta+}$···$^{\delta-}$Me−Si contacts mean the lanthanide metal centre can be regarded as 6-coordinate and the pyramidal geometry can be thought of as a distorted octahedron with a *fac* arrangement of the Ln−C σ-bonds and the Ln$^{\delta+}$···$^{\delta-}$Me−Si contacts to the (Me$_3$Si)$_2$HC$^{\ominus}$ ligands. These interactions are more electrostatic than true agostic interactions seen in transition metal complexes since the lanthanide has no accessible vacant d-orbitals into which electron density can be accepted.
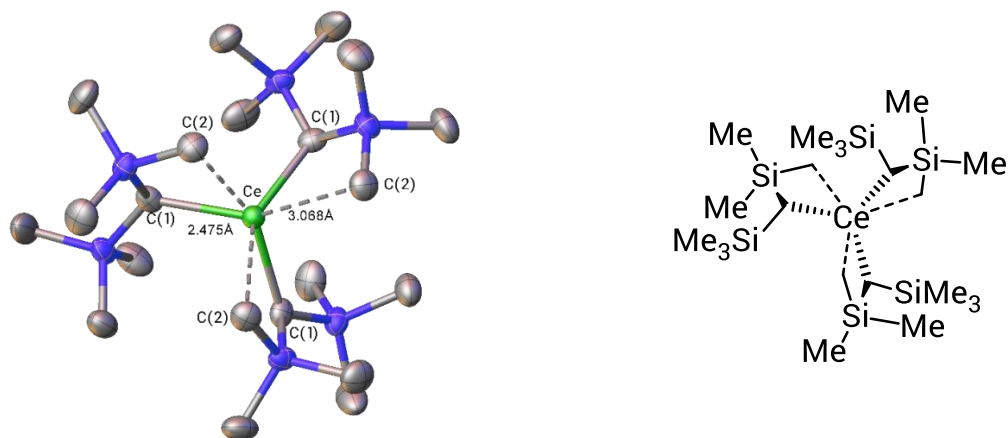
Figure 8. Structure of Ce{CH(SiMe₃)₂}₃ with hydrogen atoms omitted for clarity.

1.2.2.3   Lanthanide complexes of tris(trimethylsilyl)methyl ligands

Tris(trimethylsilyl)methyl ('trisyl') ligands have not been widely utilised in trivalent lanthanide chemistry since their steric bulk is believed to prohibit the formation of homoleptic trialkyl compounds. Heteroleptic dialkyl La(III) complexes of functionalised tris(trismethylsilyl)methyl ligands, where one methyl group of a single $-SiMe_3$ group is replaced by an $-OMe$ or $-NMe_2$ functional group have been synthesised.[48] A salt-metathesis reaction between $LaI_3(THF)_4$ and two equivalents of $[(Me_3Si)_2\{Me_2(Me_2N)Si\}C]K$ in THF at room temperature formed the heteroleptic dialkyl compound $[(Me_3Si)_2\{Me_2(Me_2N)Si\}C]_2LaI$. Crystals grown from methylcyclohexane at -20°C were suitable for X-ray crystallography.

The resulting structure (Scheme 12) shows that the complexes are solvent-free monomers and the N-donor atom enables the formation of four-membered $La-C-Si-N$ chelate rings. The same reaction with $[(Me_3Si)_2\{Me_2(MeO)Si\}C]K$ gave a mixture of dialkyl and monoalkyl products, $[(Me_3Si)_2\{Me_2(MeO)Si\}C]_2LaI$ and $[(Me_3Si)_2\{Me_2(MeO)Si\}C]LaI_2$. The dialkyl product crystallised with an additional coordinated THF molecule, and similar $La-C-Si-O$ chelate rings to $[(Me_3Si)_2\{Me_2(Me_2N)Si\}C]_2LaI$. The challenge in the formation of heteroleptic complexes is to avoid ligand redistribution by Schlenk-type equilibria, which yields mixtures of products unless a method can be found to drive the equilibrium in one

direction. Chelate ring formation often increases the stability of lanthanide complexes toward ligand redistribution, especially the exchange of monoanions.
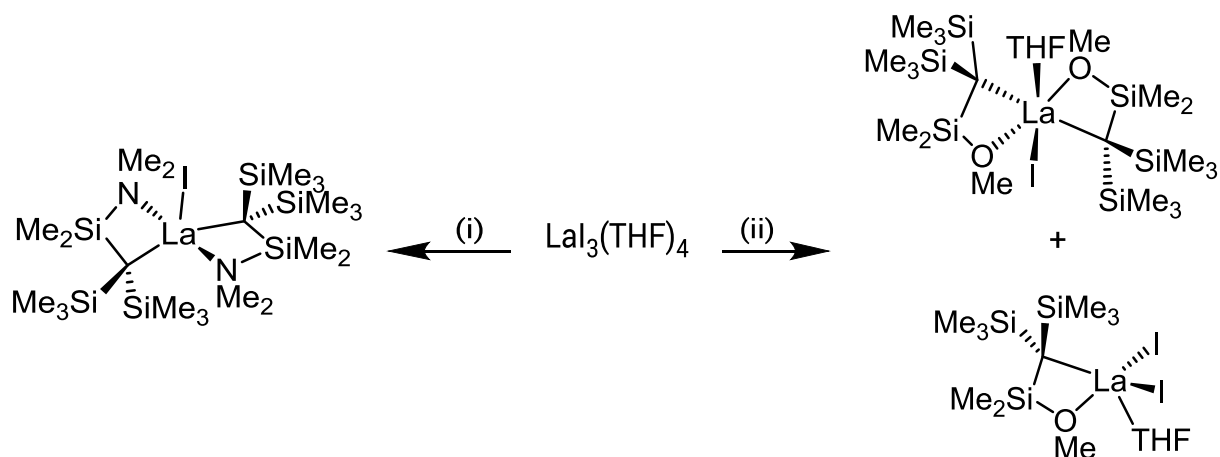
Scheme 12. Synthesis of La(III) complexes of functionalised tris(trismethylsilyl)methyl ligands: (i) 2 [(Me₃Si)₂{Me₂(Me₂N)Si}]K, THF, room temperature and (ii) 2 [(Me₃Si)₂{Me₂(MeO)Si}]K, THF, room temperature.

1.3   Divalent organo-lanthanide compounds

1.3.1   Bis(Cyclopentadienyl) Systems

Lanthanide organometallics of cyclopentadienyl-type ligands span the whole lanthanide series for both the divalent (Ln^{2+}) and trivalent (Ln^{3+}) oxidation states. For the classical lanthanide (II) ions (Eu, Sm, Yb) and some non-classical lanthanide(II) ions (Tm, Dy, Nd) soluble binary lanthanide diiodides are synthetically accessible and bis(cyclopentadienyl) complexes can be synthesised using metathesis chemistry for a range of cyclopentadienyl-type ligands (Figure 9). Complexes of non-classical lanthanide(II) ions can be synthesised as tris(cyclopentadienyl) anions with bulky non-coordinating counter-cations by reduction of the corresponding trivalent precursors using potassium graphite (KC_8). Anionic complexes of classical lanthanides can also be synthesised by this reduction route, but the ionic complexes tend to exhibit reduced reactivity, and,

since divalent complexes of the lanthanides are noted for their interesting one-electron reduction chemistry, neutral complexes are preferred.
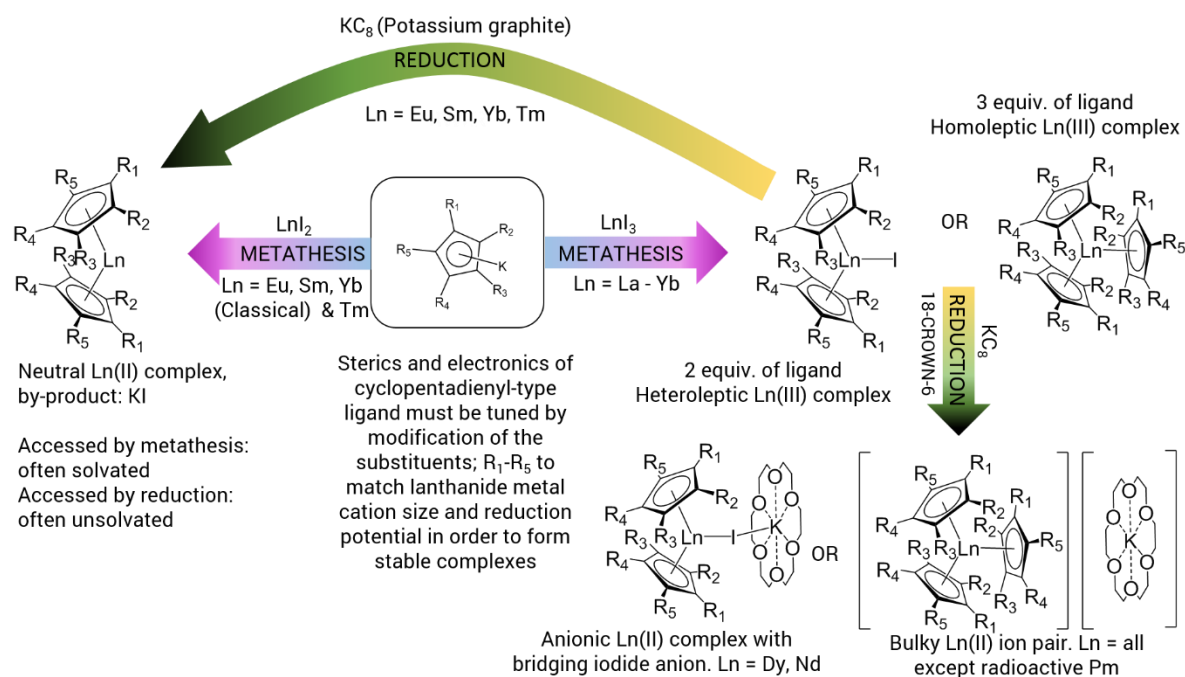
Figure 9. Overview of synthetic routes to divalent lanthanide cyclopentadienyl compounds

1.3.1.1   Synthesis by salt metathesis

The discovery of Kagan's reagent, SmI_2, in 1977 (Scheme 13) expanded the range of binary lanthanide dihalides available as starting materials for metathesis reactions with cyclopentadienide alkali-metal salts (Figure 2).[49] Previously only dihalides of Yb and Eu were routinely available because of the solubility of these metals in liquid ammonia. Two of the earliest organometallic lanthanide(II) compounds reported, Cp_2Eu and Cp_2Yb, were made in liquid ammonia from the metal and cyclopentadiene monomer.[50,51]   There are similarities between these bis(cyclopentadienyl) compounds and the previously mentioned tris(cyclopentadienyl) lanthanide compounds: crystals were grown by sublimation due to their insolubility, and more recently the solid state structures have been determined and were also found to be polymeric chains.[52] The Cp_2Yb units are

linked together in cross-linked sheets (Figure 10). Each Yb metal centre is 10-coordinated by η^5 interactions to three cyclopentadienyl rings and a further η^1 interaction to a fourth cyclopentadienyl ring. Every cyclopentadienyl ring is shared between two Yb metal centres either by η^5 interactions to both or an η^5 interaction to one Yb and an η^1 interaction to another Yb centre.

$$3\,Sm \;+\; ICH_2CH_2I \;\xrightarrow{\text{THF, rt}}\; 2\,SmI_3 \;+\; 3\,H_2C{=}CH_2 \;+\; Sm$$

$$2\,SmI_3 \;+\; Sm \;\xrightarrow{\text{THF, rt}}\; 3\,SmI_2(THF)_2$$
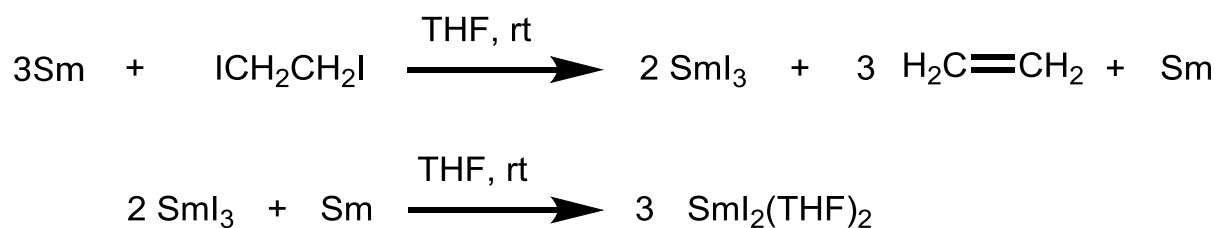
Scheme 13. Kagan's method for the synthesis of SmI$_2$(THF)$_2$ using 1,2-diiodoethane[49]

21
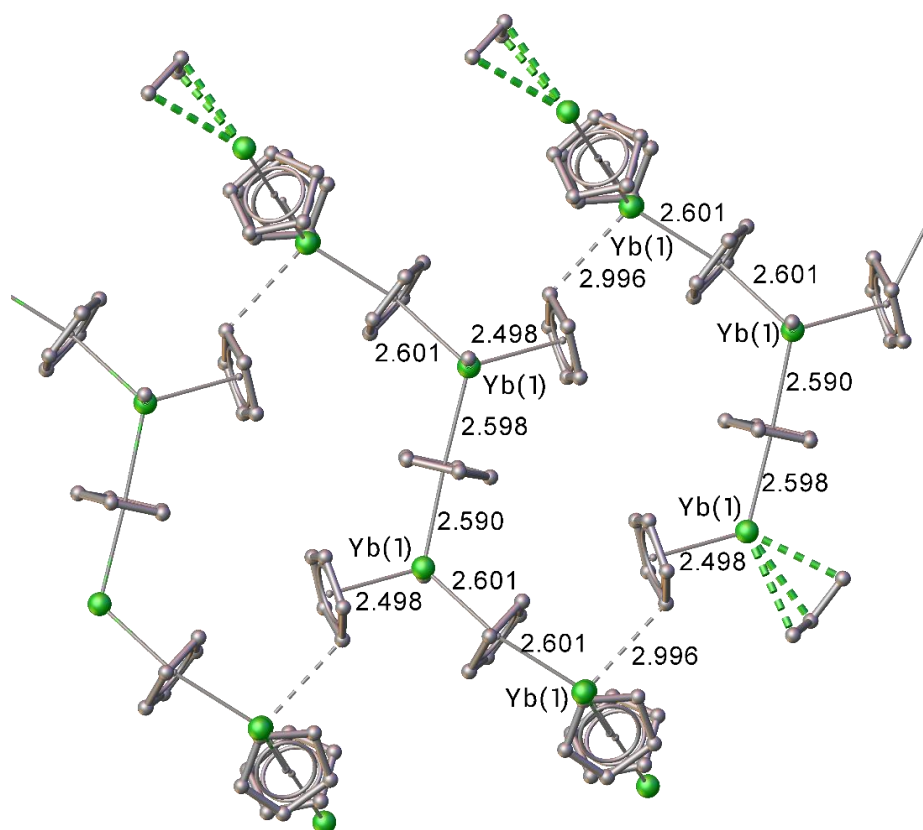
Figure 10. Sheet structure of Yb(Cp)$_2$, the solid grey lines represent η^5 interactions between cyclopentadienyl rings and Yb, the stippled grey lines represent η^1 interactions between cyclopentadienyl rings and Yb. The green stippled lines represent cross-links between this sheet and the next layer.

Kagan's reagent was investigated for its synthetic uses as a one-electron reducing agent for organic compounds, e.g. the reduction of haloalkanes and reduction of ketones to tertiary alcohols (Scheme 14).[53] The reactions result in oxidation of the lanthanide metal centre from the +2 state to the +3 state as it gains a halide anion from the haloalkane; giving SmI$_2$X. The utility of these transformations to organic synthesis generated considerable interest within organometallic chemistry in exploring the redox reactivity of organometallic divalent samarium compounds alongside synthetic method development and structural characterisation. Sm(Cp*)$_2$ and Kagan's reagent differ in their one-electron reduction chemistry, the redox potential of Sm(Cp*)$_2$ is greater than that of SmI$_2$ due to the change of ligand

and so Sm(Cp*)$_2$ will reduce many substrates such as Ph$_3$P=S that are not reduced by SmI$_2$, (Scheme 15).[54]
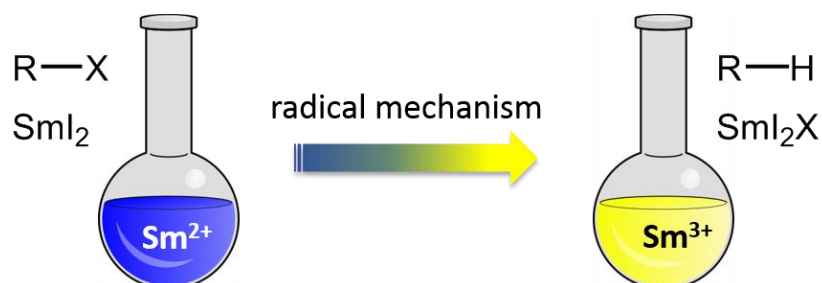
Scheme 14. Reduction of haloalkanes using Kagan's reagent. The redox potential is sensitive to the solvent and addition of strong donor ligands, so SmI$_2$ → SmI$_2^+$ + e$^-$ is -1.41 V (neat THF) and reduces only primary haloalkanes. The redox potential increases to -1.79 V with the addition of 4 equivalents of HMPA; (Me$_2$N)$_3$P=O, and will reduce secondary and tertiary haloalkanes.[55] The reactions are quite easy to follow in the lab because there is a colour change from dark blue to yellow.
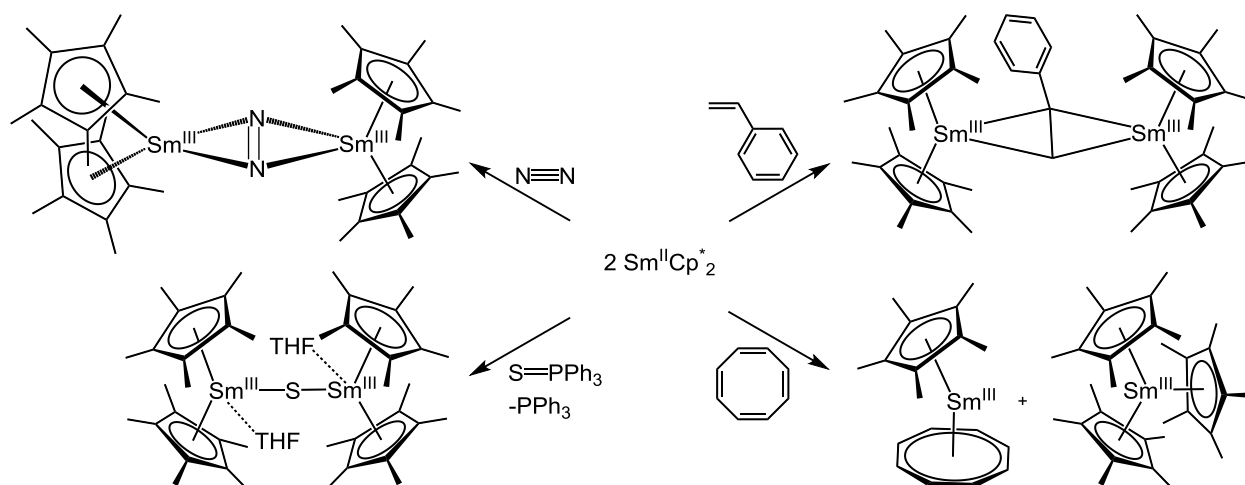
Scheme 15. Selected reduction reactions mediated by Sm(Cp)$_2$.[56−60]*

Yb(Cp*)$_2$ and Eu(Cp*)$_2$ have been prepared by metathesis of K(Cp*) with YbI$_2$ or EuI$_2$ (analogues of Kagan's reagent for these metals).[49,61,62] The solid state structures of

solvent-free $Sm(Cp^*)_2$ and $Eu(Cp^*)_2$ consist of an arrangement of dimeric units due to Sm····Me agostic-type interactions.[62]   The structures of $Yb(Cp^*)_2$ and of the analogous $Ca(Cp^*)_2$, where the divalent metal cation is smaller, are polymeric (Figure 11).[61,63] Divalent lanthanide cations are larger than trivalent cations and, since two anionic ligands instead of three provide electrostatic stabilisation, it follows that even bulkier ligands, or ligands with chelating properties are required to sterically saturate the lanthanide coordination sphere, preventing the formation of polymers.
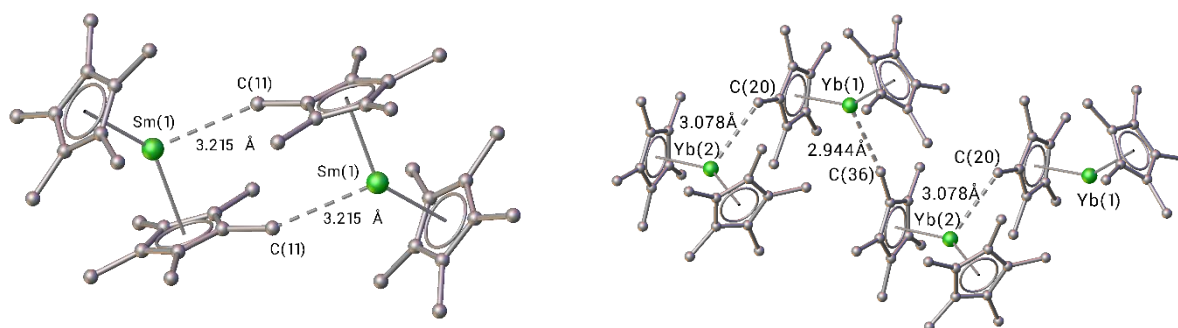
Figure 11. Solid-state structures of $Sm(Cp^*)_2$ and $Yb(Cp^*)_2$. The structure of $Sm(Cp^*)_2$ is bent in the gas phase (H atoms omitted for clarity).

Twenty years after the discovery of Kagan's reagent Bochkarev and Evans synthesised, isolated and structurally characterised the Tm analogue, $TmI_2(DME)_3$.[64] The complex decomposes slowly at room temperature both in the solid state and in solution; it was also reported that the complex is photosensitive. This compound is accessed by the two day reaction of excess Tm metal powder with iodine under vacuum in dimethoxyethane (DME) at room temperature, initially forming TmI_3.   After washing with cold DME to remove unreacted iodine, the mixture of Tm metal and TmI_3 was then heated to reflux in DME and essentially a soxhlet extraction of TmI_2 was performed.   Green crystals of $TmI_2(DME)_3$ were grown from DME at -38°C. The crystal structure with axial iodine atoms is very similar to that of $SmI_2(THF)_5$ (Figure 12) and under vacuum both compounds

readily lose solvent molecules to give powders with reduced solvation, $LnI_2(solv)_2$.[65,66]
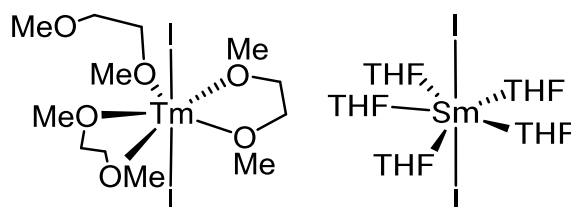
Figure 12. Structures of TmI$_2$(DME)$_3$ and SmI$_2$(THF)$_5$.

Tm(II) and Yb(II) are similar in size (Tm(II) 1.09 Å, Yb(II) 1.14 Å) but differ in reduction potential (Tm -2.3V, Yb -1.1V versus NHE) and it is suggested that this is the main reason (Cp*)$_2$Yb can be isolated but (Cp*)$_2$Tm cannot. Reported attempts to synthesise (Cp*)$_2$Tm using metathesis chemistry led to the reduction of dinitrogen and under an argon atmosphere the Tm(II) complexes attacked the Et$_2$O solvent, the connectivity of the resulting trivalent product was confirmed by X-ray crystallography (Scheme 16).[54] A very electron rich ligand acts to destabilise Ln(II) centres in that it pushes more electron density onto the divalent metal centre, increasing the reduction potential. If the ligand is sufficiently sterically bulky to prevent coordination of the solvent then oxidation of the metal via decomposition of the solvent can be avoided and a stable complex may be achieved. In order to stabilise a divalent organometallic complex of Tm(II) with cyclopentadienyl-type ligands the ligand could be modified in two ways (i) make the ligand more electron poor and/or (ii) increase the steric bulk of the ligand (Figure 13).

25
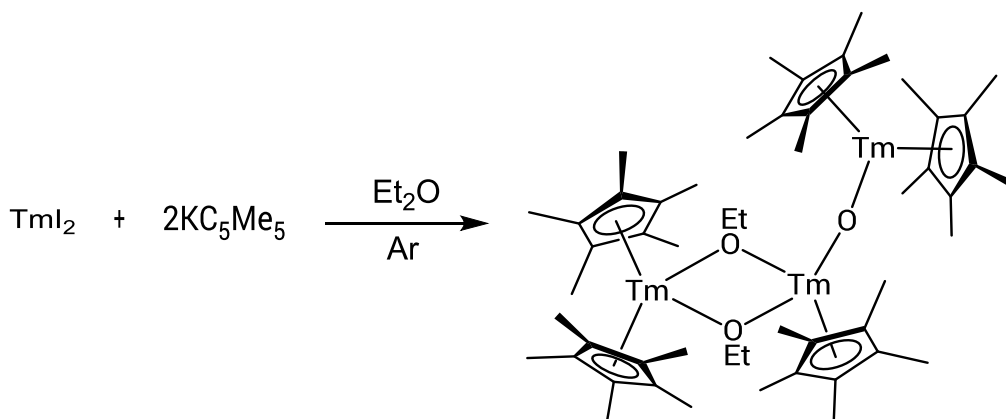
Scheme 16

A combination of both approaches was used to maximise the likelihood of success and Evans reported the first divalent organometallic complex of Tm in 2001, where the Tm(II) metal cation is coordinated by two $C_5H_3(SiMe_3)_2$ (Cp'') rings and a single THF molecule (Scheme 17).[67] The trimethylsilyl substituents act as bulky electron withdrawing substituents on the cyclopentadienyl ring. The complex is unstable in solution under argon at room temperature, as is the more electron rich Tm{$C_5H_3(^tBu)_2$}$_2$(THF) derivative [$C_5H_3(^tBu)_2$ = Cp^{tt}],[68] and both complexes react with dinitrogen. These ligands were neither electron-poor enough, nor bulky enough to prevent decomposition over several hours at room temperature, or weeks at -30°C. Adding a third *t*Bu substituent to the cyclopentadienyl ring resulted in bis(cyclopentadienyl) complexes that were stable in THF solution, Tm(Cp^{ttt})$_2$(THF), [Cp^{ttt} = 1,2,4-tris(*tert*-butyl)cyclopentadienyl] and the THF solvent is labile due to the extreme steric bulk of the ligands (Figure 13).[69]
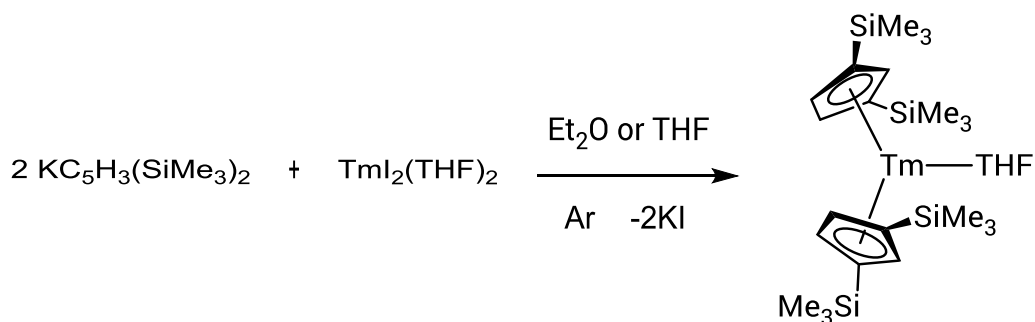
Scheme 17

Using the phosphole heterocyclic analogues of Cp″ and Cp^{tt}, in 2005 Nief created ligands with poorer π-donor abilities but similar steric bulk to that of the first complex isolated by Evans.[70] Metathesis reactions gave moderate yields of Tm(Htp)$_2$(THF), [Htp = 2,5-di-*tert*-butylphospholyl] and [Tm(Hsp)$_2$(THF)], [Hsp = 2,5-bis(trimethylsilyl)phospholyl], neither of which reacted with dinitrogen over 24 hours at room temperature in diethyl ether solution. The Tm(II) metal centre coordinated by two phospholyl anions appears to have a less negative reduction potential relative to Tm(II) complexes coordinated by (Cp*), Cp^{tt} or Cp″ anions. A divalent lanthanide metal centre can be made less reducing by decreasing the amount of electron density donated to the metal by the ligands. The reductive reactivity of the complexes was judged by comparison of their reactivity with dinitrogen.

| (Hsp)$_2$Tm(THF) = stable | (Cp″)$_2$Tm(THF) = unstable | (Cp^{ttt})$_2$Tm = stable |
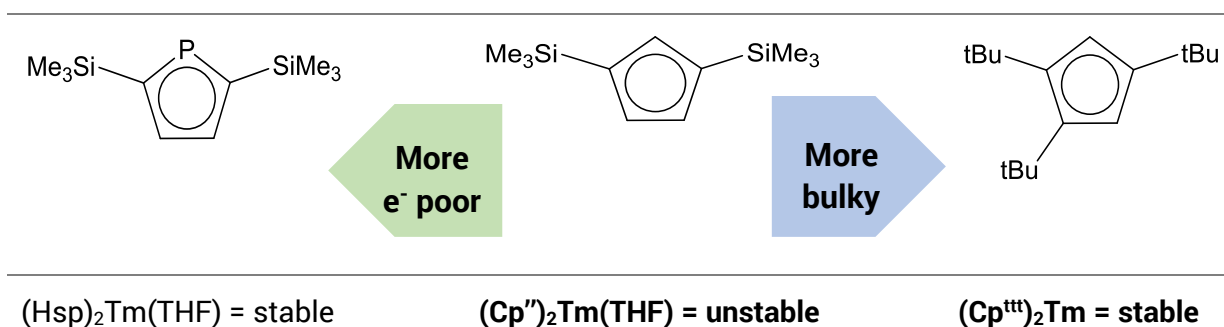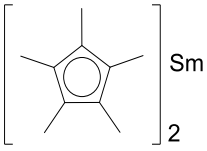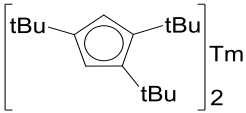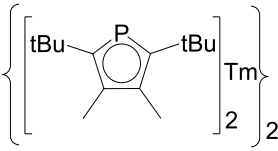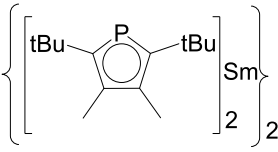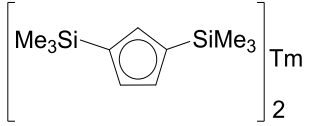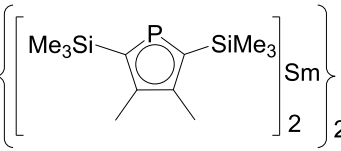
Figure 13. The Cp″ ligand (centre) was modified in two ways to stabilise Tm(II) complexes: (left) a more electron poor phospholyl ligand, (right) a more sterically bulky C$_5$H$_2$(^{t}Bu)$_3$ ligand.

Comparative reactivity studies have been carried out by Nief *et al.* between bis(phospholyl)thulium(II) complexes, bis(phospholyl)samarium(II) complexes and (Cp*)$_2$Sm.[71] Pairs of complexes with the same phospholyl ligands, [{Sm(dtp)$_2$}$_2$] and [Tm(dtp)$_2$], (dtp = 2,5-di-*tert*-butyl-3,4-dimethylphospholyl) and [{Sm(dsp)$_2$}$_2$] and [Tm(dsp)$_2$(Et$_2$O)], (dsp = 2,5-bis(trimethylsilyl)-3,4-dimethylphospholyl) were synthesised for the purpose of the study. These complexes, and the already described Tm(Cp″)$_2$(THF) and Tm(Cp^{ttt})$_2$ were reacted with a range of substrates

27

known to be reduced by (Cp*)$_2$Sm, the results are summarised in Table 3 and further discussion is given below.

Table 3. Reactivity of a series of related divalent Sm(II) and Tm(II) complexes

	THF	N$_2$	Ph$_2$P=S	PhN=NPh	Anthracene	Pyridine
[Cp*]$_2$Sm	✗	✓	✓	✓	✓	✓
[tBu,tBu,tBu-Cp]$_2$Tm	✗	✗	–	✓	–	✓
{[tBu,tBu-P(pyrrolyl)]$_2$Tm}$_2$	✗	✗	✓	✓	✗	*adduct*
{[tBu,tBu-P(pyrrolyl)]$_2$Sm}$_2$	✗	✗	✗	✓	✗	✗
[Me$_3$Si,SiMe$_3$-Cp]$_2$Tm	✓	✓	–	–	–	✗
{[Me$_3$Si,SiMe$_3$-P(pyrrolyl)]$_2$Sm}$_2$	✗	✗	✗	✓	✗	✗

TmCp''$_2$ is oxidised in solution by THF over a period of 30 minutes, probably by electron-transfer to THF, followed by ring opening. Sm(Cp*)$_2$ does not react with THF but both complexes will reduce dinitrogen to form η^2-bonded N$_2$$^{2-}$ bridged trivalent complexes (Scheme 18). (Cp*) is a more electron-rich ligand than Cp'' and hence the reducing power of Sm(Cp*)$_2$ is comparable to TmCp''$_2$ despite the difference of 0.7 V in the reduction potentials of the naked metal cations.[72] Switching the (Cp*) ligands to dsp or dtp ligands renders the Sm(II) complexes

much less reactive than Sm(Cp*)$_2$. Of the unsaturated substrates listed in Table 3, [{Sm(dsp)$_2$}$_2$] and [{Sm(dtp)$_2$}$_2$] will reduce only azobenzene in toluene (Scheme 19). The trivalent products of the one-electron reduction of azobenzene, [Sm(dsp)$_2$(N$_2$Ph$_2$] and [Sm(dtp)$_2$(N$_2$Ph$_2$) can be crystallised from pentane solutions and their structures have been determined.[71]
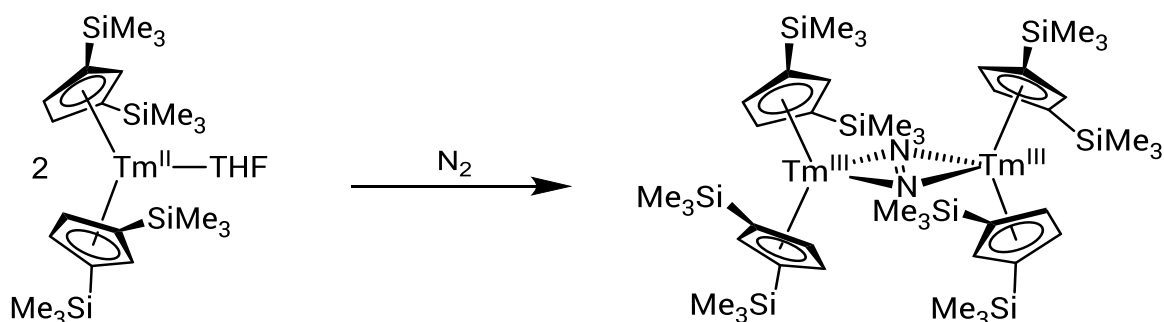
Scheme 18
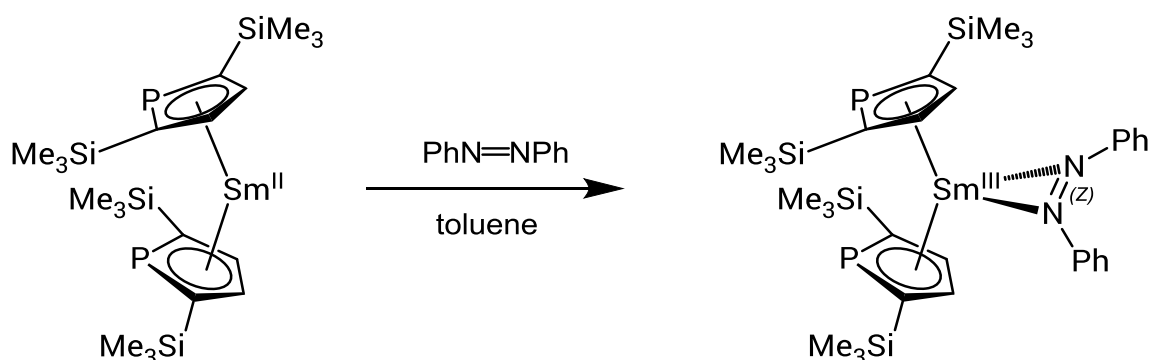
Scheme 19

The reduction potential of Tm(dtp)$_2$ is less negative than that of Sm(Cp*)$_2$ and unlike Sm(Cp*)$_2$, Tm(dtp)$_2$ will not reduce dinitrogen and anthracene which have redox potentials of -1.98 V and -2.44 V (vs. NHE), respectively (Scheme 20). [71,73] Based on the reduction potentials of the naked metal cations (Sm -1.6 V, Tm -2.3 V vs. NHE, Figure 3) the reverse trend in reductive reactivity would be expected, but the reactivity of Sm(Cp*)$_2$ and Tm(dtp)$_2$ complexes illustrates that the ligands can be used to tailor the reduction potential of a Ln(II) metal centre. A direct comparison of Tm(dtp)$_2$ and [{Sm(dtp)$_2$}$_2$] confirms expectations that Tm(dtp)$_2$ is more reducing and will reduce Ph$_3$P=S whereas [{Sm(dtp)$_2$}$_2$] cannot (Scheme 21).
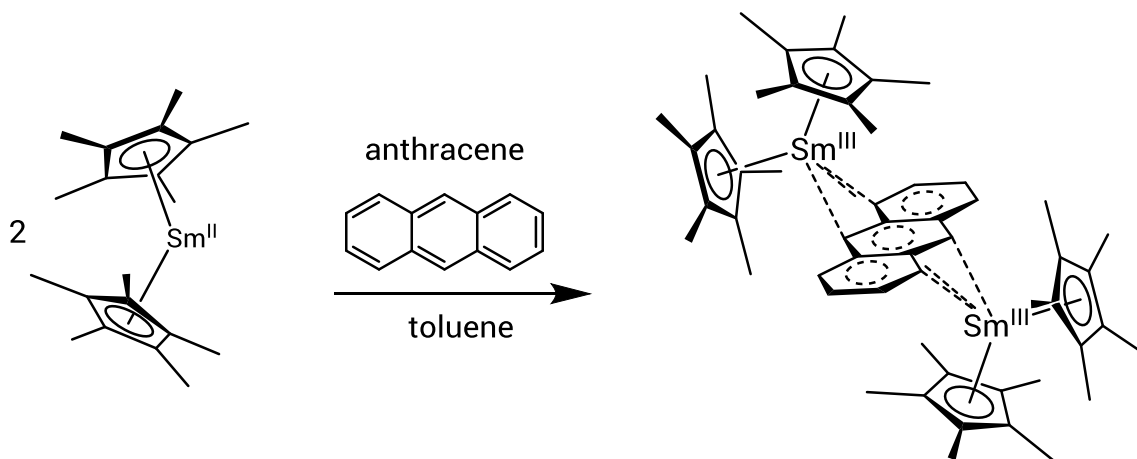
Scheme 20
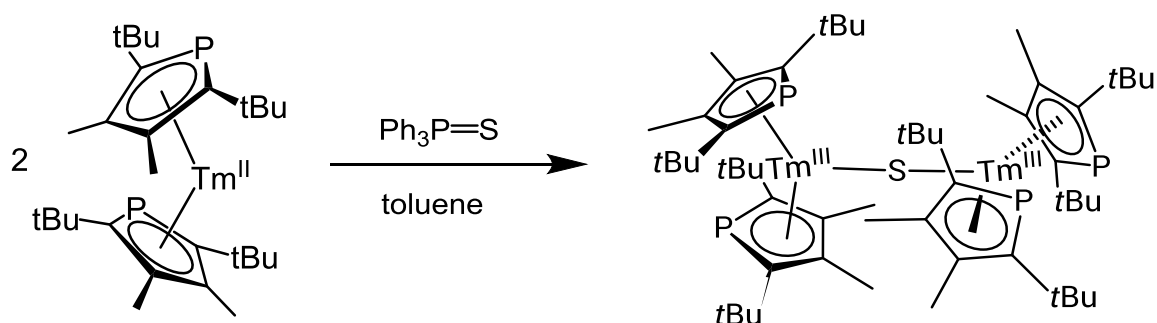
Scheme 21
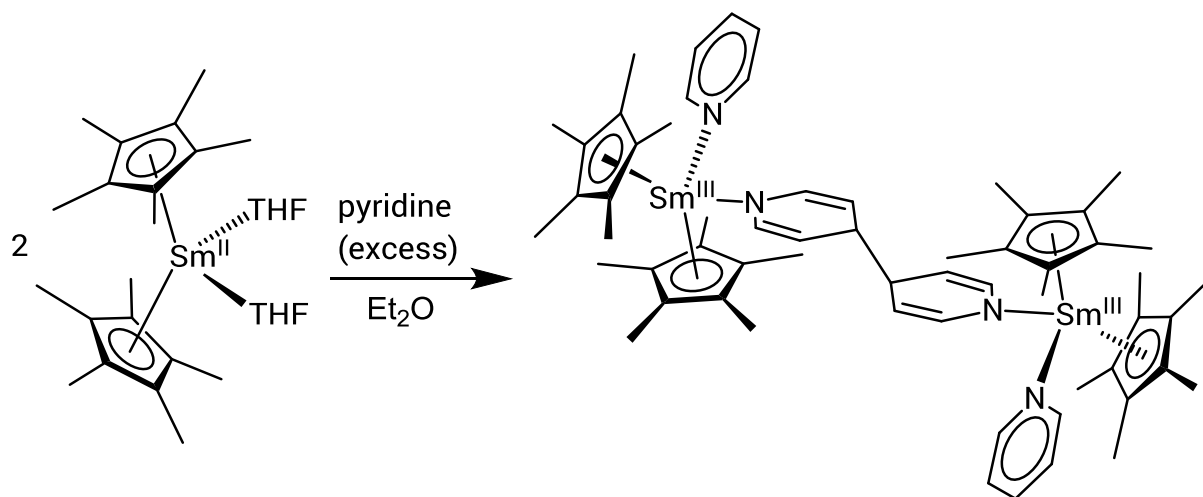
Scheme 22

A different reduction is observed for the Tm(Cp^{ttt})$_2$ complex which reductively dimerises pyridine as does TmI$_2$ and Sm(Cp*)$_2$ (Scheme 22), but more electron-poor phospholyl ligands inhibit this reaction.[72,74–76] Complexes of Tm and Sm with

phospholyl ligands form adducts with pyridine, and the structure of Sm(tmp)$_2$(pyridine)$_2$, [tmp = 2,3,4,5-tetramethylphospholyl] has been determined.[72]

Structural similarities are also apparent between SmCp$_2$* and the bulky phospholyl analogues [{Sm(dsp)$_2$}$_2$] and [{Sm(dtp)$_2$}$_2$]. All three solvent-free complexes are dimers in the solid state with one cyclopentadienyl ring of each SmL$_2$ unit effectively acting as a bridging ligand.

In the dimeric structure of SmCp$_2$* a (Cp*) ring bound η^5 to Sm(A) is linked to Sm(B) by a short agostic-type Sm(B)⋯Me contact to a peripheral methyl group of (Cp*) and vice versa (Figure 14). In the phospholyl complexes the dimers are formed by P—Sm(B) contacts from a phospholyl ligand bound η^5 to Sm(A) and vice versa. In all three compounds the interactions are weak and are broken by solvation.

The Tm(II) analogues are monomers due to the smaller size of the divalent cation (Ionic radii: Tm(II) = 1.09 Å, Sm (II) = 1.32 Å), and the less electron-rich Tm(dsp)$_2$(Et$_2$O) complex cannot be desolvated.[71]

The solvent-free divalent SmL$_2$ complexes of the smaller tmp, C$_4$Me$_4$P, or the sterically similar C$_5$Me$_4$H ligand are very insoluble polymers and no solid-state structures of the former have been determined.[77] The polymer chains form due to the same types of intermolecular interactions seen in the dimers but the contacts are shorter and stronger because the ligands are less sterically bulky. The polymeric structure of [Yb(C$_5$Me$_4$H)$_2$]$_\infty$ has been confirmed by X-ray crystallography, one C$_5$Me$_4$H ring of each YbL$_2$ unit bridges two Yb centres in a μ_2-η^5:η^1 fashion (Figure 14). The η^1-interaction is between the CH carbon of the cyclopentadienyl ring and the adjacent Yb centre.[61]
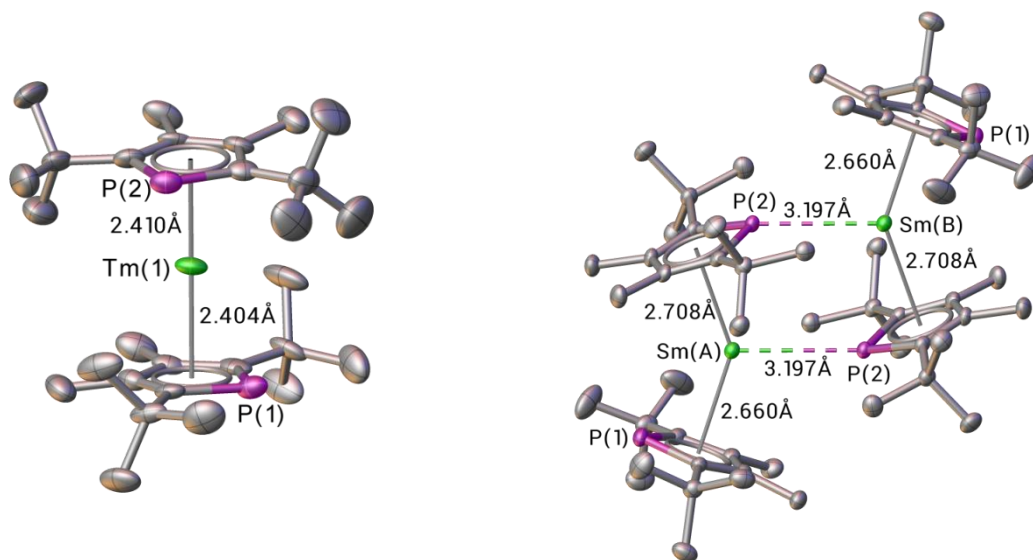
Monomeric structure of Tm(dtp)$_2$ Dimeric structure of [{Sm(dtp)$_2$}$_2$]
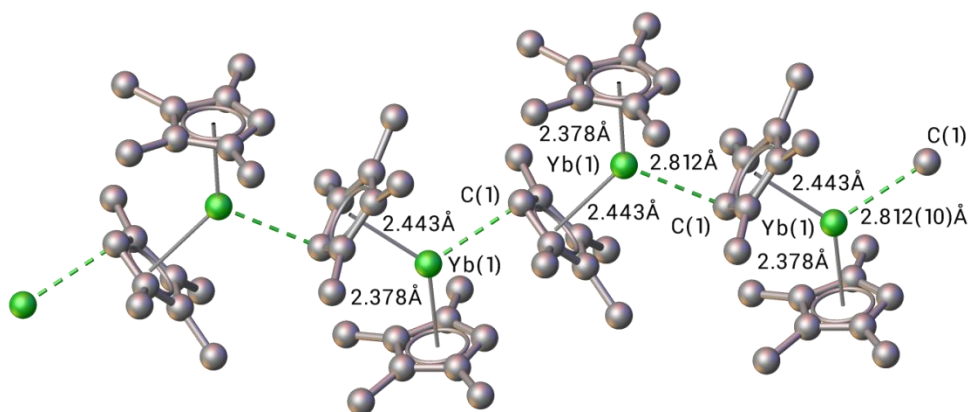
Polymeric structure of [Yb(C$_5$Me$_4$H)$_2$]$_\infty$

Figure 14. Crystal structures of Tm(dtp)$_2$, [{Sm(dtp)$_2$}$_2$] and [Yb(C$_5$Me$_4$H)$_2$]$_\infty$. (H atoms omitted).

1.3.1.2 Synthesis by reduction of trivalent precursors

Metathesis is not a viable synthetic route for the preparation of non-classical divalent lanthanide organometallic complexes with reduction potentials more negative than that of Tm(II) (E$^\theta$ = -2.3 V) and reductive routes to anionic complexes from trivalent precursors are necessary. Reduction of trivalent organolanthanide precursors with a single coordinated iodide or [BH$_4$]$^-$ anion is also a useful way to access neutral solvent-free divalent complexes of Tm and the classical lanthanide(II) ions when desolvation of the product of a metathesis reaction is

32

unsuccessful. The trivalent complexes often can be desolvated and will then dissolve in non-polar solvents.[76] The favoured reducing agent for the reduction of trivalent lanthanide complexes is KC_8 (potassium graphite). Used on its own KC_8 will reduce dimeric $[(Htp)_2TmI]_2$ to $[(Htp)_2Tm]_2$ (also a dimer) in cyclohexane or toluene with the by-product being KI.[75]

Divalent complexes of Dy and Nd have thus far proved too reducing to be stabilised as neutral complexes by adjustment of ligand sterics and electronics alone, but can be isolated as anionic complexes when 18-crown-6 is added to the reaction mixture to trap the potassium cation of the KC_8, forming a bulky counter-cation. The compounds $(Cp^{ttt})_2Dy(\mu-X)K([18]crown-6)$ {X = I, Br, BH_4} were prepared using this method in 2007 from the corresponding trivalent $(Cp^{ttt})_2LnX$ complexes (crystallised by sublimation for X = Br, I at 210°C, 0.1 mbar). The iodide, bromide or tetrahydroborate anion bridges the Ln(II) and K metal centres in the divalent products (Scheme 23).[78] The reactions were carried out at room temperature in cyclohexane from which the products precipitated as dark red solids and were extracted into toluene. The much less stable neodymium analogue $[(Cp^{ttt})_2Nd(\mu-I)K([18]crown-6)]$ was later synthesised (also in cyclohexane), but the powder was unstable at room temperature and reacted with all other solvents (hexane, benzene, toluene, diethyl ether, THF, DME). The product of the reaction with hexane was isolated by crystallisation and characterised using X-ray crystallography, which showed a trivalent anionic complex containing a pseudo-4-membered chelate ring (Nd(1)−C(34)−C(10)−ring centroid) (Figure 15).[79]
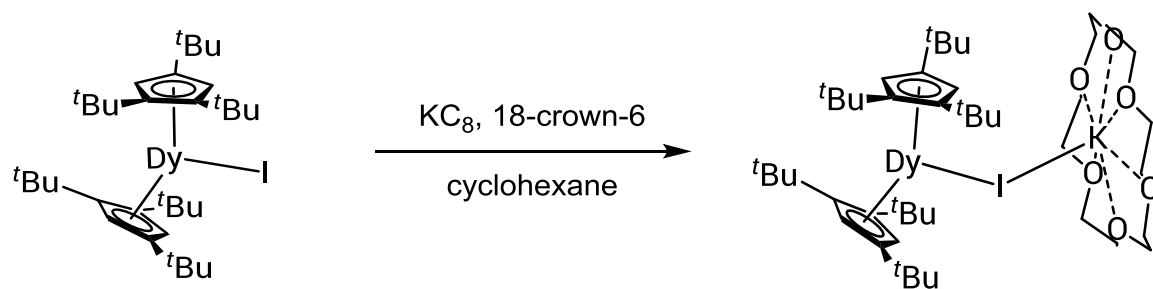
Scheme 23
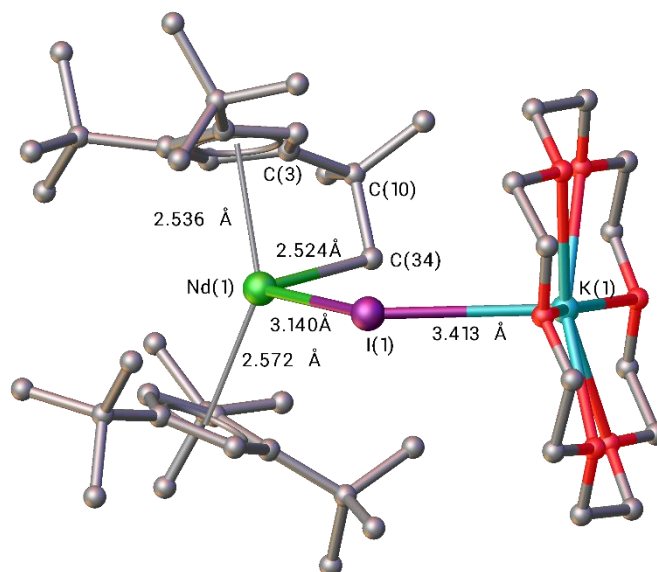
Figure 15. X-ray crystal structure of [(Cp^{ttt})$_2$Nd(μ-I)K([18]crown-6)]. Hydrogen atoms omitted for clarity.

Dy(III) and Dy(II) are both paramagnetic but the ^{t}Bu substituents of the cyclopentadienyl rings are distant enough from the paramagnetic metal centre to give useful ^{1}H NMR data. In both compounds three very broad separate signals are seen in the ^{1}H NMR spectrum, one for each ^{t}Bu substituent, meaning that the ring cannot rotate freely and the substituents are magnetically inequivalent. The paramagnetism means the actual chemical shifts cannot be rationalised but there is a distinct change in the relative chemical shifts between the trivalent reagents and the divalent products (Scheme 13). In the spectrum of trivalent (Cp^{ttt})$_2$DyI the ^{1}H NMR chemical shifts of the ^{t}Bu protons are δ -31 ppm, -168 ppm and -362 ppm, moving to 209 ppm, 99 ppm and -232 ppm in the spectrum of the divalent product

(Cp^{ttt})$_2$Dy(μ-I)K([18]crown-6).[78] The chemical shifts generally move down-field and a new peak arises around -63 pm due to the crown ether. A clear change in the chemical shift of the ^{t}Bu protons was also observed with the synthesis of the analogous neodymium complex, but the trend to a downfield shift was unclear.[79]

If homoleptic tris(cyclopentadienyl) precursors (CpR$_x$H$_{(5-x)}$)$_3$Ln (R = SiMe$_3$, x = 1 or 2, Ln = La, Ce, Ho, Er, Pr, Gd, Tb, Lu) are reduced using KC$_8$ in the presence of 18-crown-6, ionic [(CpR$_x$H$_{(5-x)}$)$_3$Ln][K([18]crown-6)] complexes can be isolated that crystallise as bulky ion pairs (Scheme 24).[80−83] More stable ionic complexes can be synthesised by using [2.2.2]-cryptand to trap the K$^+$ cation. Synthesis must be carried out at low temperature (-35°C) in diethyl ether under argon and this low temperature must be maintained during work-up.

Methods employed to ensure manipulations were carried out at low temperature included the pre-chilling of glassware, reagents and a hexane cold-bath in a glovebox freezer and passing the solution of the reagents through a pre-cooled flash chromatography column of excess KC$_8$ (30 seconds) into the cooled collection flask sitting in the cold-bath. The products precipitated in the collection flask as microcrystalline materials and were stored at <-35°C before the solvent was decanted and the products dried under vacuum (ca. 35% yield).[26] In the solid state the Ho and Er compounds are stable at room temperature. Crystals suitable for X-ray diffraction were grown by a slightly different method − a solution of (CpR$_x$H$_{(5-x)}$)$_3$Ln in diethyl ether was reacted with a potassium mirror rather than KC$_8$ at -35°C without stirring.

The crown ether or the cryptand increases the size of the potassium counter-cation to a comparable size to the anionic lanthanide organometallic moiety, which improves ion packing in the crystal structures (Figure 16).
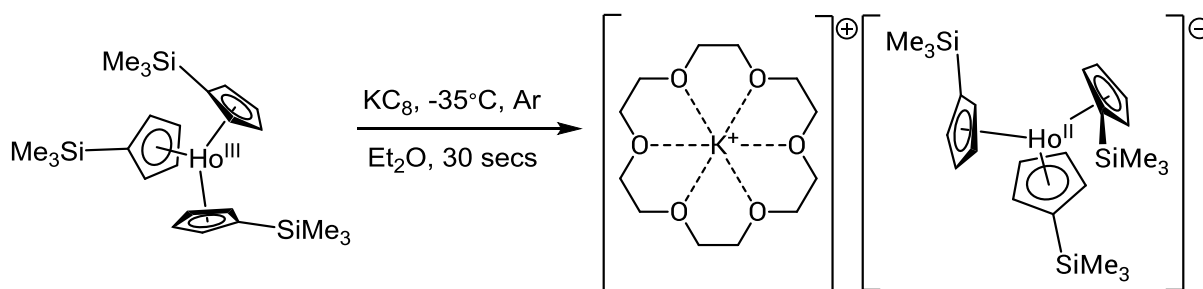
Scheme 24
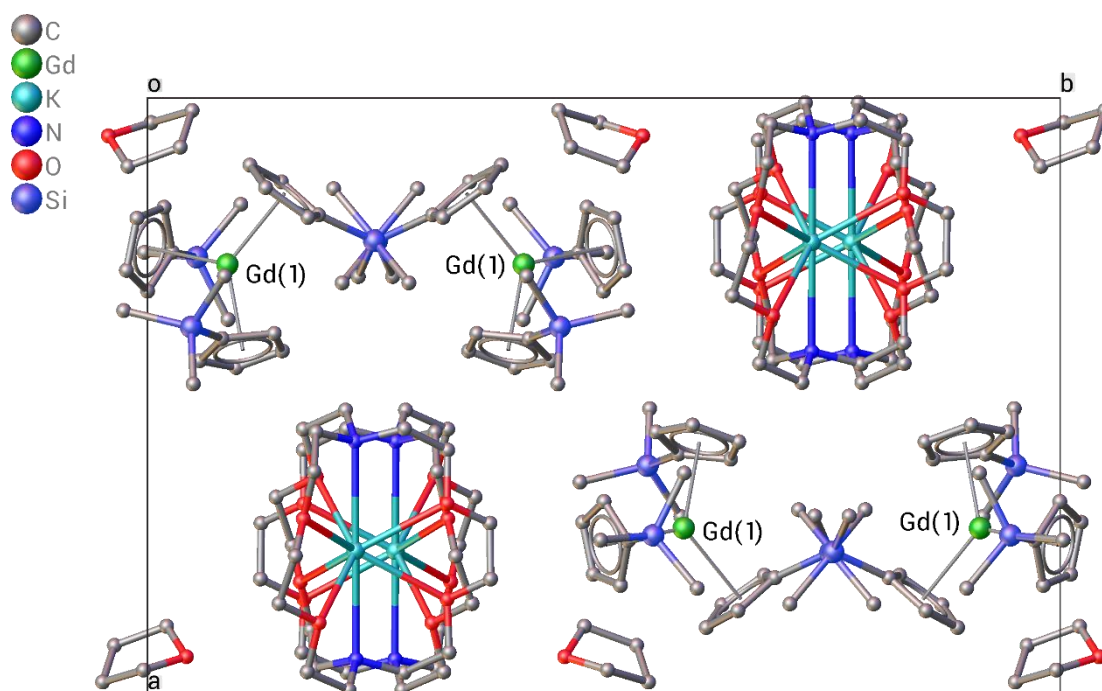
Figure 16. Unit cell packing diagram for [(CpSiMe$_3$H$_4$)$_3$Gd][K([18]crown-6)]

This reductive approach was first demonstrated by Lappert in 1998 (a good 10 years before [(Cp^{ttt})$_2$Nd(μ-I)K([18]crown-6)] was synthesised) using a potassium mirror rather than potassium graphite to reduce LaCp″$_3$. A lanthanum complex was isolated consisting of a pair of LaCp″ moieties bridged by a benzenide anion which crystallised with a chelated [K([18]crown-6)(η^2-C$_6$H$_6$)$_2$] counter-cation from benzene as dark green, photosensitive crystals (Scheme 25).[84] There is, however some

ambiguity over the oxidation state of the lanthanum metal centre in this complex. The compound is clearly paramagnetic due to the absence of a useful NMR spectrum but it is uncertain if the unpaired electron(s) reside on a La(II) metal centre or on the benzenide anion. If both La metal centres are +3 then the benzenide anion would need to carry a -3 charge which seems unlikely, but the complex could be of mixed oxidation state. A comparison of the solution EPR data for [(Cp″)$_2$La(η^6-C$_6$H$_6$)La(Cp″)$_2$][K([18]crown-6)(η^2-C$_6$H$_6$)$_2$] and [(Cp″)$_3$La][K([18]crown-6)] illustrates the uncertainty. The room temperature EPR spectrum of [(Cp″)$_2$La(η^6-C$_6$H$_6$)La(Cp″)$_2$][K([18]crown-6)(η^2-C$_6$H$_6$)$_2$] is reported to have 3 signals, a broad singlet and two octets, showing that the unpaired electron(s) couple to ^{139}La nuclei (I = 7/2), but the coupling constants (a(^{139}La)$_{av}$ = 9.5 G) are much smaller than those reported for [(Cp″)$_3$La][K([18]crown-6)] (a(^{139}La)$_{av}$ = 133.5 G) a confirmed divalent La complex, casting doubt that the unpaired electrons reside on each of the La metal centres in [(Cp″)$_2$La(η^6-C$_6$H$_6$)La(Cp″)$_2$][K([18]crown-6)(η^2-C$_6$H$_6$)$_2$].
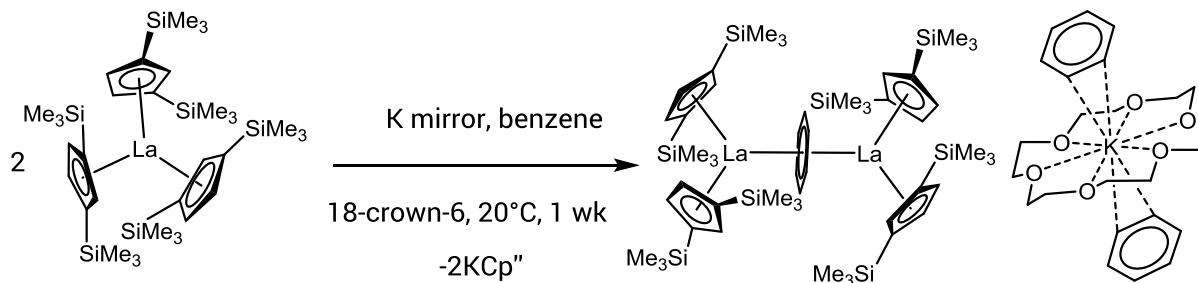
Scheme 25

When (Cp^{ttt})$_3$Sm is reduced to [(Cp^{ttt})$_3$Sm][K([18]crown-6)] in an analogous reaction to that shown in Scheme 24, the average Sm−(C)Cp^{ttt} bond lengthens by 0.147 Å. Similarly in (Cp″)$_3$Sm the average Sm−Cp″(centroid) distance is 2.486 Å, this is lengthened in the reduced complex [(Cp″)$_3$Sm] [K(18-crown-6)(toluene)$_2$] to 2.676 Å. Only very small differences (c.a. 0.025 − 0.032 Å) in the Ln−(C)Cp bond lengths are reported for the non-classical lanthanides (with the exception of Tm) which contrasts with the change in bond lengths for the Sm complexes.[85] For the non-

classical lanthanides the 4f and 5d orbitals are very close in energy and while for the naked ions the 4f is lower in energy calculations have shown that in organometallic complexes the influence of the cyclopentadienyl ligands (ligand crystal field) reverses the relative energies of the 4f and 5d orbitals. In the anionic complexes $[(CpR_x)_3Ln][K([18]crown-6)]$ and $[(CpR_x)_3Ln][K(2.2.2-cryptand)]$, (R = TMS, x = 1-2, Ln = La, Ce, Ho, Er, Pr, Gd, Tb, Lu) the electron configuration of the Ln(II) metal centre has been shown by DFT calculations to be $4f^n5d^1$ rather than $4f^{n+1}$ meaning that although there is a decrease in effective nuclear charge (+3/+2) there is no increase in electron density in the contracted 4f orbitals so the cation size increase is small relative to those Ln(II) cations with $4f^{n+1}$ electron configurations (Eu, Sm, Yb, Tm).[26,80,85]

1.3.2   Divalent lanthanide alkyl complexes

Divalent organolanthanide compounds which contain Ln-C σ-bonds are much rarer than their divalent cyclopentadienyl counterparts. The trimethylsilyl-stabilised carbanions already described for the synthesis of tris-alkyllanthanide complexes can also be used to isolate some bis-alkyl complexes of divalent classical lanthanides and their group 2 cation analogues Ca^{2+} and Sr^{2+}.

1.3.2.1   Bis(trimethylsilyl)methyl Complexes

Complexes with the intermediately sterically bulky bis(trimethylsilyl)methyl ligands have been identified only for the smallest classical divalent lanthanide Yb(II) and its group 2 cation analogue Ca^{2+}. The complex $[Yb\{CH(SiMe_3)_2\}_2(OEt_2)_2]$ has been known since 1994 (Scheme 26), but efforts to crystallise it as a neutral complex have not been successful.[86,87] Metathesis reactions between YbI_2 and $MCH(SiMe_3)_2$ (M = K, Na or Li) in non-donor solvents (hexane/benzene) yield 'ate' complexes (Scheme 26). The complex $[YbR_3]X$ (X = K or $\{Li(THF)_4\}$, R = $CH(SiMe_3)_2$) was crystallised and the structures determined in 2002.[88] Formation of these metallate

complexes cannot be avoided by altering the stoichiometry of the reaction. The [YbR$_3$]$^-$ and [CaR$_3$]$^-$ anions are trigonal pyramidal, unlike the [LnCp″$_3$]$^-$ anions of the [(CpR$_x$H$_{(5-x)}$)$_3$Ln][K([18]crown-6)] and the [(CpR$_x$H$_{(5-x)}$)$_3$Ln][K(2.2.2-cryptand)] (R = SiMe$_3$, x = 1 or 2) series of ionic complexes which are approximately trigonal planar. A neutral solvated calcium dialkyl complex with bis(trimethylsilyl)methyl ligands, [R$_2$Ca(dioxane)$_2$] was structurally characterised by X-ray crystallography in 1991 (Figure 17) but the synthesis was not standard solution chemistry, instead involving the condensation of calcium metal vapour and (SiMe$_3$)$_2$CHBr into THF at 77 K.[89]

YbI$_2$ + 2NaCH(SiMe$_3$)$_2$ $\xrightarrow[\text{-2NaI}]{\text{Et}_2\text{O, rt, 24 h}}$ Yb[CH(SiMe$_3$)$_2$]$_2$(Et$_2$O)$_2$

YbI$_2$ + 3KCH(SiMe$_3$)$_2$ $\xrightarrow[\text{-2KI}]{\text{benzene, rt, 2 days}}$ {Yb[CH(SiMe$_3$)$_2$]$_3$K}$_n$

YbI$_2$ + 2KCH(SiMe$_3$)$_2$ + LiCH(SiMe$_3$)$_2$ $\xrightarrow[\text{-2KI}]{\text{Et}_2\text{O/THF, -30°C, 4 h}}$ Yb[CH(SiMe$_3$)$_2$]$_3$Li(THF)$_4$
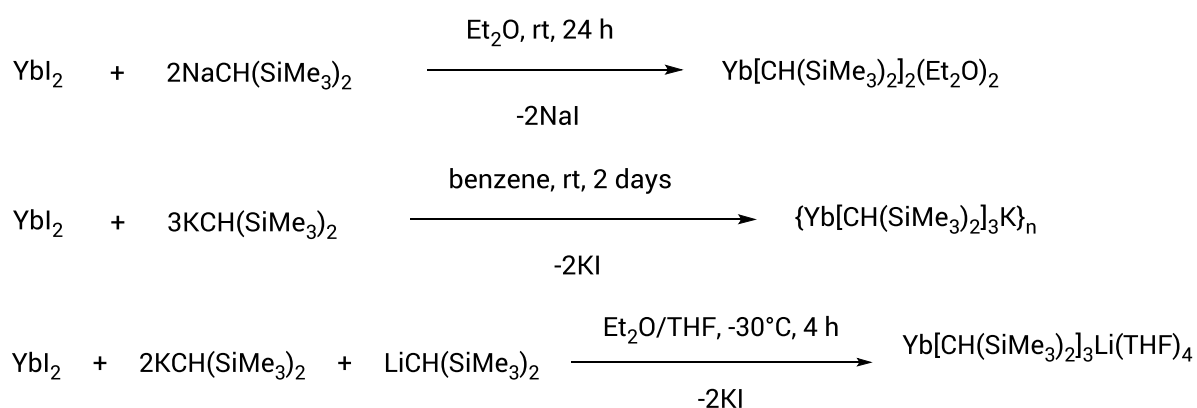
Scheme 26
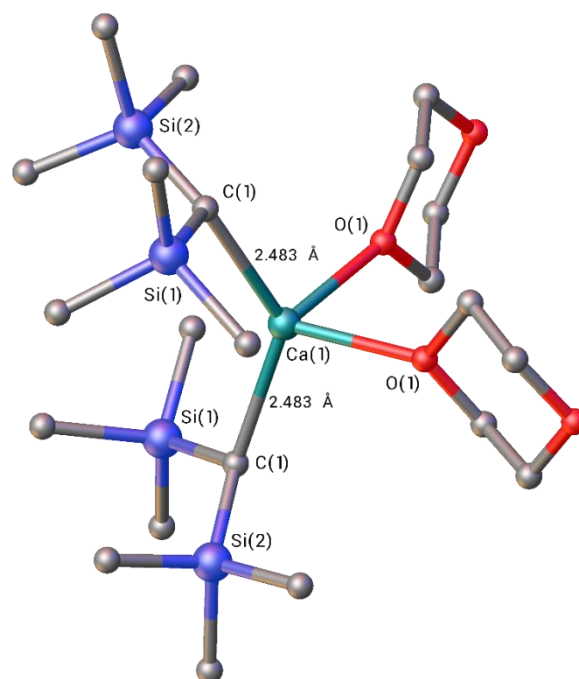
Figure 17. Structure of [{(SiMe$_3$)$_2$CH}$_2$Ca(dioxane)$_2$]. H atoms omitted for clarity.

1.3.2.2   Tris(trimethylsilyl)methyl complexes

The classical divalent lanthanides are known to be stabilised as neutral complexes (solvated monomers or unsolvated dimers) by adjustment of the sterics of cyclopentadienyl ligands and, likewise, in 1994 it was found that the extremely sterically bulky tris(trimethylsilyl)methyl ('trisyl') carbanion ligands stabilise the solvent-free monomeric dialkylytterbium(II) compound Yb{C(SiMe$_3$)$_3$}$_2$.[90] Analogous compounds have also been isolated for the larger Sm(II), Eu(II) and Ca(II) cations, but the Yb(II) derivatives remain the most studied.[91–93] The solid-state structures share features with Ln(II)(Cp*)$_2$ compounds in that they are all bent with the C—Ln—C angle ranging from 136 – 149.7° in the dialkyl compounds and from 140.1 – 147.7° in the bis(pentamethylcylopentadienyl) (Table 4). Like the bis(cyclopentadienyl) complexes of the classical divalent lanthanides these bis-alkyl complexes were synthesised by metathesis between the LnI$_2$ (Ln = Yb, Sm, Eu) and two equivalents of KC(SiMe$_3$)$_3$ in benzene (Scheme 27).
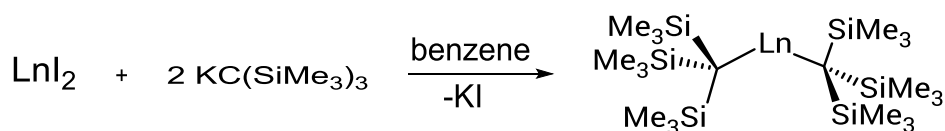
Scheme 27

Table 4. Comparison of the structural similarities between (Cp*)$_2$Ln and Ln{C(SiMe$_3$)$_3$}$_2$ (Ln = Sm, Eu, Yb and Ca). Hydrogen atoms omitted for clarity.

(Cp*)$_2$Ln unsolvated complexes **Ln{C(SiMe$_3$)$_3$}$_2$ unsolvated complexes**
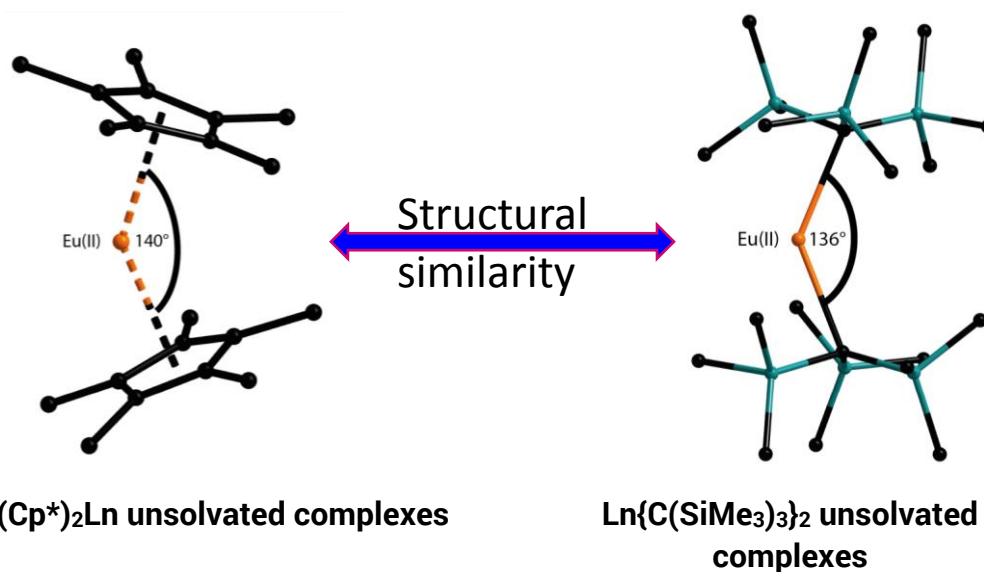
	Centroid-M-centroid angle	Average M-(C)Cp dist. (Å)	C-M-C angle (°)	M-C distance (Å)
Sm	140.1°	2.79(1)	143.4°	2.586(2)
Eu	140.3°	2.79(1)	136.01°	2.61
Yb	145.5°	2.665(4)	137°	2.495
Ca	147.7°	2.64(2)	149.7(6)°	2.459(9)

An investigation of the reactivity of Yb{C(SiMe$_3$)$_3$}$_2$ with ethers found that the reactivity could be modified by substitution of one of the methyl groups of a single SiMe$_3$ group with another functional group X to give Yb{C(SiMe$_3$)$_2$(SiMe$_2$X)}$_2$. A range of 'trisyl-like' ligands was synthesised with functional groups, X more likely to interact with the divalent Yb metal centre, potentially increasing the coordination number (Figure 18). The analogous Sm(II) compound Sm{C(SiMe$_3$)$_2$(SiMe$_2$OMe)}$_2$(THF) has also been prepared.[94] X-ray crystallography

studies showed the coordination geometry of the Sm metal centre to be a distorted square pyramid with each alkyl ligand forming a four-membered chelate ring (Sm−C−Si−O) at the base and a THF molecule occupying the top of the pyramid (Figure 19).

Me₃Si SiMe₃
SiMe₃

Me₃Si SiMe₃
PMe₂BH₃

Me₃Si SiMe₃
SiMe₂OMe

Me₃Si SiMe₃
SiMe₂CHCH₂

Me₃Si SiMe₃
SiMe₂CH₂CH₂OEt

Me₃Si SiMe₃
SiMe₂Ph
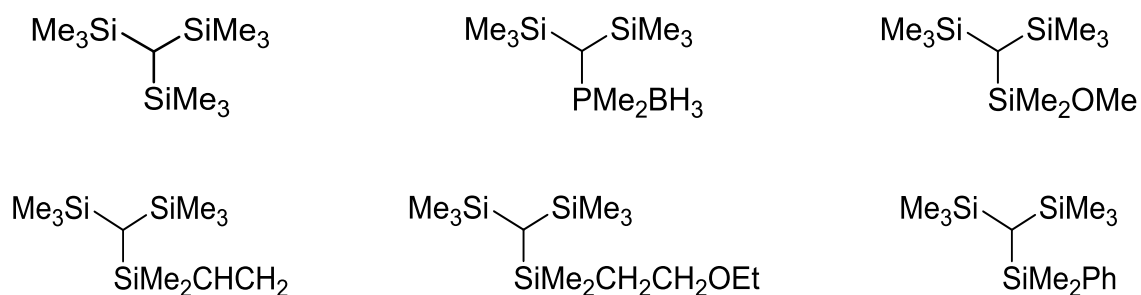
Figure 18. Examples of sterically bulky silicon-stabilised carbanion ligands, functionalisation gives multidentate ligands.
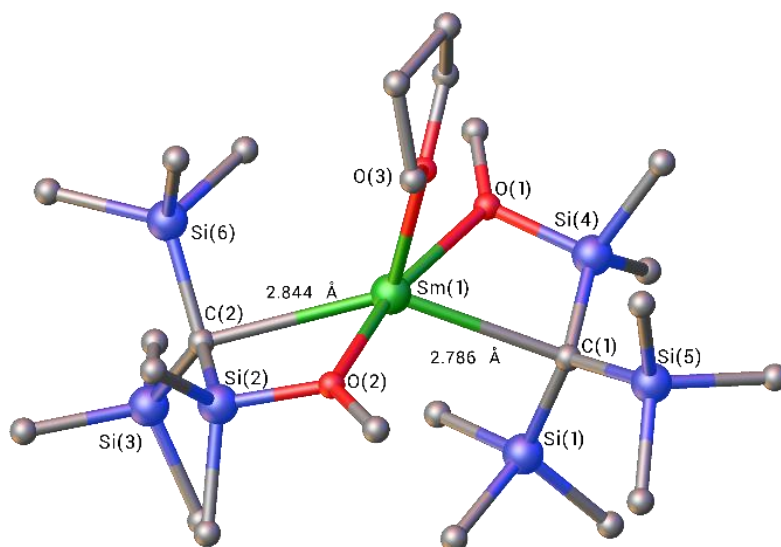
Figure 19. Crystal structure of Sm{C(SiMe₃)₂(SiMe₂OMe)}₂(THF) with hydrogen atoms omitted for clarity.

{(Me₃Si)₃C}₂Yb reacts with diethyl ether (and more slowly with bulkier ethyl ethers ROEt) whereas {(Me₃Si)₂(MeOMe₂Si)C}₂Yb does not.[91] The product of the reaction of {(Me₃Si)₃C}₂Yb with diethyl ether is tris(trimethylsilyl)methane and a solvated alkylytterbium dimer, with ethoxide anions bridging the two Yb(II) centres (Scheme

28).[87] The rate of reaction is slower (days rather than minutes) with bulkier ethyl ethers, e.g. ^{t}BuOEt, while with non-ethyl ethers, e.g. ^{i}Pr$_2$O, there is no reaction. {(Me$_3$Si)$_3$C}$_2$Yb is extremely sterically hindered as shown by a space filling model (Figure 20) and it could be that more bulky ethers are very labile and/or have difficulty coordinating to the Yb metal centre. Once coordinated, ethyl ethers undergo β-hydride elimination. Ethene is the only gas observed in NMR studies of the reaction even with ethers such as BuOEt and ^{t}BuOEt which means the Yb(II) centres in the products must be bridged by bulkier butoxide anions, although these products have not been isolated. The analogous {(SiMe$_3$)$_3$C}$_2$Ca also reacts with Et$_2$O to give tris(trimethylsilyl)methane, ethene and calcium ethoxide instead of a bridged alkylcalcium ethoxide product (Scheme 29).[93] This happens because the intermediate Ca{C(SiMe$_3$)$_3$}(OEt) reacts faster with ether than the starting material. Both {(Me$_3$Si)$_3$C}$_2$Yb and {(Me$_3$Si)$_3$C}$_2$Ca are known to react with THF. With cyclopentadienyl-like ligands divalent complexes of the classical lanthanides are usually stable in donor solvents but this is not always true for the dialkyl compounds.
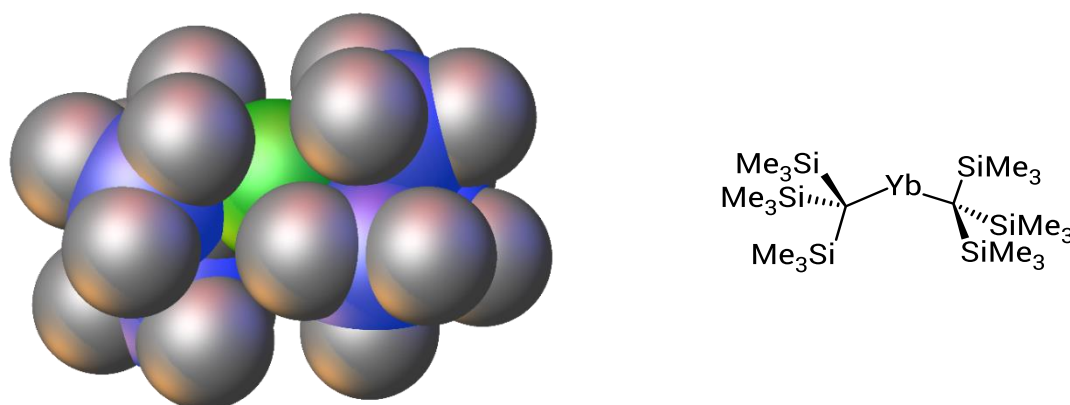
Figure 20. Space-filling model of {(Me$_3$Si)$_3$C}$_2$Yb.
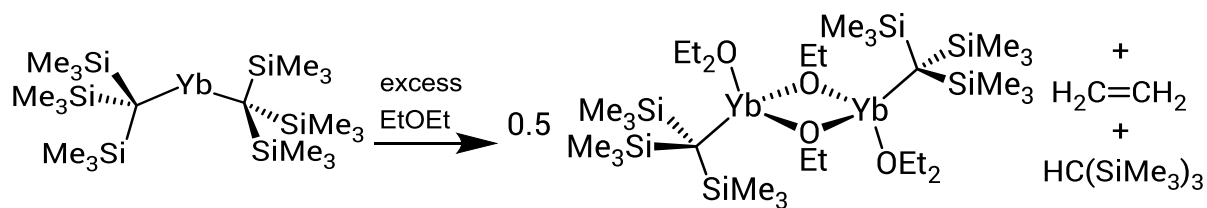
Scheme 28
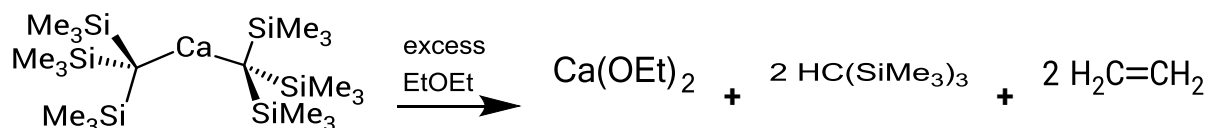
Scheme 29

An alternative synthesis of Yb{C(SiMe$_3$)$_2$(SiMe$_2$X)}$_2$, (X = Ph, CH=CH$_2$ or OMe) was found while investigating the reactivity of these compounds with alkyl halides (e.g. diiodoethane and methyliodide). Divalent bis(cyclopentadienyl)lanthanide complexes are oxidised by alkyl halides; in contrast to Yb{C(SiMe$_3$)$_2$(SiMe$_2$X)}$_2$, (X = Me, Ph, CH=CH$_2$ or OMe) undergoes ligand substitution involving the loss of an alkyl ligand and addition of an iodide ligand but the Yb(II) centre is not oxidised (Scheme 30). The product is an ytterbium Grignard analogue, YbRI. Heating this Grignard analogue at 10^{-3} Torr results in sublimation of YbR$_2$, leaving behind yellow YbI$_2$ at the bottom of the sublimation tube when X = Ph, CH=CH$_2$ or OMe but not when X = Me (Scheme 31), again showing the strong influence of the substituent, X on the reactivity of the compounds. The Grignard analogue can also be made in the usual way by reaction of an alkyl iodide with Yb metal in diethyl ether, offering another route (although less atom efficient) to YbR$_2$. Similar Grignard analogues could not be accessed for the europium analogues.
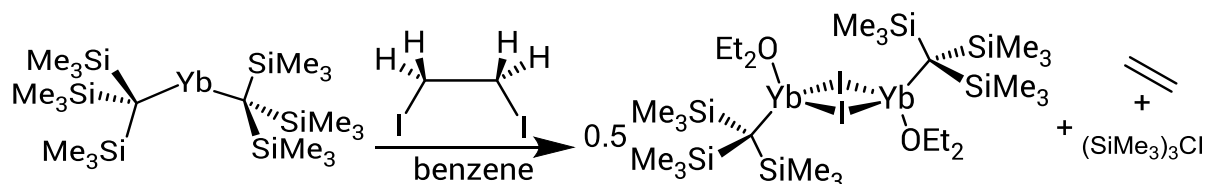
Scheme 30
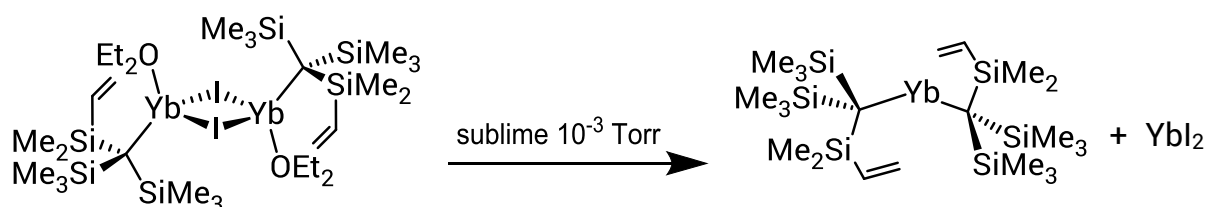
Scheme 31

1.3.2.3   Silicon-stabilised dicarbanion ligands

The successful synthesis and isolation of dialkyllanthanide(II) complexes of trisyl ligands was followed by the synthesis a ytterbium(II) dialkyls of even bulkier, multidentate, chelating, dicarbanion 'trisyl-like' ligands {(SiMe$_2$X)(SiMe$_3$)C}Me$_2$SiCH$_2$-CH$_2$SiMe$_2${C(SiMe$_3$)(SiMe$_2$X)}, (X=Me, OMe) (Figure 21).[95,96] Chelation of the Yb(II) metal centre by these ligands had the effect of slowing (X = Me) the reaction with ether from five minutes to five days or inhibiting it completely (X = OMe).   The chelated divalent Yb alkyl compounds {MeOMe$_2$Si)(Me$_3$Si)C}Me$_2$SiCH$_2$-CH$_2$SiMe$_2${C(SiMe$_3$)(SiMe$_2$OMe)}Yb(THF)   and {(SiMe$_3$)$_2$C}Me$_2$SiOSiMe$_2${C(SiMe$_3$)$_2$}Yb(THF)$_2$ crystallise as THF adducts but in the case of {(SiMe$_3$)$_2$C}Me$_2$SiOSiMe$_2${C(SiMe$_3$)$_2$}Yb(THF)$_2$ NMR experiments on aged samples indicate oxidation of diamagnetic Yb(II) to paramagnetic Yb(III), probably by reaction with THF over several days.
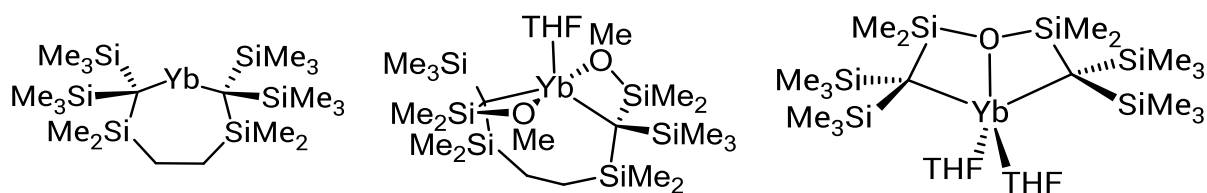
Figure 21. (left to right) Structures of {(SiMe₃)(SiMe₃)C}Me₂SiCH₂-CH₂SiMe₂{C(SiMe₃)(SiMe₃)}Yb, {MeOMe₂Si)(Me₃Si)C}Me₂SiCH₂-CH₂SiMe₂{C(SiMe₃)(SiMe₂OMe)}Yb(THF) and {(SiMe3)₂C}Me₂SiOSiMe₂{C(SiMe₃)₂}Yb(THF)₂.

It is noteworthy that these functionalised chelating ligands were unable to stabilise a divalent Tm(II) metal centre in THF solution at temperatures above -10°C. The divalent complexes may be formed at low temperature (< -10°C) and could possibly be isolated if all manipulations were carried out at low temperature. Initial reaction at -78°C gave a deep green solution upon addition of [{(SiMe₂OMe)(SiMe₃)C}Me₂SiCH₂CH₂SiMe₂{C(SiMe₃)(SiMe₂OMe)}]K₂, to TmI₂ which is characteristic of a Tm(II) species. However the colour changed to pale yellow as the reaction mixture warmed due to oxidation of the Tm(II) to Tm(III). The isolated Tm(III) complex contains a coordinated methoxide anion in addition to the dicarbanion ligand.

The only ligand known to stabilise a Tm(II) complex with a Tm-C σ-bond is the extremely bulky scorpionate ligand hydro-tris(3-*tert*-Bu-5-Me-pyrazolyl)borate (Tp'). TmI₂(THF)x is first converted to (Tp')TmI(THF) by addition of one equivalent of KTp' to a THF solution of TmI₂(THF)x at room temperature. The divalent complex (Tp')TmI(THF), which decomposes slowly above -30°C, was used as starting material for a further metathesis reaction at -40°C (allowed to warm slowly to room temperature) in Et₂O with KCH(SiMe₃)₂ to give (Tp')TmCH(SiMe₃)₂ (Scheme 32

), which was crystallised from hexane at -40°C.[97] The first Tm-C σ-bond length was reported from the X-ray crystallography study as 2.554(3) Å.
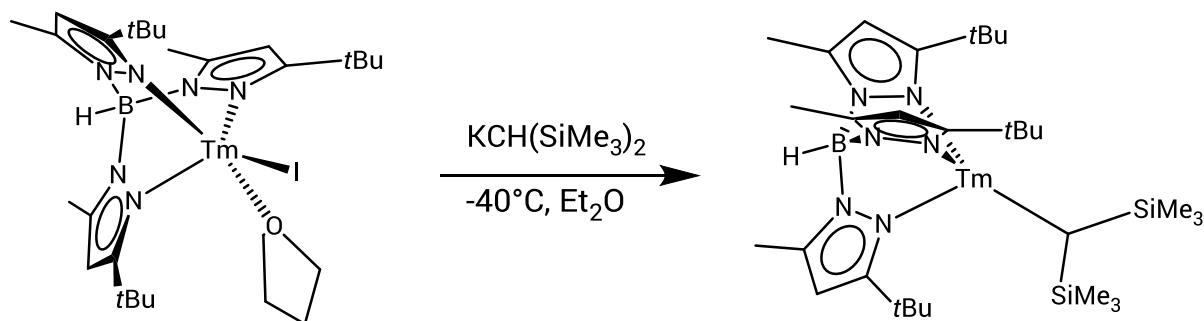
Scheme 32

1.4   References

(1)   Zimmermann, M.; Frøystein, N. Å.; Fischbach, A.; Sirsch, P.; Dietrich, H. M.; Törnroos, K. W.; Herdtweck, E.; Anwander, R. *Chem. - Eur. J.* **2007**, *13*, 8784.

(2)   Morss, L. R. *Chem. Rev.* **1976**, *76*, 827.

(3)   Evans, W. J.; Lee, D. S.; Rego, D. B.; Perotti, J. M.; Kozimor, S. A.; Moore, E. K.; Ziller, J. W. *J. Am. Chem. Soc.* **2004**, *126*, 14574.

(4)   Wilkinson, G.; Birmingham, J. M. *J. Am. Chem. Soc.* **1954**, *76*, 6210.

(5)   Lappert, M. F.; Pearce, R. *J. Chem. Soc. Chem. Commun.* **1973**, 126.

(6)   Schumann, H.; Freckmann, D. M. M.; Dechert, S. *Z.Anorg. Allg. Chem.* **2002**, *628*, 2422.

(7)   Atwood, J. L.; Hunter, W. E.; Rogers, R. D.; Holton, J.; McMeeking, J.; Pearce, R.; Lappert, M. F. *J. Chem. Soc. Chem. Commun.* **1978**, 140.

(8)   Schumann, H.; Cygon, M. *J. Organomet. Chem.* **1978**, *144*, C5.

(9)   Schumann, H.; Müller, J. *J. Organomet. Chem.* **1979**, *169*, C1

(10)   Zimmermann, M.; Anwander, R. *Chem. Rev.* **2010**, *110*, 6194.

(11)   Birmingham, J. M.; Wilkinson, G. *J. Am. Chem. Soc.* **1956**, *78*, 42.

(12) Baisch, U. Von reaktiven molecularen Vorlaufen zu hohervernetzten Lanthanoid-Oxonitr, Ludwig-Maximilians Universitat : Munich, 2006, PhD Thesis

(13) Deacon, G. B.; Forsyth, C. M.; Newnham, R. H.; Tuong, T. D. *Aust. J. Chem.* **1987**, *40*, 895.

(14) Eggers, S. H.; Hinrichs, W.; Kopf, J.; Jahn, W.; Fischer, R. D. *J. Organomet. Chem.* **1986**, *311*, 313.

(15) Rebizant, J.; Apostolidis, C.; Spirlet, M. R.; Kanellakopulos, B. *Acta Crystallogr. Sect. C* **1988**, *44*, 614.

(16) Baisch, U.; Pagano, S.; Zeuner, M.; Schmedt auf der Günne, J.; Oeckler, O.; Schnick, W. *Organometallics* **2006**, *25*, 3027.

(17) Hinrichs, W.; Melzer, D.; Rehwoldt, M.; Jahn, W.; Fischer, R. D. *J. Organomet. Chem.* **1983**, *251*, 299.

(18) Eggers, S. H.; Kopf, J.; Fischer, R. D. *Acta Crystallogr. Sect. C* **1987**, *43*, 2288.

(19) Denning, R. G.; Harmer, J.; Green, J. C.; Irwin, M. *J. Am. Chem. Soc.* **2011**, *133*, 20644.

(20) Eggers, S. H.; Schultze, H.; Kopf, J.; Fischer, R. D. *Angew. Chemie Int. Ed.* **1986**, *25*, 656.

(21) Evans, W. J.; Davis, B. L. *Chem. Rev.* **2002**, *102*, 2119.

(22) Zimmermann, M.; Anwander, R. *Chem. Rev.* **2010**, *110*, 6194.

(23) Stults, S. D.; Andersen, R. A.; Zalkin, A. *Organometallics* **1990**, *9*, 115.

(24) Burns, J. H.; Baldwin, W. H.; Fink, F. H. *Inorg. Chem.* **1974**, *13*, 1916.

(25) Hammel, A.; Schwarz, W.; Weidlein, J. *J. Organomet. Chem.* **1989**, *363*, C29.

(26) MacDonald, M. R.; Bates, J. E.; Fieser, M. E.; Ziller, J. W.; Furche, F.; Evans, W. J. *J. Am. Chem. Soc.* **2012**, *134*, 8420.

(27) Evans, W. J.; Gonzales, S. L.; Ziller, J. W. *J. Am. Chem. Soc.* **1991**, *113*, 7423.

(28) Evans, W. J.; Cano, D. A.; Greci, M. A.; Ziller, J. W. *Organometallics* **1999**, *18*, 1381.

(29) Nief, F.; Ricard, L. *Organometallics* **2001**, *20*, 3884.

(30)   Evans, W. J.; Forrestal, K. J.; Leman, J. T.; Ziller, J. W. *Organometallics* **1996**, *15*, 527.

(31)   Evans, W. J.; Perotti, J. M.; Ziller, J. W. *J. Am. Chem. Soc.* **2005**, *127*, 3894.

(32)   Evans, W. J.; Seibel, C. A.; Ziller, J. W. *J. Am. Chem. Soc.* **1998**, *120*, 6745.

(33)   Peterson, J. K.; MacDonald, M. R.; Ziller, J. W.; Evans, W. J. *Organometallics* **2013**, *32*, 2625.

(34)   Dietrich, H. M.; Raudaschl-Sieber, G.; Anwander, R. *Angew. Chemie Int. Ed.* **2005**, *44*, 5303.

(35)   Schumann, H.; Mueller, J.; Bruncks, N.; Lauke, H.; Pickardt, J.; Schwarz, H.; Eckart, K. *Organometallics* **1984**, *3*, 69.

(36)   Schumann, H.; Lauke, H.; Hahn, E.; Pickardt, J. *J. Organomet. Chem.* **1984**, *263*, 29.

(37)   Niemeyer, M. *Zeitschrift für Anorg. und Allg. Chemie* **2000**, *626*, 1027.

(38)   Cook, M. A.; Eaborn, C.; Jukes, A. E.; Walton, D. R. M. *J. Organomet. Chem.* **1970**, *24*, 529.

(39)   Aiube, Z. H.; Eaborn, C. *J. Organomet. Chem.* **1984**, *269*, 217.

(40)   Clegg, W.; Conway, B.; Kennedy, A. R.; Klett, J.; Mulvey, R. E.; Russo, L. *Eur. J. Inorg. Chem.* **2011**, *2011*, 721.

(41)   Atwood, J. L.; Lappert, M. F.; Smith, R. G.; Zhang, H. *J. Chem. Soc., Chem. Commun.* **1988**, 1308.

(42)   Schumann, H.; Müller, J. *J. Organomet. Chem.* **1978**, *146*, C5.

(43)   Hitchcock, P. B.; Lappert, M. F.; Smith, R. G.; Bartlett, R. A.; Power, P. P. *J. Chem. Soc. Chem. Commun.* **1988**, 1007.

(44)   Avent, A. G.; Caro, C. F.; Hitchcock, P. B.; Lappert, M. F.; Li, Z.; Wei, X.-H. *Dalton. Trans.* **2004**, No. 10, 1567.

(45)   Guttenberger, C.; Amberger, H.-D. *J. Organomet. Chem.* **1997**, *545-546*, 601.

(46)   Schaverien, C. J.; Orpen, A. G. *Inorg. Chem.* **1991**, *30*, 4968.

(47)   Avent, A. G.; Caro, C. F.; Hitchcock, P. B.; Lappert, M. F.; Li, Z.; Wei, X.-H. *Dalt. Trans.* **2004**, *76*, 1567.

(48) Bowman, L. J.; Izod, K.; Clegg, W.; Harrington, R. W. *Organometallics* **2006**, *25*, 2999.

(49) Girard, P.; Namy, J. L.; Kagan, H. B. *J. Am. Chem. Soc.* **1980**, *102*, 2693.

(50) Fischer, E. O.; Fischer, H. *J. Organomet. Chem.* **1965**, *3*, 181.

(51) Calderazzo, F.; Pappalardo, R.; Losi, S. *J. Inorg. Nucl. Chem.* **1966**, *28*, 987.

(52) Apostolidis, C.; Deacon, G. B.; Dornberger, E.; Edelmann, F. T.; Kanellakopulos, B.; MacKinnon, P.; Stalke, D. *Chem. Commun.* **1997**, *109*, 1047.

(53) Procter, D. J.; Flowers, R. A.; Skrydstrup, T. *Organic Synthesis using Samarium Diiodide*; Royal Society of Chemistry: Cambridge, 2009.

(54) Evans, W. J. *J. Organomet. Chem.* **2002**, *647*, 2.

(55) Inanaga, J.; Ishikawa, M.; Yamaguchi, M. *Chem. Lett.* **1987**, *16*, 1485.

(56) Evans, W. J.; Ulibarri, T. A.; Ziller, J. W. *J. Am. Chem. Soc.* **1990**, *112*, 219.

(57) Evans, W. J.; Ulibarri, T. A.; Ziller, J. W. *J. Am. Chem. Soc.* **1988**, *110*, 6877.

(58) Evans, W. J.; Rabe, G. W.; Ziller, J. W.; Doedens, R. J. *Inorg. Chem.* **1994**, *33*, 2719.

(59) Evans, W. J.; Gonzales, S. L.; Ziller, J. W. *J. Am. Chem. Soc.* **1991**, *113*, 7423.

(60) Evans, W. J.; Johnston, M. A.; Clark, R. D.; Ziller, J. W.; Doedens, R. J.; Kasai, N.; Harmon, C. A. *J. Chem. Soc. Dalt. Trans.* **2000**, *444*, 1609.

(61) Schultz, M.; Burns, C. J.; Schwartz, D. J.; Andersen, R. A. *Organometallics* **2000**, *19*, 781.

(62) Evans, W. J.; Hughes, L. A.; Hanusa, T. P. *Organometallics* **1986**, *5*, 1285.

(63) Williams, R. A.; Hanusa, T. P.; Huffman, J. C. *Organometallics* **1990**, *9*, 1128.

(64) Bochkarev, M. N.; Fedushkin, I. L.; Fagin, A. A.; Petrovskaya, T. V.; Ziller, J. W.; Broomhall-Dillard, R. N. R.; Evans, W. J. *Angew. Chem. Int. Ed. English* **1997**, *36*, 133.

(65) Evans, W. J. *Coord. Chem. Rev.* **2000**, *206-207*, 263.

(66) Evans, W. J.; Gummersheimer, T. S.; Ziller, J. W. *J. Am. Chem. Soc.* **1995**, *117*, 8999.

(67) Evans, W. J.; Allen, N. T.; Ziller, J. W. *Angew. Chem. Int. Ed.* **2002**, *41*, 359.

(68)   Nief, F.; De Borms, B. T.; Ricard, L.; Carmichael, D. *Eur. J. Inorg. Chem.* **2005**, *2005*, 637.

(69)   Jaroschik, F.; Nief, F.; Ricard, L.; Perotti, J. M.; Kozimor, S. A.; Moore, E. K.; Ziller, J. W. *Chem. Commun.* **2006**, *126*, 426.

(70)   Nief, F.; Tayart de Borms, B.; Ricard, L.; Carmichael, D. *Eur. J. Inorg. Chem.* **2005**, *2005*, 621.

(71)   Turcitu, D.; Nief, F.; Ricard, L. *Chem. - Eur. J.* **2003**, *9*, 4916.

(72)   Labouille, S.; Nief, F.; Le Goff, X.-F.; Maron, L.; Kindra, D. R.; Houghton, H. L.; Ziller, J. W.; Evans, W. J. *Organometallics* **2012**, *31*, 5196.

(73)   Evans, W. J.; Gonzales, S. L.; Ziller, J. W. *J. Am. Chem. Soc.* **1994**, *116*, 2600.

(74)   Labouille, S.; Nief, F.; Maron, L. *J. Phys. Chem. A* **2011**, *115*, 8295.

(75)   Jaroschik, F.; Nief, F.; Le Goff, X.-F.; Ricard, L. *Organometallics* **2007**, *26*, 3552.

(76)   Nief, F. *Dalton Trans.* **2010**, *39*, 6589.

(77)   Nief, F.; Mathey, F. *Synlett* **1991**, *1991*, 745.

(78)   Jaroschik, F.; Nief, F.; Le Goff, X.-F.; Ricard, L. *Organometallics* **2007**, *26*, 1123.

(79)   Jaroschik, F.; Momin, A.; Nief, F.; Le Goff, X.; Deacon, G. B.; Junk, P. C. *Angew. Chem. Int. Ed.* **2009**, *48*, 1117.

(80)   MacDonald, M. R.; Bates, J. E.; Ziller, J. W.; Furche, F.; Evans, W. J. *J. Am. Chem. Soc.* **2013**, *135*, 9857.

(81)   MacDonald, M. R.; Ziller, J. W.; Evans, W. J. *J. Am. Chem. Soc.* **2011**, *133*, 15914.

(82)   MacDonald, M. R.; Bates, J. E.; Fieser, M. E.; Ziller, J. W.; Furche, F.; Evans, W. J. *J. Am. Chem. Soc.* **2012**, *134*, 8420.

(83)   Hitchcock, P. B.; Lappert, M. F.; Maron, L.; Protchenko, A. V. *Angew. Chem. Int. Ed.* **2008**, *47*, 1488.

(84)   Cassani, M. C.; Duncalf, D. J.; Lappert, M. F. *J. Am. Chem. Soc.* **1998**, *120*, 12958.

(85)   Fieser, M. E.; Macdonald, M. R.; Krull, B. T.; Bates, J. E.; Ziller, J. W.; Furche, F.; Evans, W. J. *J. Am. Chem. Soc.* **2015**, *137*, 369.

(86) Hitchcock, P. B.; Holmes, S. A.; Lappert, M. F.; Tian, S. *J. Chem. Soc. Chem. Commun.* **1994**, 2691.

(87) van den Hende, J. R.; Hitchcock, P. B.; Holmes, S. A.; Lappert, M. F.; Tian, S. *J. Chem. Soc. Dalt. Trans.* **1995**, *39*, 3933.

(88) Hitchcock, P. B.; Khvostov, A. V; Lappert, M. F. *J. Organomet. Chem.* **2002**, *663*, 263.

(89) Cloke, F. G. N.; Hitchcock, P. B.; Lappert, M. F.; Lawless, G. A.; Royo, B. *J. Chem. Soc. Chem. Commun.* **1991**, 724.

(90) Eaborn, C.; Hitchcock, P. B.; Izod, K.; Smith, J. D. *J. Am. Chem. Soc.* **1994**, *116*, 12071.

(91) Eaborn; C.; Hitchcock, P. B.; Izod. K.; Zheng-Rong Lu, A.; Smith, J. D. *Organometallics* **1996**, *15*, 4783.

(92) Qi, G.; Nitto, Y.; Saiki, A.; Tomohiro, T.; Nakayama, Y.; Yasuda, H. *Tetrahedron* **2003**, *59*, 10409.

(93) Eaborn, C.; B. Hitchcock, P. *Chem. Commun.* **1997**, *9*, 1961.

(94) Clegg, W.; Izod, K.; O'Shaughnessy, P.; Eaborn, C.; Smith, J. D. *Angew. Chem. Int. Ed. Engl.* **1997**, *36*, 2815.

(95) Bowman, L. J.; Izod, K.; Clegg, W.; Harrington, R. W. *Organometallics* **2007**, *26*, 2646.

(96) Eaborn, C.; Hill, M. S.; Hitchcock, P. B.; Smith, J. D.; Zhang, S.; Ganicz, T. *Organometallics* **1999**, *18*, 2342.

(97) Cheng, J.; Takats, J.; Ferguson, M. J.; McDonald, R. *J. Am. Chem. Soc.* **2008**, *130*, 1544.

Chapter 2 Synthesis of hybrid pro-ligands

2.1   Introduction – Hybrid ligand design

The review of trivalent and divalent organolanthanide compounds in Chapter 1 reveals that the principal type of ligands known to form Ln−C σ-bonds are silicon-stabilised carbanions (Figure 22).   The synthesis of donor-functionalised derivatives of these carbanion ligands, $(XMe_2Si)(Me_3Si)_2C^{\ominus}$ (X = OMe, NMe$_2$, PPh$_2$) increases their denticity and enables the formation of chelate rings (for multiple examples see Chapter 1, Figure 18).[1,2] Dicarbanion ligands consisting of two linked, silicon-stabilised carbanions have allowed the isolation of divalent lanthanide complexes with a single chelating ligand, e.g. Yb(II)[{(SiMe$_3$)$_2$C}Me$_2$SiCH$_2$CH$_2$SiMe$_2${C(SiMe$_3$)$_2$}], (see Chapter 1, Figure 21).[3] The cyclopentadienyl anion has been a very useful ligand in the growth of lanthanide organometallic chemistry because it formally occupies three coordination sites when η^5-coordinated but is monoanionic. Three of these ligands give trivalent complexes a coordination number of nine. Substituents can be added to increase the ligand Tolman cone angle and achieve monomeric complexes e.g. Sm(Cp$'$)$_3$.[4]
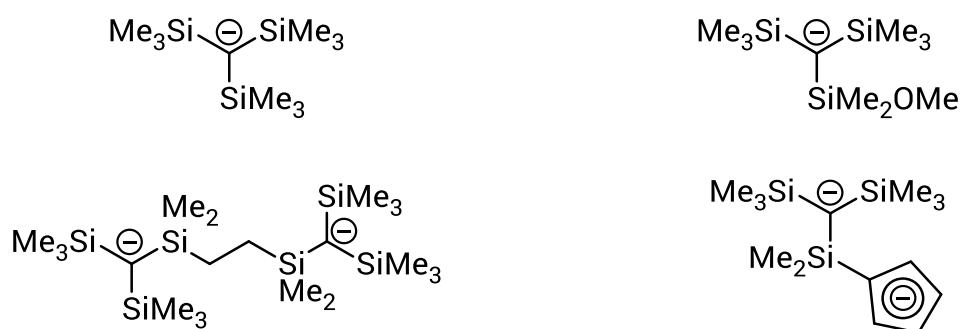
Figure 22. Selected examples of silicon-stabilised carbanions and dicarbanions used in lanthanide chemistry

53

The reactivity of divalent lanthanide and calcium compounds of silicon-stabilised carbanions, is known to be affected by the substituent, X, e.g. $\{(Me_3Si)_3C\}_2M$, (M = Yb(II), Ca) reacts with ethyl ethers whereas $\{(MeOMe_2Si)(Me_3Si)_2C\}_2M$, (M = Yb(II), Ca) does not (see Chapter 1, Scheme 28 and Scheme 29).[1,5] Incorporation of a cyclopentadienyl ligand allows investigation of the effect this aromatic carbanion substituent has on the reactivity of $\{(CpMe_2Si)(Me_3Si)_2C\}M$, (M = Yb(II), Ca) complexes towards ethyl ethers and other substrates.

The redox reactivity of $\{(Me_3Si)_3C\}_2Sm$ has not been explored extensively, in contrast to the redox reactivity of $(Cp^*)_2Sm$ which is relatively well understood (see Chapter 1, Scheme 15). The reference-point provided by $(Cp^*)_2Sm$ is useful for comparative reactivity studies. Modification of cyclopentadienyl ligands to make the ligand (i) more electron poor and/or (ii) more sterically bulky has enabled the isolation of Tm(II) complexes (with their more negative reduction potentials), see (Chapter 1). Linking a cyclopentadienyl anion to a bulky silicon-stabilised carbanion may lend itself favourably to the isolation of complexes of the more reducing divalent lanthanide cations with Ln−C σ-bonds, for example Tm(II). There is currently just one example of a Tm(II) complex with a Tm−C σ-bond, (Tp′)TmCH(SiMe₃SiMe₃)₂ (Tp′ = hydro-tris(3-*tert*-Bu-5-Me-pyrazolyl)borate).[6]

In order to probe the impact of joint alkyl and cyclopentadienyl coordination on complex stability and reactivity we have designed a new set of hybrid pro-ligands that combine these two functional groups into a single molecule (Figure 23). The steric and electronic properties of the hybrid pro-ligand can be changed by varying the type and number of substituents on the cyclopentadienyl ring or altering the bulky alkyl group.
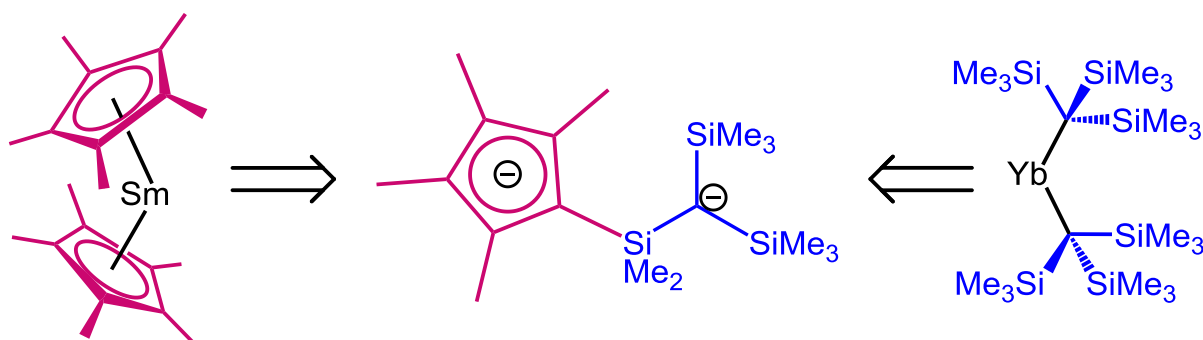
Figure 23. Design of the hybrid pro-ligand

These ligands are far more versatile than separate silicon-stabilised methanide and cyclopentadienyl ligands. They are chelating, inhibiting ligand redistribution − a known issue in the synthesis of heteroleptic lanthanide complexes. They allow the synthesis of trivalent lanthanide complexes which, with cation size optimization, could act as reductants via the mechanism of sterically induced reduction (SIR) by coordination of a (Cp*) as the third anionic ligand. Potentially these trivalent lanthanide complexes could also be reduced by potassium graphite (KC_8) to yield neutral or anionic Ln(II) complexes containing a direct Ln-C σ−bond, depending on the lanthanide metal.

2.2 Synthesis of silyl-substituted pro-ligands: {(CpH)Me$_2$Si}(Me$_3$Si)$_2$CH [5], {(Cp'H)Me$_2$Si}(Me$_3$Si)$_2$CH [6] and {(CpH^{4Me})Me$_2$Si}(Me$_3$Si)$_2$CH [7]

The hybrid pro-ligands were constructed from two separately synthesised molecular fragments: the silyl-substituted methine electrophile, $(Me_3Si)_2CHSiMe_2Br$ and the alkali metal (Li/Na/K) cyclopentadienide.

The precursor to $(Me_3Si)_2CHSiMe_2Br$ is $(Me_3Si)_2CHBr$ **[1]**, which was prepared according to the literature from bromoform, two equivalents of ^{n}BuLi and two equivalents of Me_3SiCl in THF.[7] The reaction proceeds under kinetic control (-78°C,

55

slow dropwise addition of a pre-cooled ^{n}BuLi solution) via a multiple step-wise sequence of a lithium-halogen exchange, followed by nucleophilic substitution at the silicon centre of Me$_3$SiCl (*Scheme 33*). The competing thermodynamic reaction is multiple nucleophilic substitutions at the bromoform carbon centre by ^{n}BuLi. After purification of **1** by fractional distillation at reduced pressure, another lithium-halogen exchange reaction gave {(Me$_3$Si)$_2$CH}Li [**2**], which can be purified by sublimation (~140°C, 0.01 mmHg) or by washing with light petroleum (both methods result in some loss of material).
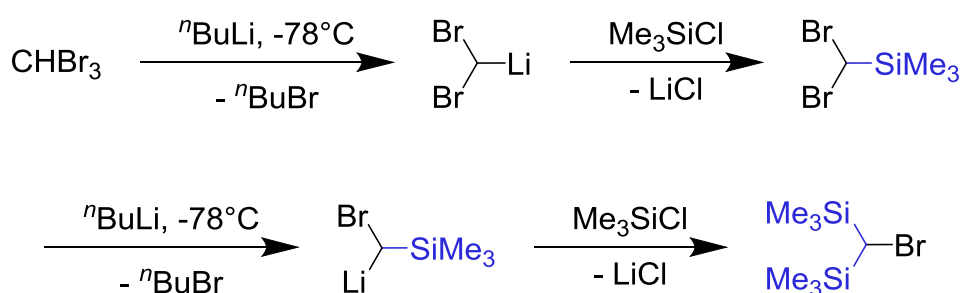
Scheme 33. Synthesis of 1

The nucleophilic substitution reaction of **2** with Me$_2$SiHCl at room temperature in diethyl ether gave (Me$_2$Si)$_2$(Me$_2$SiH)CH [**3**] which was isolated as a colourless oil (*Scheme 34*).[8] The bromosilane, (Me$_3$Si)$_2$CHSiMe$_2$Br [**4**], was prepared using an adapted literature procedure: a solution of the silane **3** in dichloromethane at 0°C was treated with bromine until an orange colour persisted. HBr was evolved from the reaction mixture, and the solvent and excess bromine were removed *in vacuo* to leave the product as a colourless solid which is sensitive to hydrolysis.[9]
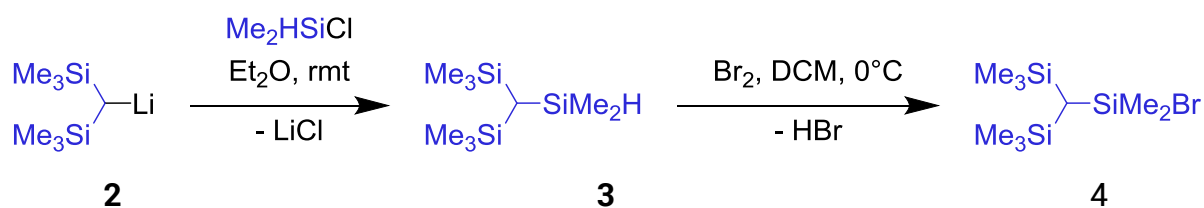
Scheme 34. Synthesis of 3 and 4

The alkali metal cyclopentadienides were synthesised from the alkali metal hydrides using well known literature procedures.[10] As will be discussed later it was found that it was best practise to isolate the alkali metal cyclopentadienide (Na/K) rather than use the lithium cyclopentadienide generated *in situ* by deprotonation with ^{n}BuLi. Preparation of HCp' involved nucleophilic substitution of Me_3SiCl by NaCp and distillation of trimethylsilylcyclopentadiene under reduced pressure (bp 41 – 43°C, 16 mmHg).[11] Cyclopentadienyl anions are weak nucleophiles due to the extensive delocalisation of the negative charge. Substitution of the cyclopentadienyl ring can reduce or enhance the nucleophilicity. Multiple electron donating groups (EDG), such as methyl- substituents increase the electron density on the cyclopentadienyl ring making it more nucleophilic. Electron withdrawing groups (EWG) such as Me_3Si- substituents remove electron density from the cyclopentadienyl ring resulting in a poorer nucleophile.

The reaction of $(Me_3Si)_2CHSiMe_2Br$ **[4]** with unsubstituted, mono-substituted or tetra-substituted lithium cyclopentadienides gives the hybrid pro-ligands **5**, **6** and **7** as substituted cyclopentadienyl compounds with one substituent being the 'trisyl-like' alkyl group (Scheme 35). Longer reaction times (3 days for Cp' versus 1 day for Cp^{4Me}) are required for poorer cyclopentadienyl nucleophiles.

	R^1	R^2	R^3	R^4	
	H	H	H	H	**5**
	H	$SiMe_3$	H	H	**6**
	Me	Me	Me	Me	**7**
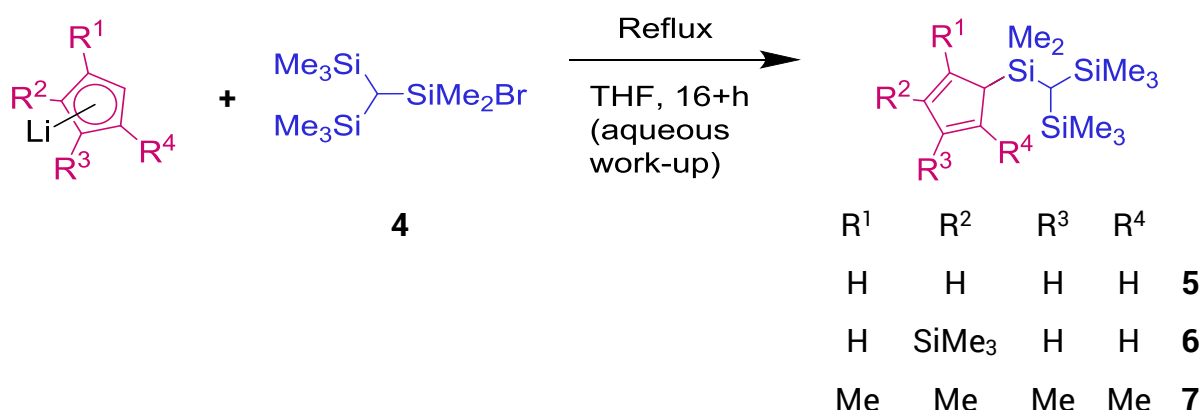
Scheme 35. The hybrid pro-ligand is constructed by reaction of an alkali metal cyclopentadienide with a silyl halide containing a tertiary alkyl group with carbanion stabilising functional groups.

Each hybrid pro-ligand derivative (**5**, **6** or **7**) was isolated, after aqueous work-up as a viscous yellow oil containing a mixture of regioisomers. There are three potential regioisomers of **5** and **7** (these are **a** - **c** in *Figure 24*), whereas **6** has four potential regioisomers. There is potentially a further group of four regioisomers for 6 where the cyclopentadienyl ring could be either 1,3-substituted (**6**) or 1,2-substitued (**6i**), but only **6** is observed by NMR spectroscopy (Figure 25). This is evidence that a — SiMe$_3$ substituent is large enough to prevent the cyclopentadienyl nucleophile reacting at the 2-position.

a   **b**   **c**   **d**
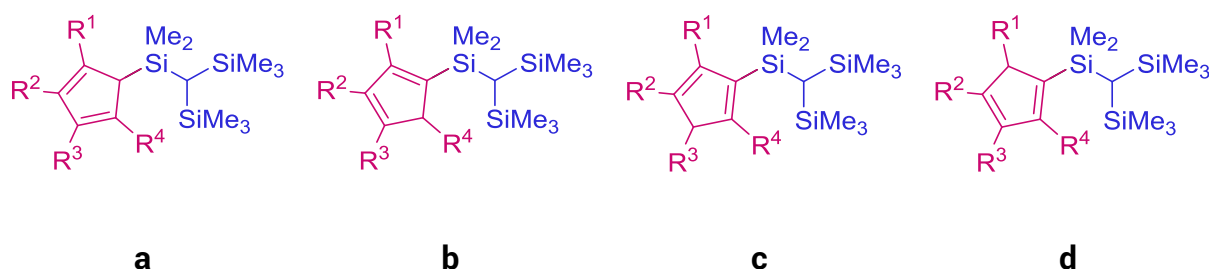
Figure 24. Regioisomers of the pro-ligands by virtue of the different possible positions of the double bonds. When R^1=R^2=R^3=R^4 three regioisomers exist but if R^2≠R^1=R^3=R^4 there are four regioisomers.

6, regioisomer **a**   **6i**, regioisomer **a**

Figure 25. A potential substitution regioisomer of the di-substituted hybrid pro-ligand

These isomeric mixtures mean the ^{1}H NMR spectra of **5** - **7** are complex, with many overlapping peaks, and it is very difficult to gauge the purity of the pro-ligand prior to deprotonation. Impurities also create issues with isolation of the corresponding dipotassium salts (see Chapter 4). For **7** unknown impurities in the HCp^{4Me} starting material (which is only 85% pure on receipt from the commercial supplier) makes accurate molar measurements impractical and potentially causes issues with deprotonation of the pro-ligand (See Chapter 4). Repetition of the pro-ligand synthesis using KCp^{4Me} purified by recrystallization increased yields and made

crystallisation of the ligand easier due to the cleaner synthesis. Crystals of regioisomer **a** of **7**; were grown from light petroleum (-24°C) as large colourless plates suitable for X-ray crystallography (Figure 26). See section 2.3.1 for a discussion of the crystal structure.
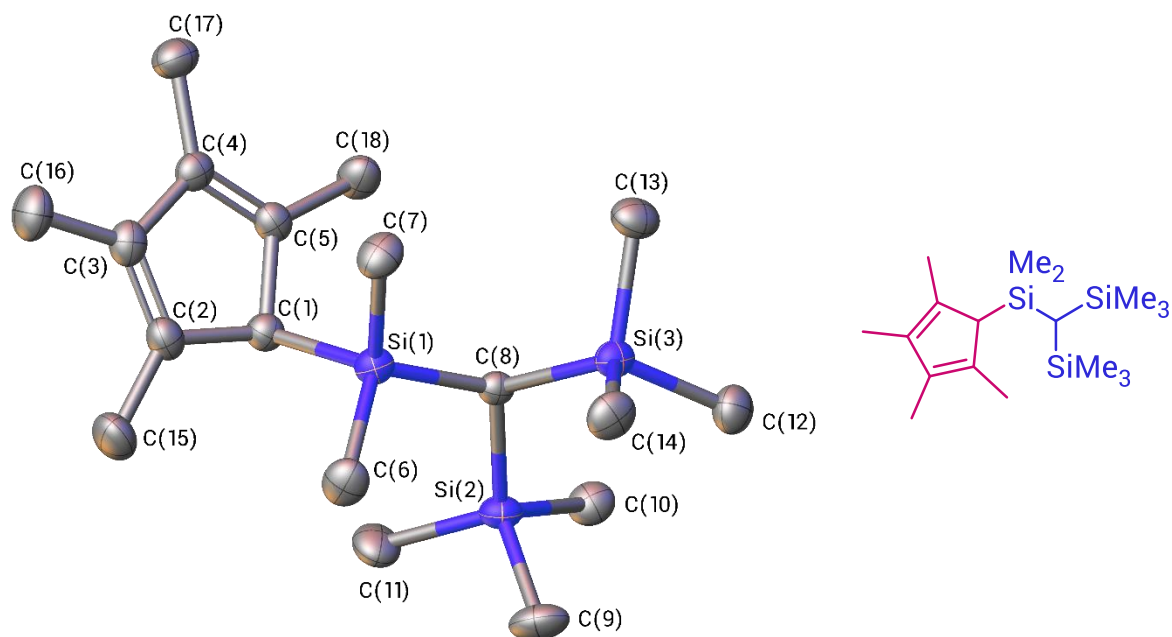
*Figure 26. Crystal structure of **7**, regioisomer **a**, with hydrogen atoms omitted for clarity.*

The most acidic alkyl proton in these pro-ligand molecules i.e. $(CpH^{4Me}Me_2Si)(Me_3Si)_2C\underline{H}$ has a pK_a >43 and the resulting tertiary carbanion is stabilised by negative hyperconjugation into the Si−C σ* orbitals (see Chapter 3). Conversion to the dianionic ligand required an extremely strong and non-bulky base. Isolation of these ligands will be discussed in Chapter 4. A new derivative with a relatively more acidic alkyl proton was also synthesised, and is discussed below.

2.3   Synthesis of mono-phosphine-borane/'Cp' hybrid pro-ligands

Exchange of one of the two SiMe$_3$ groups of the pro-ligand molecule for an isoelectronic and isosteric Me$_2$P(BH$_3$) group results in a decrease in the pK$_a$ of the methine proton of the pro-ligand. The methine proton is more acidic due to the greater stabilising effect of negative hyperconjugation into the P−C σ* orbitals of the phosphine-borane group relative to the Si−C σ* orbitals of SiMe$_3$ (Chapter 3).[12]

2.3.1   Synthesis of (CpH^{4Me}Me$_2$Si)(Me$_3$Si)CH{PMe$_2$(BH$_3$)} [10]

The bulky mono-phosphine-borane precursor (Me$_3$Si){PMe$_2$(BH$_3$)}CHSiMe$_2$Cl **[9]** must be prepared using a different route to (Me$_3$Si)$_2$CHSiMe$_2$Br because reaction of **9** with bromine would oxidise the phosphorus centre. The volatile trimethylphosphine (PMe$_3$) first converted to the phosphine-borane by addition of one equivalent of BH$_3$.SMe$_2$ (Scheme 36). Deprotonation of BH$_3$PMe$_3$ with *n*BuLi and then reaction with one equivalent of Me$_3$SiCl gave (Me$_3$Si){PMe$_2$(BH$_3$)}CH$_2$ **[8]**, which was purified by sublimation. These reactions must be carried out using greaseless Schlenk glassware since the α-lithiated phosphine-borane Me$_2$P(BH$_3$)CH$_2$Li reacts with (Me$_2$SiO)$_3$ and linear dimethylpolysiloxanes, the major components of Dow Corning vacuum grease.[13] The phosphine-borane **8** was then lithiated and reacted with an excess of Me$_2$SiCl$_2$ to give (Me$_3$Si){PMe$_2$(BH$_3$)}CHSiMe$_2$Cl **[9]**; crystals suitable for X-ray crystallography were grown from diethylether at 4°C.

The reaction of Me$_2$P(BH$_3$)CH$_2$Li with Me$_2$SiCl$_2$ must be controlled to prevent the possible formation of the di-substituted product (Me$_3$Si){(BH$_3$)Me$_2$P}CHSiMe$_2$CH{PMe$_2$(BH$_3$)}(SiMe$_3$) by a second attack of Me$_2$P(BH$_3$)CH$_2$Li on **9**. Control is achieved by using a two-fold excess of Me$_2$SiCl$_2$

as a dilute solution in THF, slow addition of $Me_2P(BH_3)CH_2Li$ and the reaction is kept at low temperature until all of the $Me_2P(BH_3)CH_2Li$ is consumed.
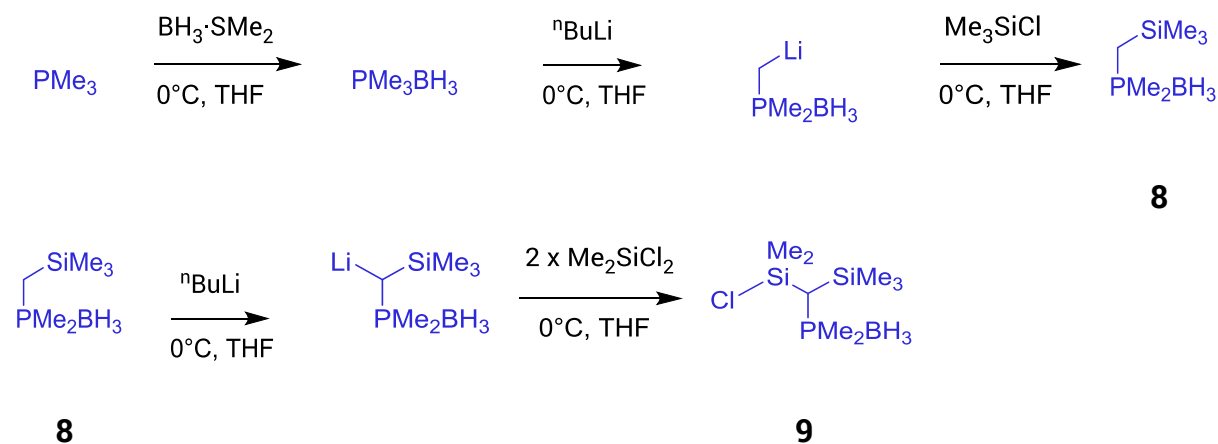
Scheme 36.

The crystal structure of the silyl chloride **9** is disordered over the silicon centres and the phosphorus centre; this is an indication of the isoelectronic and isosteric nature of the $SiMe_3$ and PMe_2BH_3 groups (Figure 27).
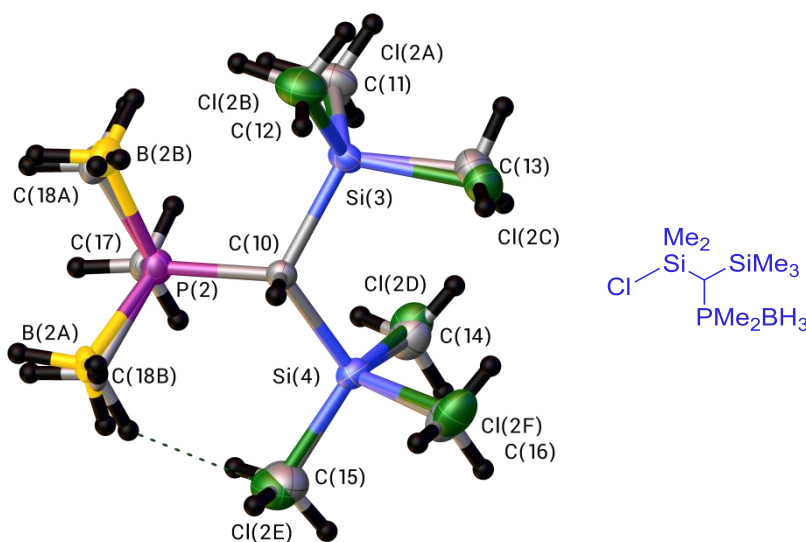
*Figure 27. X-ray crystal structure of **9** with major disorder shown*

The chlorosilane $(Me_3Si)\{PMe_2(BH_3)\}CHSiMe_2Cl$ [**9**] was reacted with either the lithium or potassium salts of tetramethylcyclopentadienide at reflux in THF to yield the phosphine-borane derivative of the penta-substituted cyclopentadienyl hybrid

ligand $(Cp^{4Me}HMe_2Si)(Me_3Si)CH\{PMe_2(BH_3)\}$ [**10**]. Aqueous work-up, extraction with diethyl ether and removal of the solvent *in vacuo* gave an oily white solid. After washing with light petroleum and drying over molecular sieves the solid product could be isolated from the impurities present in tetramethylcyclopentadiene, by recrystallization from diethyl ether at -24°C. Crystals suitable for X-ray crystallography were also grown by this method (Figure 28). The mono-phosphine-borane hybrid pro-ligand is a chiral molecule and it crystallises as a racemic mixture of enantiomers. The silicon-substituted pro-ligands **5**, **6** and **7** are liquids so could not be separated from the impurities present in $C_5Me_4H_2$, whereas the phosphine-boranes tend to be volatile solids that can be crystallised.
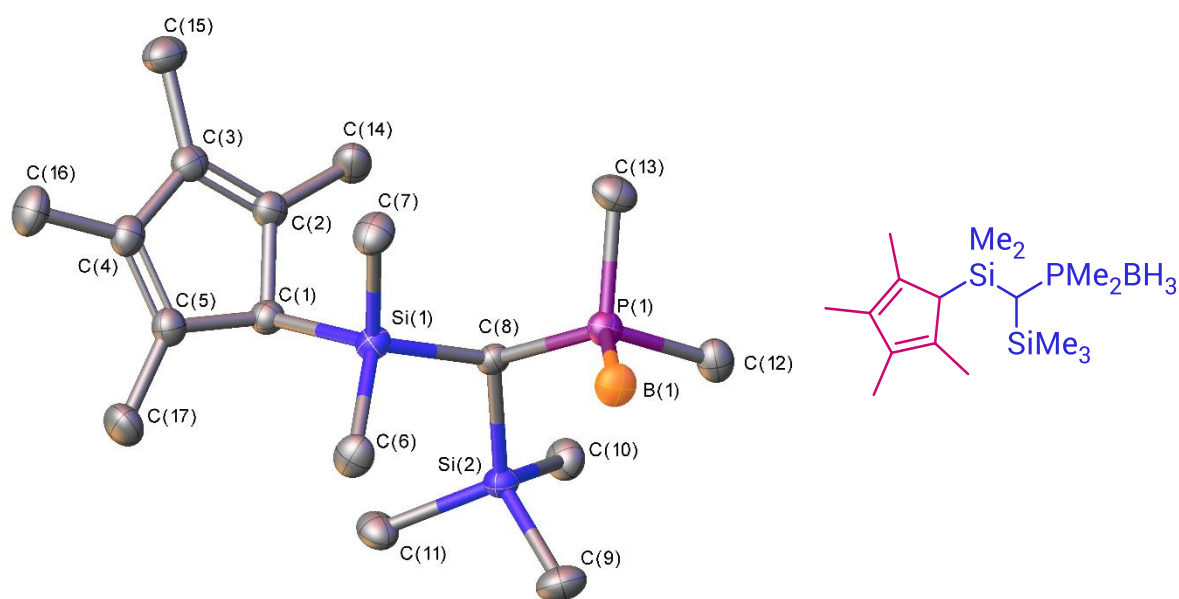
*Figure 28. Crystal structure of **10**, regioisomer **a**, with hydrogen atoms omitted for clarity.*

2.3.2   Synthesis of $(CpH^{4Me}Me_2Si)(Me_3Si)CH\{P^nPr_2(BH_3)\}$ [14]

To assess the impact of a small change in the steric demands of the alkyl group of the phosphine-borane moiety on the solid-state structures of the hybrid pro-ligands, and metalated ligands an alternative monophosphine-borane hybrid pro-ligand was synthesised containing a di-n-propylphosphine-borane group (Scheme 37).

The phosphine borane precursor was prepared by the reaction of $MePCl_2$, with two equivalents of ^nPrMgCl, followed by *in situ* addition of $BH_3.SMe_2$ to give the monophosphine-borane $(^nPr)_2PBH_3$ (**11**) as a colourless liquid in quantitative yield.

Lithiation of **11** with ^nBuLi resulted in removal of a relatively more acidic proton from the methyl group rather than from an *n*-propyl group. The metalated phosphine-borane was used *in situ*. Addition to a solution of Me_3SiCl gave $(Me_3Si)CH_2\{P^nPr_2(BH_3)\}$ [**12**] which was isolated as a viscous oil in very good yield.

From here on, the synthesis is very similar to the synthesis of $(Me_3Si)\{PMe_2(BH_3)\}CHSiMe_2Cl)$ [**9**], see section 2.3.2. Metalation of **12** with ^nBuLi gave the secondary alkyl carbanion $[(Me_3Si)CH\{P^nPr_2(BH_3)\}]Li$.

Dropwise addition of a solution of $[(Me_3Si)CH\{P^nPr_2(BH_3)\}]Li$ into a 2-fold excess of Me_2SiCl_2 gave the chlorosilane precursor $(Me_3Si)\{P^nPr_2(BH_3)\}CHSiMe_2Cl$ [**13**] provided the reaction was under kinetic control (as before) to prevent attack on newly formed **13** by the nucleophile, $(Me_3Si)\{P^nPr_2(BH_3)\}HC^{\ominus}$.

The reaction of **13** with $K(C_5Me_4H)$, (KCp^{4Me}) gave the hybrid pro-ligand $(CpH^{4Me}Me_2Si)(Me_3Si)CH\{P^nPr_2(BH_3)\}$ **14**, (Scheme 37). Crystals of a single regioisomer of **14** suitable for X-ray crystallography (Figure 29) were grown from light petroleum at 5°C.

$MePCl_2$ →($2 \times {}^nPrMgCl$, $-78°C$, Et_2O)→ ${}^nPr_2PMe$ →($BH_3 \cdot SMe_2$, $0°C$, Et_2O)→ $Me({}^nPr)_2PBH_3$

11

$Me({}^nPr)_2PBH_3$ →(${}^nBuLi$, $0°C$, THF)→ (Li)$P^nPr_2BH_3$ →(Me_3SiCl, $0°C$, THF)→ ($SiMe_3$)$P^nPr_2BH_3$

11   **12**

($SiMe_3$)$P^nPr_2BH_3$ (**12**) →(${}^nBuLi$, $0°C$, THF)→ Li($SiMe_3$)$P^nPr_2BH_3$ →($2 \times Me_2SiCl_2$, $-78°C$, THF)→ Cl—$Si(Me_2)$—($SiMe_3$)($P^nPr_2BH_3$)

12   **13**

Cl—$Si(Me_2)$—($SiMe_3$)($P^nPr_2BH_3$) (**13**) + K[C_5Me_4] →(Reflux, THF)→ $Si(Me_2)$($P^nPr_2BH_3$)($SiMe_3$)—C_5Me_4

Mixture of regioisomers

13   **14**

*Scheme 37. Synthesis of **14**.*

2.3.3   Solid-state Structures of the hybrid pro-ligands

The isosteric and isoelectronic hybrid pro-ligands **10** and **7** crystallise as monomers with similar bond lengths (Table 5) and similar molecular conformations, as seen from the torsion angles when viewed along the C(8)—Si(1) bond (Table 6). The purpose of the single crystal X-ray diffraction studies on **10** and **7** was to ascertain their steric similarity and to measure the Si—C(Me) bond lengths which are expected to be elongated upon pro-ligand metalation, the Si—C(Me) bond lengths of the pro-ligands and the metalated ligands will be compared in Chapter 4. The Si—

C(Me) bond lengths are not unusual, those for the $-SiMe_3$ and $-SiMe_2CpH^{4Me}$ groups range from 1.86 - 1.88 Å, with a typical Si$-$C bond length being 1.87 Å.[14] The Si$-$C(8) bonds are slightly longer (1.887 $-$ 1.916 Å) due to steric crowding, and the geometry around C(8) is a squashed tetrahedron (with an apical proton) with Si$-$C(8)$-$Si or Si$-$C(8)$-$P(1) angles of about 113.7°. The bond lengths and angles of **10** are closely similar to those of the previously crystallised mono-phosphine-borane $(Me_3Si)_2\{PMe_2(BH_3)\}CH$ [**15**].[15] The analogous isosteric and isoelectronic compound $(Me_3Si)_3CH$ [**16**] has also been crystallised and the bond lengths and angles are closely similar to those of **7**.[16]

*Table 5. Selected bond lengths for the hybrid pro-ligands **7** and **10***
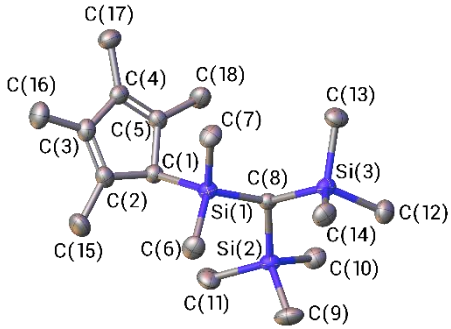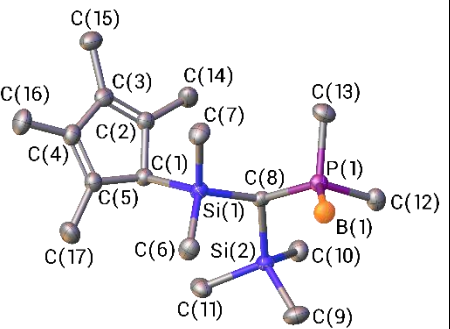
Bond lengths (Å)	7	10
C(8)−Si(1)	1.8909(19)	1.9156(19)
C(8)−Si(2)	1.8909(17)	1.9046(19)
C(8)−Si(3)/P(1)	1.8873(18)	1.8341(19)
Si(1)−C(6)	1.876(3)	1.866(2)
Si(1)−C(7)	1.8755(19)	1.870(2)
Si(2)−C(9)	1.876(3)	1.873(2)
Si(2)−C(10)	1.873(2)	1.860(2)
Si(2)−C(11)	1.870(2)	1.862(2)
Si(3)/P(1)−C(12)	1.873(2)	1.820(2)
Si(3)/P(1)−C(13)	1.872(2)	1.821(2)
Si(3)−C(14)	1.876(2)	n/a
P(1)−B(1)	n/a	1.914(2)
Si(1)−C(1)	1.926(2)	1.926(2)

*Table 6. Selected torsion angles for **7** and **10** with Newman-like views of the solid-state structures along the C(8)−Si(1) bond.*

Torsion angle (deg)	7	10
Si(2)−C(8)−Si(1)−C(6)	50.06(12)	50.76(13)
P(1)−C(8)−Si(1)−C(7)	34.87(15)	37.66(14)
P(1)−C(8)−Si(1)−1	152.01(10)	153.95(10)

The hybrid pro-ligand, (CpH^{4Me}Me$_2$Si)(Me$_3$Si)CH{P^{n}Pr$_2$(BH$_3$)} **[14]** crystallises as a racemic mixture of enantiomers (Figure 28) in the same way as **10**. The torsion angle between the phosphine-borane group and {C(13)}Cp^{4Me} is much smaller in **14** than 10 [73.68(10)°/ 153.95(10)°], with rotation around the C(1)−Si(1) bond being frozen at different dihedral angles in the two solid-state structures. The sum of the Si−C−Si and Si−C−P angles in **14** is 345.3° and the average of these angles is 115.1°. The extra steric bulk of the ^{n}propyl groups means the tetrahedron is slightly more squashed for **14** than **10**, where the sum of the sum of the Si−C−Si or Si−C−P angles is 341.1°, but otherwise the differences in the molecular structures between **10** and **14** are unremarkable.
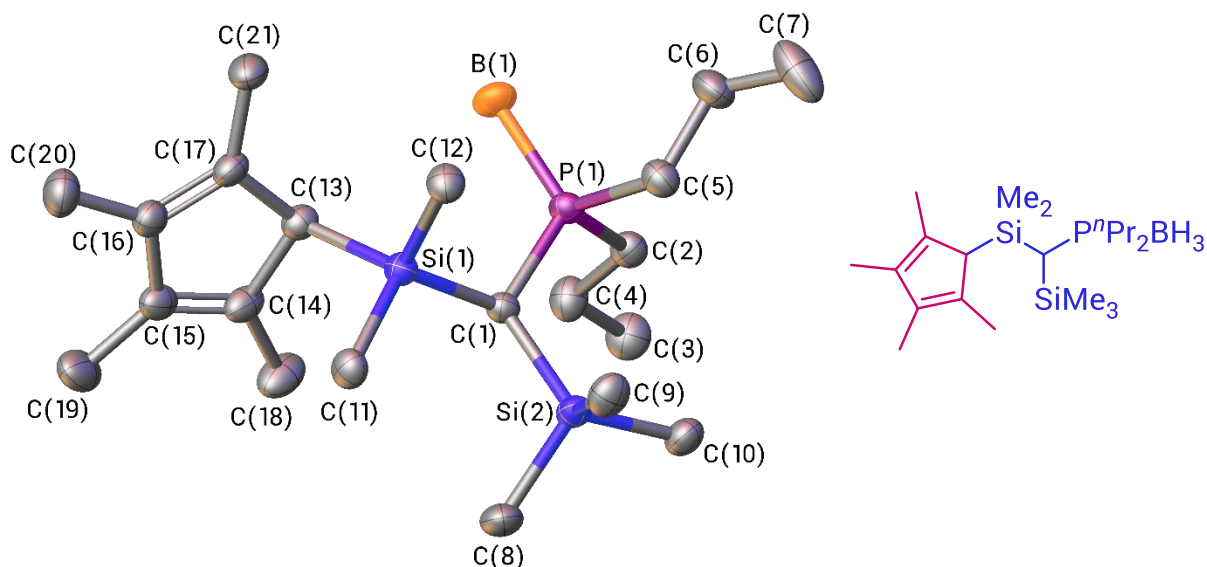
*Figure 29. Molecular structure of **14**, regioisomer **a** with 50% probability ellipsoids and with H atoms omitted for clarity. Selected bond lengths (Å) and angles (degrees): C(1)−P(1) 1.8265(16), C(1)−Si(2) 1.9125(18), C(1)−Si(1) 1.9189, Si(1)−C(13) 1.917(2), P(1)−B(1) 1.926(2), average Si−C(Me) 1.87, P(1)−C(2) 1.8239(19), P(1)−C(5) 1.8274(19), P(1)−C(1)−Si(2) 118.29(9), Si(2)−C(1)−Si(1) 114.56(9), Si(1)−C(1)−P(1) 112.46, C(13)−Si(1)−C(12) 114.18(8), C(12)−Si(1)−C(11) 106.09(9), C(11)−Si(1)−C(13) 105.22(9), P(1)−C(1)−Si(1)−C(13) 73.68(10), P(1)−C(1)−Si(1)−C(11) 169.51(9), Si(2)−C(1)−Si(1)−C(12) 86.77(10).*

2.3.4 Synthetic issues with the preparation of hybrid pro-ligands featuring less substituted cyclopentadienyl rings

Synthesis of derivatives of the hybrid pro-ligand (CpH^{TMS}Me$_2$Si)(Me$_3$Si)CH{PMe$_2$(BH$_3$)} [17] and (CpHMe$_2$Si)(Me$_3$Si)CH{PMe$_2$(BH$_3$)} [18] by reaction of (Me$_3$Si){PMe$_2$(BH$_3$)}CHSiMe$_2$Cl [9] with unsubstituted and mono-substituted lithium cyclopentadienides followed by aqueous work up initially failed (Scheme 38). Column chromatography of the isolated oily mixture of products (solvent system 3:1 petrol:DCM, switching to 1:1 petrol:DCM) followed by ^{1}H, ^{11}B{^{1}H} and ^{31}P{^{1}H} NMR spectroscopy and X-ray crystallographic analysis of crystalline material formed in some fractions identified the siloxane [(Me$_3$Si){PMe$_2$(BH$_3$)}HCMe$_2$Si]$_2$O [19], (Figure 30) as a major component.
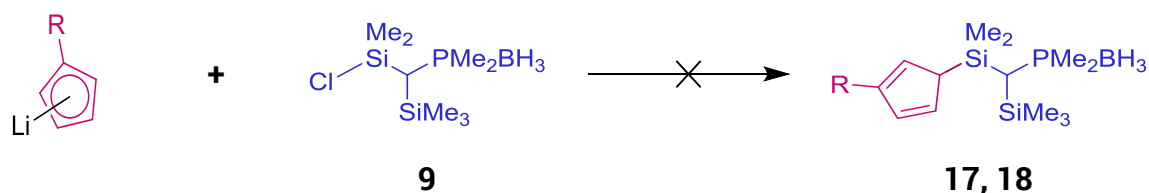
Scheme 38. Reaction conditions: reflux in THF for 16 hours followed by aqueous work-up. R = H or SiMe₃.
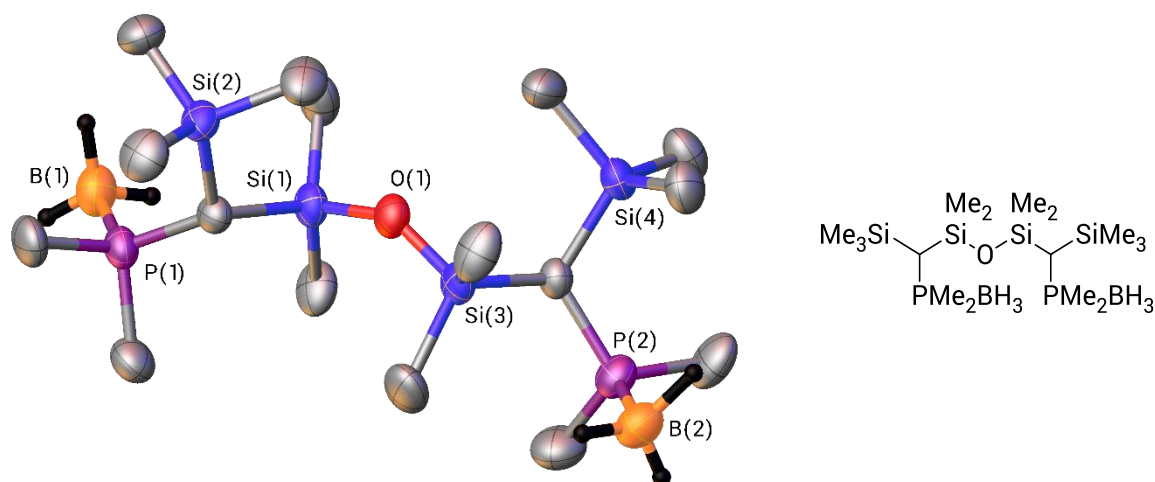
*Figure 30. Crystal structure of **19**; a siloxane formed from the self-condensation of two silanol molecules, H atoms bound to C atoms omitted for clarity.*

The data strongly suggests hydrolysis of the Si-C bond between the cyclopentadiene ring and the silicon atom during aqueous work-up (Scheme 39). Loss of the cyclopentadienyl anion as a leaving group (which is immediately protonated to form cyclopentadiene monomer and which then dimerises) leaves a silanol. Two equivalents of the silanol then undergo a self-condensation reaction to give the identified disiloxane. Ring whizz fluxionality renders the Si—C bond more labile for the unsubstituted cyclopentadiene rings versus the tetra-methylcyclopentadiene ring, and the four methyl groups of CpH^{4Me} are inductive and destabilise cyclopentadienyl anion formation.
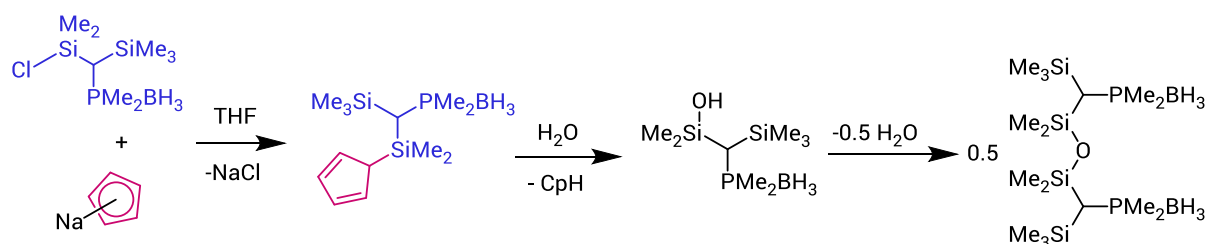
Scheme 39. Proposed decomposition reaction pathway for monophosphine-borane hybrid pro-ligands with unsubstituted or mono-substituted cyclopentadienyl rings.

It was not immediately realised that the simple cyclopentadienyl mono-phosphine-borane) hybrid pro-ligands were sensitive to hydrolysis and alternative scenarios, including that the simple cyclopentadienyl anion was too poor a nucleophile, were considered. Meanwhile derivatives of the hybrid ligand with unsubstituted or mono-substituted cyclopentadienyl rings were synthesised with silyl substituted alkyl substituents, which did not appear to be sensitive to hydrolysis. The silane pro-ligands **5** - **7** although isolated in good yield as crystalline solids, do decompose over a period of several weeks if not stored at low temperature (-24°C); it is possible that hydrolysis of the Si-(C)Cp bond is much slower for these compounds but does occur. A similar hydrolysis of the Si$-$(C)Cp bond has been reported when (Cp')$_2$CpLa(THF) was formed from reaction of KCp' with LaCl$_3$ in incompletely dry THF solvent.[17]

2.4   Synthesis of bis(phosphine-borane)/'Cp' hybrids

To further expand the range of hybrid pro-ligands chlorosilane precursors were prepared for a range of bis(phosphine)-boranes (Figure 31). The $-$SiMe$_2$Cl group must be retained to link together the alkyl part and the cyclopentadienyl part of the hybrid pro-ligand, however the remaining SiMe$_3$ group can be replaced with a second phosphine-borane group. While trimethylsilyl groups stabilise alkyl carbanions by negative hyperconjugation, phosphine-borane groups stabilise carbanions much more effectively, so increasing the number of phosphine-borane groups to give a bis(phosphine-borane)-stabilised carbanion further increases the

acidity of the methine proton. A quantitative analysis of the relative stabilities of carbanions stabilised by trimethylsilyl, phosphine and phosphine borane groups is described in Chapter 3. The stability of the carbanions increases in the order (2 x $SiMe_3$) < (1 x $SiMe_3$ and 1 x PMe_2BH_3) < (2 x PMe_2BH_3) and concomitantly the methine proton acidity increases.
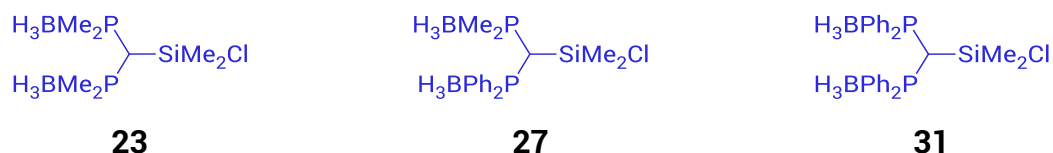
*Figure 31. Bis(phosphine-borane)-substituted chlorosilanes **23, 27** and **31**prepared to change the alkyl carbanion group of the hybrid pro-ligand to a variety of bis(phosphine)-boranes.*

2.4.1 Synthesis of $\{PMe_2(BH_3)\}_2CHSiMe_2Cl$ [**23**]

Bis(dimethylphosphino)methane [$(PMe_2)_2CH_2$] [**20**] was prepared and used *in situ* by addition of four equivalents of MeMgBr to a solution of the reactive precursor bis(dichlorophosphino)methane, prepared as described in the literature.[18,19] The reaction mixture was treated with two equivalents of $BH_3 \cdot SMe_2$ to give $\{PMe_2(BH_3)\}_2CH_2$ [**21**], which was isolated as a colourless crystalline solid following aqueous work-up.

Metalation of **21** with one equivalent of ^nBuLi followed by addition of the resulting solution to a large excess of Me_2SiCl_2 at -78°C gave $\{PMe_2(BH_3)\}_2CHSiMe_2Cl$ [**23**] as a colourless solid (Scheme 40).
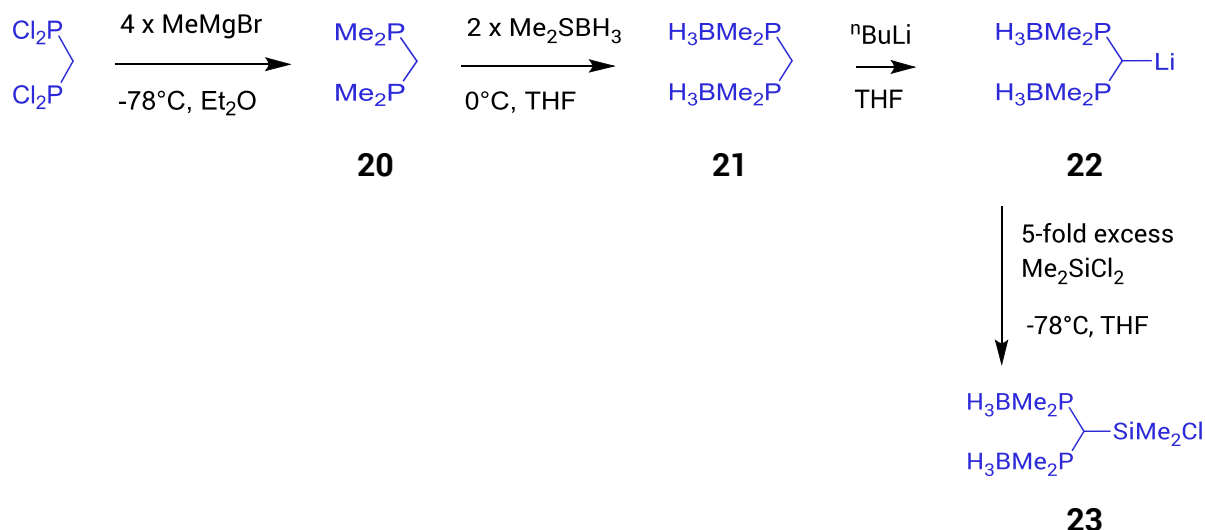
Scheme 40. Synthesis of the bis(phosphine-borane)-substituted hybrid pro-ligand chlorosilane precursor, {PMe₂(BH₃)}₂CHSiMe₂Cl [23].

The low temperature and excess Me_2SiCl_2 used in the aforementioned reaction are important for the preparation of chlorosilane precursors from bis(phosphine-borane)methanes since the tertiary alkyl carbanion of the chlorosilane [23] is further stabilised by the $ClMe_2Si-$ group, relative to the secondary bis(phosphine-borane)methane-stabilised carbanion. Warmer temperatures and stoichiometric amounts of Me_2SiCl_2 lead to metalation of the alkyl chlorosilane and recovery of the bis(phosphine-borane)methane **21** (Scheme 41).
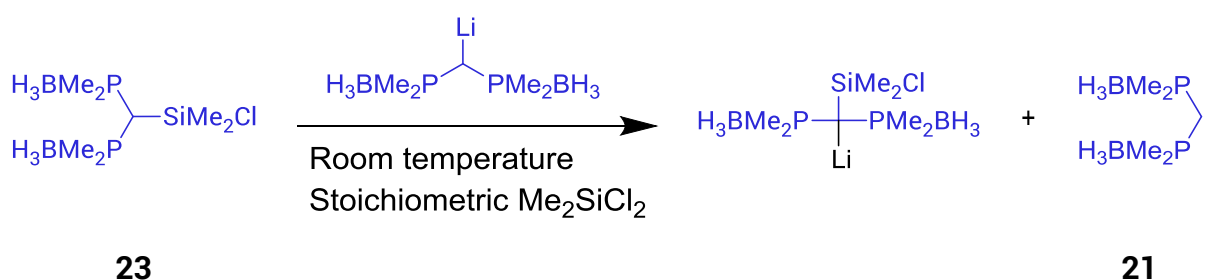
Scheme 41.

The chlorosilane molecule **23** is a symmetric bis(phosphine-borane) (Figure 32), it is achiral with a plane of symmetry that bisects the two $-PR'_2BH_3$ groups. The phosphorus centres are prochiral and the non-borane alkyl substituents on phosphorus are diastereotopic. If one $-PR'_2BH_3$ group is changed to a $-PR''_2BH_3$

72

group or SiMe$_3$ group the molecular symmetry is broken and the chlorosilane molecule becomes chiral. The effect of this is that the R substituents of the −SiR$_2$Cl group as well as the R' and R'' substituents of the phosphine-borane group(s) all become chemically inequivalent (diastereotopic). Each diastereotopic pair of chemically inequivalent R, R' or R'' alkyl substituents gives two sets of signals in the ^{1}H{^{11}B} NMR and ^{13}C{^{1}H} NMR spectra (2 doublets for −PR'$_2$BH$_3$ and −PR''$_2$BH$_3$, 2 singlets for −SiR$_2$Cl).
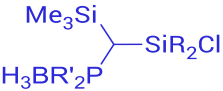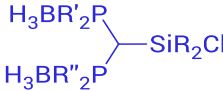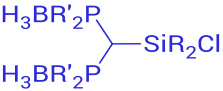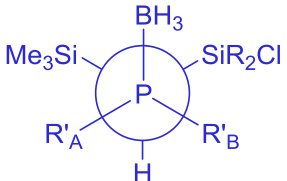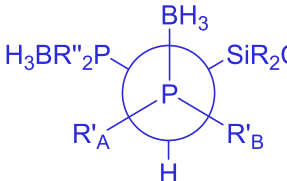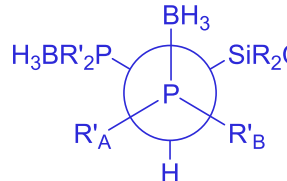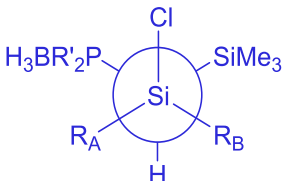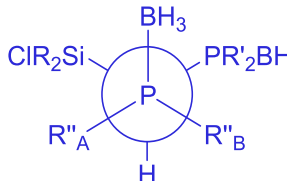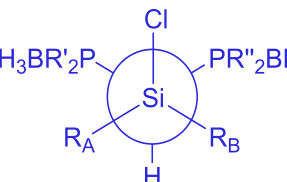
Monophosphine-borane chlorosilanes	Asymmetric bis(phosphine-borane) chlorosilanes	Symmetric bis(phosphine-borane) chlorosilanes
Me_3Si—C(SiR_2Cl)($H_3BR'_2P$)	$H_3BR'_2P$—C(SiR_2Cl)($H_3BR''_2P$)	$H_3BR'_2P$—C(SiR_2Cl)($H_3BR'_2P$)
View along P—C bond	**View along P—C bond**	**View along either P—C bond**
BH_3 / Me_3Si / SiR_2Cl / P / R'_A / R'_B / H	BH_3 / $H_3BR''_2P$ / SiR_2Cl / P / R'_A / R'_B / H	BH_3 / $H_3BR'_2P$ / SiR_2Cl / P / R'_A / R'_B / H
No mirror plane $R'_A \neq R'_B$	No mirror plane $R'_A \neq R'_B$	No mirror plane $R'_A \neq R'_B$
View along Si—C bond	**View along P—C bond**	
Cl / $H_3BR'_2P$ / $SiMe_3$ / Si / R_A / R_B / H	BH_3 / ClR_2Si / PR'_2BH_3 / P / R''_A / R''_B / H	
No mirror plane $R_A \neq R_B$	No mirror plane $R''_A \neq R''_B$	
	View along Si—C bond	
	Cl / $H_3BR'_2P$ / PR''_2BH_3 / Si / R_A / R_B / H	
	No mirror plane $R_A \neq R_B$	

Anticipated ^{1}H NMR signals (R = Me and R' = Me)		
2 singlets ($SiMe_AMe_BCl$)	2 singlets ($SiMe_AMe_BCl$)	1 singlet ($SiMe_2Cl$)
2 doublets ($BH_3PMe_AMe_B$)	2 doublets ($BH_3PMe_AMe_B$)	2 doublets ($BH_3PMe_AMe_B$)
	2 pairs of signals split into doublets ($BH_3PR''_AR''_B$)	

Figure 32. Summary of the diastereotopic groups and their anticipated effect on the appearance of NMR spectra for the chlorosilanes [9], [13] and [23, 27 and 31].

2.4.2 Synthesis of {PMe$_2$(BH$_3$)}{PPh$_2$(BH$_3$)}CHSiMe$_2$Cl [27]

BH$_3$PMe$_2$CH$_2$Li was synthesised as already described from PMe$_3$ (Scheme 36), and added as a solution in THF to diphenylchlorophosphine to give {PMe$_2$(BH$_3$)}{PPh$_2$}CH$_2$ [24] (Scheme 42). One equivalent of BH$_3$·SMe$_2$ was added to the reaction mixture to give {PMe$_2$(BH$_3$)}{PPh$_2$(BH$_3$)}CH$_2$ [25] which was isolated as a colourless solid following extraction into DCM and filtration to remove the LiCl by-product. Metalation of 25 with one equivalent of ^{n}BuLi in THF gave [{PMe$_2$(BH$_3$)}{PPh$_2$(BH$_3$)}CH]Li [26] which was used in situ by immediate addition of the orange solution to a THF solution containing a large excess of Me$_2$SiCl$_2$ at low temperature (-78C). Extraction of the product from this reaction into DCM, removal of the LiCl by-product and then removal of the excess Me$_2$SiCl$_2$ and solvent in vacuo gave the chlorosilane {PMe$_2$(BH$_3$)}{PPh$_2$(BH$_3$)}CHSiMe$_2$Cl [27] as a colourless moisture sensitive solid.
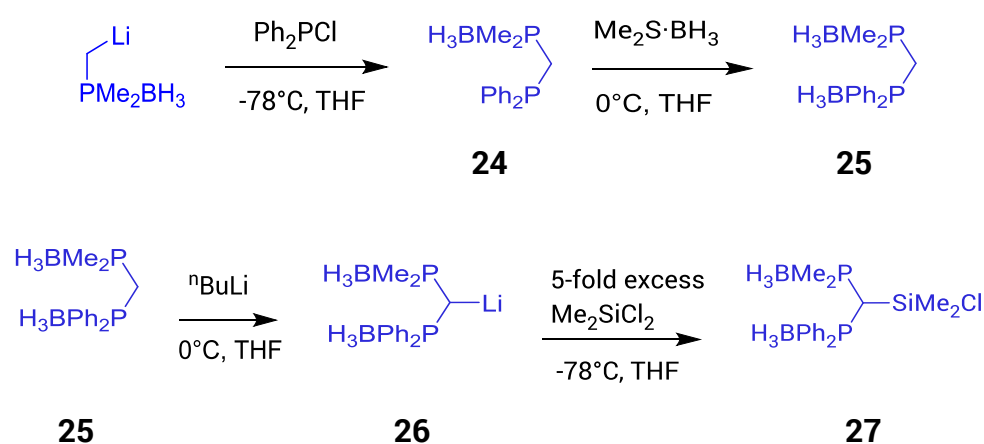
Scheme 42. Synthesis of the bis(phosphine-borane)-substituted hybrid pro-ligand chlorosilane precursor, {PMe$_2$(BH$_3$)}{PPh$_2$(BH$_3$)}CHSiMe$_2$Cl [27].

The reaction was monitored at each step using ^{31}P{^{1}H} and ^{11}B{^{1}H} NMR spectroscopy to assess the extent of the reaction. In the ^{31}P{^{1}H} NMR spectra of 25, 26 and 27 the chemical shift of the BH$_3$PPh$_2$ phosphorus atom remains roughly constant at 12 ppm in comparison to the chemical shift of the BH$_3$PMe$_2$

phosphorus atom which changes from 8.5 ppm in **25** to -7.6 ppm in **26** and 14.3 ppm in **27**. The more negative chemical shift of the BH_3PMe_2 phosphorus atom in **26** is attributed to an increase in electron density on the phosphorus atom due to stabilisation of the phosphine-borane carbanion by negative hyperconjugation. In the case of the BH_3PPh_2 group charge delocalised onto the phosphorous atom by negative hyperconjugation is then further delocalised onto the phenyl rings minimising the extra electron density on the BH_3PPh_2 phosphorus atom in the **26**. Since the electron density on the BH_3PPh_2 phosphorus atom is changed little, its chemical shift in the ^{31}P NMR spectra is essentially unchanged (12 ppm) for compounds **25** - **27**.

2.4.3 Synthesis of $\{PPh_2(BH_3)\}_2CHSiMe_2Cl$ [**31**]

Bis(diphenylphosphino)methane (dppm) [**28**] was prepared using a solution of sodium in liquid ammonia to reductively cleave a phenyl group from triphenylphosphine (Scheme 43). After removal of the ammonolysis product $NaNH_2$ by reaction with NH_4Br, half an equivalent of dichloromethane was added to yield dppm. After all the ammonia had evaporated the product **28** was extracted into DCM upon aqueous work-up and recrystallized from an IPA/DCM mixture at 4°C.
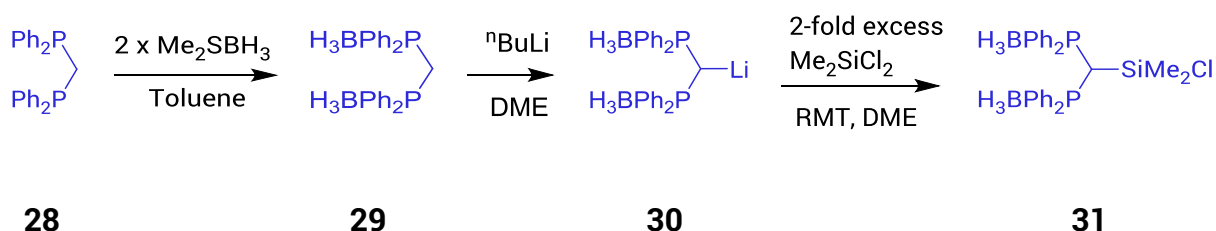
Scheme 43. Synthesis of the bis(phosphine-borane) hybrid pro-ligand chlorosilane precursor; $\{PPh_2(BH_3)\}_2CHSiMe_2Cl$ [**31**].

The BH_3 group in $\{PPh_2(BH_3)\}_2CH_2$ [**29**] is relatively labile and the P—B bond is readily cleaved by THF, preventing the use of this solvent in its synthesis. Boronation of **28** with two equivalents of $BH_3 \cdot SMe_2$ (as a solution in toluene) was

achieved using toluene as an alternative solvent as described in the literature.[20] The solvent was removed *in vacuo* to give **29** as a colourless solid in quantitative yield. Metalation of **29** was carried out in DME to avoid exchange of the borane group with THF. Previously [{PPh$_2$(BH$_3$)}$_2$CH]Li [**30**] has been prepared in Et$_2$O, by deprotonation with MeLi over 36 hours and isolated as a white solid.[21] The subsequent nucleophilic addition reaction of **30** with Me$_2$SiCl$_2$ was found not to proceed readily in Et$_2$O, hence the choice of DME solvent. The lithium salt [{PPh$_2$(BH$_3$)}$_2$CH]Li [**26**] was not isolated, but was identified by ^{11}B and ^{31}P NMR (DME) and the brown solution in DME was used in situ. Multiple phosphorous containing products were obtained from the addition of **30** to a 2-fold excess of Me$_2$SiCl$_2$ at room temperature. The reaction was not under sufficient kinetic control to prevent multiple nucleophilic attacks on the Me$_2$SiCl$_2$ despite the excess and {PPh$_2$(BH$_3$)}$_2$CHSiMe$_2$Cl [**31**] was not cleanly isolated. Lower temperatures and a larger excess of Me$_2$SiCl$_2$ are expected to resolve these issues although the re-isolation of c.a. 15% of {PPh$_2$(BH$_3$)}$_2$CH$_2$ [**29**] starting material raises the question of the stability of [{PPh$_2$(BH$_3$)}$_2$CH]Li [**30**] in DME. Alkali and alkali-earth complexes of the type [{PPh$_2$(BH$_3$)}$_2$CH]M have been found to be unstable in THF decomposing to give **29** as one of the products.[20,22]

2.5 Synthesis of bis-phosphine/'Cp' hybrids

Phosphine derivatives were investigated in their own right to investigate how the binding modes of these ligands differ to the hybrid ligands featuring silicon-stabilised and phosphine-borane-stabilised carbanions. Phosphine hybrid pro-ligands were also viewed as precursors from which to access the phosphine-borane derivatives where the cyclopentadienyl ring is not fully substituted (mono- or di-substituted cyclopentadienyl pro-ligands) by boronation of the phosphine hybrid pro-ligand as a final step. This approach was considered before it became apparent that the hybrid pro-ligands were sensitive to hydrolysis. Initial synthesis

of a bis(phosphine) pro-ligand from the bulky bis(phosphine)-substituted silyl chloride precursor and NaCp with an aqueous work-up using deoxygenated water unexpectedly gave the original bis(phosphine) in quantitative yield (Scheme 44).

Monitoring of the reaction mixture using ^{1}H and ^{31}P{^{1}H} NMR spectroscopy and visual observation of the formation of NaCl precipitate indicated that the reaction had proceeded as expected to form the bis(phosphine) hybrid pro-ligand. Upon aqueous work-up and extraction with light petroleum or DCM the bis(phosphine) was recovered in quantitative yield indicating that the Si−C bond of the chlorosilane precursor had been cleaved. The second decomposition product was expected to be $(C_5H_6SiMe_2)_2O$ from self-condensation of two molecules of $C_5H_6SiMe_2OH$ (Scheme 44), however this product was not isolated.

This bond cleavage was not anticipated because although Si−C bonds can be broken more readily than C−C bonds they are still strong bonds with a bond dissociation energy of 451 kJ/mol.[14] The formation of a very strong Si−O bond with a bond dissociation energy of 809 kJ/mol may thermodynamically drive the hydrolysis reaction. Avoidance of aqueous work-up gave the desired bis(phosphine) pro-ligand: $(CpHMe_2Si)CH(P^nPr_2)_2$.
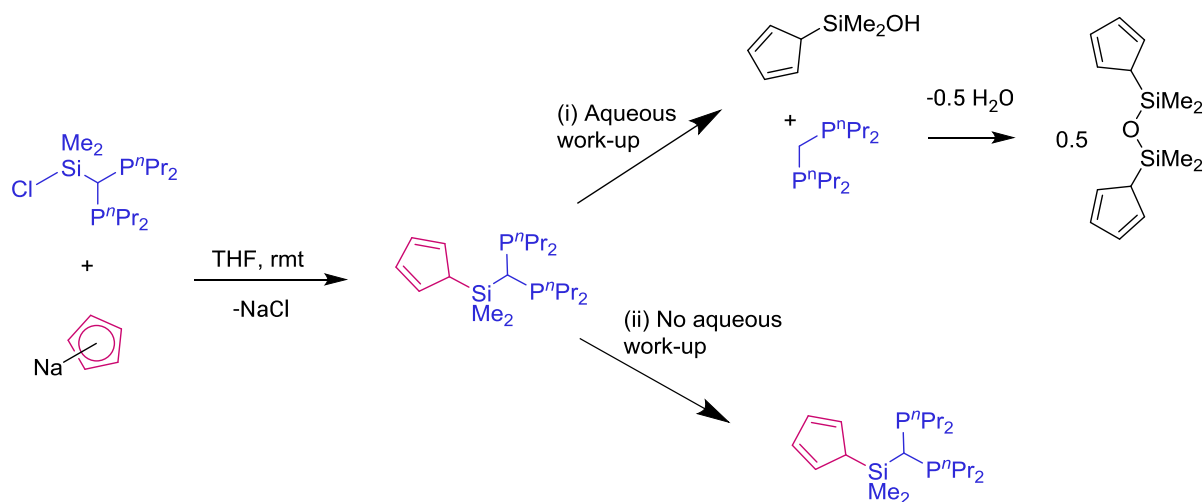
Scheme 44

Hydrolysis of the bis(phosphine) hybrid pro-ligand cleaves the Si$-$C(P^{n}Pr$_2$)$_2$ bond (Scheme 44) whereas hydrolysis of the mono(phosphine-borane) hybrid pro-ligands cleaves the Si$-$C(Cp) bond (Scheme 39). After nucleophilic attack of the SiMe$_2$ centre by water the leaving group is the most stable carbanion. To account for this difference it is suggested that the bis(phosphine) stabilised carbanion (^{n}Pr$_2$P)$_2$HC$^\ominus$ is more stable than the cyclopentadienyl anion [C$_5$H$_5$]$^\ominus$ and also that the mono(phosphine-borane) stabilised carbanion (Me$_3$Si){Me$_2$PBH$_3$}HC$^\ominus$ is less stable than the cyclopentadienyl anion [C$_5$H$_5$]$^\ominus$.

Further evidence for this conclusion that the stability of the carbanions decreases in the order (^{n}Pr$_2$P)$_2$HC$^\ominus$ > [C$_5$H$_5$]$^\ominus$ > (Me$_3$Si){Me$_2$PBH$_3$}HC$^\ominus$ comes from NBO calculations on a selection of model secondary carbanions and will be discussed in Chapter 3.

2.5.1   Synthesis of (CpHMe$_2$Si)CH(P^{n}Pr$_2$)$_2$ [33]

Bis(di-*n*-propylphosphino)methane was accessed by addition of four equivalents of ^{n}PrMgBr to a solution of the reactive precursor bis(dichlorophosphino)methane, which was prepared as described in the literature.[18]   Deprotonation of bis(di-*n*-propylphosphino)-methane as a solution in petrol using ^{t}BuLi gave a white slurry of (^{n}Pr$_2$P)$_2$CHLi (Scheme 45). The solvent was removed *in vacuo* and the product was dissolved in THF, and then added dropwise to excess Me$_2$SiCl$_2$ to form the chlorosilane reagent (^{n}Pr$_2$P)$_2$CHSiMe$_2$Cl [32].   Reaction of (^{n}Pr$_2$P)$_2$CHSiMe$_2$Cl with sodium cyclopentadienide gave the bis-phosphine-substituted hybrid pro-ligand (CpHMe$_2$Si)CH(P^{n}Pr$_2$)$_2$ [33] (Scheme 44 (ii)).
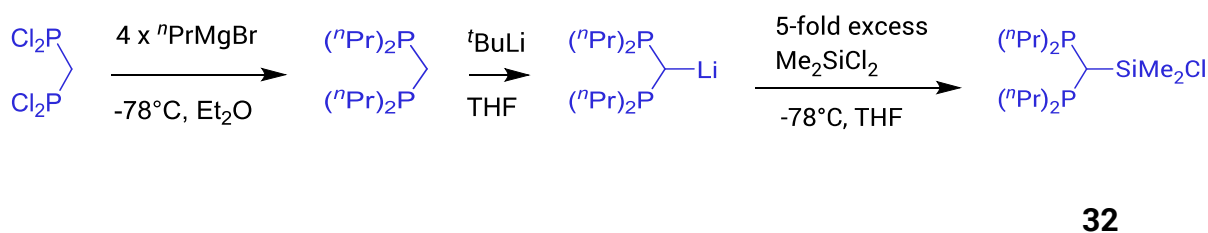
Scheme 45

This pro-ligand was contaminated with a small amount of the impurity (^{n}Pr$_2$P)$_2$CH$_2$ carried through in the reaction mixture.   To separate the product **33** from the impurity, the product was by treated with one equivalent of KH to form the monopotassium salt, [(CpMe$_2$Si)CH(P^{n}Pr$_2$)$_2$]K [34],   which was desolvated by heating under vacuum. The bis(di-*n*-propylphosphino)methane impurity was extracted into light petroleum and decanted leaving the purified product [(CpMe$_2$Si)CH(P^{n}Pr$_2$)$_2$]K [34] as a colourless solid.
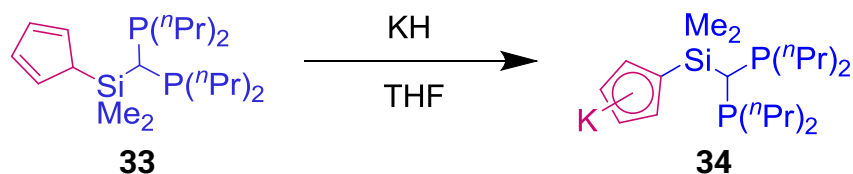
Scheme 46

2.6   Conclusion

Synthesis of the hybrid pro-ligands brings together the abundantly used cyclopentadienyl anion ligand with the silicon-, phosphine-borane and phosphine stabilised carbanion ligands previously synthesised by members of the Izod group. Combining these ligands gives a new dianionic hybrid ligand with the ability to chelate metal centres, exhibit unusual binding modes and avoid Schlenk-type equilibria in the later synthesis of lanthanide complexes.

The hybrid ligand can be easily modified and this versatility was exploited to overcome synthetic complications throughout this work. The silyl-substituted pro-ligands **5**, **6** and **7**   are usually oils and cannot be routinely purified by crystallisation, they are synthesised as a mixture of regioisomers making characterisation and assessment of compound purity by NMR spectroscopy elusive and any impurities led to issues in the subsequent metalation reaction (Chapter 4). Modification of the hybrid pro-ligand by changing one of the carbanion stabilising $SiMe_3$ groups for a significantly more carbanion-stabilising phosphine-borane group gave the hybrid pro-ligands **10** and **14** which although mixtures of regioisomers can be isolated as a crystalline solids. Hybrid pro-ligands **7** and **10** are essentially isostructural in the solid-state. To investigate the variety of different binding modes to metal centres accessible by straightforward modifications of the hybrid ligand bis(phosphine-borane) and bis(phosphine) chlorosilanes were synthesised as precursors to further hybrid pro-ligands.

Attempts to modify the cyclopentadienyl ring of the hybrid ligands by reducing the number of substituents led to the discovery that phosphine-borane-substituted hybrid pro-ligands with less than five substituents on the cyclopentadienyl ring are very sensitive to hydrolysis of the Si$-$C(Cp) bond. The bis(phosphine)-substituted hybrid pro-ligand **33** is also sensitive to hydrolysis but of the Si$-$CH(P^{n}Pr$_2$)$_2$ bond.

2.7   Experimental

2.7.1   2.6.1 General procedure

All manipulations were carried out under an inert argon atmosphere using Schlenk techniques or under nitrogen in a solvent-free glovebox. Non-halogenated solvents (diethyl ether, THF, light petroleum, toluene, benzene and hexane) were pre-dried using sodium wire. Solvents were then distilled over sodium-potassium alloy (diethyl ether, light petroleum, hexane), potassium (THF, benzene) or sodium (toluene). Dichloromethane was dried by distillation over CaH_2. THF and dichloromethane were stored under nitrogen/argon over activated 4Å molecular sieves, all other solvents were stored over a potassium film. Deuterated solvents for NMR were also dried by distillation from potassium (d$_8$-THF, C_6D_6) or CaH_2 ($CDCl_3$) and were stored over activated 4Å molecular sieves. Deuterated solvents were deoxygenated using the freeze-pump-thaw method (3 cycles).

Dicyclopentadiene was obtained from Acros Organics with 90% purity and was freshly cracked prior to use. 1,2,3,4-tetramethyl-1,3-cyclopentadiene was obtained with 85% purity from Sigma-Aldrich, stored at -24°C (in the dark) and used as supplied. 1-trimethylsilylcyclopentadiene was prepared by a previously published procedure and distilled before use.[11]

The organolithiums *n*BuLi and *t*BuLi were obtained from Sigma-Aldrich as 2.5M and 1.7M solutions in hexanes, respectively. On receipt the solution was filtered to remove LiOH. Portions (1ml) of the filtrate were quenched with 3 ml of IMS and then 5 ml of deionised water was added to dissolve the LiOH before the solution was titrated against 0.1M HCl (indicator = phenolphthalein) to determine the concentration. The solutions of *n*BuLi were typically 2.3M in hexanes and the *t*BuLi solution was 1.5M.

Borane dimethylsulfide complex (94%) was purchased from Fisher Scientific and diluted to a 2.0M solution in THF in-house. Dichlorodimethylsilane and trimethylsilane were obtained from Sigma-Aldrich and then stirred over magnesium turnings to remove HCl before distilling. The distillate was stored over magnesium turnings.

The Grignard reagents MeMgBr and ^{n}PrMgBr were obtained as 3.0M solutions in diethyl ether from Sigma-Aldrich and used as supplied. Bromine (99+% pure) was purchased from Fisher Scientific and used as received.

Trimethylphosphine, MePCl$_2$, Ph$_2$PCl and PMe$_3$ were obtained from Sigma-Aldrich and used as received. Bis(dichlorophosphino)methane, (Cl$_2$P)$_2$CH$_2$ and {(^{n}Pr)$_2$P}$_2$CH$_2$ were prepared by previously published procedures.[18,23]

2.7.1.1   NMR Spectroscopy

The NMR spectra were recorded using a Bruker Avance 300 spectrometer operating at (^{1}H 300.13; ^{13}C 75.48; ^{11}B 96.29; ^{31}P 121.49 MHz) or a Bruker Avance 400 spectrometer operating at (^{1}H 399.78; ^{13}C 100.54; ^{11}B 128.78; ^{31}P 161.83 MHz). Two-dimensional NMR experiments, HSQC and HMBC were also recorded using these instruments. Chemical shifts are quoted in ppm relative to the residual solvent peak. All NMR spectra were recorded at ambient temperature. NMR data were processed using MestReNova software.

2.7.1.2   Crystal structure determinations

Data for crystal structure determinations were collected on a Xcalibur, Atlas, Gemini ultra diffractometer at 150 K using Cu Kα radiation (λ = 1.54184 Å). Cell refinement, data collection and data reduction were undertaken via software CrysAlisPro 1.171.38.42b (Rigaku Oxford Diffraction, 2015). Intensities were corrected for absorption using CrysAlisPro. An empirical absorption correction was applied

using spherical harmonics, implemented in SCALE3 ABSPACK scaling algorithm. The structure were solved using direct methods, SHELXT and refined by SHELXL through the Olex2 interface.[24–26] All molecular graphics were generated by the author using Olex2 software.

All non-H atoms were refined anisotropically. The coordinates of H atoms were computed using a riding model constraint with the isotropic temperature factor (U_{iso}) of each H atom set to 1.2 (1.5 for methyl groups). The structures of **7**, **10** and **14** were refined with no restraints, but the structure of **19** was very disordered and convergence of the refinement required the use of restraints. The occupancies of the disordered sites were allowed to refine with isotropic atom treatment. Upon convergence of the refinement, the occupancies were fixed before anisotropy was introduced into the model. The geometries of the disordered moieties were restrained using the SAME card and the displacement parameters of all partially-occupied atoms were restrained using the SIMU card.

2.7.2   Preparation of (CpHMe$_2$Si)(Me$_3$Si)$_2$CH [**5**]

To a cold (-10°C) solution of freshly cracked Cp monomer (1.21 g, 18.29 mmol) in THF (20 ml) was added ^{n}BuLi (7.62 ml, 18.29 mmol). This reaction mixture was stirred for ca. 30 minutes and the yellow solution of LiCp was then added dropwise to a cold (-10°C) solution of (Me$_3$Si)$_2$CHSiMe$_2$Br (5.44 g, 18.29 mmol) in THF (15 ml). The reaction mixture was allowed to stir for 30 minutes and then heated under reflux for 16 h. Water (50 ml) was added and the product was extracted into diethyl ether (3 x 50 ml). The solvent was removed *in vacuo* to give a yellow oil which was dissolved in petrol (50 ml) and dried over activated 4Å molecular sieves. The solution was filtered and the solvent removed *in vacuo* to give 5 (mixture of regioisomers) as a yellow oil (yield: 3.58 g, 69.3%) which was stored at -24°C.

^{1}H NMR (300.13 MHz, CDCl$_3$, 24°C): δ -0.75, -0.55, -0.48, -0.43 ({(Cp'HMe$_2$Si)(Me$_3$Si)$_2$C*H*}, mixture of regioisomers), -0.04, 0.11, 0.13, 0.18, 0.26 (s, Si*Me$_3$*/Si*Me$_2$,* mixture of regioisomers), 2.99, 3.03 (s, Cp'*H*Me$_2$Si), 6.36, 6.50, 6.61, 6.79 (m, −Me$_2$SiCpH*H,* mixture of regioisomers).

2.7.3   Preparation of (Cp'HMe$_2$Si)(Me$_3$Si)$_2$CH [6]

To a cold (-10°C) solution of Cp'H (0.76 g, 5.48 mmol) in THF (15 ml) was added ^{n}BuLi (1.96 ml, 5.48 mmol). The reaction mixture was stirred for 30 minutes and the yellow solution of LiCp' was then added dropwise to a cold (-10°C) solution of (Me$_3$Si)$_2$CHSiMe$_2$Br (1.63 g, 5.48 mmol) in THF (30 ml). The reaction mixture was allowed to stir for 30 minutes and then heated under reflux for 16 h (79°C).

The cooled reaction mixture was added to water (50 ml) in a separating funnel and the product was extracted into diethyl ether (3 x 30 ml). The combined extracts were dried over MgSO$_4$ and filtered.

The solvent was removed *in vacuo* to give a 6 as a yellow oil, as a mixture of regioisomers (Yield = 1.26 g, 65%). It was observed during this procedure that the yellow oil did not remain dry unless stored over 4Å molecular sieves.

^{1}H NMR (300.13 MHz, CDCl$_3$, 24°C): δ -0.54, -0.51 {(CpHMe$_2$Si)(Me$_3$Si)$_2$C*H*}, mixture of regioisomers), -0.06, 0.07, 0.08, 0.13, 0.19, 0.28, 0.29 (s, Si*Me$_3$*/Si*Me$_2$,* mixture of regioisomers), 3.00 (s, Cp*H*), 6.51, 6.60, 6.61, 6.65, 6.67, 6.78 (m, CpH*H,* mixture of regioisomers).

2.7.4   Preparation of (CpH^{4Me}Me$_2$Si)(Me$_3$Si)$_2$CH [**7**]

To a cold (-10°C) solution of CpH^{4Me} (1.89 g, 15.47 mmol); (85% purity) in THF (20 ml) was added *n*BuLi (6.21 ml, 15.46 mmol). The reaction mixture was stirred for 30 min and the suspension of LiCp^{4Me} was then added dropwise to a cold (-10°C) solution of (Me$_3$Si)$_2$CHSiMe$_2$Br (4.60 g, 15.47 mmol) in THF (20 ml).§

The reaction mixture was allowed to stir for 30 min and then heated under reflux for 16h (75 °C). Water was added and the product was extracted into diethyl ether (3 x 50 ml). The solvent was removed *in vacuo* to give a yellow oil which was dissolved in petrol and dried over activated 4Å molecular sieves. The solution was filtered and the solvent removed *in vacuo* to give a yellow oil (yield: 4.28 g, 82%). Crystals of a single geometric isomer were grown from cold (-24°C) light petroleum as large colourless plates suitable for X-ray crystallography (yield: 1.16 g, 27%).

^{1}H NMR of crystalline material§ (399.78 MHz, CDCl$_3$, 23°C): -0.23 (s, 1H, CH), -0.08 (s, 6H, Si*Me$_2$*), δ 0.16 (s, 18H, Si*Me$_3$*), 1.80 (s, 6H, CpH*Me*), 1.94 (s, 6H, CpH*Me*), 3.00 (s, br, 1H, Cp*H*).

^{13}C{^{1}H} NMR of crystalline material (100.54 MHz, CDCl$_3$, 24°C): δ -0.31 (Si*Me$_2$*), 2.57 ({Me$_3$Si}$_2$*C*H, 3.68 (Si*Me$_3$*), 11.27 (CpH*Me*), 15.17 (CpH*Me*), 55.92 (*Cp*H), 133.62 (*Cp*Me), 135.93 (*Cp*Me).

§Unknown impurities in CpH^{4Me} (85%) make accurate molar measurements impractical and therefore the amount of *n*BuLi added may not be exactly one equivalent. When *n*BuLi was present in excess the reaction mixture had a yellow colour and more CpH^{4Me} was added by dropper to obtain a reaction mixture that was white to the eye. This is more important when one or both of the TMS groups is exchanged for a dimethylphosphine-borane group reducing the pK_a of the alkyl proton. It is possible that impurities carried through in the reaction mixture cause issues when the ligand is doubly deprotonated with a strong base (MeK). Repetition of the synthesis using NaCp^{4Me} purified by recrystallization to increase yields and make crystallisation of the products easier with a cleaner synthesis.

2.7.5 Preparation of (Me$_3$Si){PMe$_2$(BH$_3$)}CH$_2$ [8]

To a cold (0°C) solution of PMe$_3$ (7.35 ml, 72.3 mmol) in THF (10 ml) in a greaseless Schlenk was added BH$_3$·SMe$_2$ (36.5 ml, 73.0 mmol). ^{n}BuLi (29.0 ml, 72.3 mmol) was added slowly to the cooled (0°C) solution of *in situ* generated Me$_3$PBH$_3$ and the reaction mixture was stirred for 3 hr [^{31}P{^{1}H} NMR (no solvent): δ 0.56 (m, J_{PB} = 84 Hz)]. ^{11}B{^{1}H} NMR (no solvent): δ -33.93 (d, J_{PB} = 84 Hz)]. This solution of Me$_2$P(BH$_3$)CH$_2$Li was added to a cold (0°C) solution of Me$_3$SiCl (79.08 mmol, 10.09 ml) in THF (25 ml) and allowed to warm to room temperature with stirring for 1 h. The solvent was removed *in vacuo*, the product was extracted into diethyl ether (30 ml) and the solvent was removed from the filtrate *in vacuo*. The slightly sticky white solid was purified by sublimation onto a water cooled condenser (55°C, <0.01 mmHg) to give Me$_2$P(BH$_3$)CH$_2$SiMe$_3$ as a bright white crystalline solid (yield 10.0 g, 81%).

^{1}H{^{11}B} NMR (300.13 MHz, CDCl$_3$, 24°C): δ 0.18 (s, 9H, SiMe$_3$), 0.55 (d, J_{PH} = 16.21 Hz, 3H, BH$_3$), 0.93 (d, J_{PH} = 14.89 Hz, 2H, CH$_2$), 1.33 (d, J_{PH} = 10.24 Hz, 6H, PMe$_2$).

^{11}B{^{1}H} NMR (96.3 MHz, CDCl$_3$, 24°C): δ -36.6 (d, J$_{PB}$ = 65 Hz).

^{31}P{^{1}H} NMR (121.49 MHz, CDCl$_3$, 24°C): δ 2.7 (q, J$_{PB}$ = 65 Hz).

2.7.6 Preparation of {Me$_2$P(BH$_3$)}(SiMe$_2$Cl)CHSiMe$_3$ [9]

To a cold (0°C) solution of **8** (10.0 g, 62.8 mmol) in THF (15 ml) was added ^{n}BuLi (24.8 ml, 61.8 mmol). The reaction mixture was allowed to warm to room temperature and stirred for 1 h. The solution of [Me$_2$P(BH$_3$)CHSiMe$_3$]Li was then added dropwise to a solution of Me$_2$SiCl$_2$(14.9 ml, 123.6 mmol) in THF (30 ml). The reaction was stirred for 2 h and then the solvent was removed *in vacuo*. The product was extracted into DCM (40 ml), filtered and the solvent removed *in vacuo*

from the filtrate, giving a white solid. Yield 14.9 g, 93%. Crystals suitable for X-ray crystallography were grown from Et_2O at 4°C.

^1H NMR (300.13 MHz, $CDCl_3$, 24°C): δ 0.43 (s, 9H, Si*Me$_3$*), 0.78 (s, 3H, Si*Me$_A$*Me$_B$Cl), 0.80 (s, 3H, SiMe$_A$*Me$_B$*Cl), 0.84 (d, J_{PH} = 16.58 Hz, 1H, C*H*), 1.58 (d, 3H, J_{PH} = 9.7 Hz, BH_3P*Me$_A$*Me$_B$), 1.61 (d, 3H, J_{PH} = 9.7 Hz, BH_3PMe$_A$*Me$_B$*).

$^{13}C\{^1H\}$ NMR (75 MHz, $CDCl_3$, 25°C): δ 2.94 (d, $^3J_{PC}$ = 2.3 Hz, Si*Me$_3$*), 6.43 (m, Si*Me$_A$*Me$_B$Cl), 16.20 (d, J_{PC} = 5.05 Hz, *C*H), 16.74 (d, J_{PC} = 5.22 Hz, BH_3P*Me$_A$*Me$_B$), 17.24 (d, J_{PC} = 5.60 Hz, BH_3PMe$_A$*Me$_B$*).

$^{11}B\{^1H\}$ NMR (96.3 MHz, $CDCl_3$, 24°C): δ -34.8 (d, J_{PB} = 62 Hz). $^{31}P\{^1H\}$ NMR (121.49 MHz, $CDCl_3$, 24°C): δ 6.0 (q, J_{PB} = 62 Hz).

2.7.7 Preparation of $(CpH^{4Me}Me_2Si)(Me_3Si)CH\{PMe_2(BH_3)\}$ [10]

To a cold (-10°C) solution of CpH^{4Me} (2.58 g, 21.1 mmol) (85% purity) in THF (25 ml) was added ^nBuLi (7.20 ml, 17.9 mmol). The reaction mixture was stirred for 30 min and the suspension of $LiCp^{4Me}$ was then added dropwise to a cold (-10°C) solution of **9** (4.15 g, 16.3 mmol) in THF (20 ml).[§] The reaction mixture was allowed to stir for 30 min and then heated under reflux for 16 h (75°C). After cooling, the reaction mixture was added to water (50 ml) and the product was extracted into dichloromethane (3 x 50 ml). The solvent was removed *in vacuo* to give a white solid and a yellow oil. The oil was dissolved in petrol to give a fluorescent yellow solution and this was decanted, leaving a white solid. The solid was dissolved in diethylether and dried over activated 4Å molecular sieves. Large crystals suitable for X-ray crystallography were grown from a concentrated solution (20 ml) in diethyl ether at -24°C. Crystalline yield: 2.61g, 47%.

^1H NMR (300.13 MHz, $CDCl_3$, 24°C): δ 0.18 (s, 3H, Si*Me$_A$*Me$_B$), 0.24 (s, 3H, SiMe$_A$*Me$_B$*), 0.29 (s, 9H, Si*Me$_3$*), 0.58 (d, J_{PH} = 18.27 Hz, 1H, C*H*), 0.76 (m, 1H, Cp*H*), 1.07 (d, J_{PH} =

6.76 Hz, 3H, BH$_3$PMe_AMe$_B$), 1.08 (d, J_{PH} = 6.76 Hz, 3H, BH$_3$PMe$_A$$Me_B$), 1.53 (m, 12H, CpH$\underline{Me}$).

^{13}C{^{1}H} NMR (75 MHz, CDCl$_3$) δ -1.54, -1.50 (Si$Me_A$$Me_B$), 3.54 (d, $^3J_{PC}$ = 2.73Hz, SiMe_3), 6.05 (d, J_{PC} = 8.33 Hz, {PMe$_2$BH$_3$}{Me$_3$Si}CH), 11.95 (CpHMe), 12.48 (CpHMe), 23.46 (d, J_{PC} = 5.09 Hz, BH$_3$PMe_AMe$_B$) 39.51(d, $^3J_{PC}$ = 2.90 Hz, CpH), 46.04, 134.44 (CpMe).

^{11}B{^{1}H} NMR (CDCl$_3$): δ -15.4 (br) ^{31}P{^{1}H} NMR (CDCl$_3$): δ -0.5 (br)

2.7.8   Preparation of Me(^{n}Pr)$_2$PBH$_3$ [11]

To a cold (-78°C) solution of MePCl$_2$ (1.05 ml, 11.87 mmol) in Et$_2$O (20 ml) was added dropwise ^{n}PrMgCl (12.0 ml, 23.74 mmol) and the reaction was stirred for 16 h and allowed to warm to room temperature. BH$_3$·SMe$_2$ (5.94 ml, 11.87 mmol) was then added and the reaction mixture was stirred for 4 h. The product was extracted into Et$_2$O (3 x 15 ml) during aqueous work-up with deoxygenated water (20 ml). The solvent was removed from the combined ether extracts *in vacuo* to give Me(^{n}Pr)$_2$PBH$_3$ [11] as a colourless. Yield 1.72 g, 99%.

^{1}H{^{11}B} NMR (400 MHz, CDCl$_3$, 22°C): δ 0.38 (d, $^2J_{PH}$ = 16.03 Hz, 3H, BH_3), 0.99 (m, 6H, -PCH$_2$CH$_2$CH_3), 1.19 (d, 3H, $^2J_{PH}$ = 10.22 Hz, PCH_3), 1.52 (m, 8H, -PCH_2CH_2CH$_3$).

^{13}C{^{1}H} NMR (100.54 MHz, CDCl$_3$, 22°C): δ 8.90 (d, J_{PC} = 36.8 Hz, P$\underline{Me}$), 15.91 (d, $^3J_{PC}$ = 13.3 Hz, -PCH$_2$CH$_2$$\underline{C}H_3$), 16.45 (d, $^2J_{PC}$ = 1.96 Hz, -PCH$_2$$\underline{C}H_2CH_3$), 27.32 (d, J_{PC} = 35.82 Hz, -P$\underline{C}$H$_2$CH$_2$CH$_3$).

^{11}B{^{1}H} NMR (128.3 MHz, CDCl$_3$, 24°C): δ -39.7 (d, J_{PB} = 62.6 Hz).

^{31}P{^{1}H} NMR (161.83 MHz, CDCl$_3$, 24°C): δ 8.7 (q, J_{PB} = 62.6 Hz)

2.7.9   Preparation of {^{n}Pr$_2$P(BH$_3$)}CH$_2$SiMe$_3$ [12]

To a cooled solution (0°C) of **11** in THF (30 ml) in a greaseless schlenk flask was added ^{n}BuLi (5.12ml, 11.78 mmol) to give a yellowish-orange solution which was stirred for 4 h. This solution was added to a cooled (0°C) solution of Me$_3$SiCl (1.64 ml, 12.95 mmol) in THF (40 ml). The solvent was removed *in vacuo* and the product was extracted into dichloromethane (30 ml) and the filtered to remove LiCl. The solvent was removed *in vacuo* from the filtrate to give a viscous, colourless, oily liquid. Yield 1.79 g, 70%.

^{1}H{^{11}B} NMR (400 MHz, CDCl$_3$, 22°C): δ 0.14 (s, 9H, Si*Me$_3$*), 0.43 (d, $^2J_{PH}$ = 15.7 Hz, 3H, B*H$_3$*), 0.81 (d, $^2J_{PH}$ = 14.7 Hz, 2H, -PC*H$_2$*SiMe$_3$), 0.99 (m, 6H, -PCH$_2$CH$_2$C*H$_3$*), 1.51 (m, 8H, -PC*H$_2$*C*H$_2$*CH$_3$).

^{13}C{^{1}H} NMR (100.54 MHz, CDCl$_3$, 22°C): δ 0.77 (Si*Me$_3$*), 10.60 (d, J_{PC} = 23.1 Hz, P*Me*), 15.98 (d, $^3J_{PC}$ = 13.8 Hz, -PCH$_2$CH$_2$*C*H$_3$), 16.45 (d, $^2J_{PC}$ = 2.5 Hz, PCH$_2$*C*H$_2$CH$_3$), 28.58 (d, J_{PC} = 34.9 Hz, -P*C*H$_2$CH$_2$CH$_3$).

^{11}B{^{1}H} NMR (128.3 MHz, CDCl$_3$, 22°C): δ -38.9 (d, J_{PB} = 63.0 Hz).

^{31}P{^{1}H} NMR (161.83 MHz, CDCl$_3$, 22°C): δ 13.4 (q, J_{PB} = 63.0 Hz)

2.7.10   Preparation of {^{n}Pr$_2$P(BH$_3$)}(SiMe$_2$Cl)CHSiMe$_3$ [13]

To a cold (0°C) solution of **12** in THF (40 ml) was added ^{n}BuLi (3.57 ml, 8.30 mmol) and the reaction mixture was stirred overnight to give a dull orange solution. This solution of [(Me$_3$Si)CH{P^{n}Pr$_2$(BH$_3$)}]Li was monitored for purity by ^{31}P{^{1}H} NMR (q, 9.62 ppm, J_{PB} = 88.5 Hz) and ^{11}B{^{1}H} NMR (d, -35.9 ppm, J_{PB} = 88.5 Hz), and was then transferred dropwise to a cold (-78°C) solution of Me$_2$SiCl$_2$ (1.98ml, 16.43 mmol) in THF (40 ml). The reaction mixture was stirred overnight and allowed to warm to room temperature. The solvent was removed *in vacuo* and the product was

extracted into DCM (30 ml). After filtration to remove LiCl, removal of the solvent *in vacuo* gave a white solid **13**. Yield 2.35 g, 92%.

^{1}H{^{11}B} NMR (400 MHz, C_6D_6, 23.5°C): δ 0.26 (s, 9H, Si*Me$_3$*), 0.57 (s, 3H, Si*Me$_A$*Me$_B$Cl), 0.63 (s, 3H, SiMe$_A$*Me$_B$*Cl), 0.68 (d, $^2J_{PH}$ = 15.7 Hz, 1H, -PC*H*{SiMe$_2$Cl}SiMe$_3$), 0.79 (m, 6H, -PCH$_2$CH$_2$C*H$_3$*), 1.27 (d, $^2J_{PH}$ = 13.0 Hz, 3H, BH$_3$), 1.56 (m, 8H, -PC*H$_2$CH$_2$*CH$_3$).

^{13}C{^{1}H} NMR (100.54 MHz, C_6D_6, 23.5°C): δ 3.33 (d, $^3J_{PC}$ = 1.9 Hz, Si*Me$_3$*), 6.58 (d, $^3J_{PC}$ = 1.5 Hz, Si*Me$_A$*Me$_B$Cl), 7.05 (s, SiMe$_A$*Me$_B$*Cl), 12.51 (d, J_{PC} = 2.45 Hz, P*C*H{SiMe$_2$Cl}SiMe$_3$), 15.97 (d, $^3J_{PC}$ = 13.9 Hz, -P(^{n}Pr$_B$)C$_A$H$_2$C$_A$H$_2$*C$_A$*H$_3$), 15.99 (d, $^3J_{PC}$ =13.7 Hz, -P(^{n}Pr$_A$)C$_B$H$_2$C$_B$H$_2$*C$_B$*H$_3$), 28.79 - 29.39 (m, -P(*C$_B$*H$_2$C$_B$H$_2$C$_B$H$_3$){*C$_A$*H$_2$C$_A$H$_2$C$_A$H$_3$}), 17.11 − 17.19 Hz (m, -P(C$_B$H$_2$*C$_B$*H$_2$C$_B$H$_3$){C$_A$H$_2$*C$_A$*H$_2$C$_A$H$_3$}).

^{11}B{^{1}H} NMR (128.3 MHz, C_6D_6, 23.5°C): δ -36.8 (d, J_{PB} = 55.0 Hz).

^{31}P{^{1}H} NMR (161.83 MHz, C_6D_6, 23.5°C): δ 18.4 (br, J_{PB} = 55.0 Hz)

2.7.11 Preparation of (CpH^{4Me}Me$_2$Si)(Me$_3$Si)CH{P^{n}Pr$_2$(BH$_3$)} [**14**]

A cold (-10°C) solution of KCp^{4Me} (1.21 g, 7.56 mmol) in THF (40 ml) was added dropwise to a cold (-10°C) solution of **13** (2.35 g, 7.56 mmol) in THF (15 ml). The reaction mixture was allowed to stir for 30 min and then heated under reflux for 16 h (75°C). After the reaction mixture had cooled the solvent was removed *in vacuo* and the product was extracted into Et$_2$O (40 ml) and filtered to remove KCl. Upon cooling to 3°C a fine white powder precipitated, which was identified as excess KCp^{4Me}. The solvent was removed from the mixture *in vacuo* and the product was extracted into light petroleum (ml) and filtered to remove the excess KCp^{4Me}. The solution was concentrated (12 ml) and colourless crystals of **14** suitable for X-ray crystallography were grown from light petroleum at 3°C. Crystalline yield: 1.79 g, 60%.

^{1}H{^{11}B} NMR (400 MHz, CDCl$_3$, 25.5°C): δ -0.06 (s, 3H, SiMe_AMe$_B$), 0.26 (s, 3H, SiMe$_A$$Me_B$), 0.29 (s, 3H, Si$Me_3$), 0.68 (d, $^2J_{PH}$ = 14.30 Hz, 3H, BH_3), 0.93 (d, $^2J_{PH}$ = 16.8 Hz, 1H, (CpH^{4Me}Me$_2$Si)(Me$_3$Si)CH\{P^{n}Pr$_2$(BH$_3$)\}), 1.03 (m, 6H, -P(C$_B$H$_2$C$_B$H$_2$C$_B$$H_3$)\{C$_AH_2C_AH_2C_A$$H_3$\}), 1.40 − 1.77 (m, 8H, -P(C$_B$$H_2C_B$$H_2C_BH_3$)\{C$_A$$H_2C_A$$H_2C_AH_3$\}), 1.80 (s, 6H, Cp^{4Me}HMe_A), 1.96 (s, 6H, Cp^{4Me}HMe_B), 3.40 (m, 1H, Cp^{4Me}H).

^{13}C{^{1}H} NMR (100.53 MHz, CDCl$_3$, 23.5°C): δ -1.32 (d, $^4J_{PC}$ = 4.6 Hz, SiMe_AMe$_B$Cp^{4Me}H), 0.76 (s, SiMe$_A$$Me_B$Cp^{4Me}H), 3.80 (d, $^4J_{PC}$ = 2.1 Hz, SiMe_3), 6.26 (d, $^2J_{PC}$ = 3.4 Hz, (CpH^{4Me}Me$_2$Si)(Me$_3$Si)CH\{P^{n}Pr$_2$(BH$_3$)\}), 11.26 (d, $^6J_{PC}$ = 9.4 Hz, Cp^{4Me}HMe_A), 15.12 (d, $^6J_{PC}$ = 22.7 Hz, Cp^{4Me}HMe_B), 16.10 − 16.28 (m, P(C$_B$H$_2$C$_B$H$_2$$\underline{C_B}H_3$)\{C$_AH_2C_AH_2$$\underline{C_A}H_3$\}), 16.95 − 17.08 (m, P(C$_B$H$_2$$\underline{C_B}H_2C_BH_3$)\{C$_AH_2$$\underline{C_A}H_2C_AH_3$\}), 28.74 − 29.67 (m, P($\underline{C_B}$H$_2$C$_B$H$_2$C$_B$H$_3$)\{$\underline{C_A}$H$_2$C$_A$H$_2$C$_A$H$_3$\}), 55.12 (s, ($\underline{C}$H)Cp^{4Me}), 133.18 (d, J_{PC} = 5.13 Hz, (CMe)Cp^{4Me}H), 136.76 (d, J_{PC} = 21.2 Hz, (CMe)Cp^{4Me}H).

^{11}B{^{1}H} NMR (128.3 MHz, CDCl$_3$, 23.5°C): δ -37.1 (d, J_{PB} = 52.5 Hz).

^{31}P{^{1}H} NMR (161.83 MHz, CDCl$_3$, 23.5°C): δ 19.5 (br, J_{PB} = 52.5Hz)

2.7.12   Preparation of \{PMe$_2$(BH$_3$)\}$_2$CH$_2$ [21]

To a cold (-78°C) solution of (PCl$_2$)$_2$CH$_2$ (2.71 g, 12.44 mmol) in diethyl ether (25 ml) was added MeMgBr (18.32 ml, 54.96 mmol) dropwise and the reaction mixture was allowed to stir overnight and warm to room temperature. BH$_3$·SMe$_2$ (12.44 ml, 24.88 mmol) was added and the reaction mixture was stirred overnight.

Water (50ml) was very cautiously added and the ether layer decanted before extraction of the aqueous layer with DCM (2 x 50ml). Removal of the solvent from the combined organic extracts by rotary evaporation gave a white solid, which was dissolved in DCM (40 ml) and dried over 4Å molecular sieves. The solvent was

removed by rotary evaporation and the product purified by recrystallization from a (1:8) mixture of Et_2O and DCM at -24°C. Colourless crystals of $\{PMe_2(BH_3)\}_2CH_2$ [**21**] were isolated by filtration. Isolated yield 1.77 g, 87%.

$^1H\{^{11}B\}$ NMR of crystalline material (300.13 MHz, $CDCl_3$, 24°C): δ 0.61 (d, $^2J_{PH}$ = 15.38 Hz, 6H, BH_3), 1.52 (d, $^2J_{PH}$ = 10.24 Hz, 6H, P*Me$_2$*), 1.99 (t, $^2J_{PH}$ = 11.26 Hz, 2H, PC*H$_2$*P).

$^{31}P\{^1H\}$ NMR of crystalline material (121.49 MHz, $CDCl_3$, 24°C): δ 6.67 (q, J_{PB} = 57.5 Hz).

$^{11}B\{^1H\}$ NMR (96.29 MHz, $CDCl_3$, 24°C) δ -36.7 (d, J_{PB} = 57.5 Hz).

2.7.13   Preparation of $\{PMe_2(BH_3)\}_2CHSiMe_2Cl$ [**23**]

To a cold (0°C) solution of **21** (1.71 g, 10.44 mmol) in THF (60 ml) was added ^{n}BuLi (4.55 ml, 10.44 mmol) and the reaction mixture was stirred overnight. The resulting solution was added dropwise to a cold (-78°C) solution of Me_2SiCl_2 (6.30 ml, 52.20 mmol) in THF (40 ml) over ca. 1.5 h. The reaction was allowed to warm to room temperature and was stirred overnight before the solvent was removed *in vacuo*. The product **23** was extracted into DCM (35 ml) and separated from the precipitated LiCl by filtration. The DCM was removed *in vacuo* to give **23** as a white solid. Yield 2.42 g, 90%.

$^1H\{^{11}B\}$ NMR (300.13 MHz, $CDCl_3$, 24°C): δ 0.73 (d, $^2J_{PH}$ = 13.02 Hz, 6H, BH_3), 0.82 (s, 6H, -Si*Me$_2$*Cl), 1.57 (t, $^2J_{PH}$ = 13.26 Hz, 1H, PC*H*P), 1.65 (d, $^2J_{PH}$ = 9.4 Hz, 6H, BH_3P*Me$_A$*Me$_B$), 1.68 (d, $^2J_{PH}$ = 9.6 Hz, 6H, BH_3PMe$_A$*Me$_B$*).

$^{13}C\{^1H\}$ NMR (75.5 MHz, $CDCl_3$, 24°C): δ 6.52 (Si*Me$_2$*), 14.43 (d, J_{PC} = 41Hz, BH_3P*Me$_A$*Me$_B$), 14.75 (d, J_{PC} = 38.8 Hz, BH_3PMe$_A$*Me$_B$*), 22.50 (t, J_{PC} = 3.85 Hz, P$\underline{C}$HP).

$^{11}B\{^1H\}$ NMR (96.29 MHz, CDCl$_3$, 24°C) δ -32.9 (d, J_{PB} = 49.1 Hz).

$^{31}P\{^1H\}$ NMR (121.49 MHz, CDCl$_3$, 24°C): δ 11.5 (br q, J_{PB} = 49.1 Hz).

2.7.14   Preparation of {PMe$_2$(BH$_3$)}{PPh$_2$(BH$_3$)}CH$_2$ [**25**]

To a cold (-78°C) solution of Ph$_2$PCl (5.15 ml, 28.09 mmol) in THF (15 ml) in a greaseless Schlenk flask was added Me$_2$PBH$_3$CH$_2$Li (28.09 mmol) as a solution in THF (40 ml). The reaction mixture was allowed to stir for 12 hours while warming slowly to room temperature. The orange-coloured reaction mixture was cooled to 0°C and excess Me$_2$S·BH$_3$ (21.72 ml, 36.5 mmol) was added. The solvent was removed *in vacuo* and the product was washed with ca. 15 ml of Et$_2$O to remove a yellow oily impurity. The product was extracted into DCM (30 ml) and decanted from the LiCl. The solvent was removed *in vacuo* to give a white solid (Yield 6.06 g, 75%).

$^1H\{^{11}B\}$ NMR (400MHz, CDCl$_3$, 23°C): δ 0.52 (d, $^2J_{PH}$ = 15.8 Hz, 3H, B*H*$_3$PMe$_2$), 1.15 (d, $^2J_{PH}$ = 15.4 Hz, 3H, B*H*$_3$PPh$_2$), 1.36 (d, $^2J_{PH}$ = 10.2 Hz, 6H, BH$_3$P*Me*$_2$), 2.64 (m, 2H, PC*H*P'), 7.62 (m, 10H, BH$_3$P*Ph*$_2$).

$^{11}B\{^1H\}$ NMR (128.27 MHz, CDCl$_3$, 23°C): -38.3 Hz (br d, J_{PB} = 48.5 Hz, PPh$_2$*B*H$_3$), -35.4 (br d, 61 Hz, PMe$_2$*B*H$_3$).

$^{31}P\{^1H\}$ NMR (162 MHz, CDCl$_3$, 23°C): 8.5 (br d, J_{PB} = 61.0 Hz, *P*Me$_2$BH$_3$), 11.8 (br d, J_{PB} = 48.5 Hz, *P*Ph$_2$BH$_3$).

2.7.15   Preparation of {PMe$_2$(BH$_3$)}{PPh$_2$(BH$_3$)}CHSiMe$_2$Cl [**27**]

To a cold (0°C) solution of **25** (4.85 g, 16.84 mmol) in THF (20 ml) was added ^{n}BuLi (7.3 ml, 16.84 mmol) and this mixture was stirred for 1 hour. The reaction mixture was then added to a cold (-78°C) solution of Me$_2$SiCl$_2$ (10.87 ml, 90 mmol) in THF (25 ml) and stirred for 16 h while warming to room temperature. The solvent was

removed *in vacuo* and the product was extracted into DCM (30 ml) and filtered to remove the LiCl. The solvent was removed from the filtrate *in vacuo* to give a white solid **27**. Yield = 4.98g, 78%.

^{1}H{^{11}B} NMR (CDCl$_3$, 23°C): δ 0.40 (s, 3H, Si*Me$_A$*Me$_B$Cl), 0.54 (s, 3H, SiMe$_A$*Me$_B$*Cl), 0.76 (d, $^2J_{PH}$ = 13.8 Hz, 3H, B*H$_3$*PMe$_A$Me$_B$), 1.08 (d, $^2J_{PH}$ = 9.6 Hz, 3H, BH$_3$P*Me$_A$*Me$_B$), 1.35 (d, $^2J_{PH}$ = 13.9 Hz, 3H, B*H$_3$*PPh$_A$Ph$_B$), 1.63 (d, $^2J_{PH}$ = 9.8 Hz, 3H, BH$_3$PMe$_A$*Me$_B$*), 2.82 (m, 1H, PC*H*P), 7.48 (m, 5H, BH$_3$P*Ph$_A$*Ph$_B$), 7.89 (m, 5H, BH$_3$PPh$_A$*Ph$_B$*).

^{11}B{^{1}H} NMR (128.27 MHz, CDCl$_3$, 23°C): -38.4 (br, PPh$_2$BH$_3$), -32.6 (br, PMe$_2$BH$_3$).

^{31}P{^{1}H} NMR (161.83 MHz, CDCl$_3$, 23°C): 14.3 (d, J_{PB} = 61.8 Hz, *P*Me$_2$BH$_3$), 12.7 (d, J_{PB} = 53.2 Hz, *P*Ph$_2$BH$_3$).

2.7.16   Preparation of {PPh$_2$(BH$_3$)}$_2$CH$_2$ [**29**]

To a cold (0°C) solution of **28** (2.55g, 6.63 mmol) in toluene (25 ml) was added BH$_3$·SMe$_2$ (7.90 ml, 13.27 mmol) as a solution in toluene. The reaction mixture was allowed to stir for 12 h before the solvent was removed *in vacuo* to give **29** as a white solid in quantitative yield.

^{1}H{^{11}B} NMR (CDCl$_3$, 23°C): δ 0.92 (d, 6H, B*H$_3$*), 3.25 (t, 2H, C*H$_2$*), 7.31 – 7.66 (m, 20H, Ar*H*).

^{31}P{^{1}H} NMR (121.49 MHz, CDCl$_3$, 24°C): δ 14.6 (br m). ^{11}B{^{1}H} NMR (CDCl$_3$): δ -37.44 (br d).

2.7.17   Preparation of {PPh$_2$(BH$_3$)}$_2$CHSiMe$_2$Cl [**31**]

A portion of [**29**] (1.52g, 3.69 mmol) was dissolved in DME (25 ml), to this solution was added *n*BuLi (1.60ml, 3.69 mmol) and the reaction was monitored by NMR.

^{31}P{^{1}H} NMR 14.54 (m); ^{11}B{^{1}H} NMR (no solvent): δ -33.21 (d, J_{PB} = 56.73 Hz).

This solution of [**30**] was added dropwise to a room temperature solution of Me$_2$SiCl$_2$ (0.89 ml, 7.38 mmol) in DME (30 ml). The expected product **31** could not be isolated; ^{11}B and ^{31}P NMR data indicate that multiple species were produced.

2.7.18   Preparation of {(^{n}Pr)$_2$P}$_2$CHSiMe$_2$Cl [**32**]

To a solution of {(^{n}Pr)$_2$P}$_2$CH$_2$ (3.93 g, 15.83 mmol) in light petroleum (20 ml) at room temperature was added ^{t}BuLi (9.31 ml, 15.83 mmol) and the reaction mixture was left to stir overnight. The solvent was removed from the white slurry of {(^{n}Pr)$_2$P}$_2$HCLi *in vacuo* and the residue was dissolved in THF (50 ml). This solution was added dropwise to a cold (-78°C) solution of Me$_2$SiCl$_2$ (9.5 ml, 79.0 mmol) in THF (30 ml). The reaction was allowed to warm to room temperature and was stirred overnight before the solvent was removed *in vacuo*. The product was extracted into diethyl ether (30 ml) and separated from the LiCl by filtration. Removal of the solvent from the filtrate gave a crude product which was contaminated by a small amount of {(^{n}Pr)$_2$P}$_2$CH$_2$. This contaminant was distilled off (oil bath temperature 125 °C, 10^{-2} Torr) to give **32** as a viscous golden-yellow oil. Yield 3.04 g, 59%.

^{1}H NMR (300.13 MHz, CDCl$_3$, 25°C): δ 0.45 (s, 6H, -Si*Me$_2$*Cl), 0.59 (t, $^2J_{PH}$ = 3.4 Hz, 1H PC*H*P), 0.90 (br, $^4J_{PH}$ = 7.4 Hz, 12H, -PCH$_2$CH$_2$C*H$_3$*), 1.25 − 1.40 (m, 8H, -PCH$_2$C*H$_2$*CH$_3$), 1.46 − 1.68 (m, 8H, -PC*H$_2$*CH$_2$CH$_3$).

^{13}C{^{1}H} NMR (75.48 MHz, CDCl$_3$, 25°C): δ 5.03 (t, $^3J_{PC}$ = 3.2 Hz, -Si*Me$_2$*Cl), 15.65 − 15.87 (m, -PCH$_2$CH$_2$*C*H$_3$), 18.55 (t, J_{PC} = 42.8 Hz, P*C*HP), 19.82 − 20.28 (m, -PCH$_2$*C*H$_2$CH$_3$), 28.70 − 29.20 (m, -P*C*H$_2$CH$_2$CH$_3$).

^{31}P{^{1}H} NMR (121.49 MHz, CDCl$_3$, 25°C): δ -25.4 (s).

2.7.19   Preparation of (CpKMe$_2$Si)(^{n}Pr$_2$P)$_2$CH [**34**]

To a cold (-10°C) solution of **32** (1.04 g, 3.05 mmol) in THF (20 ml) was added a solution of NaCp (0.32 g, 3.66 mmol) in THF (15 ml). Immediate formation of a white precipitate was observed and the reaction mixture was allowed to stir overnight and attain room temperature. The solvent was removed *in vacuo* and the product extracted into light petroleum (30 ml). This solution was filtered to afford separation of the product from NaCl and excess NaCp. The solvent was removed *in vacuo* from the filtrate to give **33** as an extremely viscous golden oil, which was immediately dissolved in THF (20 ml) and added slowly to a cold (0°C) slurry of KH (0.15 g, 3.66 mmol) in THF (20 ml). The reaction mixture was stirred overnight and allowed to warm to room temperature, before filtering to remove excess KH. The solvent was removed from the filtrate *in vacuo* and the product was desolvated by heating (80°C) under vacuum (10^{-2} Torr), to give **34** as a fine beige powder. Yield 0.95 g, 76%.

^{1}H NMR (300.13 MHz, C$_6$D$_6$/d$_8$-THF (referenced to benzene), 25°C): δ 0.42 (s, 6H, -Si*Me$_2$*Cl), 0.96 (t, $^2J_{PH}$ = 4.6 Hz, 1H, PC*H*P), 1.05 (t br, $^4J_{PH}$ = 7.3 Hz, 12H, -PCH$_2$CH$_2$C*H$_3$*), 1.46 − 1.60 (m, 8H, -PCH$_2$C*H$_2$*CH$_3$), 1.60 − 2.00 (m, 8H, -PC*H$_2$*CH$_2$CH$_3$).

^{13}C{^{1}H} NMR (75.48 MHz, C$_6$D$_6$/d$_8$-THF (referenced to benzene), 25°C): δ 3.71 (t, $^3J_{PC}$ = 3.0 Hz, -Si*Me$_2$*Cl), 16.32 (d, $^3J_{PC}$ = 1.9 Hz, -PC$_A$H$_2$C$_A$H$_2$*C$_A$*H$_3$), 16.49 (d, $^3J_{PC}$ = 2.1 Hz, -PC$_B$H$_2$C$_B$H$_2$*C$_B$*H$_3$), 20.95 (d, $^2J_{PC}$ = 20.1 Hz, -PC$_A$H$_2$*C$_A$*H$_2$C$_A$H$_3$), 21.02 (d, $^2J_{PC}$ = 19.6 Hz, -PC$_B$H$_2$*C$_B$*H$_2$C$_B$H$_3$), 30.01 (m, -P*C*H$_2$CH$_2$CH$_3$), 108.72 ({CH}Cp), 112.01 ({C}Cp), 112.35 ({CH}Cp).

^{31}P{^{1}H} NMR (121.49 MHz, C$_6$D$_6$/d$_8$-THF , 25°C): δ -23.6.

Elemental analysis (%) calculated for: C$_{20}$H$_{39}$KP$_2$Si: C 58.78, H 9.6; found C 54.60. H 8.87.

2.8   References

(1)   Eaborn, C.; Hitchcock, P. B.; Izod, K.; Lu, Z.-R.; Smith, J. D. *Organometallics* **1996**, *15*, 4783.

(2)   Eaborn, C.; Hill, M. S.; Hitchcock, P. B.; Smith, J. D.; Zhang, S.; Ganicz, T. *Organometallics* **1999**, *18*, 2342.

(3)   Bowman, L. J.; Izod, K.; Clegg, W.; Harrington, R. W. *Organometallics* **2007**, *26*, 2646.

(4)   Fieser, M. E.; Macdonald, M. R.; Krull, B. T.; Bates, J. E.; Ziller, J. W.; Furche, F.; Evans, W. J. *J. Am. Chem. Soc.* **2015**, *137*, 369.

(5)   Eaborn, C.; B. Hitchcock, P. *Chem. Commun.* **1997**, *9*, 1961.

(6)   Cheng, J.; Takats, J.; Ferguson, M. J.; McDonald, R. *J. Am. Chem. Soc.* **2008**, *130*, 1544.

(7)   Wiberg, N.; Wagner, G.; Müller, G.; Riede, J. *J. Organomet. Chem.* **1984**, *271*, 381.

(8)   Seyferth, D.; Lang, H. *Organometallics* **1991**, *10*, 551.

(9)   Gupta, S. K.; Yumnam, S.; Hitchcock, P. B. *J. Mol. Struct.* **2012**, *1018*, 137.

(10)   Odera, R.; Garratt, S.; Saly, M.; Kanjolia, R. Molybdenum allyl complexes and use thereof in thin film deposition. PCT/US2013/022260, Patent.

(11)   Kraihanzel, C. S.; Losee, M. L. *J. Am. Chem. Soc.* **1968**, *90*, 4701.

(12)   Izod, K.; Wills, C.; Anderson, E.; Harrington, R. W.; Probert, M. R. *Organometallics* **2014**, *33*, 5283.

(13)   Izod, K.; Wills, C.; Clegg, W.; Harrington, R. W. *Organometallics* **2007**, *26*, 2861.

(14)   *CRC handbook of chemistry and physics*, 84th ed.; Lide, D. R., Ed.; CRC Press, **2003**;

(15)   Izod, K.; Wills, C.; Clegg, W.; Harrington, R. W. *Organometallics* **2006**, *25*, 5326.

(16) Antipin, M. Y.; Chernega, A. N.; Struchkov, Y. T.; Romanenko, V. D. *Met. Khimiya* **1991**, *4*, 358.

(17) Peterson, J. K.; MacDonald, M. R.; Ziller, J. W.; Evans, W. J. *Organometallics* **2013**, *32*, 2625.

(18) Hietkamp, S.; Sommer, H.; Stelzer, O.; Balch, A. L.; Linehan, J. C.; Oram, D. E. *Inorg. Synth.* **1989**, *25*, 120 - 121

(19) Schumann, H.; Muller, J. *J. Organomet. Chem.* **1978**, *146*, C5.

(20) Langer, J.; Görls, H. *Dalt. Trans.* **2014**, *43*, 458

(21) Blug, M.; Grünstein, D.; Alcaraz, G.; Sabo-Etiene, S.; Le Goff, X-F.; Le Floch, P.; Mézailles, N. *Chem. Commun.* **2009**, *53,* 4432

(22) Langer, J.; Pálfi, V. K.; Görls, H.; Reiher, M.; Westerhausen, M. *Chem. Commun.* **2013**, *49,* 1121

(23) Izod, K.; McFarlane, W.; Tyson, B. V. *European J. Org. Chem.* **2004**, *2004*, 1043.

(24) Dolomanov, O. V.; Bourhis, L. J.; Gildea, R. J.; Howard, J. A. K.; Puschmann, H. *J. Appl. Crystallogr.* **2009**, *42*, 339.

(25) Sheldrick, G. M. *Acta Crystallogr. Sect. A* **2007**, *A64*, 112.

(26) Sheldrick, G. M. *Acta Crystallogr. Sect. A* **2015**, *A71*, 3.

Chapter 3 DFT studies on the relative extent of negative hyperconjugation for a model series of silicon-, phosphine- and phosphine-borane-stabilised carbanions

3.1 Introduction

Trimethylsilyl, phosphine and phosphine-borane functional groups all stabilise α-carbanions by negative hyperconjugation (Figure 33). This stabilising interaction involves overlap of a filled p-orbital on the carbanion carbon with one or more Si—C(R) or P—C(R) σ* orbitals (R = an alkyl group, e.g. methyl, iso-propyl, phenyl). The p-orbital overlaps with the lobe of the σ* orbital that resides on the heteroatom because this is closest. Previous computational studies have found that a pyramidal methyl anion adjacent to a SiH_3 group, $[CH_2SiH_3]^-$ is stabilised by about 99 kJ/mol, while a pyramidal methyl anion adjacent to a PH_2 group $[CH_2PH_2]^-$ is stabilised by 89 kJ/mol.[1,2]
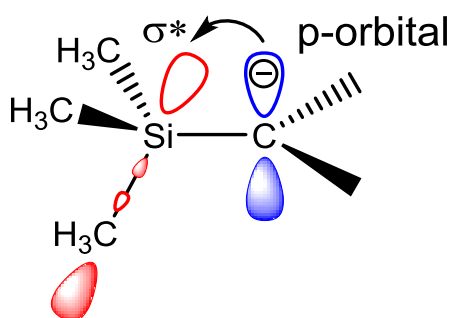
Figure 33.Negative hyperconjugation in a silicon-stabilised carbanion

Negative hyperconjugation results in elongation of the P−H/Si−H bonds by up to 0.055 Å or the P−C(R)/Si−C(R) bonds by up to 0.016 Å, due to a decrease in the bond order caused by the delocalisation of electron density into the antibonding orbital.[1,3] Another effect of this delocalisation is that the P−H/Si−H hydrogens become more hydridic or the P−C(R)/Si−C(R) carbon atoms acquire a partial negative charge. In the metallated anions the bond between the carbanion carbon and the heteroatom of the stabilising group (Si or P) is shorter than in the protonated molecules.[4] Part of this bond shortening can be attributed to an increase in multiple-bond character due to delocalisation of the carbanion lone-pair into the P−C(R)/Si−C(R) σ* orbitals, but another contributing factor is the change in hybridisation at the carbanion carbon from sp^3 to sp^2 on metalation. The effects of negative hyperconjugation on molecular structure can be observed both in the calculated optimised geometry at the global energy minimum and experimentally in structures determined by X-ray crystallography.[3]

Phosphine-borane-stabilised carbanions have been found to be significantly more stabilised than their trimethylsilyl analogues. Practical evidence from the laboratory is that deprotonation of mono(phosphine-boranes) is easily achieved with BnK (preferred for subsequent synthesis of lanthanide complexes) or ^{n}BuLi.[3,5–7] Deprotonation of tris(trimethylsilanes) requires MeK, which is more difficult to handle (see Chapter 4) and bis(trimethylsilanes) are usually metalated by lithium-halogen exchange reactions (see Chapter 2).[8] The rationale behind the greater stabilising effect of phosphine-borane functional groups over trimethylsilyl and phosphine groups is that when the lone-pair on the phosphorus atom becomes a bonding pair in the P−B bond the electron density on the phosphorus atom is reduced giving it a partial positive charge. In a polarised bond the larger coefficient of the antibonding orbital lies on the more δ⁺ atom, which is the phosphorus atom in the P−C(R) bonds. As a result, orbital overlap between the filled p-orbital on the carbanion carbon and the σ* antibonding orbital on the phosphorus atom is

improved, and delocalisation of electron density into the P—C(R) σ* orbitals is more extensive, increasing overall stabilisation of the carbanion.

The extent of electron density delocalisation due to molecular orbital interactions can be analysed quantitatively using Natural Bond Orbital (NBO) analysis.[3,9] The NBO program chooses a best-fit Lewis structure representation of the molecular wavefunction of a calculated structure. The structural model consists of filled Lewis-type NBOs (occupancy 2 for closed shell systems) and empty non-Lewis-type NBOs; these are called donor and acceptor orbitals respectively. Then the program evaluates how the energies of these orbitals are perturbed for all possible mixing combinations of a pair of donor and acceptor orbitals.[9]

The concept that the overlap and mixing of filled and empty orbitals with similar energies is energy stabilising is a familiar result from quantum mechanics (Figure 34). In the case of structures of phosphine- and phosphine-borane-stabilised carbanions previously analysed with the NBO program the most energy stabilising orbital interactions were between the filled donor orbital on the carbanion carbon with >96% p-character and an empty acceptor antibonding orbital of a P—C bond.[3] The E(2), second-order perturbation stabilisation energies computed by the NBO program give numerical values to the extent of carbanion stabilisation by negative hyperconjugation for different functional groups (Figure 34).
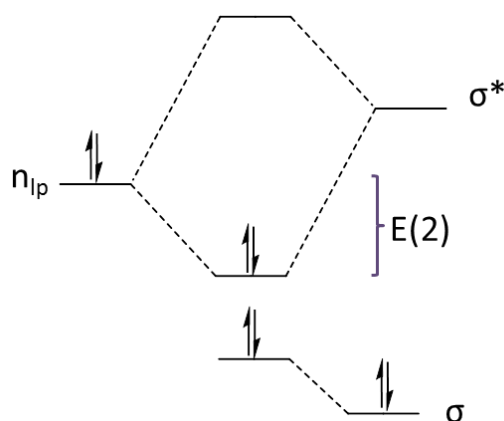
Figure 34. Negative hyperconjugation is energy stabilising

With the foregoing in mind the principle aim of this study was to be able to place the functional groups −SiMe$_3$, -PMe$_2$ and −PMe$_2$BH$_3$ in order of their α-carbanion-stabilising capability, after taking into account the dependence of negative hyperconjugation on the dihedral angle between the donor and acceptor orbitals.

3.2　　A model system for the quantitative comparison of carbanion-stabilising functional groups

The series of five organolithium compounds **35**, **36**, **37**, **38** and **39** used in the current computational study are shown in Figure 35. All the compounds have *N,N,N′,N′*-tetramethylethylenediamine (tmeda) as a common coligand to occupy two coordination sites of the lithium cation and prevent the formation of polymeric extended structures as seen for dipotassium salts of the hybrid ligands (Chapter 4), making them unsuitable for investigation using computational methods.

The ground-state geometry of the calculated structures was optimised at the wB97XD/6-311G(2d,p) level, similarly to the series of compounds: [{Ph$_2$P(BH$_3$)}CHP^{i}Pr$_2$]Li(tmeda), [Ph$_2$PCH{P(BH$_3$)^{i}Pr$_2$}]Li(tmeda), [{Ph$_2$P(BH$_3$)}CH{P(BH$_3$)^{i}Pr$_2$}]Li(tmeda) and [Ph$_2$PCHP^{i}Pr$_2$]Li(tmeda) previously synthesised by the Izod group and analysed using DFT and NBO methods.[3]　An advantage of the current series of compounds over those in the previous study of hyperconjugation in phosphine- and phosphine-borane carbanions is that the bis(trimethylsilyl), bis(phosphine) and bis(phosphine-borane) derivatives are all symmetrical (Figure 35). The alkyl groups attached to the silicon or phosphine atoms are all the same (methyl groups) so differing inductive or charge delocalisation effects do not need to be taken into account and will not mask differences in stabilisation due to negative hyperconjugation.

35

36

37

38

39
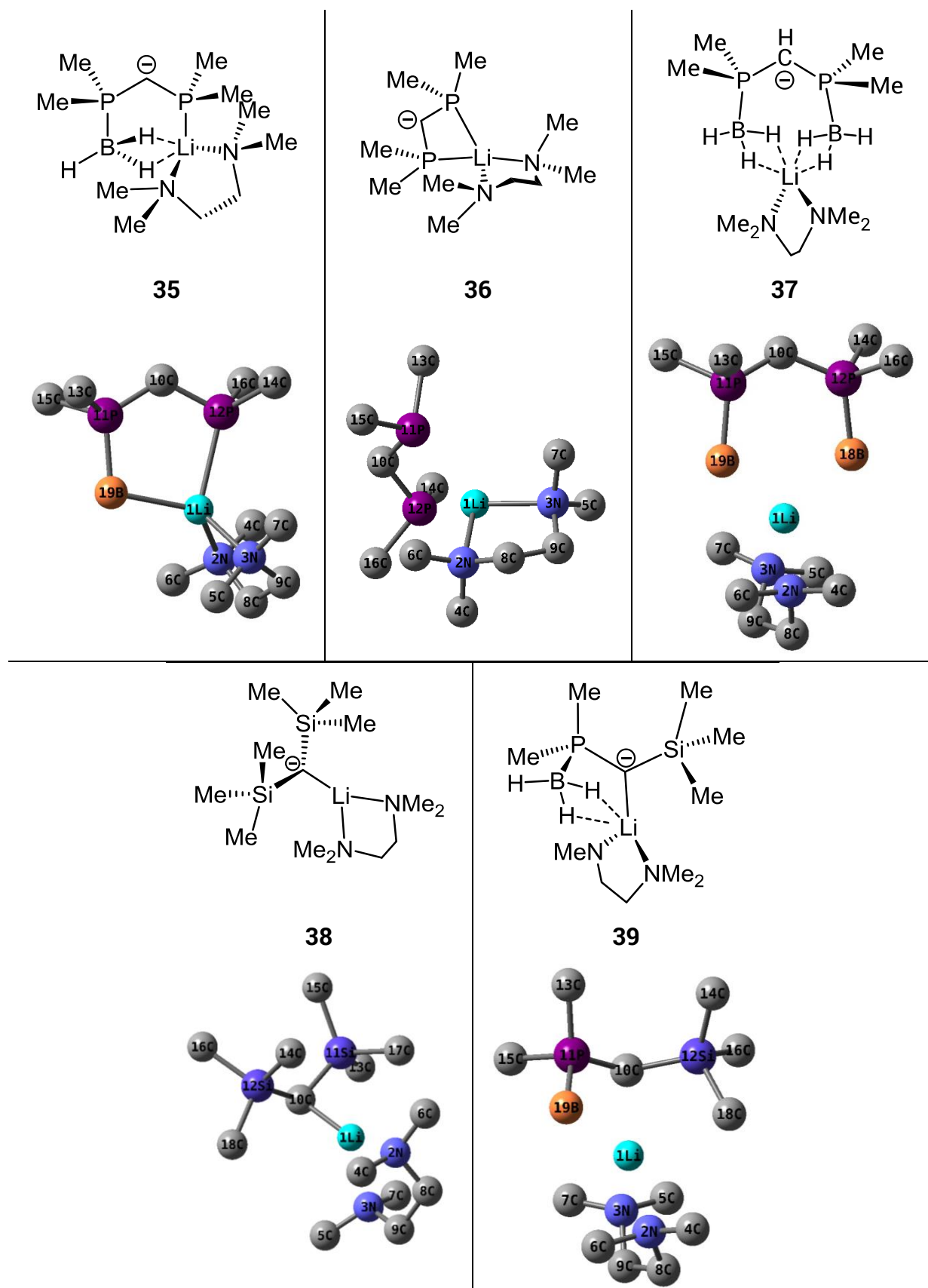
Figure 35. Structures, optimised geometries and atom numbering scheme for the five organolithium compounds analysed using NBO analysis

No solvent was included in the calculations and the justifications for this are the structure of the compounds could very well be different in solution to in the solid-state, particularly in a donor solvent such as THF; for example separated ion pairs could be present in solution. In addition, with the exception of compound **38** these compounds are insoluble in non-donor solvents (e.g. toluene).

3.3 Calculated Structures

For this study relative differences in geometry between the five carbanion fragments (**35** - **39**) are the primary concern rather than differences in their interaction with the [Li(tmeda)]$^+$ cation fragment. A comparison of Li$-$C(10) bond distances in calculated structures with Li$-$C(α) distances reported in the literature would require geometry optimisations of the exact compounds (with equivalent co-ligands) rather than closely similar compounds. Changes in geometry on metalation not discussed because this is a relative comparison. Geometrical changes in bond lengths that occur on metalation are discussed for the hybrid pro-ligands versus metalated hybrid ligands in chapter 4.

3.3.1 The calculated structure of [Me$_2$PCH{P(BH$_3$)Me$_2$}]Li(tmeda) [35]

In the calculated structure of [Me$_2$PCH{P(BH$_3$)Me$_2$}]Li(tmeda) **35** the planar mixed phosphine/phosphine-borane coordinates the lithium cation via the P donor atom and η^2 through the borane hydrogens of the Me$_2$PBH$_3$ group. The only solid-state structures of α-metalated mixed phosphine/phosphine-borane-stabilised carbanions are the structures of [{Ph$_2$P(BH$_3$)}CHP^{i}Pr$_2$]Li(tmeda) and [Ph$_2$PCH{P(BH$_3$)^{i}Pr$_2$}]Li(tmeda).[3] In both of these structures the lithium cation is bound to the phosphine and the borane-hydrogens of the phosphine-borane group.

3.3.2   The calculated structure of [(Me$_2$P)$_2$CH]Li(tmeda) [36]

In the calculated structure of [(Me$_2$P)$_2$CH]Li(tmeda) **36** the planar diphosphinomethanide acts as a $\kappa^2 P,P$ donor.   The diphosphinomethanides [(Ph$_2$P)$_2$CH]Li(tmeda) and [Ph$_2$PCHP^{i}Pr$_2$]Li(tmeda) and have the same coordination mode in their solid-state structures determined by X-ray crystallography.[3,10] The structure of [Ph$_2$PCHP^{i}Pr$_2$]Li(tmeda) has also been calculated using the wb97XD functional method[11] and the 6-311+G(d,p) basis set (the same as used in this work) and the bond lengths were overestimates relative to the crystal structures by ≤ 0.02Å. The calculated structure of **36** and [Ph$_2$PCHP^{i}Pr$_2$]Li(tmeda) **[40]**, and the structures of **40** and [(Ph$_2$P)$_2$CH]Li(tmeda) **[41]** determined by X-ray crystallography are largely consistent; they are both monomeric, and each 4-coordinate lithium cation is bound to the phosphorus atoms of the carbanion and to the nitrogen atoms of the tmeda co-ligand with a spiro-like geometry around the Li cation (Figure 35 and Figure 36).[3,10]

Figure 36. Structures of [Ph$_2$PCHP^{i}Pr$_2$]Li(tmeda) [40] and [(Ph$_2$P)$_2$CH]Li(tmeda) [41].

The crystal structure of **36** is unknown, the closest analogue with a known structure is the dimer [{(Me$_2$P)$_2$CH}Li(THF)]$_2$ **[42]**.[12] Changing the co-ligand from bidentate tmeda to monodenate THF alters the coordination mode of the diphosphinomethanide, [(Me$_2$P)$_2$CH]$^-$ anion from a $\kappa^2 P,P$ donor to a $\kappa^2 P,P$: κC bridging ligand (with the ligand bridging two lithium cations to form a dimer). The same change in coordination mode is observed for the [(Ph$_2$P)$_2$CH]$^-$ ligand. Due to the large change in structural morphology caused by the change in co-ligand the structures of **36** and [{(Me$_2$P)$_2$CH}Li(THF)]$_2$ **[42]** will not be compared in more detail.

The planar carbanion fragments of the calculated structure of **36** and the structures of [Ph$_2$PCHP^{i}Pr$_2$]Li(tmeda) [**40**] and (Ph$_2$P)$_2$CH]Li(tmeda) [**41**] (Figure 36) have highly similar bond lengths and P−C(α)−P angles. The difference in length between the longest and the shortest P−C(α) bonds over all three structures is 0.02 Å (c.a. 1%), (

Table 7). These small differences can be attributed to the extent of delocalisation of the charge on the carbanion onto the phosphorus atoms by negative hyperconjugation, and hence the degree of double bond character. The ^{i}Pr$_2$P−C(α) and Me$_2$P−C(α) bond lengths are identical (1.738 Å), however the Ph$_2$P−C(α) bonds (for both compounds) are slightly shorter (1.722(3) Å) indicating that switching an alkyl group to a phenyl group slightly increases the carbanion-stabilising ability of a PR$_2$ substituent.

The differences in the P−C(R) bond lengths of the three carbanion fragments are also small, 0.03 Å (c.a. 2 %) and can largely be attributed to the differences between P−C(sp^3) and P−C(sp^2) bond lengths. The lengthening of P−C(R) bond lengths as a result of negative hyperconjugation is so small, ≤ 0.014 Å for the five model compounds included in this study (Figure 35) that it is meaningless to make comparisons across PR$_2$ substituents with different alkyl groups.

The P−Li bond lengths vary across the three compounds **36**, [Ph$_2$PCHP^{i}Pr$_2$]Li(tmeda) [**40**] and [(Ph$_2$P)$_2$CH]Li(tmeda) [**41**] by a factor of ten more than the bond lengths within the carbanion fragment. The shortest P−Li bond is 2.477 Å in the calculated structure of **36**, and the longest is 2.582(2) Å in the crystal structure of **41**. The Me$_2$P−Li bond is shorter because this phosphorus atom is more nucleophilic than the Ph$_2$P phosphorus atom and so it is more strongly attracted to the lithium cation. The nucleophilicity of the phosphorus atom is influenced by the nature of the alkyl groups. The methyl alkyl groups of −PMe$_2$ have a positive inductive effect and any electron density donated to the phosphorus atom by negative hyperconjugation is localised on the phosphorus

atom, both these factors increase the nucleophilicity of the phosphorus atom. The phenyl rings of the $-PPh_2$ group have a weakly negative inductive effect and act to further delocalise any charge donated onto the phosphorus atom through negative hyperconjugation, both these factors decrease the nucleophilicity of the phosphorus atom.

The P−C−P bond angle is largest for the calculated structure **36** (116.50°) and smallest for $[(Ph_2P)_2CH]Li(tmeda)$ [**41**] (114.8°), which is also consistent with more negative charge being localised on the phosphorus atoms of **36**. The P−C−P bond angle of $[Ph_2PCHP^iPr_2]Li(tmeda)$ [**40**] is intermediate (115.54°).

A related compound with methyl alkyl groups on the phosphorus atoms and a known crystal structure, utilising the same tmeda co-ligand, is the monomeric tertiary carbanion $[(Me_2P)_2\{SiMe_3\}C]Li(tmeda)$ [**43**].[13] The P−Li bond lengths in **43** are slightly longer than in **36** because the presence of a third carbanion-stabilising functional group, -SiMe₃ means delocalised electron density is shared between the three heteroatom-stabilising functional groups so the $-PMe_2$ groups are slightly less nucleophilic. The steric bulk of the $-SiMe_3$ substituent acts to reduce the P−C−P angle by >9°.

3.3.3 The calculated structure of [{P(BH₃)Me₂}₂CH]Li(tmeda) [37]
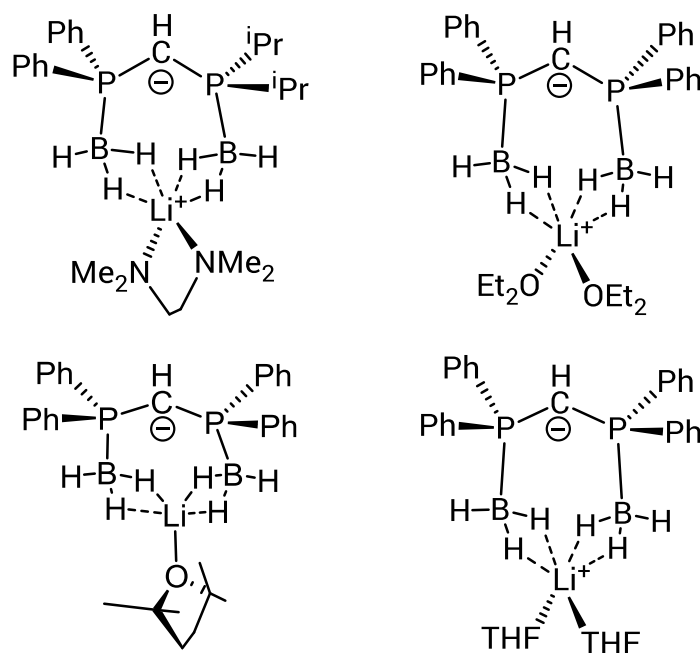
*Figure 37. Clockwise from top left: the structures of [{Ph₂P(BH₃)}CH{P(BH₃)ⁱPr₂}]Li(tmeda) [**44**], [{Ph₂P(BH₃)}₂CH]Li(OEt₂)₂ [**45**], [{Ph₂P(BH₃)}₂CH]Li(Me₄THF)₂ [**46**] and [{Ph₂P(BH₃)}₂CH]Li(THF)₂.[**47**].*

In the calculated structure of [{Me₂P(BH₃)}₂CH]Li(tmeda) [**37**] the planar bis(phosphine-borane)methanide is coordinates the lithium cation $\kappa^2 H,H$ with both of the BH₃ groups (Figure 35). The crystal structure of [{Me₂P(BH₃)}₂CH]Li(tmeda) is unknown, however monomeric solid-state structures of [{Ph₂P(BH₃)}₂CH]Li(co-ligand)ₓ with the same $\kappa^2 H,H$ coordination mode of both the borane groups as in **37** are known for several different monodentate co-ligands: diethyl ether, THF and 2,2,5,5-tetramethyltetrahydrofuran (Me₄THF), see Figure 37.[13,14] The structure with the bidentate co-ligand 1,2-dimethoxyethane (DME) is a separated ion pair: [{Ph₂P(BH₃)}₂CH][Li(dme)₃].[14] Nevertheless it is suggested that the nature of the co-ligand appears to have less of an effect on the structures of the lithium bis(phosphine-borane)methanides than the diphosphinomethanides since the solid-state structure of the unsymmetrical bis(phosphine-borane)methanide [{Ph₂P(BH₃)}CH{P(BH₃)ⁱPr₂}]Li(tmeda) has been determined and found to be

monomeric with the bis(phosphine-borane) carbanion coordinated $\kappa^2 H,H$ by both of the BH_3 groups; a very similar structure to all the compounds in Figure 37.

Once again there are only small differences in the bond lengths and $P-C(\alpha)-P$ angles of the planar carbanion fragment between the calculated structure of **37** and the similar compounds shown in Figure 37. All the $P-C$ bonds are shorter by 0.02 – 0.06 Å in the bis(phosphine-borane)methanides relative to the diphosphinomethanides due to the partial positive charge on the phosphorus atom after formation of a BH_3 adduct.

The $Me_2P-C(\alpha)$ bond lengths of the calculated structure of **37** are 1.7203 Å and 1.7219 Å (Table 7) which are close (but slightly shorter) to the $(^{i}Pr)_2P-C(\alpha)$ bond length (1.7242(16) Å) found in the crystal structure of $[\{Ph_2P(BH_3)\}CH\{P(BH_3)^{i}Pr_2\}]Li(tmeda)$ **[44]**, but longer than the $Ph_2P-C(\alpha)$ bond length (1.7061(16)Å). The $(^{i}Pr)_2P-C(\alpha)$ bond length and the $Ph_2P-C(\alpha)$ bond length found in the solid state structure of **44** are the longest and shortest bond lengths respectively of all the compounds in Figure 37. This is perhaps expected because the Ph_2P group is a better acceptor of electron density than the $^{i}Pr_2P$ group, so in the presence of a poorer acceptor the Ph_2P group accepts more electron density than it would in the presence of another Ph_2P group, resulting in a shorter than usual $Ph_2P-C(\alpha)$ bond length. In compound **37** more electron density is delocalised onto the $-PMe_2BH_3$ group in the absence of a better acceptor $-PPh_2BH_3$ group resulting in slightly shorter $P-C(\alpha)$ bond lengths than that found for the $(^{i}Pr)_2P-C(\alpha)$ bond in **44**.

3.3.4   The calculated structure of $[(Me_3Si)_2CH]Li(tmeda)$ [38]

The $Li-C(10)$ bond in the calculated structure of **38** is very short at 2.069 Å indicating a polarised bond with significant covalent character as expected by Fajan's rules. The solid-state structure of the similar organolithium compound,

Li{CH(SiMe₃)₂}(pmdeta) [**48**] determined by X-ray crystallography also has a short Li−C(α) bond length of 2.13(5) Å.[15] The key geometry of the calculated structure of Li{CH(SiMe₃)₂}(tmeda) [**38**] is consistent with the reported solid-state structure of Li{CH(SiMe₃)₂}(pmdeta) [**48**]. Both structures are monomeric with a pyramidal (a squashed tetrahedron) carbanion, where the Li−C(α) bond occupies the apex (Figure 35 and Figure 38). The Si−C(α)−Si angle is 122.9° in calculated structure of **38** and 124(2)° in the structure of **48** respectively. The sum of the angles around C(10) in **38**, where all atoms are in calculated positions is 344.57°.
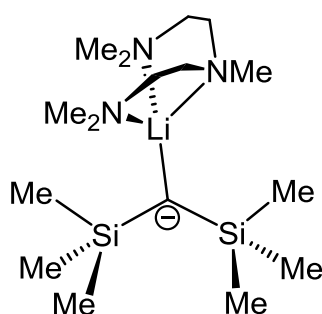
*Figure 38. Structure of Li{CH(SiMe₃)₂}(pmdeta) [**48**].*

3.3.5   The calculated structure of [{Me₂P(BH₃)}CH(SiMe₃)]Li(tmeda) [39]

In the calculated structure of **39** the lithium cation is coordinated by the C(10) carbanion carbon and κ² *H,H* by the BH₃ group in addition to the TMEDA co-ligand. The carbanion [{Me₂P(BH₃)}CH(SiMe₃)]Li(donor)ₓ has been synthesised in solution, but was used *in situ* and has not been crystallised.[16] The Li−C(10) bond length is 2.321 Å, which is slightly longer than the Li−C bond lengths (2.249(8) Å and 2.252(8) Å) in the more sterically hindered compound (THF)₃Li{(Me₃Si)₂CPMe₂(BH₃)}₂Li [**49**] (Figure 39) but is consistent with increased coordination number of the lithium cation in **39**.[17] The coordination environment of the lithium cation in is different to that of the carbanion bound lithium cation in **49**, where one lithium cation is bound to two carbanion carbon atoms and is also η¹

coordinated by a BH₃ group. The second lithium cation in the contact ion-pair is coordinated $\kappa^3 H,H,H$ by another BH₃ group and is also solvated by three molecules of THF.
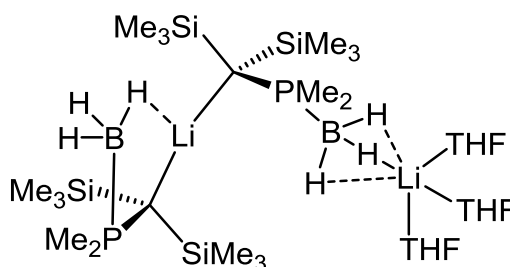
Figure 39. Structure of (THF)₃Li{(Me₃Si)₂CPMe₂(BH₃)}₂Li **[49]**.

The bond lengths within the carbanion fragment of **39**, Me₂P—C(α) (1.738 Å) and C(α)—SiMe₃ (1.826 Å) are comparable with those found in (THF)₃Li{(Me₃Si)₂CPMe₂(BH₃)}₂Li, Me₂P—C(α) (1.750(5) Å and 1.755(5) Å) and C(α)—SiMe₃ (average 1.86 Å), the slightly shorter bond lengths in **39** can be attributed to the structure having one less carbanion stabilising substituent.

Table 7. Selected bond lengths (Å) and angles (degrees) for the calculated structures shown in Figure 37

	35	**36**	**37**	**38**	**39**
P/Si(12)−B/C(18)	n/a	n/a	1.92818	1.89865	1.89551
P/Si(11)−B/C(19)	1.9335	n/a	1.92421	1.90841	1.92646
C(10)−P/Si(12)	1.73493	1.73994	1.72191	1.80859	1.82614
C(10)−P/Si(11)	1.71540	1.73880	1.72031	1.81244	1.73841
P/Si(12)−C(14)	1.8528	1.85129	1.82461	1.89952	1.88812
P/Si(12)−C(16)	1.8523	1.85610	1.83456	1.88918	1.88340
P/Si(11)−C(13)	1.8312	1.85268	1.83400	1.88917	1.83448
P/Si(11)−C(15)	1.8325	1.85431	1.82547	1.89193	1.82255
P(12)−Li(1)	2.5117	2.50029	n/a	n/a	n/a
P(11)−Li(1)	n/a	2.47683	n/a	n/a	n/a
C(10)−Li(1)	n/a	2.87575	4.1000	2.06909	2.32052
B/C(18)−Li(1)	n/a	n/a	2.36996	2.82954	2.70701
B(19)/C(17)−Li(1)	2.3390	n/a	2.37845	3.37722	2.42915
Li(1)−N(2)	2.1286	2.09808	2.12664	2.13996	2.25265
Li(1)−N(3)	2.0913	2.06502	2.12550	2.06232	2.11158

3.3.6 Measurement of the angles between the filled p-orbital on C(10) and the σ* orbitals involved in negative hyperconjugation

The magnitude of the angles between the lone-pair containing p-orbital on C(10) and the vacant σ* orbitals with which it interacts to stabilise the carbanion were calculated from measurements of dihedral angles in the calculated structures. For the planar carbanions of compounds **35**, **36** and **37** the angle between the filled p-orbital on C(10) and the P(11)−C(15) σ* orbital was obtained as follows (the example is for **35**); a measurement of the dihedral angle P(12)−C(10)−P(11)−C(15) was obtained in GaussView as -122.853° and 90° was subtracted from the magnitude of the dihedral angle measurement to give the angles between the lone-pair containing p-orbital on C(10) and the vacant σ* orbitals as 32.85° (By geometry the p-orbital on C(10) is orthogonal to the plane containing P(12), C(10) and P(11) and the lobe of the σ* orbital residing on P(11) lies antiparallel to the P(11)−C(15) bond (Figure 40). The dihedral angle measures the angle between the plane of the carbanion and the σ-bonding orbital so deducting 90° gives the angle between the orbitals since opposite angles are congruent.
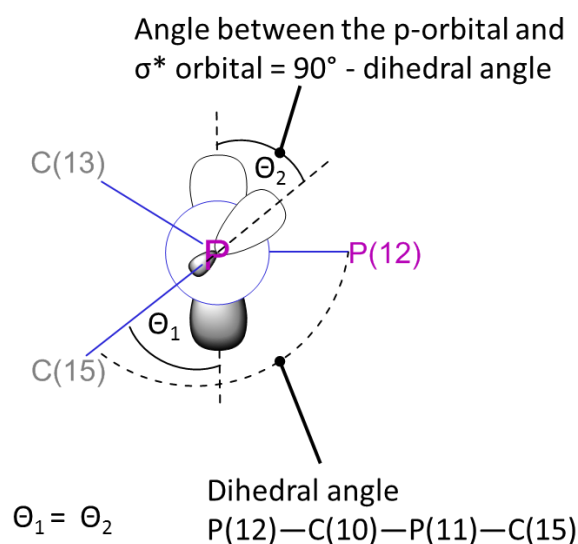
Figure 40. Geometric construction (along P(11)−C(10) bond) of the planar carbanion for
35

For the pyramidal carbanion in structures **38** and **39**, the C(10) carbanion carbon interacts directly with the lithium cation and the orbital containing the lone-pair, which has >92% p-character lies along this C−Li bond. The angle between this p-orbital and the Si(11)−C(15) σ* orbital in **38** was obtained by measurement of the dihedral angle Li(1)−C(10)−Si(11)−C(15) as 176.11°, and then subtracting this value from 180° to give 3.59° (Figure 41). The major lobe of the σ* orbital residing on Si(11) that overlaps with the p-orbital on C(10), points in a direction that is antiparallel to the direction of the Si(11)−C(13) σ-bond and therefore the angle between the orbitals is 180° minus the magnitude of the Li(1)−C(10)−Si(11)−C(13) dihedral angle (Table 8).
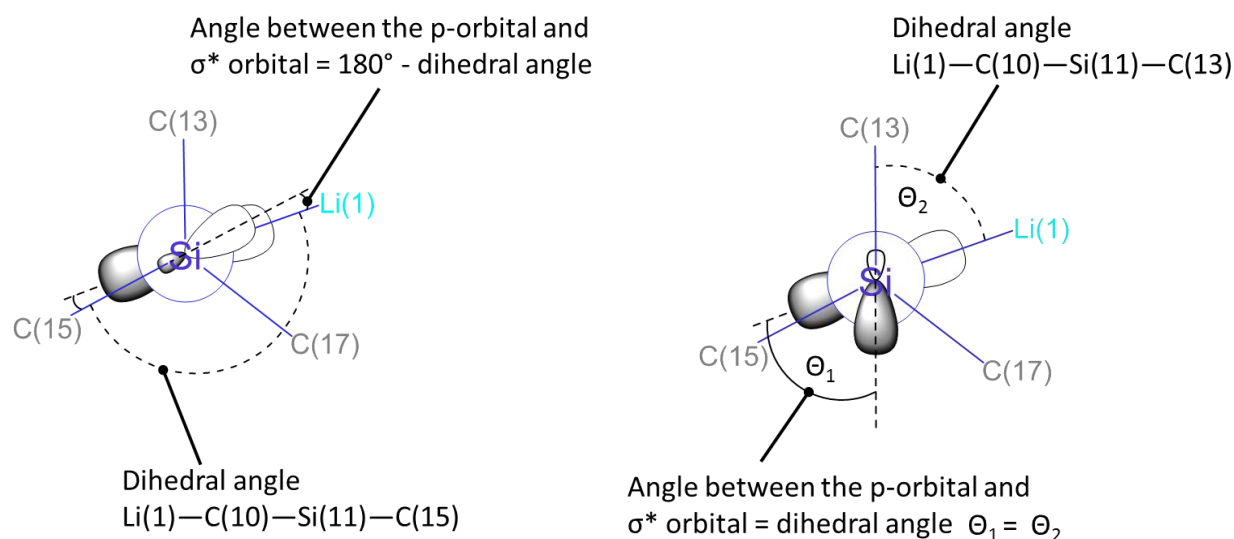
Figure 41. Geometric construction (view along Si(11)−C(10) bond) of the pyramidal carbanion for compound 38. (Left-hand side) Measurement of the angle between the p-orbital and the Si(11)−C(15) σ orbital. (Right-hand side) Measurement of the angle between the p-orbital and the Si(11)−C(13) σ* orbital.*

Table 8. Magnitudes of the angles between the filled p-orbital on C(10) and the σ*
orbitals involved in negative hyperconjugation

	35	36	37	38	39
Planarity {Sum of angles around C(10)}	358.92	358.71	357.41	344.57	345.45
l.p.−C(10)−P/Si(11)−C(13)	36.18	52.73	12.65	100.50	36.03
l.p.−C(10)−P/Si(11)−C(15)	32.85	22.74	57.64	44.09	76.46
l.p.−C(10)−P/Si(12)−C(14)	36.72	50.61	64.60	54.88	57.61
l.p.−C(10)−P/Si(12)−C(18)	n/a	n/a	n/a	61.58	1.96
l.p.−C(10)−P/Si(11)−C(17)	n/a	n/a	n/a	16.69	n/a
l.p.−C(10)−P/Si(12)−C(16)	39.47	24.70	5.75	3.59	64.61

3.4 Natural Bond Orbital (NBO) Analyses – insights into negative hyperconjugation

All NBO analyses were performed using the NBO *6.0* program and could not be run using the NBO *3.0* program due to the program making an inappropriate choice of Lewis structure representation. The default best-fit Lewis structure chosen by the NBO *3.0* program had a C=P multiple bond and the extent of hyperconjugation could not be assessed using this structure. Attempts to use the $CHOOSE keylist in the NBO *3.0* program to select an alternative Lewis structure were not fruitful, however the $CHOOSE keylist was successfully used in the NBO *6.0* program to ensure the Lewis-structure bonding pattern for all compounds included a lone pair on the carbanion carbon (C(10)) atom (where this was not the default choice).

No solvent was included in the calculations and the justifications for this are the structure of the compounds could very well be different in solution to in the solid-state, particularly in a donor solvent such as THF; for example separated ion pairs could be present in solution. In addition, with the exception of compound **38** these compounds are insoluble in non-donor solvents (e.g. toluene).

NBO analysis shows that in all of the carbanions the lone-pair on C(10) occupies an orbital with > 92% p-character and that all of the carbanions are stabilised by negative hyperconjugation into P—C or Si—C σ* orbitals, with E(2) stabilisation energies for individual interactions ranging from 13 – 101 kJ/mol (Table 9). A plot of normalised P—C bond lengths versus E(2) stabilisation energy shows a strong positive correlation (Figure 42). The bond lengths were normalised by first plotting the bond length (

Table 7 7) against E(2) stabilisation energies for the phosphine bonds and the phosphine-borane bonds separately to give two parallel lines. The y-axis intercept of these lines was deducted from the bond lengths to give the normalised values. For phosphine and phosphine-borane groups this suggests that more extensive delocalisation into the P—C σ* orbitals leads to longer bond lengths. There was no definitive correlation between Si—C bond length and E(2) stabilisation energy, however the longest Si—C bonds in compounds **38** and **39** were the Si(12)—C(18) bonds. The carbon atoms in these bonds have short contacts with the Li cation and these interactions also lengthen the Si—C bond.

Table 9. E(2) Energies (kJ/mol) of selected delocalisations, the percentage p-character of the carbon {C(10)} lone pair and its occupancy for **35** *-* **39**

	35	**36**	**37**	**38**	**39**
$n_{C(10)} \rightarrow \sigma^*_{P/Si(11)-B(19)/C(17)}$	0.00	n/a	0.00	48.26	15.82
$n_{C(10)} \rightarrow \sigma^*_{P/Si(12)-B/C(18)}$	n/a	n/a	4.85	13.64	40.21
$n_{C(10)} \rightarrow \sigma^*_{P/Si(12)-C(16)}$	64.98	90.54	106.11	92.72	0.00
$n_{C(10)} \rightarrow \sigma^*_{P/Si(12)-C(14)}$	69.33	52.97	34.81	4.23	60.12
$n_{C(10)} \rightarrow \sigma^*_{P/Si(11)-C(15)}$	84.52	88.57	45.65	101.04	0.00
$n_{C(10)} \rightarrow \sigma^*_{P/Si(11)-C(13)}$	77.53	57.61	97.73	0.00	48.24
% character $n_{C(10)}$	99.77	99.59	98.11	99.09	92.79
Occupancy $n_{C(10)}$	1.68	1.65	1.72	1.69	1.77
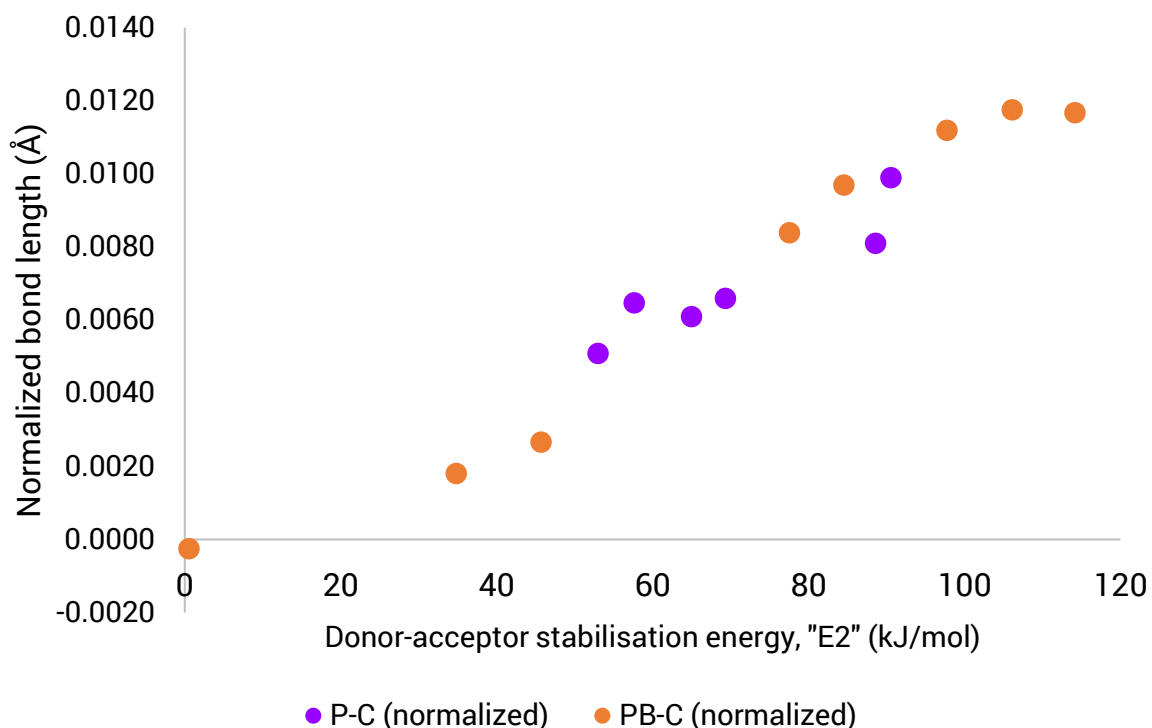
Figure 42. Correlation of bond length and E(2) stabilisation energy of the $n_{C(10)} \rightarrow \sigma^*_{P-C}$ interaction

The dependence of the extent of electron density delocalisation and therefore carbanion stabilisation on the angle between the filled p-orbital and vacant σ* acceptor orbital appears to be approximately linear. The parallel gradients in (Figure 43) suggest, perhaps as expected that the dependence of the extent of negative hyperconjugation on the angle between the orbitals is essentially the same for the σ* orbitals of all the functional groups in this series of organolithium compounds **35** – **39**.
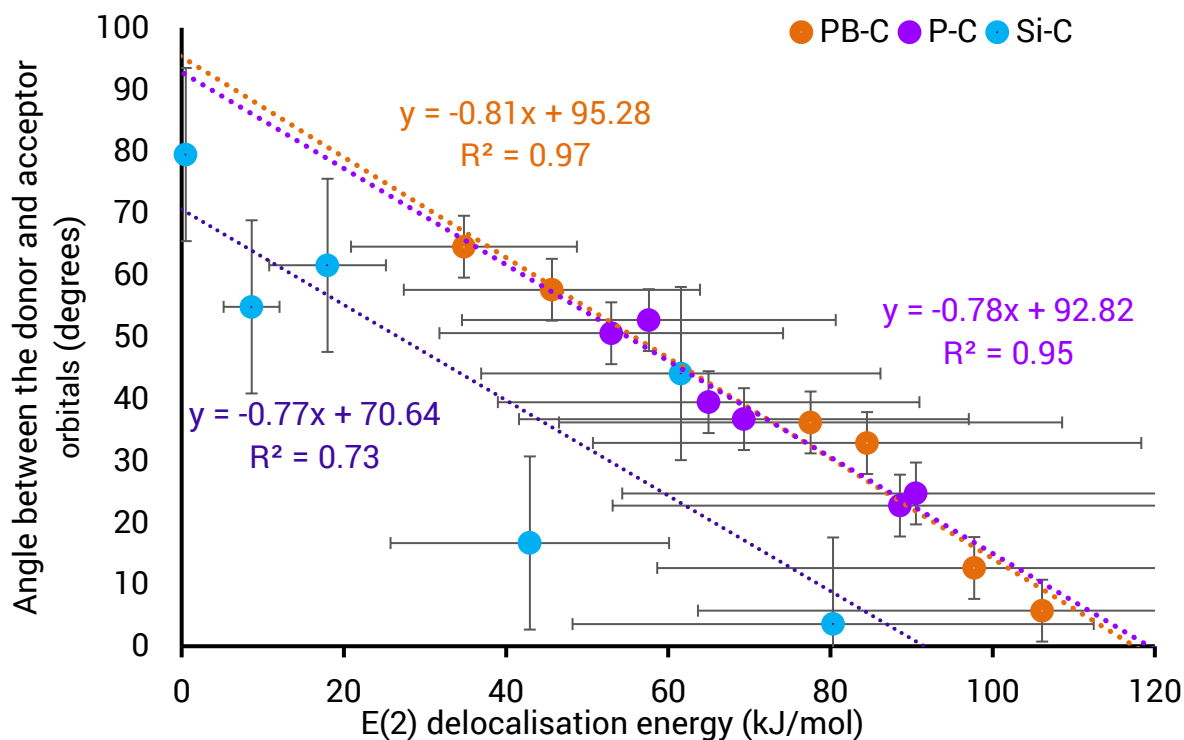
Figure 43. Dependence of the extent of delocalisationon the angle between the donor p-orbital on C(10) and the acceptor σ* orbital for each functional group.

Addition of a borane group reduces the electron density on the phosphorus atom as the lone pair that previously resided on the phosphorus atom becomes a bonding pair of electrons in the P—B bond. The effect of this is that the phosphorus atom has a partial positive charge and the H_3BP—C(Me) bonds are shortened relative to P—C(Me) bonds by about 0.023 Å. The other effect of the partial positive charge on the phosphorus atom is that the σ*-antibonding orbital of the P—C(Me) bond has a larger coefficient on the phosphorus atom, which makes for better orbital overlap with the filled p-orbital of the C(10) carbanion carbon atom. The expectation was that after allowing for the orbital orientation, negative hyperconjugation would be more energy stabilising for phosphine-borane groups than for phosphine or trimethylsilyl groups. The data are inconsistent with this hypothesis (Figure 43) and appear to show that the negative hyperconjugation interaction is equally stabilising for phosphine-borane groups and phosphine groups in these model

systems. The stabilisation energies do span a wider range for the phosphine-borane groups, but so do the angles between the lone-pair on C(10) and the P—C(Me) σ*-orbitals (Figure 43). The average stabilisation energies are not statistically different at 70.67 kJ/mol for a phosphine group and 72.53 kJ/mol for a phosphine-borane group. Trimethylsilyl groups are, however found to be less stabilising than phosphine and phosphine-borane groups by about 30±12kJ/mol at any given orientation.

The trend in the dependence of stabilisation energy on the angle between the p-orbital on C(10) and the overlapping σ* orbital is less clear for the trimethylsilyl functional groups. It is suggested that this could be attributed to the fact that carbanions containing this functional group are pyramidal rather than planar causing undefined variations in orbital overlap. Orbital overlap is also poorer for these carbanions since silicon atoms are less electropositive than the phosphorus atom of a phosphine-borane group so the lobe of the σ* orbital residing on silicon is smaller. The difference in orbital size may account for the differing intercepts at different angle values on the y-axis. Since the lobe of the σ* orbital residing on silicon is smaller than the lobe of the σ* orbital residing on phosphorus the angle at which there is no appreciable overlap appears to be <90°. For the phosphine and phosphine-borane groups the intercept angle value is approximately 90°; there is no orbital overlap when the orbitals are orthogonal.

Lithium is a very small, polarizing alkali-metal cation and phosphine lone-pair(s) interact preferentially with this cation even in the presence of a carbanion centre for these compounds. It is suggested that electron density on the phosphorus atom of phosphine groups is reduced by this P—Li bond and that this would partially explain the similarities in the energy stabilisation shared by phosphines and phosphine-boranes for this series of compounds. A larger alkali-metal cation such as potassium would be likely to interact preferentially with the lone-pair on the

carbanion carbon atom, C(10) rather than the phosphorus lone-pair and this might give a different trend in the relative α-carbanion stabilising ability of phosphine and phosphine-borane functional groups.

In Figure 43 the E(2) delocalisation energies for each donor-acceptor orbital interaction are plotted as a function of the angle between the donor and acceptor orbitals. This data is re-plotted in Figure 44 as the sum of the E(2) delocalisation energies for each functional group in a particular molecule. For compound **35**, which contains a phosphine-borane group and a phosphine group the electron density does appear to be delocalised more extensively onto the phosphine-borane group (sum = 134.31 kJ/mol for the phosphine group and 162.07 kJ/mol for the phosphine-borane group)(Figure 44). The overall E(2) stabilisation energies for compounds **35**, **36** and **37** are similar 296.46, 284.30 and 289.69 (kJ/mol) respectively. The phosphine-borane group of compound **39** stabilises the carbanion by 113.94 kJ/mol, considerably less than in compounds **35** and **37**. It is suggested that this is due to the pyramidal structure of the carbanion of compound **39** which allows for poorer orbital overlap, whereas compounds **35** and **37** have planar carbanions and better overlap between donor and acceptor orbitals involved in negative hyperconjugation.
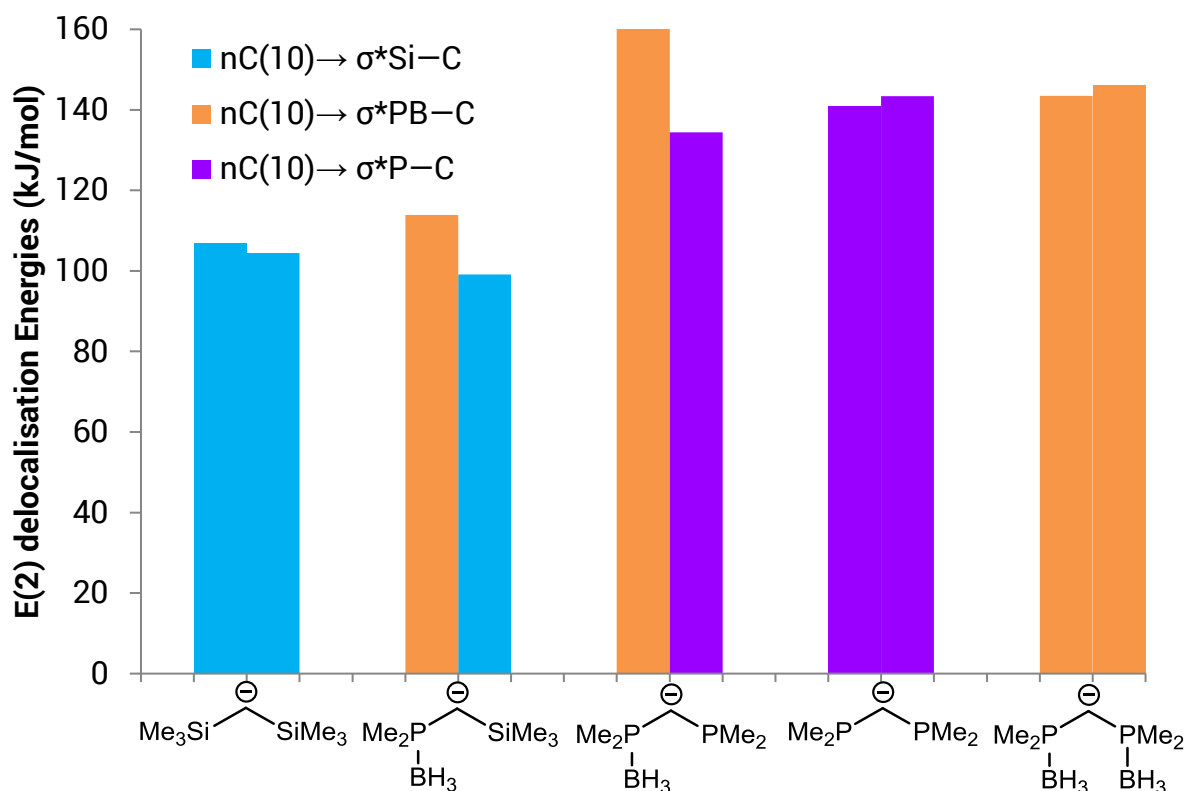
*Figure 44. Comparison of the E(2) delocalisation energies for the model series of carbanions **35 - 39***

3.5   Conclusion

There is a strong correlation between P—C bond length in the −PMe$_2$ and −PMe$_2$BH$_3$ groups of compounds **35 - 37** and **39** and the degree of carbanion stabilisation due to negative hyperconjugation. The more electron density is delocalised from the carbanion carbon into the σ*$_{P-C}$ orbital the more the P—C bond is elongated. The correlation is much weaker for the −SiMe$_3$ groups of compounds **38** and **39** because some of the Si—Me bonds are involved in agostic-type interactions with the lithium cation and these also serve to elongate the Si—Me bonds. Separation of these two contributory factors to Si—Me bond lengthening is difficult, since Si—Me bonds involved in agostic-type interactions are also involved in negative hyperconjugation unless the alignment of the Si—Me bond is perpendicular to the donor lone-pair orbital on the carbanion.

123

For all functional groups in the organolithium compounds **35** - **39** the smaller the angle between donor and acceptor orbitals the larger the E(2) delocalisation energy. The relationship between the E(2) delocalisation energy (kJ/mol) and the angle between the donor and acceptor orbitals is that the E(2) delocalisation energy is a multiple of -1.25 times the angle between donor and acceptor orbitals plus a constant. To put it another way the closer the donor and acceptor orbitals are to an eclipsed arrangement the better they overlap and the more effectively the carbanion is stabilised by negative hyperconjugation.

The calculated E(2) delocalisation energy data shows that $-PMe_2$ and $-PMe_2BH_3$ functional groups at any given orientation of donor and acceptor orbitals have very similar capacities to energetically stabilise the carbanions in compounds **35** - **37** and **39** by negative hyperconjugation. The $-SiMe_3$ group at any given orientation of donor and acceptor orbitals is more poorly stabilising by approximately 30 kJ/mol. These findings contradict experimental observations in the laboratory where a stronger base is required to synthesise $[\{Me_2P\}CH(SiMe_3)]Li$ than compound **39**. The laboratory is a different system in which solvation and kinetic effects come into play, whereas these calculations model only the thermodynamic stabilisation of the carbanion. The carbanions $[\{Me_2P\}CH(SiMe_3)]Li$ and compound **39** could be energetically stabilised by similar amounts due to negative hyperconjugation but the metalation reaction pathways to these products could have different energy barriers.

3.6   Experimental

3.6.1   DFT Calculations

All calculations were carried out with the Gaussian09 package.[18]   Ground-state geometry optimizations of **35, 36, 37, 38** and **39** were computed using the wB97XD hybrid functional method[11] and the 6-311G(2d,p) all-electron basis set was used on

all atoms.[19–22] Minimum energy conformations of **35, 36, 37, 38** and **39** were first optimised at the HF/3-21G* level. These geometries were then reoptimised at the wB97XD/6-311G(2d,p) level. For compounds **35, 36** and **37** the geometry was confirmed as the energy minima by the absence of imaginary vibrational frequencies. For compounds **38** and **39** the optimised geometries were not energy minima and imaginary vibrations were present. The geometries of **38** and **39** were reoptimised using a tight geometry optimisation. Natural bond orbital analyses were performed using the NBO 6.0 program from with the Gaussian interface.[23] No solvent was included in the calculations. All output files from the calculations are available as an electronic appendix to this chapter.

3.6.2 Error bars

Representative uncertainties in the E(2) energies, displayed as error bars in Figure 43 were calculated as the percentage difference between the E(2) stabilisation energy and the variational deletion [ΔE($DEL)] for each donor-acceptor negative hyperconjugation interaction of orbitals. Deletion calculations recalculate the energy of the molecule at the current optimised geometry in the absence of one or more energy stabilising donor-acceptor orbital interactions and report the energy difference, ΔE($DEL).[9] Differences between the ΔE(2) and ΔE($DEL) values relate to inherent differences in the approximations made by each calculation method. Since the values of ΔE(2) and ΔE($DEL) are strongly correlated both are consistent with relative comparisons between molecular structures, however the actual energy values must be treated as imprecise and the difference between the values reported by ΔE(2) and ΔE($DEL) values serves as a useful measurement of their uncertainty. The results of calculations of the percentage difference between the E(2) stabilisation energy and the variational deletion ΔE($DEL) energy for each donor-acceptor negative hyperconjugation interaction in all of the five structures are given in Table 10 – Table 14 and these percentage values are used as the error bars in Figure 43.

Table 10. Comparison of ΔE(2) and ΔE($DEL) (kJ/mol) estimates of stabilisation energies for negative hyperconjugation interactions in compound 35

Donor → Acceptor	NBOs	ΔE(2)	ΔE($DEL)	% difference
$n_{C(10)} \to \sigma^*_{P(12)-C(14)}$	29 → 78	69.33	38.73	-44.1
$n_{C(10)} \to \sigma^*_{P(12)-C(16)}$	29 → 79	64.98	36.07	-44.5
$n_{C(10)} \to \sigma^*_{P(11)-C(13)}$	29 → 82	77.53	42.86	-44.7
$n_{C(10)} \to \sigma^*_{P(11)-C(15)}$	29 → 83	84.52	47.06	-44.3
Sum		**296.36**	**164.72**	**-44.4**

Table 11. Comparison of ΔE(2) and ΔE($DEL) (kJ/mol) estimates of stabilisation energies for negative hyperconjugation interactions in compound 36

	NBOs	ΔE(2)	ΔE($DEL)	% difference
$n_{C(10)} \to \sigma^*_{P(12)-C(16)}$	28 → 73	90.54	50.58	-44.1
$n_{C(10)} \to \sigma^*_{P(12)-C(14)}$	28 → 74	52.97	28.24	-46.7
$n_{C(10)} \to \sigma^*_{P(11)-C(15)}$	28 → 77	88.57	48.68	-45.0
$n_{C(10)} \to \sigma^*_{P(11)-C(13)}$	28 → 78	57.61	30.60	-46.9
Sum		**289.69**	**158.10**	**-45.4**

Table 12. Comparison of ΔE(2) and ΔE($DEL) (kJ/mol) estimates of stabilisation energies for negative hyperconjugation interactions in compound 37

	NBOs	ΔE(2)	ΔE($DEL)	% difference
$n_{C(10)} \to \sigma^*_{P(12)-C(14)}$	29 → 82	34.81	19.18	-44.9
$n_{C(10)} \to \sigma^*_{P(12)-C(16)}$	29 → 83	106.11	63.09	-40.5
$n_{C(10)} \to \sigma^*_{P(12)-B(18)}$	29 → 84	4.85	2.77	-42.9
$n_{C(10)} \to \sigma^*_{P(11)-C(13)}$	29 → 117	97.73	57.61	-41.1
$n_{C(10)} \to \sigma^*_{P(11)-C(15)}$	29 → 118	45.65	25.53	-44.1
Sum		**289.15**	**168.18**	**-41.8**

*Table 13. Comparison of ΔE(2) and ΔE($DEL) (kJ/mol) estimates of stabilisation energies for negative hyperconjugation interactions in compound **38***

	NBOs	$\Delta E(2)$	ΔE($DEL)	% difference
$n_{C(10)} \rightarrow \sigma^*_{Si(12)-C(16)}$	29 → 117	92.72	55.55	-40.1
$n_{C(10)} \rightarrow \sigma^*_{Si(12)-C(17)}$	29 → 130	48.24	27.72	-42.5
$n_{C(10)} \rightarrow \sigma^*_{Si(11)-C(15)}$	29 → 125	101.04	41.15	-59.3
$n_{C(10)} \rightarrow \sigma^*_{Si(12)-C(14)}$	29 → 129	4.23	5.31	+25.5
$n_{C(10)} \rightarrow \sigma^*_{Si(11)-C(18)}$	29 → 121	13.64	11.28	-17.31
Sum		**259.87**	**141.01**	**-45.7**

*Table 14. Comparison of ΔE(2) and ΔE($DEL) (kJ/mol) estimates of stabilisation energies for negative hyperconjugation interactions in compound **39***

	NBOs	$\Delta E(2)$	ΔE($DEL)	% difference
$n_{C(10)} \rightarrow \sigma^*_{P(11)-B(19)}$	29 → 81	15.82	9.48	-40.1
$n_{C(10)} \rightarrow \sigma^*_{P(11)-C(13)}$	29 → 83	48.24	27.74	-42.5
$n_{C(10)} \rightarrow \sigma^*_{Si(12)-C(14)}$	29 → 116	60.12	24.47	-59.3
$n_{C(10)} \rightarrow \sigma^*_{Si(12)-C(18)}$	29 → 127	40.21	50.46	+25.5
Sum		**164.39**	**112.15**	**-45.7**

The energy change given by the sum of the individual deletion calculations in is less than the energy change given by the combined deletion calculation. This stabilisation energy given by the combined deletion calculation lies between the values for the sum of the negative hyperconjugation stabilisation energies (less by 29%) and the sum of the individual deletion calculations (more by 27%). Removal energy stabilising orbital interactions (in these systems negative-hyperconjugation) from the model for one pair of orbitals, can be partially compensated by extra negative hyperconjugation between the remaining orbitals with the correct energy and orbital overlap so it is less destabilising than removal of all negative hyperconjugation.

3.7 References

(1)   El-Nahas, A. M.; Schleyer, P. V. R. *J. Comput. Chem.* **1994**, *15*, 596.

(2)   Izod, K. *Coord. Chem. Rev.* **2002**, *227*, 153.

(3)   Izod, K.; Wills, C.; Anderson, E.; Harrington, R. W.; Probert, M. R. *Organometallics* **2014**, *33*, 5283.

(4)   Izod, K.; Wills, C.; Clegg, W.; Harrington, R. W. *Organometallics* **2006**, *25*, 5326.

(5)   Izod, K.; Dixon, C. M.; McMeekin, E.; Rodgers, L.; Harrington, R. W.; Baisch, U. *Organometallics* **2014**, *33*, 378.

(6)   Izod, K.; Wills, C.; Clegg, W.; Harrington, R. W. *Organometallics* **2010**, *29*, 4774.

(7)   Izod, K.; Wills, C.; Clegg, W.; Harrington, R. W. *Organometallics* **2006**, *25*, 38.

(8)   Eaborn, C.; Hitchcock, P. B.; Izod, K.; Jaggar, A. J.; Smith, J. D. *Organometallics* **1994**, *13*, 753.

(9)   Weinhold, F.; Landis, C. R. *Discovering chemistry with natural bond orbitals*; John Wiley and Sons Inc., Hoboken, NJ, USA, **2012**.

(10)   J. Brauer, D.; Hietkamp, S.; Stelzer, O. *J. Organomet. Chem.* **1986**, *299*, 137.

(11)   Chai, J.-D.; Head-Gordon, M. *Phys. Chem. Chem. Phys.* **2008**, *10*, 6615.

(12)   Karsch, H. H.; Grauvogl, G.; Mikulcik, P.; Bissinger, P.; Müller, G. *J. Organomet. Chem.* **1994**, *465*, 65.

(13)   Karsch, H. H.; Deubelly, B.; Müller, G. *J. Organomet. Chem.* **1988**, *352*, 47

(13)   Langer, J.; Geitner, R.; Görls, H. *Eur. J. Inorg. Chem.* **2014**, *2014*, 5940.

(14)   Langer, J.; Wimmer, K.; Görls, H.; Westerhausen, M. *Dalt. Trans.* **2009**, 2951.

(15)   Lappert, M. F.; Engelhardt, L. M.; Raston, C. L.; White, A. H. *J. Chem. Soc. Chem. Commun.* **1982**, 1323.

(16)   Izod, K.; Wills, C.; Clegg, W.; Harrington, R. W. *Organometallics* **2009**, *28*, 5661.

(17) Izod, K.; Wills, C.; Clegg, W.; Harrington, R. W. *Organometallics* **2006**, *25*, 38.

(18) Frisch, M. J.; Trucks, G. W.; Schlegel, H. B.; Scuseria, G. E.; Robb, M. A.; Cheeseman, J. R.; Scalmani, G.; Barone, V.; Petersson, G. A.; Nakatsuji, H.; Li, X.; Caricato, M.; Marenich, A. V.; Bloino, J.; Janesko, B. G.; Gomperts, R.; Mennucci, B.; Hratch, D. J. *Gaussian 09, Revisions B.01,C.01 and D.01*; Gaussian Inc.:Wallingford, CT **2009**.

(19) McLean, A. D.; Chandler, G. S. *J. Chem. Phys.* **1980**, *72*, 5639.

(20) Krishnan, R.; Binkley, J. S.; Seeger, R.; Pople, J. A. *J. Chem. Phys.* **1980**, *72*, 650.

(21) McGrath, M. P.; Radom, L. *J. Chem. Phys.* **1991**, *94*, 511.

(22) Curtiss, L. A.; McGrath, M. P.; Blaudeau, J.; Davis, N. E.; Binning, R. C.; Radom, L. *J. Chem. Phys.* **1995**, *103*, 6104.

(23) E. D. Glendening, J, K. Badenhoop, A. E. Reed, J. E. Carpenter, J. A. Bohmann, C. M. Morales, C. R. Landis, and F. W. *NBO 6.0*, Theoretical Chemistry Institute, University of Wisconsin, Madison **2013**.

Chapter 4 Metalation of hybrid pro-ligands

4.1   Introduction

The synthesis of the organometallic lanthanide compounds described in Chapter 1, invariably involved the use of an alkali-metal organometallic compound (metalated ligand) as a carbanion source: NaCp, KCp*, KCp' and (Me$_3$Si)CK are among the more common ligands.   The metalation of these compounds (and some phosphine-borane-stabilised carbanions similar to those discussed in Chapter 3) and their solid-state structures are briefly discussed here as a prelude to metalation of the hybrid pro-ligands. Many of these air-sensitive compounds were used in synthesis long before developments in X-ray crystallography enabled determination of their solid-state structures.   The familiar sodium cyclopentadienide was used in synthesis for 95 years before its solid-state structure was determined using powder diffraction techniques with synchrotron radiation.[1]

The protons of the cracked cyclopentadiene monomer are relatively acidic (pKa) since deprotonation generates an aromatic anion with substantial charge delocalisation. The bases ^{n}BuLi, NaH and KH can all be used to metalate the cyclopentadiene monomer and substituted derivatives.[1]   LiCp and NaCp are isostructural and their structures consist of linear chains of alternating alkali metal cations and η^5-coordinated cyclopentadienyl anions.   KCp has a regular zig-zag structure with a potassium cation at each point in the polymeric chain.[1,2] Each potassium cation is coordinated η^5 by two cyclopentadienyl rings in a bent conformation, with the Cp$_{centroid}$−K−Cp$_{centroid}$ angle being 137.95(8)°.   The potassium cations are also coordinated η^2 by cyclopentadienyl rings from two adjacent zig-zag chains. The larger ionic radius of the potassium cations (1.51 Å) explains their preference for a higher coordination number (formally 8-coordinate)

versus the smaller Li (0.76 Å) and Na (1.02 Å) cations which are formally 6-coordinate.[3]

The Cp* ring is larger and more sterically demanding (cf. Chapter 1, section 1.2.1 on tris{cyclopentadienyl systems}) but the structures of LiCp* and NaCp* are again isostructural and similar to that of LiCp with disordered Cp* rings and a slightly shorter Li−Cp$_{centroid}$ distance (1.911(3) Å) than in the structure of LiCp (1.969(1) Å).[4] The pyridine adduct NaCp*(py)$_3$ is a monomer. The crystal structure of KCp* has been determined as several pyridine and THF adducts: [KCp*(py)$_2$], [KCp*(THF)$_2$] and [KCp*(THF)]. In all these compounds the extended structure is a zig-zag polymer chain with a bent arrangement of the Cp* rings around the K cations (Figure 45), the Cp$_{centroid}$−K−Cp$_{centroid}$ angles and K−Cp$_{centroid}$ distances are: [KCp*(py)$_2$] (138°, 2.79 Å) and [KCp*(THF)$_2$] (137.9°, 2.821 Å), for [KCp*(THF)] only the atom connectivity was determined.[2,5]
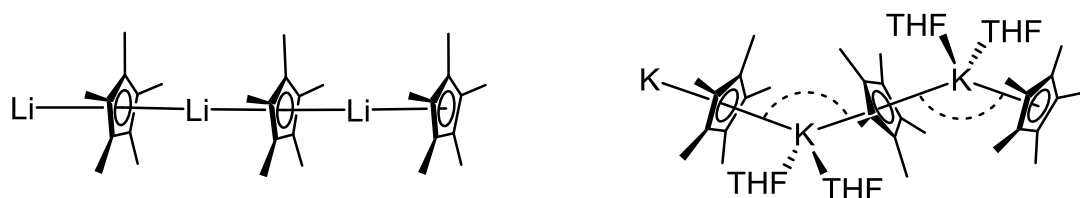
Figure 45. Linear structure of LiCp and zig-zag structure of [KCp*(THF)$_2$].*

There are considerable differences between the solid state structures of α-metalated silicon-stabilised carbanions with smaller and larger alkali metal cations.[6] For instance [Li{C(SiMe$_2$Ph)$_3$}(THF)] crystallises as a monomer with coordinated solvent, whereas [K{C(SiMe$_2$Ph)$_3$}]$_\infty$ crystallises solvent-free, with a polymeric structure involving η^6 coordination of the phenyl rings to the K cations (Figure 46).[7,8] The larger K cations have an affinity for interaction with the π-electron density of arene rings, whereas the smaller Li cations are highly polarising and interact preferentially with the localised negative charge on the carbanion carbon atom (see Chapter 3). The structures of benzyl potassium (BnK) and benzyl

lithium (BnLi) which have been crystallised as the adducts KBn(PMDTA) and LiBn(TMEDA)(THF) serve as a better known example of the same structural trend.
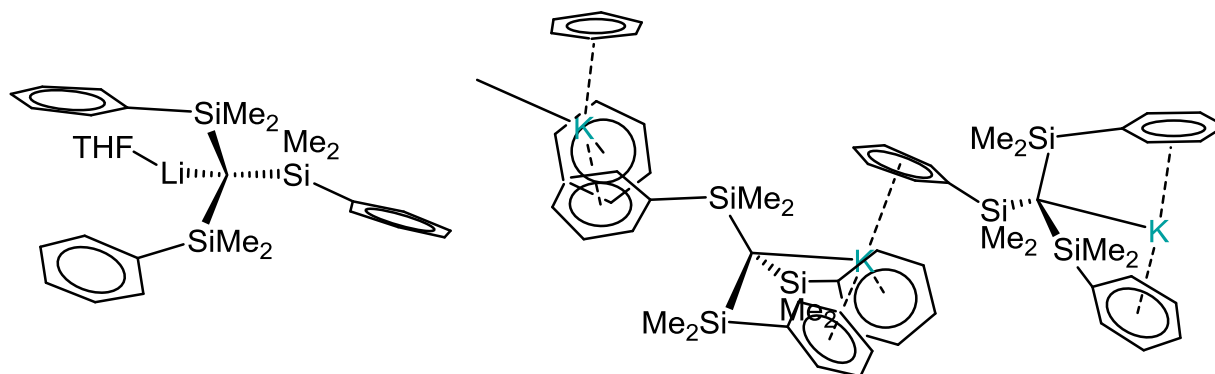
Figure 46. Structures of the [Li{C(SiMe$_2$Ph)$_3$}(THF)] monomer (left) and the [K{C(SiMe$_2$Ph)$_3$}]$_\infty$ polymer (right).

Whilst many phosphine-borane-stabilised carbanions have been prepared and used in situ as a synthetic route to chiral and achiral phosphines, structurally characterised α-metalated phosphine- boranes are uncommon and most of those known were prepared by Wills in our group one decade ago.[6,9−11]   Typically deprotonation of phosphine-borane has been carried out with BuLi, MeK or MeNa but we have since found that the more accessible BnK is sufficiently basic to deprotonate mono-phosphine-borane adducts.[12]

The silicon-stabilised alkyl carbanion (Me$_3$Si)C$^-$ and the phosphine-borane-stabilised carbanion (Me$_3$Si)$_2${Me$_2$P(BH$_3$)}C$^-$ are isosteric and isoelectronic. Differences in the stability of the carbanions and the polarity of the P−B bond versus the Si−C bond influence the reactivity and the solid-state structures of potassium complexes of these two carbanions (cf. Chapter 3).   Both potassium complexes crystallise solvent free, but the carbanion ligands adopt very different binding modes (Figure 47 and Figure 48).[9]
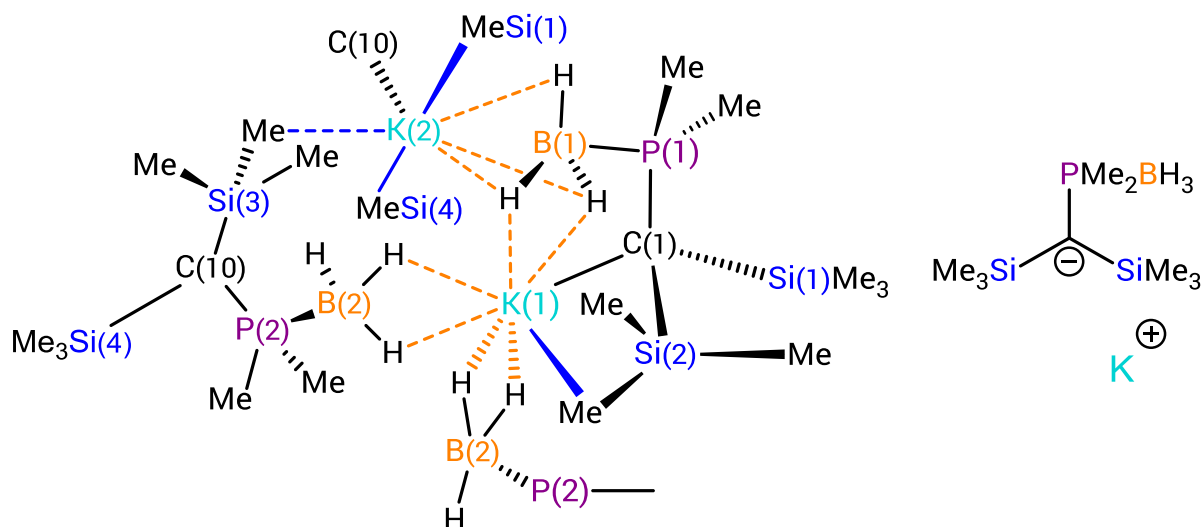
Figure 47. Coordination geometry of the potassium cations K(1) and K(2) in the solid-state structure of the metalated phosphine-borane-stabilised carbanion ligand (Me₃Si)₂{Me₂P(BH₃)}CK. Each K(I) cation is coordinated κ² H,H by three BH₃ groups, one carbanion carbon C(1) and a single Si−Me····K agostic-type interaction. Each K(2) cation is coordinated κ³ H,H,H by one BH₃ group, one carbanion carbon C(10) and three Si−Me····K agostic-type interactions.
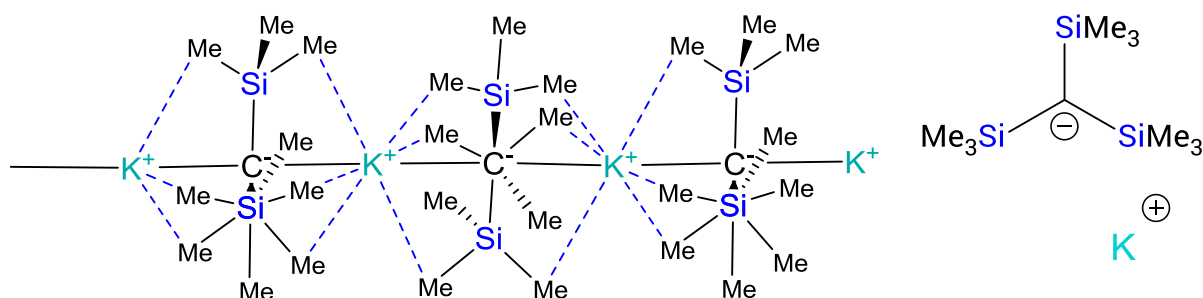
Figure 48. Coordination geometry of the potassium cations in the solid-state structure of the metalated silicon-stabilised-carbanion ligand (Me₃Si)CK (N.B The silicon atoms of two −SiMe₃ groups are eclipsed in the first and last carbanions in the illustrated section of the polymer, and in middle carbanion the carbanion carbon atom and Si atom of the third −SiMe₃ group are eclipsed). Each K cation can be described as formally 8-coordinate. The cations are sandwiched between two carbanion carbon atoms and are also coordinated by six Si−Me····K agostic-type interactions.

Metalated hybrid ligands were prepared as dipotassium salts from mixtures of pro-ligand regioisomers. Organopotassium compounds were chosen because they are less likely to form 'ate' complexes when subsequently used in metathesis reactions with lanthanide halides.[13] The potassium halide by-product has a large lattice energy and so usually precipitates and is easily separated from the more soluble

lanthanide organometallic product by filtration. The use of organolithium precursors often results in the incorporation of solvated lithium cations (separated ion pairs) or LiCl (Ln−Cl−Li(solvate)$_x$ with an η^2-bridging chloride anion) in the solid state structures of the organolanthanide compounds (see chapter 1 and chapter 5).

Studies of the effect of cation size on the structures of alkali metal complexes of the hybrid ligands could uncover information that is important to understand the structures, bonding and reactivity of these ligands, but since here their synthesis was an intermediate step in the synthesis of lanthanide complexes of the hybrid ligands, discussion is largely confined to potassium salts.

4.2 Synthesis of potassium complexes of [(R′Me$_2$Si)C(Me$_3$Si)$_2$]$^{2-}$ (R′ = Cp, Cp′ or Cp^{4Me}) and [(Cp^{4Me}Me$_2$Si)(Me$_3$Si)C{PR″$_2$(BH$_3$)}]$^{2-}$ (R″ = Me or ^{n}Pr)

4.2.1 Synthesis of [(R′Me$_2$Si)C(Me$_3$Si)$_2$]K$_2$(L)$_{0.5}$, {R′ = Cp [50], Cp^{4Me} [51] or Cp′ [52], L = OEt$_2$ or C$_6$H$_6$}

Initially our focus was on hybrid ligands incorporating a trimethylsilyl-stabilised carbanion. Treatment of (R′HMe$_2$Si)CH(Me$_3$Si)$_2$ with base such as ^{n}BuLi or LDA led only to removal of the cyclopentadienyl protons, leaving the methine proton of the hybrid pro-ligand unaffected. Similarly, the methine proton is not removed on treatment of (R′HMe$_2$Si)CH(Me$_3$Si)$_2$ with two equivalents of BnK, even after heating at reflux for several hours indicating that the proton adjacent to the SiMe$_3$ groups has a pK$_a$ greater than the pK$_a$ of toluene (pK$_a$>43), and close to the pK$_a$ of the 'trisyl' ligand described in Chapter 1.[14,15] However, the pro-ligands **5**, **6**, **7** were successfully doubly deprotonated using the powerful base MeK.

The reaction of the hybrid pro-ligands, as mixtures of regioisomers, with four equivalents of MeK in diethyl ether at -78°C gave the compounds [(R'Me$_2$Si)C(Me$_3$Si)$_2$]K$_2$(Et$_2$O)$_{0.5}$, {R' = Cp [50], Cp^{4Me} [51] or Cp' [52]} (*Scheme 47*) on warming to room temperature. Filtration followed by removal of the solvent *in vacuo* from the filtrate gave the products as dark beige foams or powders depending on the purity of the pro-ligand starting material in approximately 40% yield. It is necessary to use large excess of MeK as this compound reacts with the diethyl ether solvent.

R^1 − R^4 = H [50]

R^1 − R^4 = Me [51]

R^1, R^2, R^4 = H, R^3 = SiMe$_3$ [52]
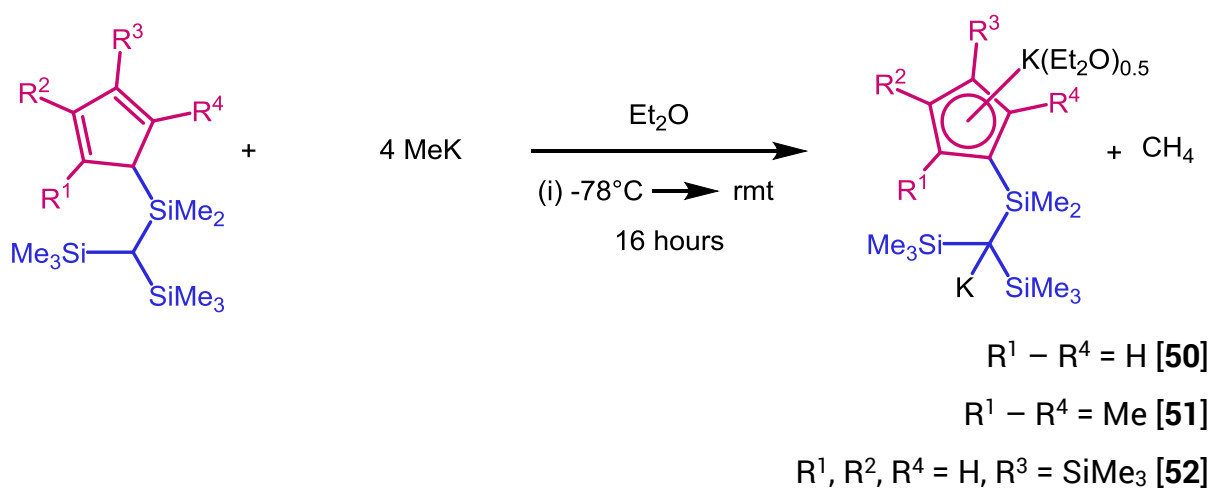
Scheme 47. Synthesis of 50, 51 and 52.

The purity of the hybrid pro-ligands was paramount to the purity of the dipotassium salt products. Impurities carried through in the reaction mixture from the synthesis of the hybrid pro-ligands may be attacked by the MeK base used to doubly deprotonate the pro-ligand. This not only generates contaminating impurities but also reduces the stoichiometric excess of MeK, meaning the reaction did not always go to completion and a mixture of mono- and dipotassium salts was obtained (Figure 49). MeK reacts with diethyl ether above 0°C to give KOEt, methane and ethane. Deprotonation does not occur at very low temperature due to a thermodynamic barrier, so competing reactions with the pro-ligand and the solvent necessitate a large excess of MeK for the reaction to go to completion.
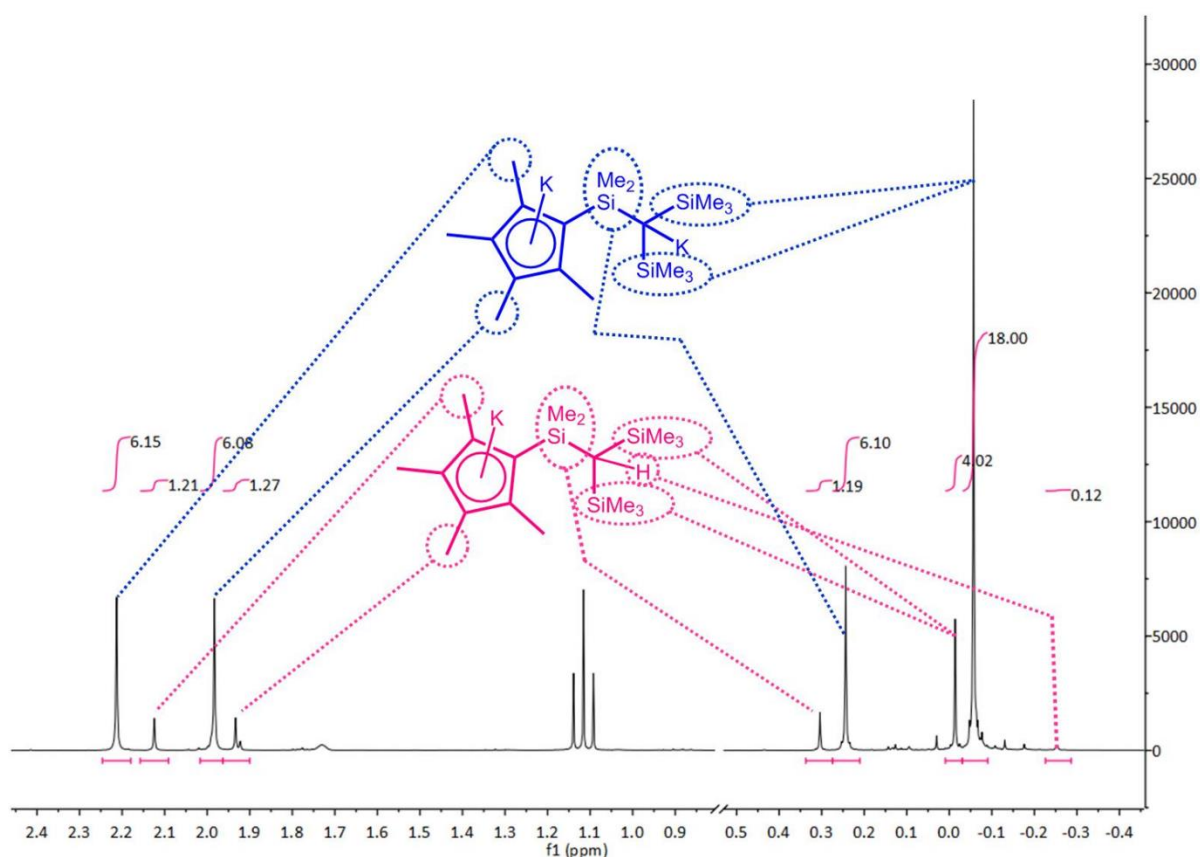
Figure 49. ^{1}H NMR spectrum of a mixture of mono and dipotassium salts obtained from an incomplete metalation reaction.

Mixtures of mono and dipotassium salts created issues with crystallisation – solutions were very oily with the dipotassium salt being less soluble. But in the presence of monopotassium salt impurities, the dipotassium salt tended to form in diethyl ether as a precipitate rather than crystallise. The poor solubility of the dipotassium salts in diethyl ether was a factor affecting reaction yields because the excess MeK was removed by filtration.

The dipotassium salt **52** and the compound $[(Me_3Si)_3CK]_\infty$ are both soluble in benzene and can be crystallised from this solvent.[15] The cyclopentadienyl groups of the dipotassium salts **50** and **51**, and the phenyl groups of the compound $[K\{C(SiMe_2Ph)_3\}]_\infty$ make these compounds much less soluble in benzene and addition of a small amount of diethyl ether or THF is required to fully dissolve them. All of these compounds attack toluene due to their extremely high pK_a (very strong

bases) to give orange benzylpotassium and the corresponding mono-potassium salt. They also decompose slowly in THF at room temperature – observed as the formation of mixtures of monopotassium and dipotassium salts in sealed NMR samples (C_6D_6/d_8-THF mixtures) left to stand for several weeks.

The dipotassium salts **50 - 52** and were isolated as the diethyl ether hemisolvates. Compounds **50** and **51** are sparingly soluble in benzene. The donor solvent was removed from **50** by heating at reflux in benzene for two days, whereby the unsolvated dipotassium salt $[(CpMe_2Si)C(Me_3Si)_2]K_2$ **[50']** precipitates as a very pale grey powder. The dipotassium salts **50** and **51** were crystallised as the alternate solvates $[(CpMe_2Si)C(Me_3Si)_2]K_2(Et_2O)$ **[50.Et$_2$O]** and $[(Cp^{4Me}Me_2Si)C(Me_3Si)_2]K_2(Et_2O)$ **[51.Et$_2$O].** Due to the better solubility of **52** in benzene, this compound was crystallised from benzene as the solvate $[(Cp'Me_2Si)C(Me_3Si)_2]K_2(C_6H_6)$ **[52.C$_6$H$_6$]**. Exposure of crystals of **[50.Et$_2$O]**, **[51.Et$_2$O]** and **[52.C$_6$H$_6$]** to vacuum resulted in solvent loss and isolation of the hemisolvates **50 - 52** , and the reported NMR data relates to these compounds.

4.2.2 Synthesis of $[(Cp^{4Me}Me_2Si)(Me_3Si)C\{PR''_2(BH_3)\}]K_2(THF)_{0.5}$ {R'' = Me [53] or ^nPr [54]}

To address the difficulties with the synthesis of **51**, including poor yields, high pK_a of the methine proton, incomplete deprotonation, instability of the reagents and products, and crystallisation issues, one of the $-SiMe_3$ groups in the hybrid pro-ligands was replaced with an isoelectronic and isosteric $-PMe_2(BH_3)$ group. The dipotassium salt $[(Cp^{4Me}Me_2Si)(Me_3Si)C\{PMe_2(BH_3)\}]K_2(THF)_{0.5}$ **53**, which is isoelectronic with $[(Cp^{4Me}Me_2Si)(Me_3Si)_2C]K_2(Et_2O)_{0.5}$ **51** was synthesised by reaction of a solid crystalline mixture of regioisomers of the pro-ligand with 2 equivalents of BnK in THF at room temperature (*Scheme 48*). Similarly, treatment of **14** with two equivalents of BnK in THF gives the dipotassium salt as the hemisolvate $[(Cp^{4Me}Me_2Si)(Me_3Si)C\{P^nPr_2(BH_3)\}]K_2(THF)_{0.5}$ **54** in good yield.
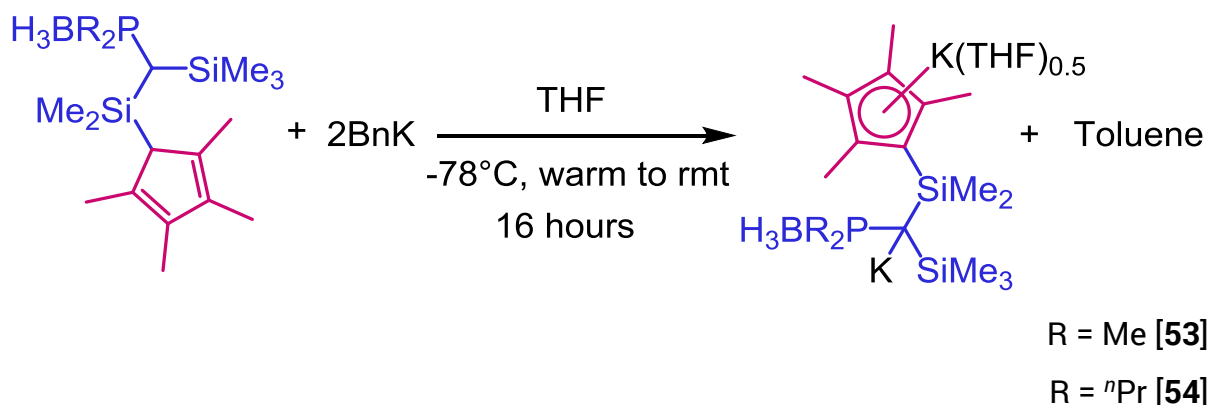
Scheme 48. Synthesis of 53 (R = Me) and 54 (R = ^{n}Pr).

This ligand synthesis highlights many synthetic advantages of phosphine-boranes. The pro-ligand starting material is readily purified by recrystallization from cold (-24°C) diethyl ether (see Chapter 2) so no impurities are carried through to the subsequent metalation step. The $PMe_2(BH_3)$ group stabilises the adjacent carbanion centre to a greater degree than the $-SiMe_3$ group it replaced, resulting in a decrease in pK_a of the methine proton of the pro-ligand. Deprotonation can be achieved with a stoichiometric number of equivalents of BnK, which can be prepared in large batches and which does not react with the THF solvent at room temperature.

The progress of the reaction can be monitored by $\{H^1\}^{31}P$ and $\{H^1\}^{11}B$ NMR spectroscopy to ensure complete conversion to the dipotassium salt and to monitor decomposition. For instance, monitoring of the synthesis of **54** by $\{H^1\}^{31}P$ and $\{H^1\}^{11}B$ NMR spectroscopy showed that the chemical shift of the monopotassium salt in the reaction mixture is 18.6 ppm with an unresolved J_{PB} coupling constant of about 50 Hz whereas the chemical shift of the dipotassium salt is 7.0 ppm with J_{PB} = 89 Hz (Figure 50). The coupling constant approximately doubles when the methine carbon adjacent to the phosphorus atom is metalated to give a tertiary carbanion. The J_{PB} coupling constant of **54** is very similar to that of **53** (J_{PB} = 93.8 Hz) and to other examples of α-metalated phosphine-borane-stabilised carbanions including $(Me_2Si)_2\{Me_2P(BH_3)\}CLi$ (J_{PB} = 89.4 Hz),

[(Me$_3$Si)$_2${Ph$_2$P(BH$_3$)}CK(OEt$_2$)$_2$] (J_{PB} = 107.3 Hz) and (THF)$_2$Li{(Me$_3$SiCH)$_2$-P(BH$_3$)Ph}Li(THF)$_3$ (J_{PB} = 107.9 Hz).[9,16] A similar increase in the J_{PB} coupling constant of 30 – 50 Hz is observed upon metalation for all of these compounds as can be seen from the coupling constants of the corresponding protonated phosphine-borane adducts: (Me$_2$Si)$_2${Me$_2$P(BH$_3$)}CH (J_{PB} = 59.5 Hz), (Me$_3$Si)$_2${Ph$_2$P(BH$_3$)}CH (J_{PB} = 66.1 Hz) and {(Me$_3$Si)CH$_2$}$_2$P(BH$_3$)Ph (J_{PB} = 58.8 Hz).
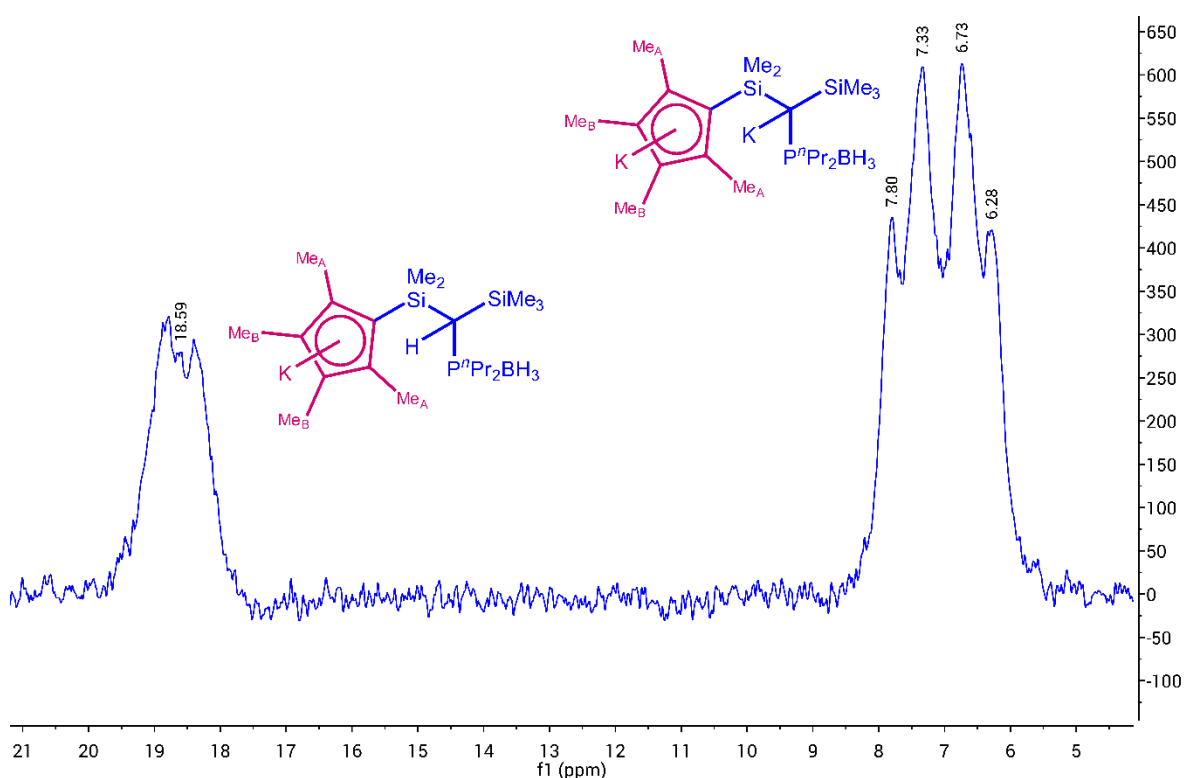
Figure 50. Monitoring of an incomplete metalation reaction by ^{31}P{^{1}H} NMR spectroscopy.

The products are stable in THF and crystals of the alternative solvate [(Cp^{4Me}Me$_2$Si)(Me$_3$Si)C{PMe$_2$(BH$_3$)}]K$_2$(THF) **[53.THF]** were grown from benzene containing a few drops of THF at room temperature. Overall, hybrid ligands combining phosphine-borane-stabilised carbanions with substituted

cyclopentadienyl rings can be prepared in higher yields (ca. 90%), in more straightforward reactions using easier to handle reagents, that can be monitored in situ to ensure higher purity products and isolated using simpler procedures than hybrid ligands with silicon-stabilised carbanions.

4.3 Solid-state structures of hybrid ligands featuring silicon-stabilised carbanions

Since these ligands are hybrids of substituted cyclopentadienyl rings and trimethylsilyl stabilised alkyl carbanions it is relevant to draw comparisons between the compounds $[(Me_3Si)CK]_\infty$ and $[K\{C(SiMe_2Ph)_3\}]_\infty$ and also dicarbanions such as $[[\{Me_3Si)_2C(SiMe_2)\}_2O]K_2](OEt_2)$ and the dipotassium salts **51** and **52**.[15,17] Comparisons between the structures of the cyclopentadienyl organopotassium compounds: $[(THF)_2K(Cp^*)]$ and $[(py)_2K(Cp^*)]$ and the dipotassium salts **51** and **52** will be considered similarly.[5,18]

The dipotassium salts of the silyl hybrid ligands crystallise as the solvates $[(Cp^{4Me}Me_2Si)(Me_3Si)_2C]K_2(OEt_2)$ **[51.Et₂O]** and $[(Cp'Me_2Si)(Me_3Si)_2C]K_2(C_6H_6)$ **[52.C₆H₆]**. **[51.Et₂O]** was crystallised from diethyl ether at 3°C and **[52.C₆H₆]** was crystallised from benzene at 5°C. Solvent loss occurs readily under vacuum and the solid powders are less solvated according to the acquired NMR data (**50, 51, 52**), with half a molecule of coordinated solvent in the molecular formula of the bulk materials versus one molecule in the crystalline solids.

With the notable exception of KCp' which has been crystallised solvent-free, most potassium cyclopentadienides have only been crystallised as THF solvates or with coordinating bases such as pyridine.[19] In contrast, $[(Me_3Si)_3CK]_\infty$, and $[K\{C(SiMe_2Ph)_3\}]_\infty$, crystallise with solvent-free structures even in the presence of a donor solvent (see above, Figure 47 and Figure 48).

4.3.1   Solid-state structure of [{(Cp^{4Me}Me$_2$Si)C(Me$_3$Si)$_2$}K$_2$(Et$_2$O)]$_\infty$ [51.Et$_2$O]

Half of the potassium cations in the asymmetric unit of **[51.Et$_2$O]** are solvent-free and these cations are sandwiched between a trisyl-like carbanion and the cyclopentadienyl ring of a different hybrid ligand.   The extended structure of **51.Et$_2$O** consists of chelated [(hybrid ligand)K(Et$_2$O)]$^-$ anionic units linked nose to tail by potassium cations in a zig-zag polymer chain (Figure 51 and Figure 52). The structure bears resemblance to the structure of [[{Me$_3$Si)$_2$C(SiMe$_2$)}$_2$O]K$_2$](OEt$_2$) **[55]**, also a zig-zag polymer featuring alternately solvated and solvent-free K cations and a chelating, sterically-hindered silicon-stabilised dicarbanion ligand (Figure 53).
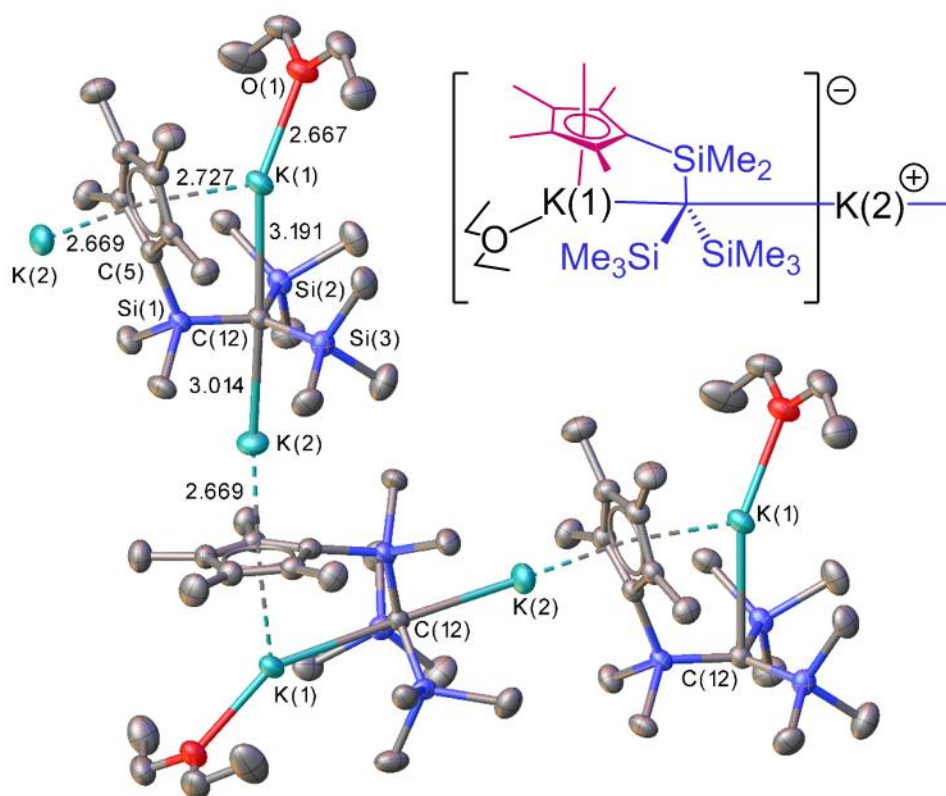
*Figure 51. Extended structure of **[51.Et$_2$O]**, with agostic-type contacts omitted, showing the chelated [(hybrid ligand)K(Et$_2$O)]$^-$ anionic units linked nose to tail by K cations in a non-linear polymer chain.*

142
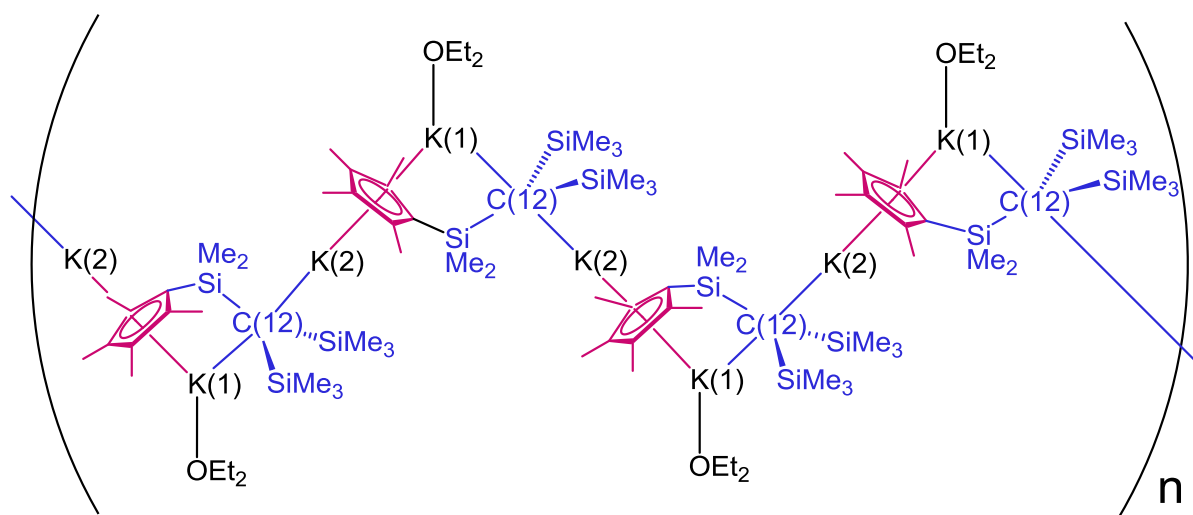
*Figure 52. Polymer chain structure of **51.Et₂O***
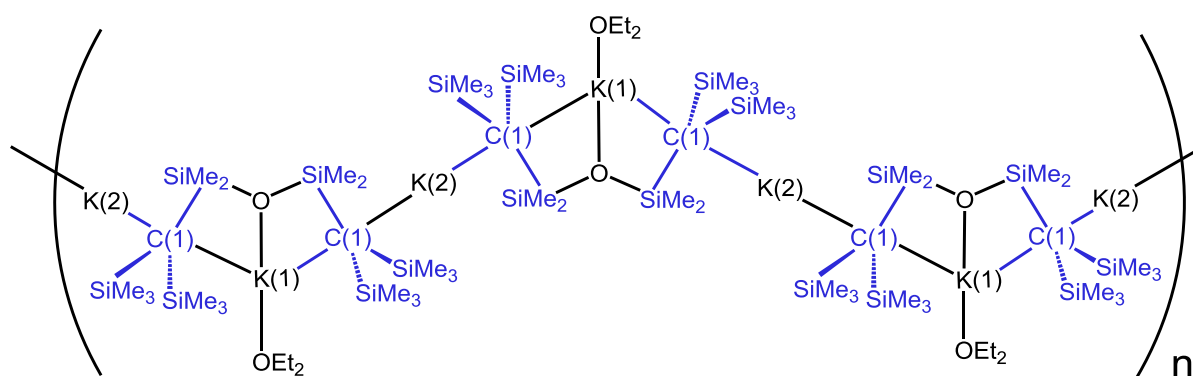
*Figure 53. Polymer chain structure of **55***

The K(1)—C(12) and K(2)—C(12) bond lengths of **51.Et₂O** are 3.1910(19) Å and 3.0138(9) Å, respectively. These are similar to the corresponding distances found in [[{Me₃Si}₂C(SiMe₂)}₂O]K₂](OEt₂), where the K(1)—C(1) and K(2)—C(1) distances are 3.2302(18) Å and 3.0132(19) Å respectively, with the K(2) cations being unsolvated in both structures (*Figure 51*, *Figure 52* and *Figure 53*). The structure of **51.Et₂O** appears to be a mixture of the structures of [(Me₃Si)₃CK]∞ (see above, Figure 48) and [KCp*(THF)₂] (see above, Figure 45) in that it has structural similarities with both. While **51.Et₂O** crystallises with a zig-zag polymeric structure also seen for [KCp*(THF)₂], the zig-zag chain changes direction only every other chelated K(1) potassium cation. The K(2) cations in **51.Et₂O** are unsolvated and not chelated, and

are linearly sandwiched between a 'trisyl-like' carbanion, C(12) the cyclopentadienyl ring of a symmetry equivalent hybrid ligand. The K(2)−C(12) distance is 3.0138(9) Å and the K(2)−Cp^{4Me}(centroid) distance is 2.6687(10) Å (see below, Table 15). The K(1)−C(12) and K(1)−Cp^{4Me}(centroid) distances are slightly longer at 3.1910(19) Å and 2.7273(10) Å (see below, Table 15) respectively.

The symmetry inequivalent potassium cations K(1) and K(2) in **51.Et$_2$O** are not equidistant from the C(12) carbanion carbon, unlike in [(Me$_3$Si)$_3$CK]$_\infty$ where each potassium cation is located equidistant between two trisyl carbanions with a K−C distance of 3.104(11) Å, which is intermediate with the two K−C distances in **51.Et$_2$O**. The K(2)−C(12) contacts are shorter than in [(Me$_3$Si)$_3$CK]$_\infty$, perhaps because the planar cyclopentadienyl ring opposite offers less steric hindrance.

4.3.2 Solid-state structure of [(Cp'Me$_2$Si)(Me$_3$Si)$_2$C]K$_2$(C$_6$H$_6$) 2C$_6$H$_6$ [52.C$_6$H$_6$]

There are two distinct types of polymer chain in the structure of **52.C$_6$H$_6$** and these chains are cross-linked by a short contact between K(4) and C(15) of the −SiMe$_3$ substituent of the Cp' ring (Figure 54). Cross-linking of polymer chains is also observed in the structures of KCp and KCp', where staggered parallel −K−Cp'−K−Cp'− chains are cross-linked by weak η^2 interactions between a Cp' ring in one chain and a K cation in the adjacent chain. One of the polymer chains in **52.C$_6$H$_6$** is similar to the chains found in the structure of **51.Et$_2$O** with chelated [(hybrid ligand)K(1)(C$_6$H$_6$)]$^-$ anionic units linked by solvent-free K(2) cations (Figure 52). In the other type of polymer chain there is no chelation of the K(3) cation by the dianionic hybrid ligand (Figure 55). The ligand coordinates K(3) in an η^5 manner by the cyclopentadienyl ring and the silicon-stabilised carbanion coordinates through two agostic-type K····Me contacts rather than the carbanion carbon atom C(31). The K(3)····C(31) distance is 3.740(6) Å (see below, Table 15), far longer than any known K−C σ-bond lengths which are typically 2.91 − 3.10 Å.[2] K(3) is also

coordinated by an η^6 benzene ring showing the affinity of potassium cations for the π-electron density of arene rings similarly to in the structure of $[K\{C(SiMe_2Ph)_3\}]_\infty$. The carbanion carbon C(31) does coordinate to the adjacent K(4) cations in the same polymer chain, and these are wedged between the carbanion and a cyclopentadienyl ring of different hybrid ligands. Both the polymer chain connecting the K(2) and K(1) cations and the polymer chain connecting the K(3) and K(4) cations in **52.C$_6$H$_6$** are zig-zags with the chain changing direction every other potassium cation {K(1) or K(3)} in a similar way to in the structure of **51.Et$_2$O**. The unsolvated K cations of each polymer chain {K(2) or K(4)} have a more bent coordination geometry than the linearly coordinated K(2) cations in **51.Et$_2$O**. The Cp'$_{centroid}$—K(2)—C(8) angle in **52.C$_6$H$_6$** is 154.51(12)° and the Cp'$_{centroid}$— K(4)—C(31) angle is 153.09(13)°, making the zig zag pattern less distinctive.
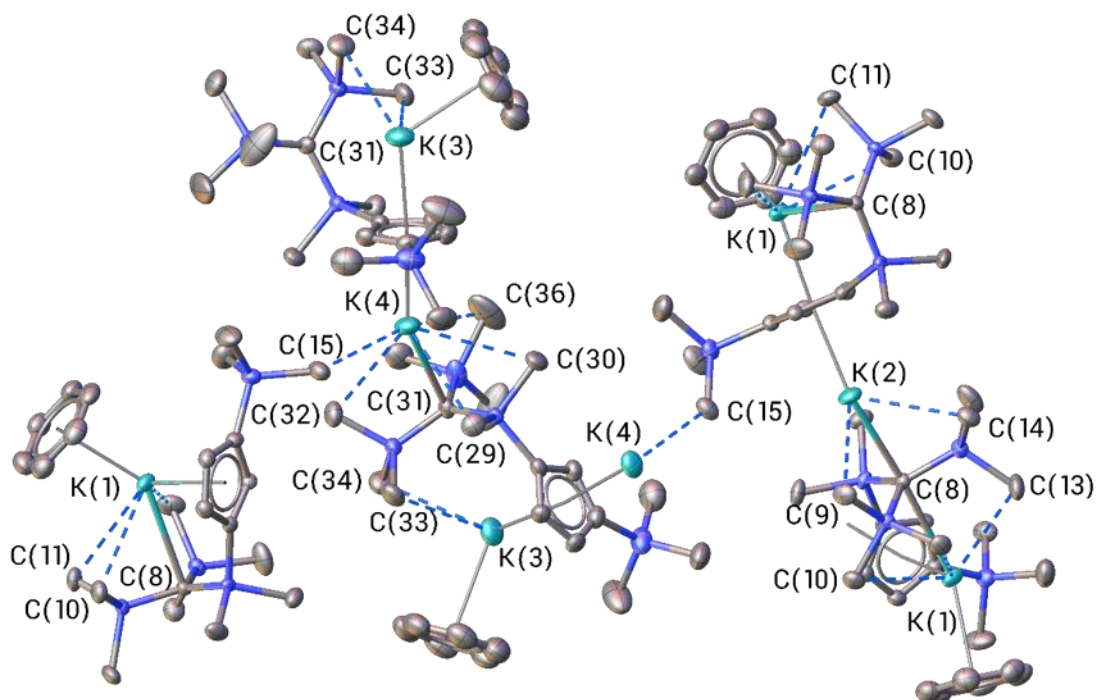
*Figure 54. Extended structure of **52.C$_6$H$_6$** showing the K(4)····C(15) cross-links and the agostic-type K····Me contacts. Solvent of crystallisation and H atoms are omitted for clarity.*
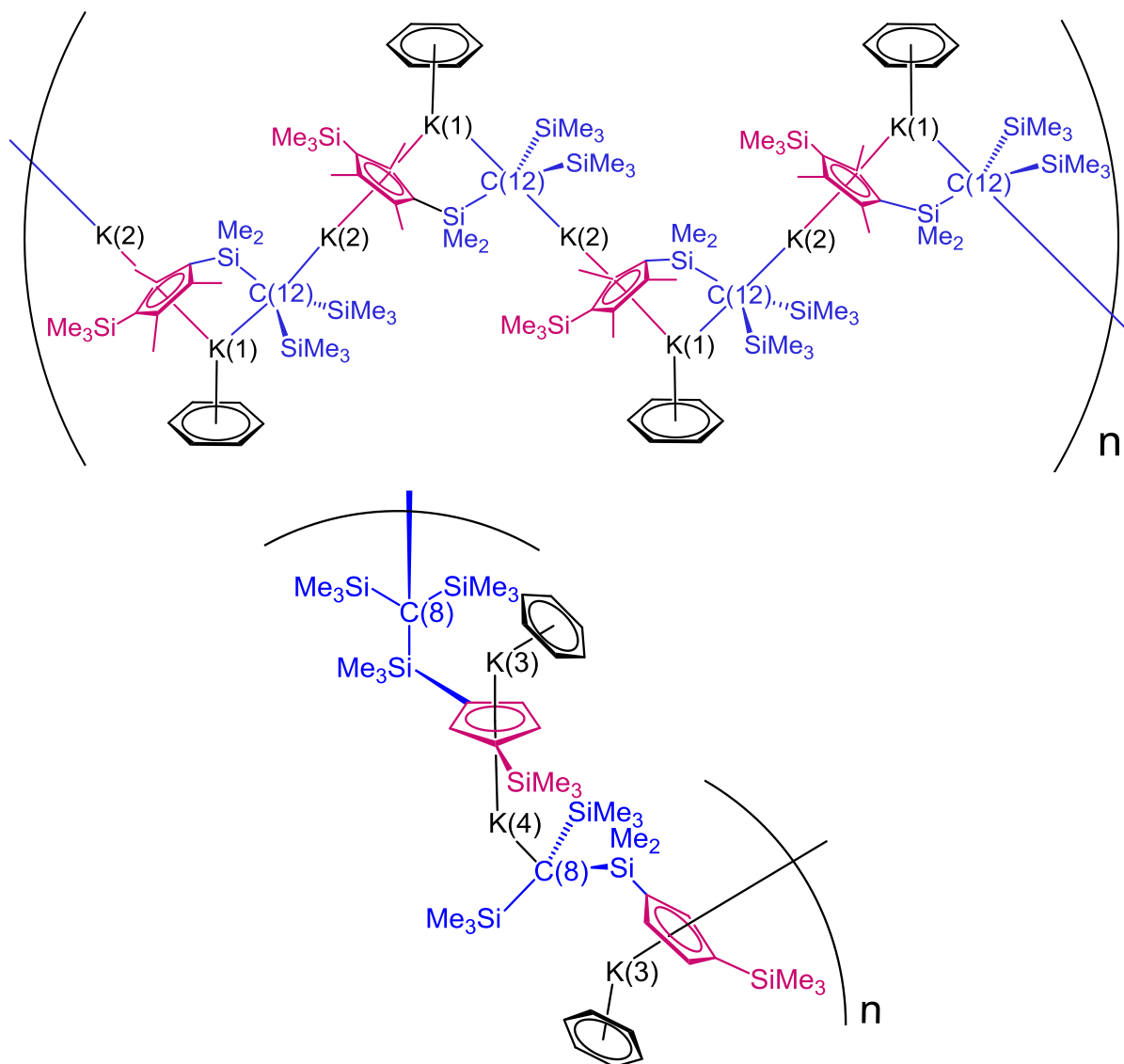
*Figure 55. The two different polymer chains in the structure of **52.C₆H₆**. Top: a similar polymer chain to that seen in the structure of where the ligand chelates the solvated K(1) cations, the ether solvent is replaced by benzene. Bottom: the ligand does not chelate any of the K(3) or K(4) cations in this polymer chain.*

146

Table 15. Comparison of the lengths of the main ionic interactions in the dipotassium salts of the hybrid ligands

	51.Et$_2$O	52.C$_6$H$_6$
C$^\ominus$·····K$_{(solvated)}$[1] / Å	K(1)−C(12) = 3.1910(19)	K(1)−C(8) = 3.225(5)
		K(3)····C(31) = 3.740(6)
C$^\ominus$·····K$_{(unsolvated)}$ / Å	K(2)−C(12) = 3.0138(9)	K(4)−C(31) = 3.031(6)
		K(2)−C(8) = 2.984(5)
Ring centroid[2]···· K$_{(solvated)}$ / Å	K(1)−Cp^{4Me} = 2.7273(10)	K(1)−Cp′ =2.716(3)
		K(3)−Cp′ = 2.391(3)
Ring centroid[2]···· K$_{(unsolvated)}$ / Å	K(2)− Cp^{4Me} = 2.6687(10)	K(2)−Cp′ = 2.693(3)
		K(4)−Cp′ = 2.732(3)
Solvent[3]·····K /	K(1)−OEt$_2$ = 2.6671(14)	K(1)−C$_6$H$_6$ = 3.007(3)
		K(3)−C$_6$H$_6$ = 3.177(4)

[1] **Solvent is diethyl ether or benzene**

[2] **Centroid of cyclopentadienyl anion**

[3] **Centroid of benzene molecule**

4.3.3   Agostic-type interactions in the polymeric solid-state structures of the hybrid ligands

Short Si−Me····K contacts between peripheral methyl carbon atoms of the carbanion-stabilizing −SiMe$_3$ groups and the K cations are common to all the K cations in the structures of the hybrid ligand complexes. In **51.Et$_2$O** only one of the

eight silyl methyl groups {C(17) in Figure 56} lies close to the plane of the alkyl carbanion and so is non-coordinating, four of the Si−Me groups form short contacts with unsolvated K(2) cations and three with solvated K(1) cations rendering each of these ions effectively 8-coordinate (the Cp^{4Me} ring formally occupies three coordination sites of K(1) and K(2)). These interactions are also found in [(Me$_3$Si)$_3$CK]$_\infty$, where there are six Si−Me····K interactions for each potassium cation with distances ranging from 3.16 - 3.31 Å, the remaining three non-coordinating methyl groups lie in the plane of the carbanion (Figure 56).

The electrostatic interactions between the K cations and the peripheral methyl groups of the silicon-stabilised carbanion are longer than usual in compound **51.Et$_2$O** (3.18 − 3.69 Å) compared with the expected range of 3.20 − 3.30 Å for distances between K cations and methyl groups on the anion periphery in organopotassium compounds.[2] It is suggested that geometry constraints imposed by η^5 coordination of the cylopentadienyl anion to the potassium cations and the formation of a chelate ring are responsible for the slight elongation of the Si−Me····K short contacts. The cyclopentadienyl ring is perpendicular to the plane of the alkyl carbanion (Torsion angle C(5)−Si(1)−C(12)−Si(2) = 90.46(8)°) as is one Me group of each of the two −SiMe$_3$ groups (Torsion angles: C(13)−Si(2)−C(12)−Si(3) = 89.45(10)° and C(16)−Si(3)−C(12)−Si(2) = 97.74(10)°). These two perpendicular Me groups form the two shortest K····C(Me) distances for this compound K(2)····C(13) = 3.182(2) Å and K(1)····C(16) = 3.346(2) Å (Figure 56).
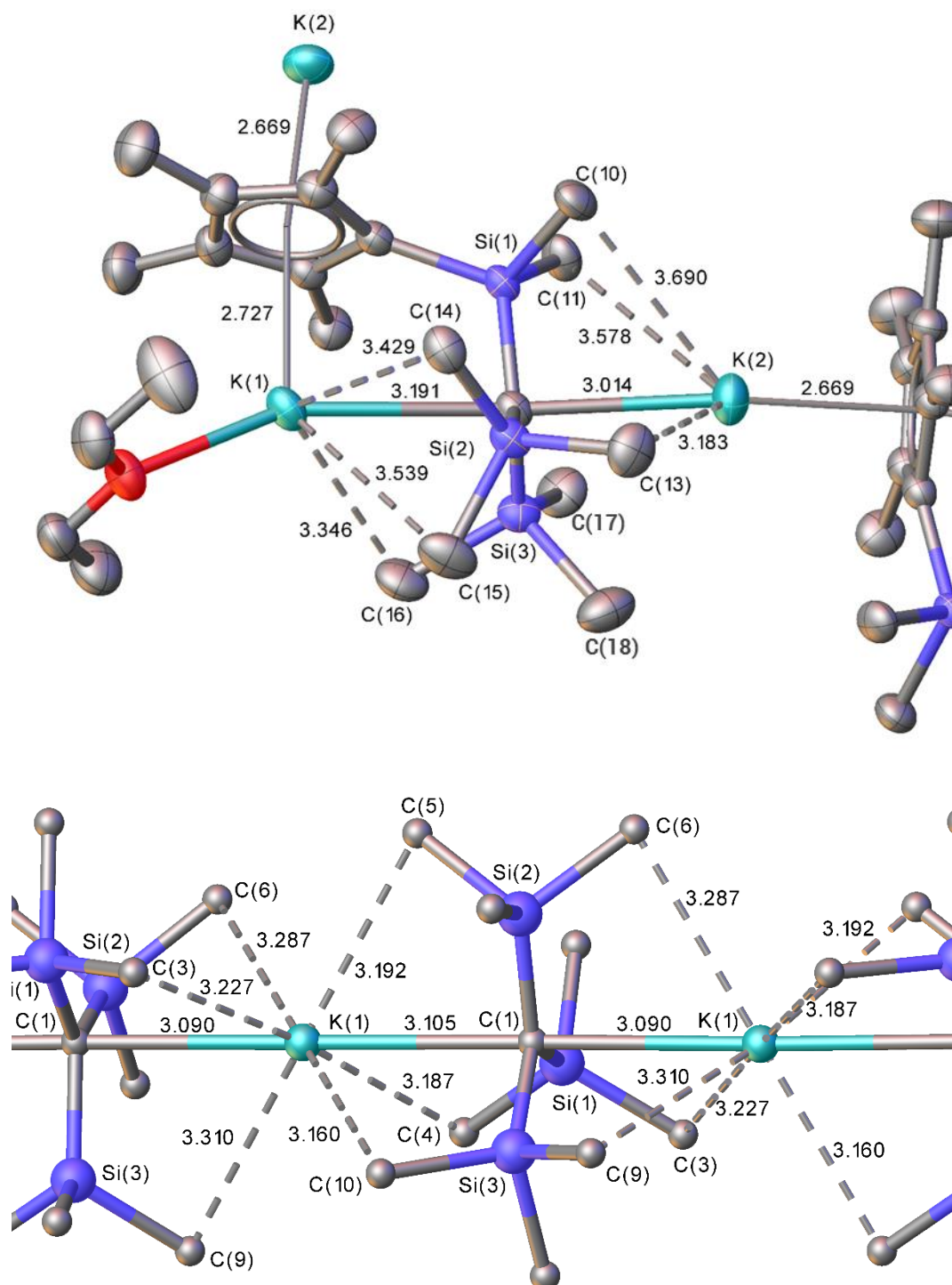
*Figure 56. Agostic-type Si−Me····K interactions in **51.Et$_2$O** and [(Me$_3$Si)$_3$CK]$_\infty$.*

In **52.C$_6$H$_6$** the conformation of the −SiMe$_3$ groups of the silicon-stabilised carbanion is again influenced by the perpendicular arrangement of the cyclopentadienyl anion relative to the plane of the carbanion, and this (on average) elongates the K····Me contacts (average K····Me distance is ca. 3.5 Å, range 3.01 −

149

3.75 Å) relative to expected values (3.20 − 3.30 Å).[2] There is also more of a spread of K⋯Me distances, since very short contacts are observed, e.g. K(2)⋯C(9) = 3.103(6) Å for those Si−Me groups lying at almost 90° degrees to the plane of the carbanion. Only two methyl groups can adopt this conformation, either parallel or antiparallel to the cyclopentadienyl anion.   There are a large number of K⋯Me contacts which are listed in Table 16.

Taking into account the agostic-type Me⋯K contacts the unchelated K(3) cation of **52.C$_6$H$_6$** is 8-coordinate (η^5-Cp', η^6-C$_6$H$_6$ and two Me⋯K contacts). The unsolvated cation K(4) in the same polymer chain is 9-coordinate (η^5-Cp', η^1-carbanion and 5 Me⋯K contacts) including the Me⋯K cross-linking interaction to the Cp' ring coordinating K(1) and K(2) in the next polymer chain. The chelated K(1) cation is 10-coordinate (η^5-Cp', η^1-carbanion, η^6-C$_6$H$_6$ and three Me⋯K contacts).   It is unsurprising that two of the longest Me⋯K contact distances are for the K(1) and K(4) cations with their high coordination numbers (Table 16).   Shorter Me⋯K contact distances are found for K(2) which has a coordination number of seven (η^5-Cp', η^1-carbanion and three Me⋯K contacts).

*Table 16. Agostic-type K⋯Me contacts (Å) for **52.C$_6$H$_6$***

K(1)⋯C(10)	3.440(6)	K(3)⋯C(33)	3.753(7)
K(1)⋯C(11)	3.728(6)	K(3)⋯C(34)	3.354(7)
K(1)⋯C(13)	3.243(7)	K(4)⋯C(29)	3.500(7)
K(2)⋯C(7)	3.615(6)	K(4)⋯C(30)	3.685(7)
K(2)⋯C(9)	3.103(6)	K(4)⋯C(32)	3.468(7)
K(2)⋯C(14)	3.368(7)	K(4)⋯C(36)	3.727(11)

The dianionic hybrid ligand chelates the K(1) cations in both **51.Et₂O** and **52.C₆H₆** by coordinating though both the cyclopentadienyl ring and the planar alkyl carbanion, forming a strained pseudo-four-membered ring (The average of the internal angles α, β, γ and ε of the polygon in Table 17 is approximately 93°) (Table 17). The ring centroid−K(1)−C(12) angle (α) in **52.C₆H₆** is acute (87.43(4)°) due to chelation of the ligand.

Table 17. Geometry of the pseudo-four-membered chelate rings
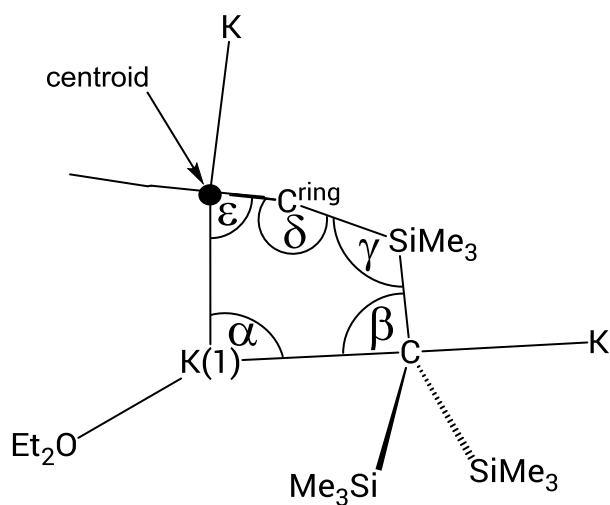
Bond lengths (Å) and angles (deg)	$[K\{C(SiMe_2Ph)_3\}]_\infty$	51.Et$_2$O	52.C$_6$H$_6$
K(1)−C	3.26(2)	3.1910(19)	3.225(5)
C−Si	1.82(2) / 1.869(14)	1.8382 (19)	1.831(5)
Si−C(ring)	1.94(2) / 1.91(2)	1.8838(19)	1.862(5)
C(ring)−centroid	1.397(18) / 1.411(19)	1.2336(16)	1.229(4)
Si−centroid	3.333(10) / 3.317(10)	3.0966(10)	3.077(3)
Centroid−K(1)	2.949(11) / 3.000(7)	2.7273(10)	2.716(3)
Centroid−K(1)−C (α)	86.1(4) / 85.3(3)	87.43(4)	85.78(11)
K(1)−C−Si (β)	91.9(7) / 91.7(7)	86.59(7)	86.93(17)
C−Si−C(ring) (γ)	109.7(10) / 107.4(8)	113.3(2)	115.23(8)
Si−C(ring)−centroid (δ)	173.8(13) / 176.9(14)	169.1(4)	166.47(13)
C(ring)−centroid−K(1) (ε)	77.2(9) / 74.7(5)	83.6(2)	83.88(8)

4.4 Solid-state structure of a hybrid ligand featuring a phosphine-borane-stabilised carbanion

4.4.1 Solid-state structure of $[(Cp^{4Me}Me_2Si)(Me_3Si)C\{PMe_2(BH_3)\}]K_2(THF)$ [53.THF]

Complex **53.THF** is the first organopotassium compound incorporating both a cyclopentadienyl anion and a phosphine-borane-stabilised carbanion. The molecules of **53.THF** pack with relatively high symmetry resulting in the higher symmetry space group $I4_1/a$ (Figure 57). The packing and formation of network structures is encouraged by agostic-type intermolecular interactions from the borane-hydrogens. There are two symmetry inequivalent K cations in the asymmetric unit and a single hybrid ligand molecule. One of the K cations, K(1) is coordinated by a THF solvent molecule, the Cp^{4Me} ring of the hybrid ligand, an κ^2 *H,H* coordinated BH_3 group of the same ligand and a short K····Me−P contact. There is no contact between the carbanion centre and K(1). The carbanion centre coordinates the solvent-free K(2) cation, and this ligand also forms a number of agostic-type interactions with K(2): two K····Me−Si contacts and one K····Me−P contact. The cyclopentadienyl ring of an adjacent ligand also coordinates K(2) cation and there is a K····Me−Si contact between K(2) and the −SiMe$_2$− linking substituent of the cyclopentadienyl ring.
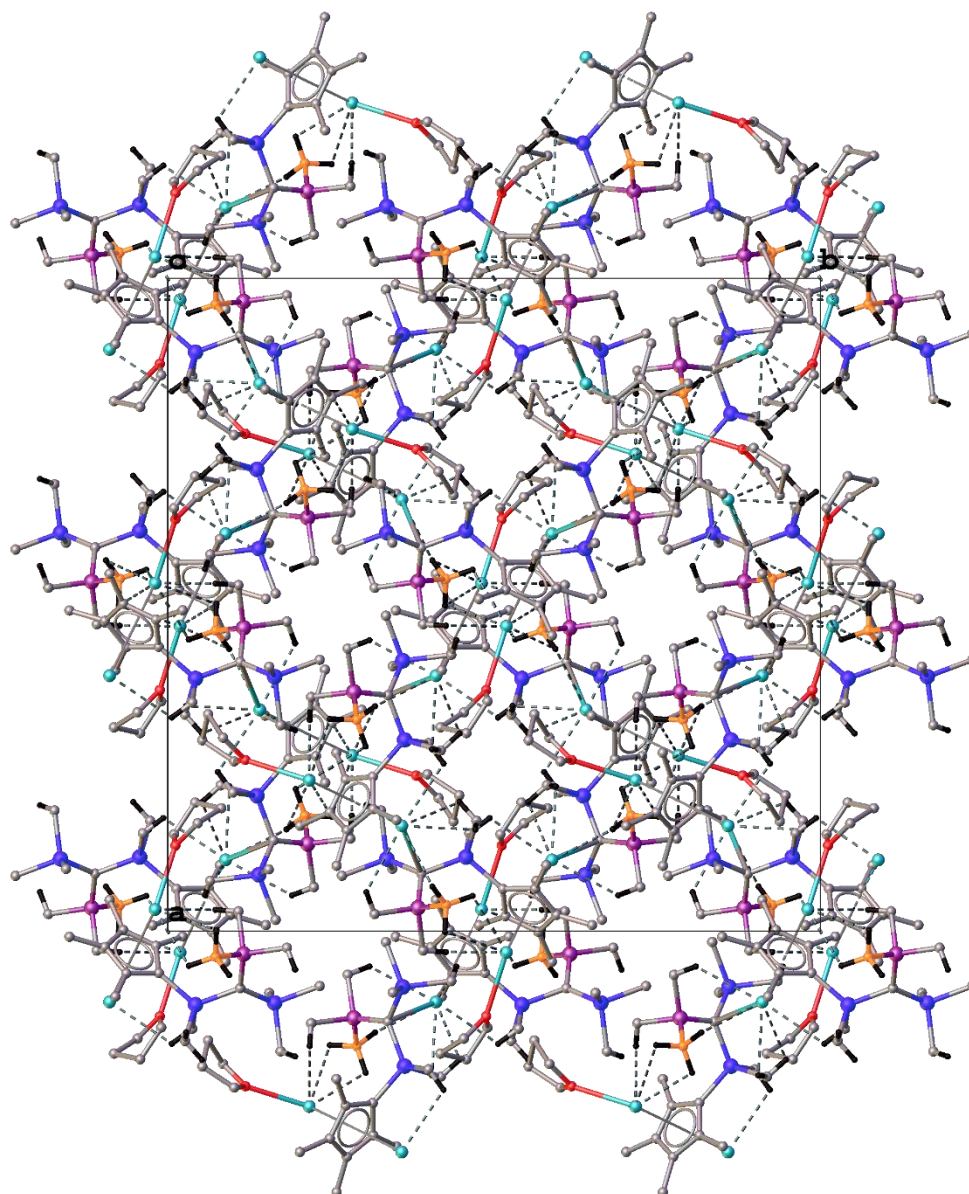
*Figure 57. Unit cell diagram of **53.THF**, viewed along the 001 direction highlighting the four-fold symmetry of the overall structure.*

Coordination of the K cations is completed by the formation of a 3D polymeric network structure through multiple agostic-type B−H····K contacts. The extended structure shows remarkable similarity with the structure of $[[(Me_3Si)_2\{Me_2P(BH_3)\}C]K]_\infty$, one of the first structurally characterised alkali-metal complexes of a phosphine-borane-stabilised carbanion.[9]

In both the structures two K(1) cations symmetry related by inversion, K(1a) and K(1b) in **53.THF** (Figure 58), are linked by two μ_2 bridges formed by two BH_3 groups. The μ_2 bridges in **53.THF** are best described as follows, both of the K centres are coordinated κ^2 *H,H* by one of the BH_3 groups and κ^3 *H,H,H* by the other BH_3 group. This mode of bridging is most similar to the μ_2 bridging of the symmetry inequivalent Rb(1) and Rb(2) cations in $[[(Me_3Si)_2\{Me_2P(BH_3)\}C]Rb]_\infty$.[9]

In **53.THF** the μ_2 bridges between the symmetry inequivalent K(2) and K(1) cations are rather like one of the two bridges in the dimeric compound $[[(Me_3Si)_2\{Me_2P(BH_3)\}C]Cs(pmdeta)]_2$, where both caesium cations are coordinated in an η^1-fashion by one BH_3 group and κ^3 *H,H,H* by the other BH_3 group. In **53.THF** there is only one borane hydrogen bridge rather than two between K(2) and K(1). K(2) is coordinated in an η^1-fashion by the BH_3 group and K(1) is coordinated κ^3 *H,H,H* by the same BH_3 group.

Overall in **53.THF** each BH_3 group forms six B—H···K contacts, linking three K cations K(1a), K(1b) and K(2). The two bridging BH_3 groups are symmetry related by a four-fold screw axis in **53.THF**. In $[[(Me_3Si)_2\{Me_2P(BH_3)\}C]K]_\infty$ and $[[(Me_3Si)_2\{Me_2P(BH_3)\}C]Rb]_\infty$ the two bridging BH_3 groups are from different symmetrically inequivalent ligand molecules.
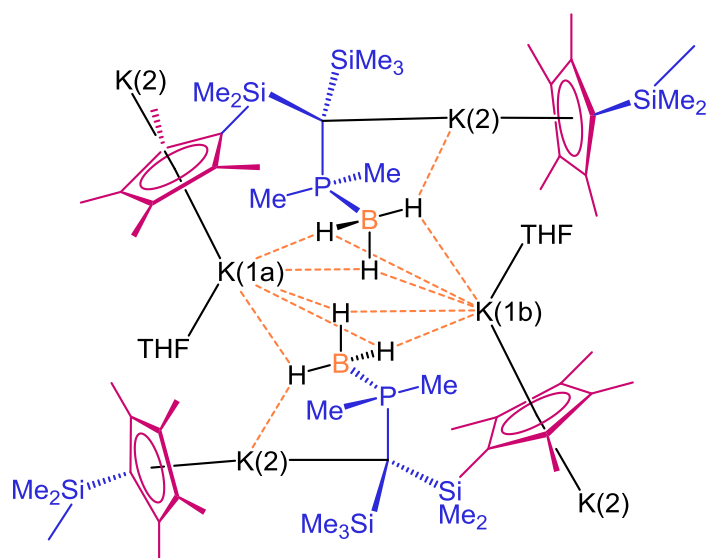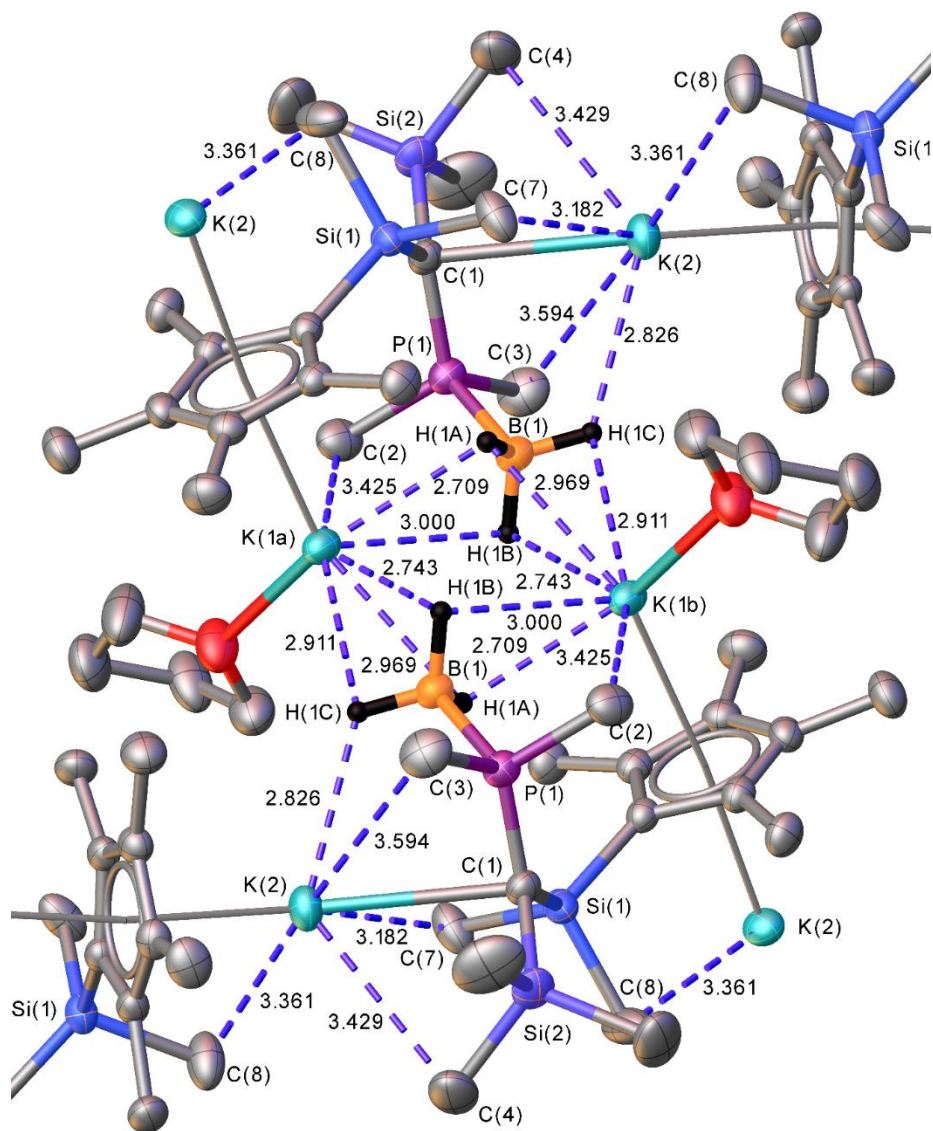
Figure 58. Coordination diagram of **53.THF** showing all the agostic-type B—H····K and Me····K contact distances (Å).

156

4.5   Conclusion

The hybrid pro-ligands **5** – **7** successfully doubly deprotonated with an excess of MeK in diethyl ether to give the dipotassium salts **50** – **52** with yields of 40%. Issues with the metalation reactions that led to the lower than desirable yields include (i) the high pK_a of the methine proton, which could not be removed with BnK (pK_a = 43) even when heated at reflux, (ii) the competing reaction of the MeK base with the diethyl ether solvent above 0°C, since there is a thermodynamic barrier to deprotonation elevation to room temperature is necessary and a large excess of MeK used to achieve complete double deprotonation of the pro-ligand (iii) impurities in the pro-ligand **7** (an oil) synthesised as described in chapter 2 led to impurities in **51**, these difficulties were later circumvented by changing the starting material in the synthesis of **7** from $LiCp^{4Me}$ generated and used in situ to KCp^{4Me} isolated as a crystalline solid from cold THF (iv) poor solubility of compounds **50** and **51** in benzene and their slow decomposition in donor solvents such as diethyl ether and THF made them challenging to crystallise.

Exchange of one $-SiMe_3$ group in the hybrid pro-ligand **7** for an isosteric and isoelectronic phosphine-borane group to give hybrid pro-ligand **14** resolved all of the issues with the metalation reactions observed in the synthesis of **50** - **52**. The hybrid pro-ligand **14** was doubly deprotonated with BnK in THF to give the dipotassium salt **53** in quantitative yield. Obvious advantages of the phosphine-borane ligands are the use the easily synthesised soluble molecular base, BnK and the 60% increase in metalation reaction yields. Further advantages are (i) the pro-ligand can be purified by recrystallization as it is a solid, (ii) the progress of the metalation reactions can be followed using ^{31}P and ^{11}B NMR spectroscopy as the J_{PB} coupling constant almost doubles from 55 Hz in **14** to 94 Hz in **53** and (iii) the dipotassium salt **53** does not decompose in donor solvents at low temperature, and is more soluble in non-donor solvents making crystal growth easier.

Compound **51.Et₂O** was crystallised rapidly from a cold (3°C) solution in diethyl ether, compound **52.Et₂O** was crystallised from a cold (3°C) solution in benzene and their structures were determined by x-ray crystallography. In the solid-state, compounds **51.Et₂O** and **52.Et₂O** have structural features in common with both potassium cyclopentadienides and the alkylpotassium compound $(Me_3Si)_3CK$, which is perhaps as expected given their hybrid nature.

The structure of **51.Et₂O** is a polymer with zig-zag chains similar to those found for $KCp^*(THF)_2$ and $KCp^*(py)_2$ (Figure 45). A key difference between the structure of **51.Et₂O** and $KCp^*(THF)_2$ is the degree of solvation of the potassium cations, **51.Et₂O** is a monosolvate where only every other potassium cation in the polymer chain has a coordinated molecule of diethyl ether and the polymer chain changes direction at these cations similarly to in the structure of $KCp^*(THF)_2$. The solvated potassium cations are chelated by the hybrid ligand. In between the solvated potassium cations are linearly coordinated unsolvated potassium cations which are sandwiched between the alkyl carbanion and the cyclopentadienyl ring of different hybrid ligands. The coordination environment of these unsolvated potassium cations bears resemblance to the linear polymer structure of $[(Me_3Si)_3CK]_\infty$ (Figure 46).The structure of **52.C₅H₆** contains two different polymer chains, one chain is similar to the polymer chain of **51.Et₂O** with the coordinated diethyl ether solvent replaced by η^6-coordinated benzene molecules. In the second type of polymer chain the hybrid ligand does not chelate any of the potassium cations.

Compound **53** was crystallised from deuterated benzene containing a few drops of deuterated THF. The solid-state structure of compound **53.THF** is a 3D network rather than a polymer chain since the borane group increases the denticity of the ligand. Each BH_3 group connects three potassium cations, with each of the borane hydrogens bridging between two potassium cations.

4.6   Experimental

4.6.1   General Procedure

All manipulations were carried out under an inert argon atmosphere using Schlenk techniques or under nitrogen in a solvent-free glovebox. Non-halogenated solvents (diethyl ether, THF, light petroleum, toluene, benzene and hexane) were pre-dried using sodium wire. Solvents were then distilled over sodium-potassium alloy (diethyl ether, light petroleum, hexane), potassium (THF, benzene) or sodium (toluene). Dichloromethane was dried by distillation over CaH_2. THF and dichloromethane were stored under nitrogen/argon over activated 4Å molecular sieves, all other solvents were stored over a potassium film. Deuterated solvents for NMR were also dried by distillation from potassium (d_8-THF, C_6D_6) or CaH_2 ($CDCl_3$) and were stored over activated 4Å molecular sieves. Deuterated solvents were deoxygenated using the freeze-pump-thaw method (3 cycles).

The organolithiums ^{n}BuLi and ^{t}BuLi were obtained from Sigma-Aldrich as 2.5M and 1.7M solutions in hexanes, respectively. On receipt the solution was filtered to remove LiOH. Portions (1 ml) of the filtrate were quenched with 3 ml of IMS and then 5 ml of deionised water was added to dissolve the LiOH before the solution was titrated against 0.1M HCl (indicator = phenolphthalein) to determine the concentration. The solutions of ^{n}BuLi were typically 2.3M in hexanes and the ^{t}BuLi solution was 1.5M.

Methyl potassium was prepared by a previously published procedure.[15]

Benzyl potassium was prepared by a procedure adapted from the literature.[20]

4.6.1.1   NMR Spectroscopy

The NMR spectra were recorded using a Bruker Avance 300 spectrometer operating at (^{1}H 300.13; ^{13}C 75.48; ^{11}B 96.29; ^{31}P 121.49 MHz), a Bruker Avance 400 spectrometer operating at (^{1}H 399.78; ^{13}C 100.54; ^{11}B 128.78; ^{31}P 161.83 MHz) or a Bruker Avance 700 spectrometer operating at (^{1}H 700.13; ^{13}C 176.06). Two-dimensional NMR experiments, HSQC and HMBC were also recorded using these instruments.   Chemical shifts are quoted in ppm relative to TMS (^{1}H and ^{13}C), $BF_3(OEt_2)$ (^{11}B) and 85% H_3PO_4 (^{31}P). All NMR spectra were recorded at ambient temperature. NMR data were processed using MestReNova software.

4.6.1.2   Crystal structure determinations

Data for crystal structure determinations were collected on a Xcalibur, Atlas, Gemini ultra diffractometer at 150 K using CuKα radiation (λ = 1.54184 Å). Cell refinement, data collection and data reduction were undertaken via software CrysAlisPro 1.171.38.42b (Rigaku Oxford Diffraction, 2015). Intensities were corrected for absorption using CrysAlisPro. An empirical absorption correction was applied using spherical harmonics, implemented in SCALE3 ABSPACK scaling algorithm. The structure were solved using direct methods, SHELXT and refined by SHELXL through the Olex2 interface.[21−23] All molecular graphics were generated by the author using Olex2 software.

All non-H atoms were refined anisotropically. The coordinates of H atoms were computed using a riding model constraint with the isotropic temperature factor (U_{iso}) of each H atom set to 1.2 (1.5 for methyl groups). The structure of **51.Et$_2$O** was refined with no restraints, but the structures of **52.C$_6$H$_6$** and **53.THF** contained disordered solvent molecules and convergence of the refinement required the use of restraints.

4.6.2 Preparation of [(CpMe$_2$Si)(Me$_3$Si)$_2$C]K$_2$(Et$_2$O)$_{0.5}$ [50]

To a cold (-78°C) flask containing MeK (ca. 2.1 g, > 4 equivalents) in diethyl ether (20 ml) was added a cold (-78°C) solution of (CpHMe$_2$Si)Me$_3$Si)$_2$CH (2.70g, 9.55 mmol) in diethyl ether (15 ml). The reaction mixture was stirred overnight then allowed to warm slowly to room temperature. The resulting reaction mixture was filtered and solvent was removed under vacuum to give a yellow-orange foam.

The solvated product, [(CpMe$_2$Si)(Me$_3$Si)2C]K$_2$(Et$_2$O)$_{0.5}$ **50** was characterised by NMR spectroscopy. Benzene was added to the flask at room temperature and the product partially dissolved. The product was desolvated by heating at reflux in benzene for 2 days and during this time the unsolvated dipotassium salt precipitated as a very pale grey powder. The powder, [(CpMe$_2$Si)(Me$_3$Si)$_2$C]K$_2$ **50'** was isolated by filtration. Yield 1.34g, 39%.

Solvated compound **50**:

^{1}H NMR (300.13 MHz, d$_8$-THF, 21°C): δ -0.10 (s, 18H, SiMe$_3$), 0.22 (s, 6H, SiMe$_2$), 1.11 (t, 3H, Et$_2$O), 3.38 (q, 2H, Et$_2$O), 5.87 (m, 4H, Cp).

^{13}C{H^1} NMR (75.48 MHz, d$_8$-THF, 21°C): δ 4.07 ({Me$_3$Si}$_2$CK), 8.25 (Cp*Me*$_2$Si), 9.16 ({*Me*$_3$Si}$_2$CK), 15.87 ({*C*H$_3$CH$_2$}$_2$O), 66.39 ({CH$_3$*C*H$_2$}$_2$O), 107.34 ({*C*H}Cp), 111.84 ({*C*H}Cp), 126.85 ({*C*}Cp).

Desolvated compound: **50'**

^{1}H NMR (300.13 MHz, C$_6$D$_6$/d$_8$-THF (21°C): δ 0.48 (s, 18H, SiMe$_3$), 0.75 (s, 6H, SiMe$_2$), 6.27 (m, 4H, Cp).

^{13}C {H^1}NMR (75.48 MHz, C$_6$D$_6$/d$_8$-THF (21°C): δ 4.15 ({Me$_3$Si}$_2$*C*K), 8.31(Cp*Me*$_2$Si), 9.26 ({*Me*$_3$Si}$_2$CK), 107.25 ({*C*H}Cp), 111.73 ({*C*H}Cp), 127.54 ({*C*}Cp).

Elemental analysis (%) calculated for unsolvated **50'** $C_{14}H_{28}K_2Si_3$: C 46.01, H 7.87; found: C 42.11, H 7.11.

The low carbon analysis is often observed for organometallic compounds because of the formation of stable metal carbonates and metal carbides. These issues are exacerbated in compounds with a high silicon content due to the formation of stable silicon carbide.[24] Formation of all these compounds traps the carbon so less carbon dioxide is evolved from combustion of the sample.

4.6.3   Preparation of [(Cp^{4Me}Me$_2$Si)(Me$_3$Si)$_2$C]K(OEt$_2$)$_{0.5}$ [51]

To a cold (-78°C) flask containing MeK (ca. 1.3 g, > 4 equivalents) in diethyl ether (30 ml) was added a cold (-78°C) solution of (CpH^{4Me}Me$_2$Si)(Me$_3$Si)$_2$CH (1.16g, 3.42 mmol) in diethyl ether (20 ml). The reaction mixture was stirred overnight and allowed to warm slowly to room temperature. The resulting reaction mixture was a brown, yellow-tinged suspension which was filtered to remove the excess MeK to give an orange-red filtrate. The solvent was removed from the filtrate under vacuum to give a dull amber coloured powder **51**. Crystals of the alternate solvate [(Cp^{4Me}Me$_2$Si)(Me$_3$Si)$_2$C]K(Et$_2$O), **51.THF** suitable for X-ray crystallography were grown from a cold (3°C), concentrated solution in diethyl ether, over a period of three days. Yield 0.64g, 41.5%.

^{1}H NMR (300.13 MHz, C$_6$D$_6$/d$_8$-THF 21°C): δ 0.50 (s, 18H, SiMe$_3$), 0.72 (s, 6H, SiMe$_2$), 1.11 (t, 3H, Et$_2$O), 2.27 (s, 6H, Cp*Me$_A$*), 2.53 (s, 6H, Cp*Me$_B$*) 3.26 (q, 2H, Et$_2$O).

^{13}C{H^1} NMR (75.48 MHz, C$_6$D$_6$/d$_8$-THF, 21°C): δ 3.69 ({Me$_3$Si}$_2$*C*K), 9.34 ({*Me$_3$*Si}$_2$CK), 11.23 (Cp*Me$_2$*Si),   11.81 (Cp*Me$_A$*),   15.28 (Cp*Me$_B$*), 15.58 ({*C*H$_3$CH$_2$}$_2$O), 65.91 ({CH$_3$*C*H$_2$}$_2$O), 111.96 ({*C*Me}Cp), 115.41 ({*C*Me}Cp), 116.01 ({*C*}Cp^{4Me}).

Elemental analysis (%) calculated for C$_{20}$H$_{41}$K$_2$Si$_3$O$_{0.5}$: C 53.15, H 9.14; found: C 41.32, H 8.20.

4.6.4 Preparation of [(Cp^{4Me}Me$_2$Si)(Me$_3$Si)C{PMe$_2$(BH$_3$)}]K$_2$(THF)$_{0.5}$ [53]

To a cold (-78°C) solution of (Cp^{4Me}HMe$_2$Si)(Me$_3$Si)CH{PMe$_2$(BH$_3$)} (0.48 g, 1.41 mmol) in THF (15 ml) was added a cold (-78°C) solution of BnK (0.37g, 2.85 mmol) in THF (15 ml). The reaction was stirred for 16 hours and allowed to warm slowly to room temperature. Once the reaction was complete the solvent was removed *in vacuo* to leave [(Cp^{4Me}Me$_2$Si)(Me$_3$Si)C{PMe$_2$(BH$_3$)}]K$_2$(THF)$_{0.5}$, **53** as red foam (0.70g, 100%). Crystals of an alternative solvate [(Cp^{4Me}Me$_2$Si)(Me$_3$Si)C{PMe$_2$(BH$_3$)}]K$_2$(THF), **53.THF** suitable for X-ray diffraction were grown at room-temperature in an NMR tube from a 10:1 mixture of C$_6$D$_6$ and d$_8$-THF.

^{1}H{^{11}B} NMR (700.16 MHz, C$_6$D$_6$, d$_8$-THF, 298 K): δ 0.52 (s, 9H, Si*Me*$_3$), 0.66 (s, 6H, Si*Me*$_2$), 1.43 (m, 2H, THF C*H*$_2$), 1.63 (d, 6H, $^2J_{PH}$ = 9.3 Hz, -PC*H*$_3$), 2.18 (s, 6H, Cp*Me*$_A$), 2.62 (s, 6H, Cp*Me*$_B$), 3.51 (m, 2H, THF -OC*H*$_2$).

^{11}B{^{1}H} NMR (96.3 MHz, C$_6$D$_6$, d$_8$-THF, 298 K): δ -29.7 (d, J_{PB} = 93.8 Hz).

^{31}P{^{1}H} NMR (100 MHz, C$_6$D$_6$, d$_8$-THF, 298 K): δ -7.5 (poorly resolved q, J_{PB} = 93.8 Hz).

^{13}C{^{1}H} NMR (75.5 MHz, C$_6$D$_6$, d$_8$-THF, 298 K): δ 8.98 (d, $^3J_{PC}$ = 2.4 Hz, Si*Me*$_3$), 10.10 (d, $^3J_{PC}$ = 7.2 Hz, Si*Me*$_2$), 11.49 (Cp^{4Me}*Me*$_A$), 14.96 (Cp^{4Me}*Me*$_B$), 22.04 (d, -P*C*H3, coupling obscured by d$_8$-THF signal), 25.87 (s, THF *C*H$_2$), 67.83 (s, THF -O*C*H$_2$), 110.71 ({*C*Me$_B$}*Cp*^{4Me}), 117.26 ({*C*Me$_A$}*Cp*^{4Me}). Note: Two quaternary carbon atoms for ({*C*}*Cp*^{4Me} and KCp^{4Me}Me$_2$Si}{Me$_3$Si}{Me$_2$PBH$_3$}*C*K were not visible in this spectrum.

4.6.5   Preparation of [(Cp^{4Me}Me$_2$Si)(Me$_3$Si)C{P^{n}Pr$_2$(BH$_3$)}]K$_2$(THF)$_{0.5}$ [54]

To a cold (-78°C) solution of (Cp^{4Me}HMe$_2$Si)(Me$_3$Si)CH{P^{n}Pr$_2$(BH$_3$)} (1.59 g, 4.30 mmol) in THF (30 ml) was added a cold (-78°C) solution of BnK (1.12g, 8.61 mmol) in THF (20 ml). The reaction was stirred for 48 hours and allowed to warm slowly to room temperature. Once the reaction was complete the solvent was removed *in vacuo* to leave [(Cp^{4Me}Me$_2$Si)(Me$_3$Si)C{P^{n}Pr$_2$(BH$_3$)}]K$_2$(THF)$_{0.5}$ as a beige powder (1.81g, 89%).

^{1}H{^{11}B} NMR (700.16 MHz, C$_6$D$_6$, d$_8$-THF, 298 K): δ 0.49 (s, 9H, SiMe$_3$), 0.60 (s, 6H, SiMe$_2$), 0.64 (d, J_{PH} = 13.5 Hz, 3H, BH$_3$), 1.08 (t, 6H, -PCH$_2$CH$_2$C*H$_3$*), 1.75 (m, 4H, PCH$_2$CH$_2$CH$_3$), 1.86 (m, 2H, -PCH$_2$CH$_2$CH$_3$), 2.06 (m, 2H, -PCH$_2$CH$_2$CH$_3$), 2.15 (s, 6H, Cp*Me$_A$*), 2.58 (s, 6H, Cp*Me$_B$*).

^{11}B{^{1}H} NMR (96.3 MHz, C$_6$D$_6$, d$_8$-THF, 298K): δ -35.36 (d, J_{PB} = 90.1 Hz).

^{31}P{^{1}H} NMR (C$_6$D$_6$, d^8-THF, 298K): δ 6.2 (poorly resolved q, J_{PB} = 90.1 Hz).

^{13}C{^{1}H} NMR (176.07 Hz, C$_6$D$_6$, d$_8$-THF, 298K): δ -2.14 (d, J_{PC} = 30.9 Hz, *C*K), 8.86 (d, SiMe$_3$, $^3J_{PC}$ = 1.6 Hz), 10.61 (d, $^3J_{PC}$ = 6.8 Hz, SiMe$_2$), 11.43 (Cp^{4Me}Me$_A$), 15.09 (Cp^{4Me}Me$_B$), 17.15 (d, $^3J_{PC}$ = 13.6 Hz, -PCH$_2$CH$_2$*C*H$_3$), 18.34 (s, -PCH$_2$*C*H$_2$CH$_3$), 38.60 (d, J_{PC} = 36.1 Hz, -P*C*H$_2$CH$_2$CH$_3$,), 110.38 ({*C*Me$_B$}*Cp*^{4Me}), 114.75 ({*C*}*Cp*^{4Me}), 117.20 ({*C*Me$_A$}*Cp*^{4Me}).

4.7   References

(1)   Dinnebier, R. E.; Behrens, U.; Olbrich, F. *Organometallics* **1997**, *16*, 3855.

(2)   Smith, D. J. *Adv. Organomet. Chem.* **1999**, *43*, 267.

(3)   Shannon, R. D. *Acta Cryst.* **1976**, *32*.

(4)   Dinnebier, R. E.; Schneider, M.; van Smaalen, S.; Olbrich, F.; Behrens, U. *Acta Cryst. Sect. B.* **1999**, *55*, 35.

(5)   Evans, W. J.; Brady, J. C.; Fujimoto, C. H.; Giarikos, D. G.; Ziller, J. W. *J. Organomet. Chem.* **2002**, *649*, 252.

(6)   Izod, K.; Wills, C.; Clegg, W.; Harrington, R. W. *Organometallics* **2006**, *25*, 38.

(7)   Eaborn, C.; Hitchcock, P. B.; Smith, J. D.; Sullivan, A. C. *J. Chem. Soc. Chem. Commun.* **1983**, 1390.

(8)   Eaborn, C.; Hitchcock, P. B.; Izod, K.; Jaggar, A. J.; Smith, J. D. *Organometallics* **1994**, *13*, 753.

(9)   Izod, K.; Wills, C.; Clegg, W.; Harrington, R. W. *Organometallics* **2006**, *25*, 5326.

(10)   Izod, K.; Wills, C.; Clegg, W.; Harrington, R. W. *Inorg. Chem.* **2007**, *46*, 4320.

(11)   Izod, K.; Wills, C.; Clegg, W.; Harrington, R. W. *J. Organomet. Chem.* **2007**, *692*, 5060.

(12)   Izod, K.; Dixon, C. M.; McMeekin, E.; Rodgers, L.; Harrington, R. W.; Baisch, U. *Organometallics* **2014**, *33*, 378.

(13)   Albrecht, I.; Schumann, H. *J. Organomet. Chem.* **1986**, *310*, C29.

(14)   Zimmermann, M.; Anwander, R. *Chem. Rev.* **2010**, *110*, 6194.

(15)   Eaborn, C.; Hitchcock, P. B.; Izod, K.; Jaggar, A. J.; Smith, J. D. *Organometallics* **1994**, *13*, 753.

(16)   Izod, K.; Wills, C.; Clegg, W.; Harrington, R. W. *Organometallics* **2010**, *29*, 4774.

(17)   Bowman, L. J.; Izod, K.; Clegg, W.; Harrington, R. W.; Smith, J. D.; Eaborn, C.; Guagliardi, A.; Moliferni, A. G. G.; Polidori, G.; Rizzi, R. *Dalton. Trans.* **2006**, *32*, 502.

(18)   Jutzi, P.; Leffers, W.; Hampel, B.; Pohl, S.; Saak, W. *Angew. Chem. Int. Ed. English* **1987**, *26*, 583.

(19)   Rabe, G.; Roesky, H. W.; Stalke, D.; Pauer, F.; Sheldrick, G. M. *J. Organomet. Chem.* **1991**, *403*, 11.

(20)   Lochmann, L.; Trekoval, J. *J. Organomet. Chem.* **1987**, *326*, 1.

(21)   Dolomanov, O. V.; Bourhis, L. J.; Gildea, R. J.; Howard, J. A. K.; Puschmann, H. *J. Appl. Crystallogr.* **2009**, *42*, 339.

(22)   Sheldrick, G. M. *Acta Cryst. Sect. A.* **2007**, *A64*, 112.

(23)   Sheldrick, G. M. *Acta Cryst. Sect. A.* **2015**, *A71*, 3.

(24)   Culmo, R. F. *The Elemental Analysis of Various Classes of Chemical Compounds Using CHN*; PerkinElmer Inc., Shelton, CT, **2013**, Industrial report.

Chapter 5 Trivalent lanthanide and calcium complexes of bulky hybrid ligands

5.1   Introduction

The synthesis of trivalent heteroleptic monocylopentadienyl lanthanide complexes with one or more σ-bonded alkyl ligands is known to be problematic. The high Lewis acidity of the lanthanide metal centres can lead to 'ate-complex' formation when complexes are prepared using metathesis chemistry.[1] An alternative route that avoids the incorporation of alkali metals is an alkane ($SiMe_4$) elimination reaction starting from $Ln(CH_2SiMe_3)_3$ precursors discussed in Chapter 1.[2,3] Unfortunately it has been demonstrated that this method sometimes leads to ligand rearrangement giving mixtures of the intended product, biscyclopentadienyl $Cp*_2Ln(CH\{SiMe_3\}_2)$ and starting material.[1] The complexes $Cp*Ln(CH\{SiMe_3\}_2)_2$, Ln = Ce, La (and THF solvates) and $Cp*Y(CH\{SiMe_3\}_2)(OAr)$ [OAr = $O\text{-}2,6\text{-}C_6H_3\text{-}^tBu_2$] are the only neutral monocylopentadienyl complexes with a σ-bonded alkyl ligand to have been structurally characterised in the solid state.[4,5]   Halide containing complexes of this type are known only for lutetium and are anionic, with solvated or chelated lithium counter-cations linked to the lanthanide metal centre by μ_2-bridging chloride anions (Figure 59).[6]
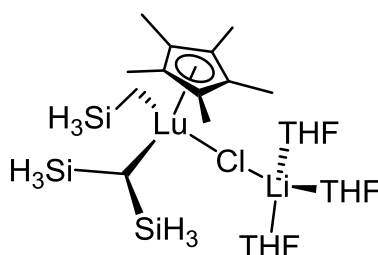
Figure 59. Structure of an ionic monocylopentadienyl 'ate' complex of lutetium

The majority of lanthanide monocyclopentadienyl complexes with an additional σ-bonded alkyl ligand are constrained geometry complexes (CGCs).[7] The first constrained geometry complex was the dimeric rare earth [(Cp*SiN^{t}Bu)(PMe$_3$)Sc]$_2$(μ-H)$_2$ complex prepared by Bercaw in 1990 (Scheme 49) and the analogous dimers are now known for several trivalent lanthanides including Lu and Yb.[8–10]
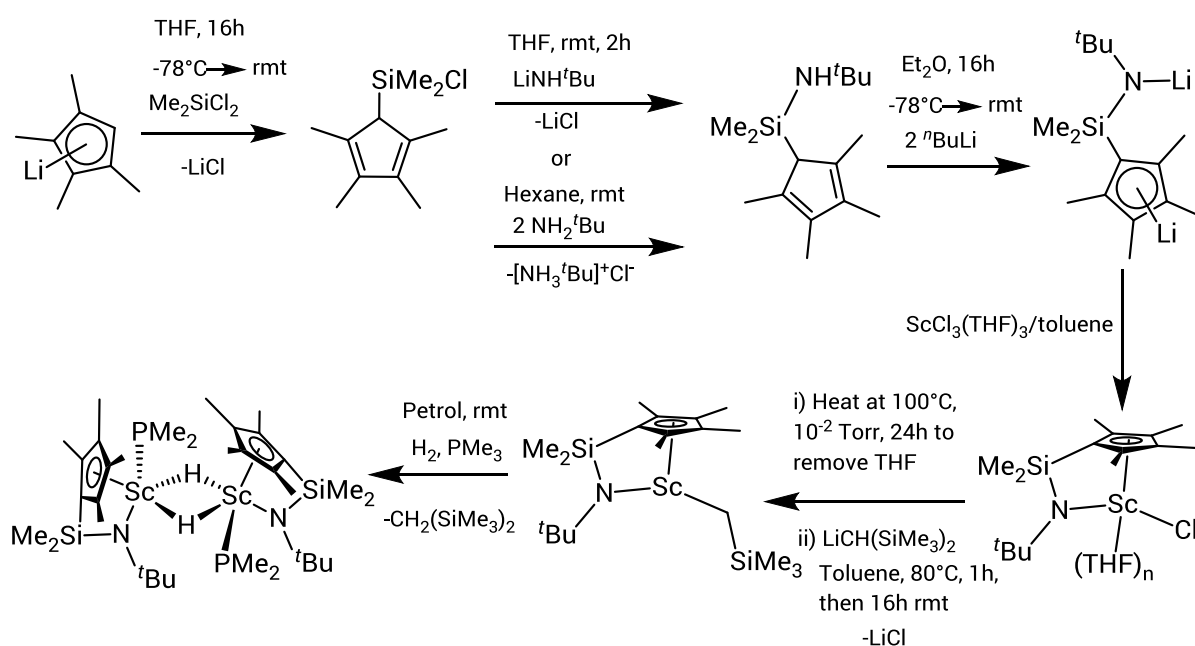
Scheme 49

The monomeric constrained geometry complexes prepared as precursors in the synthesis of the dimeric hydrido complexes of Sc/Lu/Yb can be prepared as THF adducts in ca. 90% yield from the aforementioned Ln(CH$_2$SiMe$_3$)$_3$ precursors in an alkane (SiMe$_4$) elimination reaction (Scheme 50), and the chelate rings formed by the linked ligands help prevent ligand redistribution. The complexes have been structurally characterised by X-ray crystallography for Ln = Sc (R = ^{t}Bu, n =1),[9] Ln = Y, Yb, Lu (R = Ph, n = 2),[11] Ln = Lu (R = 1,3-dimethylphenyl, n= 1)[12] and for Ln = Y (R = Me$_2$EtC, n = 1).[7] CGCs were also synthesised in solution as precursors, but no crystal structures were determined for Ln = Y, Lu, Yb, Er, Tb (R = ^{t}Bu, n =1).[3]
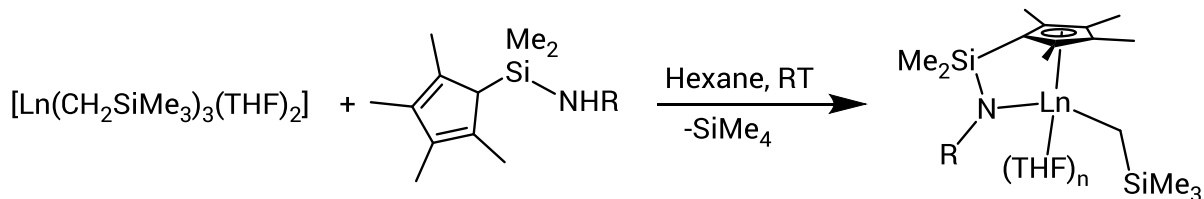
Scheme 50

A related series of lanthanide CGC's with Ln−C σ-bonds was more recently prepared over the full size range of the lanthanide trivalent cations from $[Ln(CH_2C_6H_4NMe_2\text{-}o)_3]$ precursors (Ln = Y, La, Pr, Nd, Sm, Gd, Lu), (Scheme 51).[13] In addition a few constrained geometry complexes of divalent lanthanides are also known, for example $[(Cp^{4Me}Me_2SiNPh)]Yb(THF)_3$ and $[(Cp^{4Me}Me_2SiPAr)]Sm(THF)_3$ (Ar = $C_6H_2{}^tBu_3\text{-}2,4,6$).[14,15]
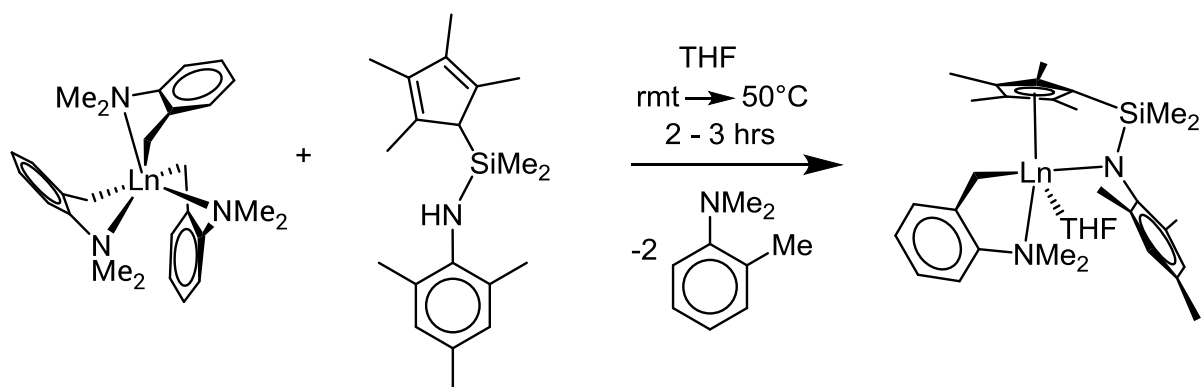
Scheme 51

Monomeric constrained geometry complexes of group 4 transition metal elements were developed industrially and patented as ethene polymerisation catalysts and copolymerisation catalysts for ethene with other more bulky α-olefins.[16] The catalytically active species is believed to be the cation and this has been observed in the case of the titanium benzyl cation $[Ti(\eta^5:\eta^1\text{-}C_5Me_4SiMe_2NCH_2CH_2NMe_2)(CH_2Ph)]^+$ generated by the reaction of $[Ti(\eta^5:\eta^1\text{-}C_5Me_4SiMe_2NCH_2CH_2NMe_2)(CH_2Ph)_2]$ with $B(C_6F_5)_3$ and this cationic species is isoelectronic (valance only) with neutral rare earth or lanthanide CGCs.[3] Prior to the

169

discovery of constrained geometry complexes most organometallic complexes used as catalysts were bis(cyclopentadienyl) metallocenes or metallocenophanes where the two cyclopentadienyl rings are linked by a short hydrocarbon chain, silicon or boron bridge.[17] In CGCs one of the linked cyclopentadienyl rings of the metallocenophanes is replaced by an amide or phosphide group to give η^5:η^1 coordinating chelating dianionic ligand systems with heteroatom-containing functional groups. The hybrid ligands presented herein can be described as a modification of these constrained geometry ligand systems, where the amide or phosphide is exchanged for a silicon-stabilised or phosphine-borane-stabilised carbanion, providing complexes with both Ln—C(Cp) and Ln—C σ-bonds. Complexes where the amide group is replaced with a carbanion are known for some transition metal elements, but so far not for lanthanide or rare earth metals.

Polymer properties are controlled by tweaking catalyst symmetry and geometry, so CGCs were very attractive for development as catalysts since the geometry of the pseudo-four-membered chelate ring (Cp—Si—N—M), while very constrained, can be modified systematically by variation of the cyclopentadienyl ring, the amide/phosphide functional group, the linking 'bridge' or the metal centre. Other advantageous features of CGCs for catalysis include that the chelate ring bite angle ($Cp_{centroid}$—Ln—N) is about 90 − 100∘ degrees, opening up the coordination sphere for the substrate to bind to the metal centre while still providing electronic saturation. The metal tends to be more Lewis acidic than in the corresponding bis(cyclopentadienyl) complexes because less electron density is donated to the metal centre (electron-counting models) by the constrained geometry ligand systems. The effect of this is that the metal centre 'holds' its ligands strongly enough that chain-transfer reactions of the growing polymer chain are less frequent resulting in higher molecular weight polymers.

Lanthanide complexes of the hybrid ligands have much in common with known constrained geometry complexes (CGCs) of the rare earth and lanthanide elements.

5.2   Synthesis of a lanthanum complex of a silicon-stabilised dicarbanion hybrid ligand

The lanthanum complex [(Cp^{4Me}Me$_2$Si)(Me$_3$Si)$_2$C]LaI(THF)$_2$ [**56**] was prepared by a metathesis reaction between the organopotassium compound [(Cp^{4Me}Me$_2$Si)(Me$_3$Si)$_2$C]K$_2$(Et$_2$O) **51** and LaI$_3$(THF)$_4$ (Scheme 52). Upon addition of the dark red solution of the dipotassium salt in THF to a slurry of LaI$_3$(THF)$_4$ the reaction mixture immediately became pale yellow in colour and formation of a colourless precipitate was observed. The product [(Cp^{4Me}Me$_2$Si)(Me$_3$Si)$_2$C]LaI(THF)$_2$, **56** was isolated by filtration to remove KI followed by removal of the solvent *in vacuo.* Crystallisation of the resulting yellow foam was successful from toluene and THF at -24°C and from analysis of the colourless crystals by X-ray crystallography the solid-state structure shown in (Figure 62) was determined.

The lanthanum complex **56** appears to be more stable in THF than the dipotassium salt **51** and, unlike the dipotassium salt, does not deprotonate toluene. Compound **56** has limited solubility in toluene but readily dissolves in this solvent upon addition of a few drops of THF. This behaviour resembles that of the dipotassium salt **51**.

Scheme 52

171
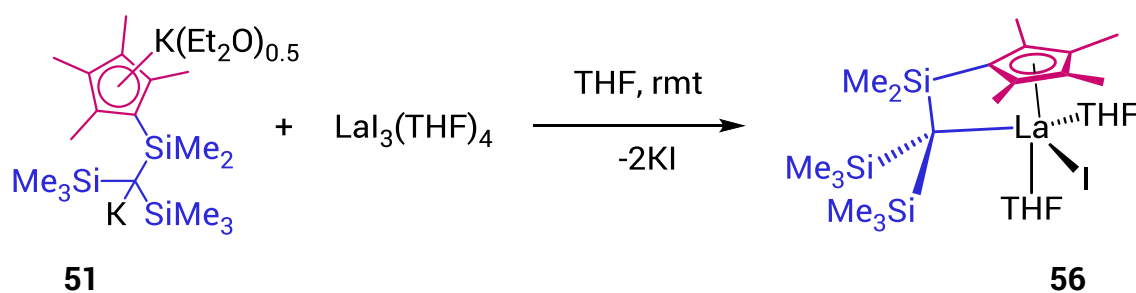
Crystals of [(Cp^{4Me}Me$_2$Si)(Me$_3$Si)$_2$C]LaI(THF)$_2$, **56** were sensitive to solvent loss and, according to ^{1}H NMR spectroscopy of a sample which was sealed under vacuum, one molecule of coordinated THF was lost very readily to give [(Cp^{4Me}Me$_2$Si)(Me$_3$Si)$_2$C]LaI(THF), **[56a]** (Figure 58). This behaviour is known for halide-containing constrained geometry complexes of the lanthanides, for example THF solvent is removed from the complex [(Cp^{4Me}Me$_2$Si)N^{t}Bu]ScCl(THF)$_n$ (see Scheme 49 above) by heating at 100°C under vacuum (10^{-2} Torr).[18]

56a
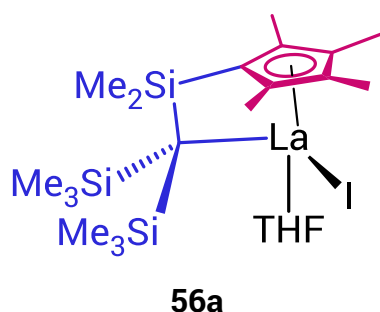
*Figure 60. Less solvated form of the lanthanum complex **56a** found in the NMR sample*

Variable temperature NMR studies of [(Cp^{4Me}Me$_2$Si)N^{t}Bu]Y(CH$_2$SiMe$_3$)(THF) have revealed that the THF solvent is labile in solution on the NMR timescale.[19] A decrease in temperature results in an upfield shift of the THF protons since the solvent molecules are coordinated to the metal for more of the time on average at lower temperatures. If more than one equivalent of THF is present in the NMR sample then the THF signals are shifted downfield to approximately the same chemical shifts as free THF.

5.3   Synthesis of a samarium complex of a phosphine-borane-stabilised dicarbanion hybrid ligand

The samarium complex [(Cp^{4Me}Me$_2$Si)(Me$_3$Si)C{PMe$_2$(BH$_3$)}]SmI(THF)$_3$ **[57]**, was prepared by a metathesis reaction between the organopotassium compound [(Cp^{4Me}Me$_2$Si)(Me$_3$Si)C{PMe$_2$(BH$_3$)}]K$_2$(THF)$_{0.5}$ **53** and SmI$_3$(THF)$_{3.5}$ (Scheme 53). The dipotassium salt was prepared as described in chapter 4 and used *in situ* as a

dark red solution in THF. Initially the ligand was added to the $SmI_3(THF)_{3.5}$ at low (-78°C) temperature. The reaction mixture was allowed to warm to room temperature overnight with stirring to yield a bright red suspension consisting of a bright red solution and a colourless precipitate of KI. The $^{11}B\{^1H\}$ NMR spectrum of the reaction mixture showed the appearance of a very broad peak at -47.2 ppm, but also a sharp doublet at -34.5 ppm (J_{PB} = 111 Hz), the latter of which was attributed to the dipotassium salt starting material **53**. The reaction mixture was stirred for a further 16 hours before removal of the solvent *in vacuo* and extraction into diethyl ether, followed by filtration to remove the KI. Concentration of this oily red diethyl ether solution readily yielded crystalline material. The growth of the crystals was slowed by storing the solution in a refrigerator and large red crystals suitable for X-ray crystallography were obtained.
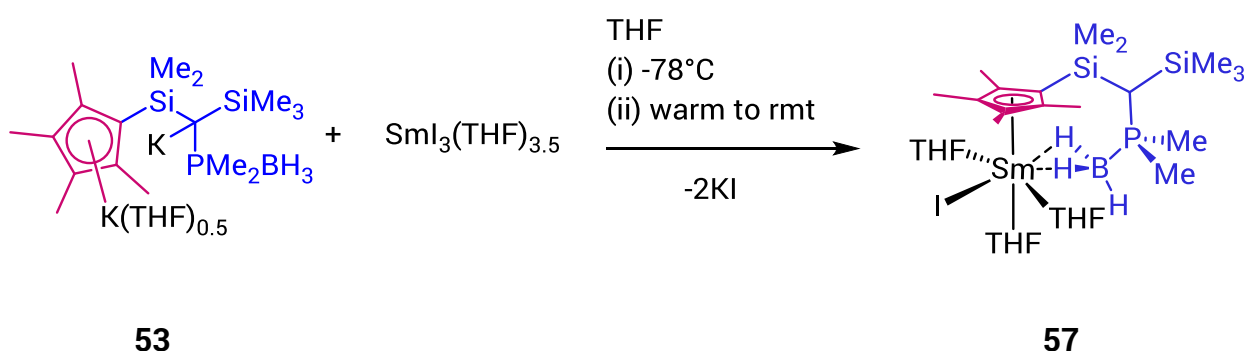
Scheme 53

5.3.1   NMR analysis of the paramagnetic samarium complex

Despite the paramagnetism of the Sm(III) metal centre the complex could be usefully characterised by $^1H\{^{11}B\}$ and $^{13}C\{^1H\}$ NMR spectroscopy. The unpaired electrons of paramagnetic compounds give rise to a magnetic moment. The effective magnetic moment, μ_{eff} is given by *equation 1* as:

$$\mu_{eff} = g_J\sqrt{J(J+1)} \qquad \text{(Equation 1)}$$

$$g_J = \frac{J(J+1) + (S+1) - L(L+1)}{2J(J+1)}$$

(Equation 2)

Where g_J is the Landé factor (given by e*quation 2*).[20] *S* is total spin angular momentum, for Sm(III) *S* = 5/2, *L* is the total orbital angular momentum, for Sm(III) *L* = 5 and *J* is the total angular momentum, for Sm *J* = 5/2. By equations (1) and (2) this gives the Landé factor for Sm(III) as g_J = 2/7 and μ_{eff} = 0.845 BM. respectively. This effective magnetic moment is very small in comparison to other lanthanides, an example at the other extreme is Dy(III) *J* = 15/2, g_J = 4/3 and μ_{eff} = 10.3 BM.[21,22]

The uneven occupation of the f-orbitals by unpaired electrons means with the exception of Gd(III) the electron distribution of the Ln(III) cations is anisotropic.[21,23,24] This means that when a paramagnetic Ln(III) complex is exposed to a magnetic field, for example in an NMR spectrometer the Ln(III) complex is anisotropically susceptible to the applied magnetic field of the spectrometer.

Both the size of the effective magnetic moment and the magnetic susceptibility anisotropy produce the changes in chemical shift observed in the NMR spectra of ligands coordinated to paramagnetic Ln(III) cations.   There are two main contributions to the change in chemical shift, these are called the contact shift and the pseudocontact shift.[25] The contact shift is due to the sharing of some of the electron density of the unpaired electrons through chemical bonds and decreases sharply at distances that exceed coordinative 'bond lengths'.[21] In many lanthanide complexes heteroatom donors (O, N) are the atoms that bind to the Ln(III) cation, especially in the context of the use of lanthanide shift reagents (LSRs) in NMR spectroscopy and MRI scans and it is more unusual that a carbon or a hydrogen atom (^{1}H and ^{13}C being the routine NMR nuclei) bind to the Ln(III) cation.[25] In heteroatom donor complexes and in all complexes for atoms not involved in coordination at the metal centre the contact shift is negligible. Another reason the

contact shift is often ignored is that the bonding in lanthanide complexes is ionic, but for some organolanthanide and organoactinide complexes the contact shift can be observed.[26]

The pseudocontact shift is the origin of the changes in chemical shift most commonly observed in NMR spectra of paramagnetic lanthanide compounds. It is related to the magnitude of the magnetic moment, the anisotropic magnetic susceptibility and the ligand crystal field.[27] A theory that describes these relationships mathematically, given by *equation 3* for an axially symmetrical complex (with a three-fold axis or higher) was put forward by Bleaney in 1972.[28] Where C_J is the Bleaney constant given by *equation 4*, μ_B is the Bohr magneton, k is the Boltzmann constant, T is temperature, r is the distance between the nuclei being observed and the Ln(III) cation, θ is the angle between the vector r and the principle symmetry axis of the complex and B_0^2 is a second-order crystal field splitting parameter. In the equation for the Bleaney constant (*equation 4*) g_J is the Lande factor, J is the total angular momentum and $<J\|\alpha\|J>$ is a numerical coefficient determined by Bleaney that factors in the anisotropy in the magnetic susceptibility.[28]

$$\Delta\delta_{pseudo} = \frac{C_J\mu_B^2}{60(kT)^2}\left[\frac{(3cos^2\theta - 1)}{r^3}B_0^2\right]$$

(Equation 3)

$$C_J = g^2J(J + 1)(2J - 1)(2J + 3)<J\|\alpha\|J>$$ (Equation 4)

Using Bleaney's theory a very approximate estimate of the order of magnitude of the pseudocontact shifts that can be expected for an axially symmetrical samarium complex was calculated (Figure 61). The calculation was motivated by the huge changes in chemical shift of the carbanion carbon of - 50 ppm in the ^{13}C NMR spectrum and the coordinated BH$_3$ hydrogen atoms by -17 ppm in the ^{1}H NMR spectrum, which seemed contradictory to the small magnetic moment of Sm(III). Please note that the calculation was only ever intended as a guide to ballpark

values and the most obvious limitation when interpreting the results is that the isolated complex does not have axial symmetry, however later terms have a smaller contribution to the overall result and the limitations of Bleaney's theory are still the subject of recent research.[21,28,29] The details of the calculation are given as an appendix to this chapter. The structure of the complex is only known in the solid-state, and since phosphine-borane-stabilised carbanions are known to have variable binding modes we wanted to consider the possibility that the carbanion is bound directly to the metal when the complex is in solution. If the structure in solution is the same as in the solid-state, where the carbanion is located 4.7 Å from the Sm(III) cation then Bleaney's theory of the pseudocontact shift should predict the order of magnitude of the change in chemical shift. If the carbanion carbon is bonded directly to the metal then perhaps there is a contributing factor from the contact shift.
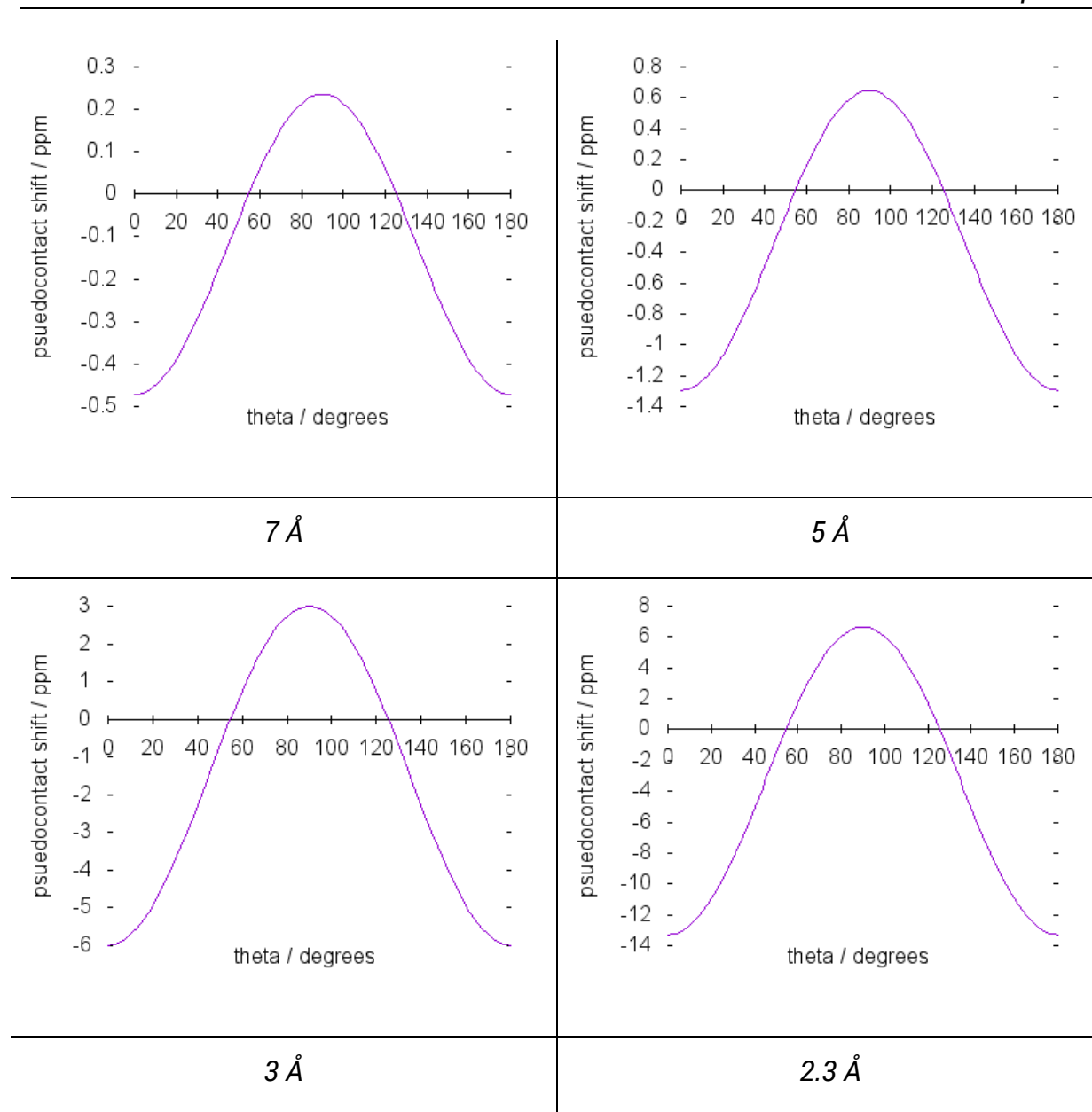
Figure 61. Crude estimates of pseudocontact shifts for an axially symmetrical Sm(III) complex for nuclei at distances of 2.3 Å, 3 Å, 5 Å and 7 Å from the Sm(III) centre.

The chemical shifts of the protons for the −SiMe$_3$, -SiMe$_2$, -PMe$_2$ and methyl groups on the cyclopentadienyl ring in the ^{1}H NMR spectra of the complex were compared with the average chemical shift of the same protons in the organopotassium compounds **53** and **54**, (Chapter 4) and the calcium complex **58** (see below, Section 5.7.4). The chemical shifts of the −SiMe$_3$ protons in the diamagnetic compounds of the hybrid ligand **53**, **54** and **58** are 0.48, 0.49 and 0.52 ppm respectively. The chemical shift of the −SiMe$_3$ protons in the Sm(III) complex, **57** is 0.3 ppm, which is a shift of -0.2 ppm. The approximate Sm(III)−C(Me) distance for the −SiMe$_3$ group

in the solid-state structure of **57** is 7Å. This shift falls within the plausible calculated pseudocontact shift range of -0.5 - +0.2 ppm (Figure 61).

Similarly the chemical shifts of the $-SiMe_2$ protons in the diamagnetic compounds of the same ligand **58**, **53** and **54** are 0.89, 0.60 and 0.66 ppm respectively. The chemical shift of the $-SiMe_2$ protons in the Sm(III) complex **57** is -0.5 ppm, which is a shift of c.a -0.7 ppm. The approximate Sm(III)$-$C(Me) for the $-SiMe_2$ group in the solid-state structure of is 5 Å. Again this shift falls within the plausible calculated pseudocontact shift range of -1.3 - +0.6 ppm. The protons of the $-PMe_2$ group did not show any pseudocontact shift presumably due to their orientation with respect to the principle symmetry axis of the molecule. The chemical shifts of the two chemically inequivalent methyl substituents of the cyclopentadienyl ring in compounds **58** and **53** are 2.14/2.59 and 2.18/2.62 ppm respectively. In the Sm(III) complex, **57** the chemical shifts of the same protons are 0.90 and 1.44 ppm respectively, a pseudocontact shift of ca. -1.2 pm. The approximate Sm(III)$-$C(Me) distance for the methyl substituents of the cyclopentadienyl ring distance in the solid-state structure of is 4 Å. The shifts of all hydrogen nuclei located at a distance of ≥4 Å from the Sm(III) metal centre can be attributed to the pseudocontact shift.

The chemical shifts of the borane protons in **58** and **53** are 0.67 and 0.64 ppm respectively. In the Sm(III) complex the chemical shift of the analogous borane protons is -17.02 ppm. This is a shift change of almost -16.5 ppm. The approximate B$-$H$\cdots$Sm(III) distance in complex is 2.4 Å, although this vector is a slight underestimate, since bonds to hydrogen atoms are systematically underestimated by X-ray crystallography. Nevertheless the shift of this κ^2 *H,H* coordinated BH_3 group has changed more than it is suggested is plausible, if the effect is attributed solely to the pseudocontact shift (Figure 61). The change in shift of the borohydride protons of the $[BH_4]^-$ anion in $(Cp^{4Me}Me_2SiNPh)Sm(BH_4)(THF)_2$ appears to be much smaller with the chemical

shift moving from -0.25 ppm in diamagnetic $Mg(BH_4)(THF)_3$ to -1.4 ppm in the paramagnetic Sm(III) compound (C_6D_6).[30] It could be that due to the very unsymmetrical nature of these complexes higher order crystal field splitting parameters not included in this calculation would significantly alter the calculation results, giving a larger pseudocontact shift range, but an ambitiously large crystal field splitting parameter, of 1000 cm^{-1} was chosen with this in mind.[21] It would also be expected that the pseudocontact shifts of some of the peripheral protons would be outside the plausible ranges estimated by the calculation if too small a crystal field splitting parameter was chosen. Finally one of the known limitations of the pseudocontact shift theory is that within 4 Å of the paramagnetic metal ion the theory is inaccurate since other effects (contact shift) contribute to the overall change in chemical shift.

5.4   Synthesis of a calcium complex of a phosphine-borane-stabilised dicarbanion hybrid ligand

The calcium complex $[(Cp^{4Me}Me_2Si)(Me_3Si)C\{PMe_2(BH_3)\}]Ca$ (THF)$_2$ [**58**], was prepared by a metathesis reaction between the organopotassium compound $[(Cp^{4Me}Me_2Si)(Me_3Si)C\{PMe_2(BH_3)\}]K_2$ **53** and CaI$_2$ (Scheme 54). The calcium complex was synthesised as a precedent to the synthesis of the Yb(II) complex, since the Ca^{2+} cation is very similar in size to the Yb(II) cation (Chapter 1, Table 2) but is not susceptible to oxidation.
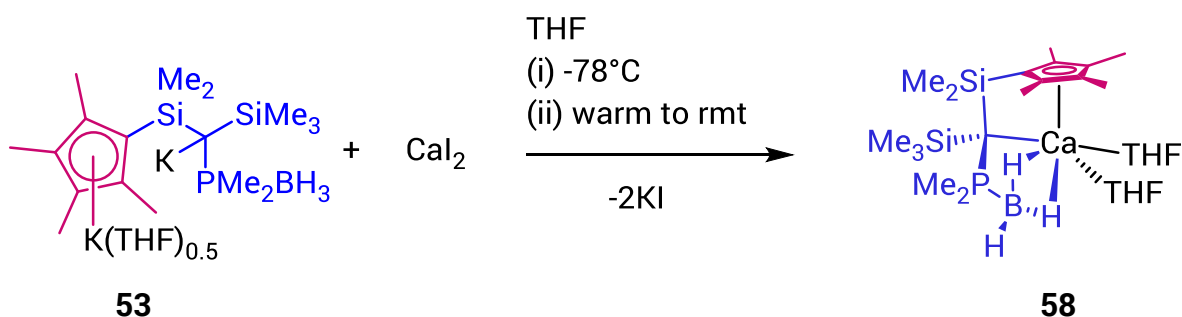
Scheme 54

Complex **58** was prepared in a very similar way to that described for **56** and **57**. A dark red solution of the metalated ligand **53** in THF was added to a cooled (-78°C) slurry of CaI$_2$ in THF. The red solution was immediately discoloured and a colourless precipitate formed. After warming to room temperature overnight the solvent was removed *in vacuo,* the product was extracted into diethyl ether and filtered to remove KI. Concentration of the pale yellow diethyl ether solution and cooling to -24 °C yielded colourless crystalline material. The crystals rapidly lose crystallinity upon solvent loss and initial attempts to pick a crystal under oil for X-ray diffraction were unsuccessful. At ambient temperatures the mother liquor became oily and yellow in colour and this was attributed to decomposition, therefore the mother liquor was decanted and the colourless solid re-dissolved in the minimum amount of a 1:1 mixture of cold (0°C) diethyl ether and toluene. The cold solution was quickly filtered and stored in the freezer. A second crop of crystals were obtained and with haste a crystal suitable for X-ray crystallography was mounted and the solid state-structure shown in Figure 68 was determined.

5.5 Solid-state structures

5.5.1 Solid-state structure of a lanthanum complex with a silicon-stabilised hybrid ligand

The monomeric solid-state structure of the constrained geometry lanthanum complex, [(Cp^{4Me}Me$_2$Si)(Me$_3$Si)$_2$C]LaI(THF)$_2$ **[56]** is shown in Figure 62. The monomeric structure of **56** contrasts with the previously determined structures of halide containing constrained geometry complexes of smaller lanthanides and alkaline-earth cations [{(Cp^{4Me}Me$_2$Si)PMes*} SmI(THF)]$_2$ (Mes* = 2,4,6-^{t}BuC$_6$H$_2$) **[59]**, [{(Cp^{4Me}Me$_2$Si)NMe$_2$Et}YCl(THF)]$_2$ **[60]** and [{(Cp^{4Me}Me$_2$Si)NPh}ScCl(THF)]$_2$ **[61]** which are dimeric (Figure 63).[10,15,31] It is possible that the less solvated complex [(Cp^{4Me}Me$_2$Si)(Me$_3$Si)$_2$C]LaI(THF) **56a** that was observed in the NMR spectrum (see above) would have an analogous dimeric structure in the solid state.
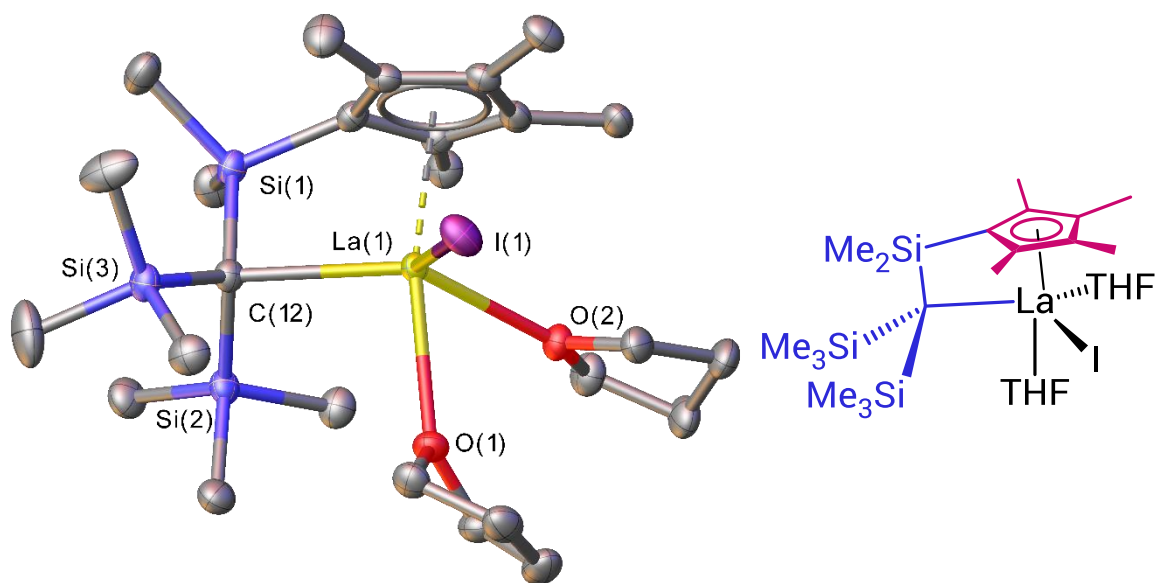
*Figure 62. Molecular structure of **56**, with 40% probability ellipsoids and with H atoms omitted for clarity.*

The constrained geometry pseudo-four membered ring is formed by η^5-coordination of the cyclopentadienyl ring and η^1-coordination of the silicon-stabilised carbanion to the La(III) metal centre (Figure 62). The La−centroid (ring centroid of the cyclopentadienyl ring) distance is 2.508(1) Å. A very similar La−centroid distance is of 2.540(3) Å is found for the only other constrained geometry complex known for La, [(Cp^{4Me}Me$_2$Si)NAr]LaPPh$_2$(THF)$_2$ **[62]** The differences in geometry between the constrained geometry chelate rings stem from the longer La−C$^{\ominus}$ bond from the bridging silicon atom to the carbanion carbon. The La−C$^{\ominus}$ contact distance for **56** is 2.710(3) Å, whereas the La−N$^{\ominus}$ contact distance for **62** is shorter at 2.416(2) Å. The C$^{\ominus}$−SiMe$_2$ distance for **56** is 1.859(3) Å and the N$^{\ominus}$−SiMe$_2$ distance for **62** is shorter [1.716(4) Å]. With the La−centroid and C(ring)−Si bond lengths being so similar the effect of the elongated La−C$^{\ominus}$ and C$^{\ominus}$−SiMe$_2$ distances is to skew one half of the chelate ring such that the La−C$^{\ominus}$−Si angle in **56** [93.16(11)°] is reduced compared to the corresponding angle La−N$^{\ominus}$−Si in **62** [99.1(3)°]. Size optimization of the trivalent lanthanide cation has the potential to allow fine control over the geometry of the chelate ring.

60   **62**
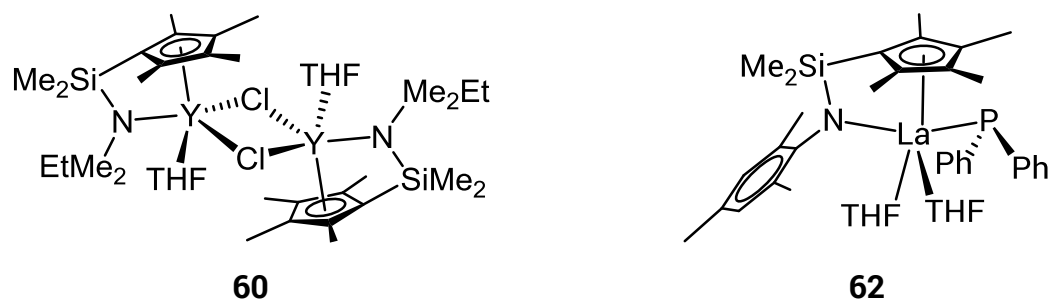
Figure 63. Structures of the constrained geometry complex 62 and the dimeric halide containing constrained geometry complex [{(Cp⁴ᴹᵉMe₂Si)NMe₂Et}YCl(THF)]₂.

The La(1)−C(12) σ-bond length is 2.710(3) Å which is very similar to the La−C σ-bond lengths in [{(Me₃Si)(Me₂MeOSi)C(SiMe₂CH₂)}₂]LaI(THF) **[63]** of 2.711(2) Å and comparable to those in [(Me₃Si)₂{Me₂(MeO)Si}C]₂LaI(THF) **[64]** of 2.813(4) and 2.714(4) Å (Figure 64). The La−C bond lengths in [(Me₃Si)₂{Me₂(Me₂N)Si}C]₂LaI **[65]** are slightly shorter (2.663(4)/2.680(3) Å), perhaps because this complex is solvent-free and formally only 5-coordinate (Figure 64). The constrained geometry La(III) complex of the hybrid ligand containing a silicon-stabilised carbanion has, in common with the La complexes **63**, **64**, and **65**, a chelate ring involving a silicon-stabilised carbanion and also coordination of an iodide anion. The La−I distance in **56** is 3.1521(4) Å, which is very similar to the La−I distances in **63** 3.1744(5) Å, **64** 3.1734(3) Å and **65** 3.1447(3) Å.[32]

63   **64**   **65**
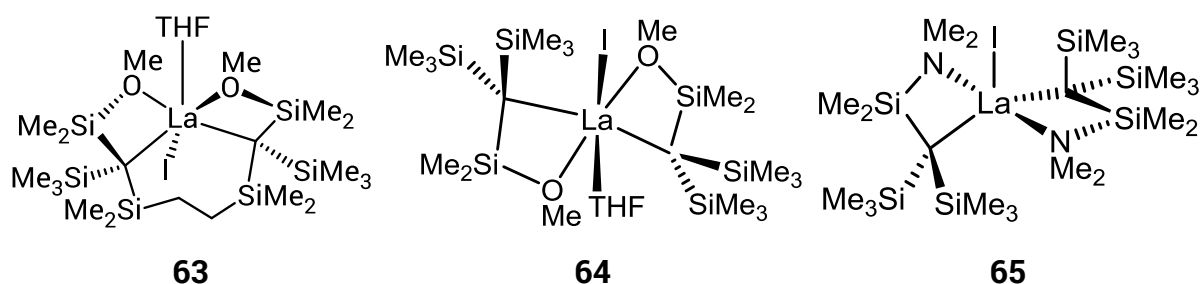
Figure 64. Structures of [{(Me₃Si)(Me₂MeOSi)C(SiMe₂CH₂)}₂]LaI(THF) 63, [(Me₃Si)₂{Me₂(MeO)Si}C]₂LaI(THF) 64 and [(Me₃Si)₂{Me₂(Me₂N)Si}C]₂LaI 65.

The silicon-stabilised carbanion in **56** is distorted from planarity; the sum of the Si−C(12)−Si angles around C(12) is 343.2° (Figure 62), and C(12) protrudes 0.335 Å out of the mean plane defined by the atoms Si(1), C(12), Si(2) and Si(3) towards the La(III) cation. The effect of this pyramidalisation is to increase the localisation of

negative charge on the carbanion carbon, C(12). The filled p-orbital on C(12) does not overlap as-effectively with the antibonding Si−C σ*-orbitals of the −SiMe$_3$ groups to delocalise the charge from the carbanion by negative hyperconjugation if the carbanion is non-planar (see Chapter 3).

There is a statistically significant difference (two-sample t (16) = 3.883, p = 0.001)[4] in the average length of Si−C bonds of the -SiMe$_3$ groups for the potassium compound (See Chapter 4) and the lanthanum complex **56** of the silicon-stabilised hybrid ligands. The Si−C bonds are significantly longer, on average by 0.012 Å for the dipotassium salt compound **51** Than the lanthanum complex compound **56**. Two factors are suggested to contribute to the elongation of the Si−C bonds in **51** relative to **56**, (i) increased negative hyperconjugation due to the more planar carbanion in **51** and (ii) agostic-type Si−Me····K interactions found in the solid state structure of **51**, which decrease the Si−C bond order. In **56** there is an absence of agostic-type Si−Me····La interactions, with the shortest approach of a methyl group to the La centre measuring 3.372(3) Å. The Si−(Me)C····La distances for Cp*La{CH(SiMe$_3$)$_2$}$_2$ measured from structures obtained using both X-ray and neutron diffraction techniques were approximately 2.97 Å. The neutron diffraction study determined that the hydrogen atoms of the methyl groups do not have the correct orientation for these close contacts to be true agostic interactions and there is no significant elongation of the C−H bonds. On the basis of this evidence the interaction is better described as an electrostatic interaction between the Si−C(Me) bond (which is elongated) and the lanthanum metal centre. The average elongation between agostic and non-agostic Si−C bonds is given as 0.036Å. [5]

---

[4] A two-sample t-test compares the means of two groups with unknown but equal variances. Where "p" is the probability of obtaining a test-statistic this extreme if the means of the two groups of bond lengths are assumed to be the same (the null hypothesis). The statistic "t(df)" tells us about the magnitude and direction of the difference in the means of the two groups of bond lengths, df is degrees of freedom; the two groups consist of 16 bond lengths.

There is no mention of negative hyperconjugation which also contributes to Si−C bond elongation and since this effect depends on Si−C bond orientation it is very difficult to separate the two effects.

5.5.2 Solid-state structure of a samarium complex with a phosphine-borane-stabilised hybrid ligand

The monomeric solid-state structure of the samarium complex $[(Cp^{4Me}Me_2Si)(Me_3Si)C\{PMe_2(BH_3)\}]SmI(THF)_3$ **[57]** is shown in Figure 65. An unstrained pseudo-six-membered ring is formed by the η^5-coordination of the cyclopentadienyl ring and the κ^2 *H,H* coordination of the BH_3 group to the Sm(III) metal centre. The phosphine-borane-stabilised carbanion centre does not interact with the Sm(III) cation. The coordination sphere of the monomer is completed by three molecules of THF and an iodide anion. The formally 8-coordinate Sm(III) complex has a distorted octahedral geometry with the $-BH_3$ group and the iodide anion arranged trans to each other and together with the cyclopentadienyl ring form a meridional arrangement. The three THF ligands are also approximately meridionally arranged.

The coordination of the phosphine-borane-stabilised carbanion part of the hybrid ligand to the Sm(III) metal centre by only κ^2 *H,H* coordination of the borane hydrogens is one of several conceivable coordination modes. As discussed at the beginning of chapter 4 a monophosphine-borane-stabilised monocarbanion can coordinate to a metal centre through the residually hydridic borane hydrogens (κH − κ^3 *H,H,H*), a M−C σ-bond or both, forming a 4-membered chelate ring. In polymeric compounds the ligand often bridges multiple metal centres by binding to them via alternating coordination modes.
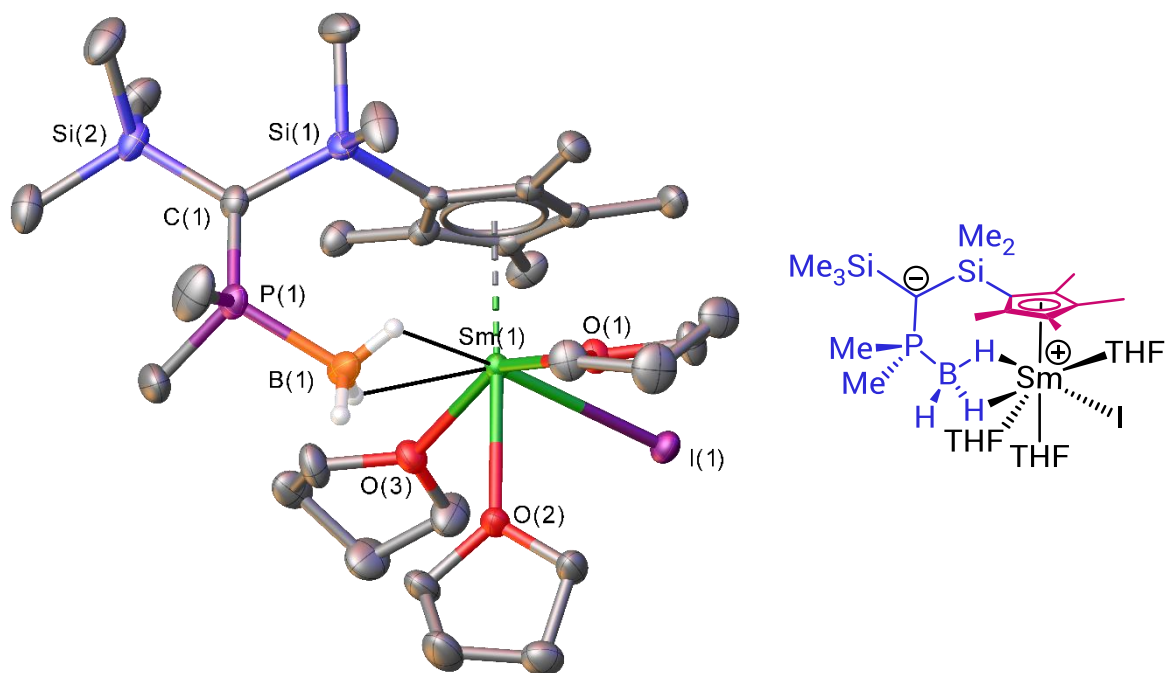
*Figure 65. X-ray crystal structure of **57**, with 40% probability ellipsoids and C-bound H atoms omitted for clarity.*

Coordination of phosphine-borane stabilised carbanions to Sm(II) cations has shown that these ligands also exhibit variable binding modes with lanthanide metals. The dialkylsamarium(II) compounds $[(Me_3Si)_2\{Me_2P(BH_3)\}C]_2Sm(THF)_n$ (n = 1 or 3) have been previously synthesised from the potassium salt $[(Me_3Si)_2\{Me_2P(BH_3)\}C]K$ and $SmI_2(THF)_2$. (Figure 8) In the solid-state structure the binding mode of the phosphine-borane-stabilised carbanion ligands to the Sm(II) cation depends on the number of coordinated molecules of THF. In the mono-THF adduct [**66a**] the phosphine-borane ligands coordinate the Sm(II) cation through the carbanion carbon atom and the BH_3 group forming two 4-membered chelate rings. In the tris-THF adduct [**66b**] the chelate ring of one of the phosphine-borane ligands is opened, and the ligand is bound to the Sm(II) metal centre in a similar way to that in **57** by only an κ^3 *H,H*,H coordination of the borane hydrogen atoms. This coordination mode, in which the phosphine-borane-stabilised carbanion is coordinated to the metal centre by only the BH_3 group with a remote planar carbanion, has also been observed in the solid-state structures of

[(Me$_3$Si)$_2${Me$_2$(H$_3$B)P}C]$_2$Ca(THF)$_4$ [**67**] and [(Me$_3$Si)$_2${Me$_2$(H$_3$B)P}C]$_2$M(THF)$_5$ (M = Sr [**68**] or Ba [**69**]).[33]

66a   **66b**
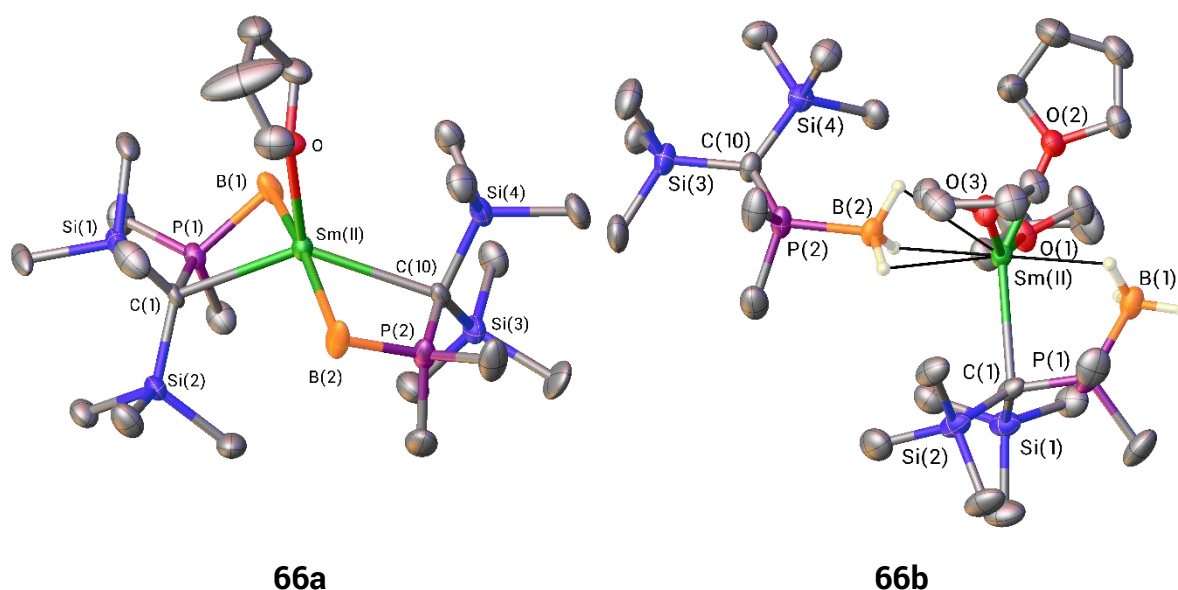
Figure 66.   Molecular structures of [(Me$_3$Si)$_2${Me$_2$P(BH$_3$)}C]$_2$Sm(THF)$_n$ (n = 1 or 3) with C-bound H atoms omitted for clarity.

The Sm(III)····H−B contact distances in **57** are 2.3508(3) Å and 2.5670(3) Å and the Sm(III)−B(1) distance is 2.884(4) Å. On the basis of Shannon ionic radii (see Figure 1, chapter 1) a difference of 0.2 Å is expected between the Sm(III)····H−B contacts and Sm(III)−B distance in **57** and the corresponding Sm(II)····H−B and Sm(II)−B(1) distances in **66a**. The Sm(II)····H−B distances of the κ^3 *H,H,H* coordinated BH$_3$ group in **66a** are 2.55(3), 2.61(2) and 2.60(3) Å and the Sm(II)−B(2) distance is 2.782(4) Å. As anticipated the shortest Sm(III)····H−B contact distance is approximately 0.2 Å shorter than the shortest Sm(II)····H−B distance; otherwise the average difference between the Sm····H−B and Sm−B distances is ≤0.1 Å. It is suggested that this lower than expected difference can be attributed to the lower coordination number of the Sm(II) complex which is formally 6-coordinate. The Sm(III)····H−B and Sm(III)····B(1) contact distances are also similar to the corresponding distances in Sm(III) borohydride complexes with cyclopentadienyl ligands or constrained geometry ligands, for example (C$_5$Me$_4$^{n}Pr)$_2$Sm(BH$_4$)(THF) [Sm(III)····H−B   2.40(4)-2.51(3)   Å,   Sm(III)····B   2.621(5)]   and

(Cp^{4Me}Me$_2$SiNPh)Sm(BH$_4$)(THF)$_2$ [Sm(III)····H—B 2.31(4)−2.60(5) Å, Sm(III)····B$_{average}$ 2.69 Å].[30,34] The Sm(III)····B distances are shorter for the κ^3 *H,H,H* coordinated BH$_4$ groups versus the κ^2 *H,H* coordinated BH$_3$ group in complex **57** as expected.

As in the structure of **57**, where the carbanion carbon atom is 4.710(3) Å from the Sm(III) metal centre, the carbanion carbons in **66a** (5.80 Å), **67** (5.79 Å), **68** (5.98 Å) and **69**(6.09 Å) are also a long way from the metal cation, and the distant separation of charge makes the structures zwitterions. The geometry of the carbanion carbon in **57** is planar, with the sum of the angles around C(1) being 358.1°; the remote carbanions in **66a**, **67**, **68** and **69** are similarly planar with the sum of the angles around the carbanion carbon atom being 354.6°, 354.1°, 357° (average) and 358.0° respectively.
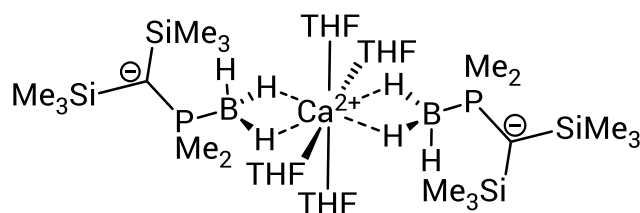
*Figure 67. Structure of [(Me$_3$Si)$_2${Me$_2$(H$_3$B)P}C]$_2$Ca(THF)$_4$ **[67]***

The ring centroid—Sm(1)—B(1) bite angle in **57** is 102.61(9)° which is slightly larger than in an archetypal constrained geometry complex where the ring centroid—metal—heteroatom anion bite angle is about 95°. Despite the larger bite angle, the steric environment around the samarium metal centre is more open than in a constrained geometry complex. The effect of the hybrid ligand binding to the Sm(III) cation through the borane hydrogen atoms and not the carbanion carbon is that the sterically bulky —SiMe$_3$ substituent is located further from the metal centre outside the periphery of the cyclopentadienyl ring and the Tolman cone angle is reduced relative to that of the silicon-stabilised carbanion hybrid ligands.

5.5.3 Solid-state structure of a calcium complex of a phosphine-borane-stabilised hybrid ligand

The monomeric solid-state structure of the constrained geometry calcium complex [(Cp^{4Me}Me$_2$Si)(Me$_3$Si)C{PMe$_2$(BH$_3$)}]Ca(THF)$_2$ **[58]**, is shown in Figure 68. The hybrid ligand coordinates the Ca metal cation in a tridentate fashion, with η^5-coordination of the cyclopentadienyl ring, κ^2 *H,H* coordination of the BH$_3$ group and η^1-coordination of the carbanion carbon to form a C−Ca σ-bond. The tridentate coordination mode results in two fused pseudo-four-membered chelate rings, the first is formed by Cp^{4Me}, Si(1), C(1) and Ca(1) and the second is formed by C(1), P(1), B(1) and Ca(1). The angle between the planes of the two chelate rings is about 115°. The Ca cation is formally 7-coordinate, with two molecules of THF completing the coordination sphere.
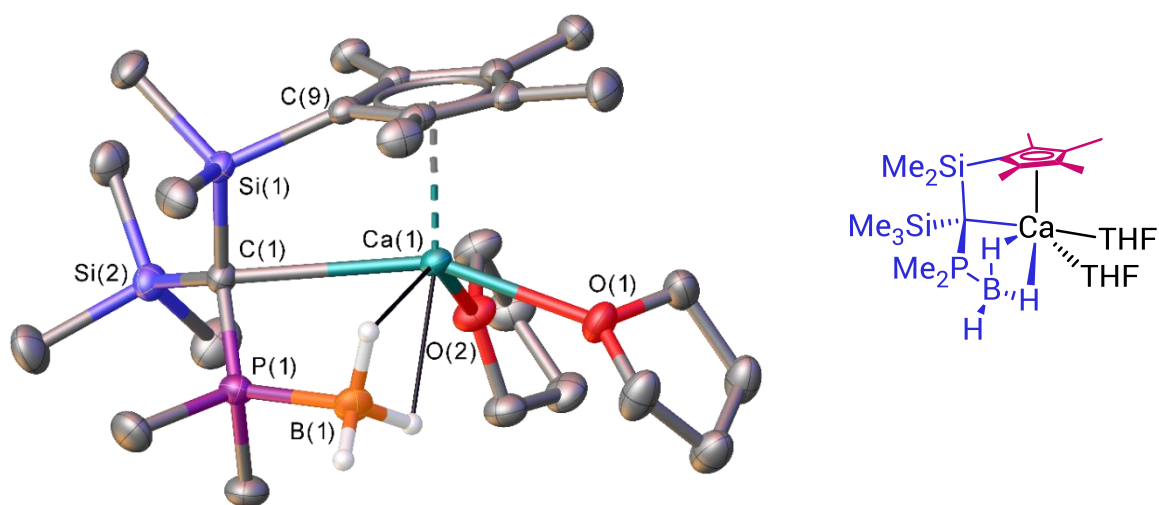
*Figure 68. Molecular structure of [(Cp^{4Me}Me$_2$Si)(Me$_3$Si)C{PMe$_2$(BH$_3$)}]Ca(THF)$_2$ **[58]**, with 40% probability ellipsoids and C-bound H atoms omitted for clarity.*

The length of the Ca−C(1) σ-bond in **58** is 2.985(3) Å, much longer than the Ca−C σ-bond lengths in the dimeric calcium complex of the 1,3-monophosphine-borane-stabilised dicarbanion ligand [{PhP(BH$_3$){CH(SiMe$_3$)}$_2$}Ca(OEt$_2$)]$_2$ **[70]** which range from 2.550(3) − 2.683(3) Å.[35] Comparison with (PhCH$_2$)$_2$Ca(THF)$_4$ where the Ca−C distance ranges from 2.568(5) − 2.595(5) Å confirms that the Ca−C(1) bond in **58** is longer than expected by about 0.3 Å. The trend towards M−C σ-bonds that are

longer than usual as a consequence of M−carbanion−P−B chelate ring formation has been previously observed for the unsolvated magnesium complex [(Me$_3$Si)$_2${Me$_2$(H$_3$B)P}C]$_2$Mg [**71**], where the Mg−C bond lengths are longer than expected by approximately 0.2 Å.[33] The compound [(Me$_3$Si)$_2${Me$_2$(H$_3$B)P}C]$_2$Ca is also known, but the structure has not been determined by X-ray crystallography, therefore complex **58** is the only example of a monomeric solid-state structure where the calcium centre is bound by the carbanion carbon and the BH$_3$ group of the *same* phosphine-borane-stabilised carbanion ligand. The Ca····H−B distances in **58** of 2.38(4) and 2.37(4) Å are similar to those in **67** (2.40(2) and 2.43(2) Å where the BH$_3$ group of the remote carbanion is also κ^2 *H,H* coordinated to a 6-coordinate Ca cation (see above).
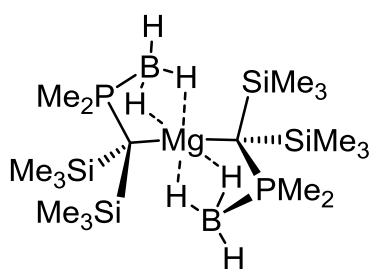
Figure 69. Structure of [(Me$_3$Si)$_2${Me$_2$(H$_3$B)P}C]$_2$Mg [71]

Comparison of **58** with constrained geometry complexes of Ca [**72**] and Yb(II) [**73**] (Figure 70) shows that the long Ca−C(1) σ-bond in **58** has the effect of skewing the geometry of one side of the pseudo-four-membered chelate ring formed by Cp^{4Me}, Si(1), C(1) and Ca (Figure 68). The Ca−C(1) bond length is >0.5 Å longer than the Ca−N distance in **72** [2.452(2) Å] and the Yb(II)−N distance in **73** [2.359(8) Å]. In **58** the Ca−C(1)−Si(1) angle becomes acute [83.16(10)°], while for **72** [99.62(9)°] and **73** [100.1(4)°] the corresponding angles are obtuse angles.

72   **73**
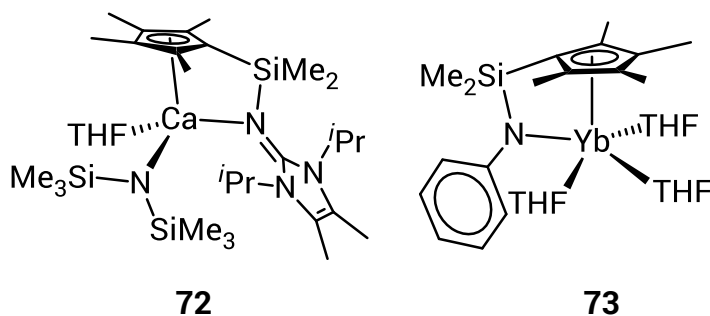
Figure 70. Structures of 72 and 73

5.6   Conclusion

The hybrid ligands **51** and **53** can be transferred to trivalent and divalent lanthanide cations and their cation analogues using metathesis chemistry. The diamagnetic La(III) complex **56** was synthesised from the metathesis reaction of the dipotassium salt **51** with $LaI_3(THF)_4$ in THF at room temperature with 47% yield. Compound **56** was crystallised from cold (-24°C) toluene containing a few drops of THF. The structure is monomeric and the hybrid ligand chelates the La(III) cation forming a pseudo-four-membered ring. The La(III) cation has a coordination number of and the coordination geometry of **56** bears close resemblance to the lanthanum constrained geometry complex [(Cp^{4Me}Me$_2$Si)NAr]LaPPh$_2$(THF)$_2$ [**74**]. Compound **56** is the first example of a lanthanide constrained geometry complex incorporating an alkyl carbanion in the place of the more usual amide or phosphide groups. Desolvation of **56** is facile as shown by the loss of one of the two coordinated THF molecules during preparation of the NMR sample (sealed under vacuum) to give **56a**. The solid-state structure of **56a** was not determined so it is unknown if this less solvated compound crystallises as a dimer, analogous to previously crystallised halide containing lanthanide constrained geometry complexes. There are no agostic-type Si—Me····La short contacts in **56** in contrast to the monocyclopentadienyl complex and iodide containing chelated lanthanum alkyl complexes where the solid-state structures all have Si—Me····La agostic-type interactions.

The zwitterionic Sm(III) complex **57** was synthesised from the metathesis reaction of the dipotassium salt **53** with $SmI_3(THF)_{3.5}$ in initially cold THF (-78°C) with 32% yield. Compound **57** was crystallised from a concentrated cold (3°C) diethyl ether solution. Crystals of **57** are deep red in colour which is unusual for a trivalent samarium complex due to the forbidden nature of f-f transitions and it is suggested that a ligand to metal charge transfer (LMCT) process is responsible for the red colour. In this complex the Sm(III) cation has a coordination number of eight, the hybrid ligand coordinates κ^2 *H,H* through the borane hydrogens and η^5 through the cyclopentadienyl ring, the remaining four coordination sites are occupied by three molecules of THF solvent and an iodide anion. There is no contact between the carbanion carbon and the Sm(III) metal centre and the distance between them is 4.7 Å. Sm(III) is paramagnetic, but since the effective magnetic moment is only 0.845 BM the shift in the peripheral (atoms not directly bonded to metal) ligand signals in the ^{1}H and ^{13}C NMR spectra is only small (< ±1.5ppm). The much larger shift of 17ppm observed for the borane hydrogens is evidence for a contribution from the coxntact shift to the change in chemical shift. The quaternary carbanion carbon C(1) is shifted by 50 ppm in the ^{13}C NMR spectrum which suggests that the structure of compound **57** is different in solution to in the solid-state, with the Sm(III) being additionally coordinated by the carbanion carbon in solution.

In the calcium complex **58** also synthesised from the metathesis reaction of the dipotassium salt **53** with CaI_2 in THF (yield = 36%) the hybrid ligand exhibits a different coordination mode to in complex **57**. In complex **58** the hybrid ligand binds to the calcium metal centre in a tridentate fashion via the cyclopentadienyl anion, the carbanion carbon and κ^2 *H,H* through the borane hydrogens. Compound **58** is the only example of crystal structure of an organocalcium compound where the calcium metal is chelated by both the carbanion carbon and the BH_3 group of the same phosphine-borane-stabilised carbanion ligand. Phosphine-borane carbanion ligands are well known to adopt versatile coordination modes and the

191

hybrid ligand **53** is no exception, as it is able to chelate the metal by η^5-coordination of the cyclopentadienyl ring and either the borane hydrogens alone or the borane hydrogens and the carbanion carbon. The tridentate binding mode of hybrid ligand **53** seen in complex **58** is much more sterically demanding than the bidentate binding mode seen in complex **57**.

The synthesis of complex **58** is a useful precedent for the synthesis of divalent lanthanide complexes since calcium cations are the redox inert analogues of divalent ytterbium cations. Future work should aim to synthesise divalent lanthanide complexes of these hybrid ligands followed by an investigation of their redox chemistry. Of particular interest is the redox chemistry of divalent samarium complexes of the hybrid ligands which could be compared to the redox chemistry of Sm(Cp*)$_2$. There are several potential areas of interest for further investigation of the trivalent lanthanide complexes **56** and **57** synthesised in this work, (i) trivalent lanthanide complexes of the hybrid ligands may reduce substrates by sterically induced reduction (SIR) if the iodide anion is first substituted by a cyclopentadienyl anion. These complexes offer the opportunity lanthanides to size optimise both the lanthanide cation and the cyclopentadienyl anion(s) to achieve the desired reactivity. (ii) The trivalent lanthanide complex **56** which resembles the precursor to previously synthesised rare earth and lanthanide constrained geometry complexes should be desolvated, then treated with LiCH$_2$SiMe$_3$ and perhaps converted to dimeric hydrido complexes of the type. The catalytic activity of these complexes towards the polymerisation of α-olefins could then be investigated. (iii) Reduction of desolvated derivatives of **56** and **57** with KC$_8$ at low temperature (-35°C) in the presence of [18]crown-6 should be investigated as a synthetic route to access divalent lanthanide complexes of the hybrid ligands as separated ion pairs.

5.7 Experimental

5.7.1 General procedure

All manipulations were carried out under an inert argon atmosphere using Schlenk techniques or under nitrogen in a solvent-free glove-box. Non-halogenated solvents (diethyl ether, THF, light petroleum, toluene, benzene and hexane) were pre-dried using sodium wire. Solvents were then distilled over sodium-potassium alloy (diethyl ether, light petroleum, hexane), potassium (THF, benzene) or sodium (toluene). Dichloromethane was dried by distillation over CaH_2. THF and dichloromethane were stored under nitrogen/argon over activated 4Å molecular sieves, all other solvents were stored over a potassium film. Deuterated solvents for NMR were also dried by distillation from potassium (d_8-THF, C_6D_6) or CaH_2 ($CDCl_3$) and were stored over activated 4Å molecular sieves. Deuterated solvents were deoxygenated using the freeze-pump-thaw method (3 cycles).

The lanthanide triiodide THF solvates were prepared from the lanthanide metals and diiodine as described in the literature and stored in a glovebox.[36]

Anhydrous calcium diiodide was purchased from Sigma-Aldrich and used as supplied.

5.7.1.1 NMR Spectroscopy

The NMR spectra were recorded using a Bruker Avance 300 spectrometer operating at (^{1}H 300.13; ^{13}C 75.48; ^{11}B 96.29; ^{31}P 121.49 MHz), a Bruker Avance 400 spectrometer operating at (^{1}H 399.78; ^{13}C 100.54; ^{11}B 128.78; ^{31}P 161.83 MHz) or a Bruker Avance 700 spectrometer operating at (^{1}H 700.13; ^{13}C 176.06).Two-dimensional NMR experiments, HSQC and HMBC were also recorded using these instruments. Chemical shifts are quoted in ppm relative to TMS (^{1}H and ^{13}C),

$BF_3(OEt_2)$ (^{11}B) and 85% H_3PO_4 (^{31}P). All NMR spectra were recorded at ambient temperature. NMR data were processed using MestReNova software.

5.7.1.2   Crystal structure determinations

Data for crystal structure determinations were collected on a Xcalibur, Atlas, Gemini ultra diffractometer at 150 K using CuKα radiation (λ = 1.54184 Å) for **56** and **58**, for **57** MoKα (λ = 0.71073) was used.   Cell refinement, data collection and data reduction were undertaken via software CrysAlisPro 1.171.38.42b (Rigaku Oxford Diffraction, 2015). Intensities were corrected for absorption using CrysAlisPro. An empirical absorption correction was applied for **56** and **57** using spherical harmonics, implemented in SCALE3 ABSPACK scaling algorithm. Intensities were corrected for absorption using a numerical absorption correction based on a multi-faceted crystal model using the program 'sadabs' for **58**. The structures were solved using direct methods, SHELXT and refined by SHELXL through the Olex2 interface.[37−39]   All molecular graphics were generated by the author using Olex2 software.

All non-H atoms were refined anisotropically. The coordinates of the non-borane H atoms were computed using a riding model constraint with the isotropic temperature factor (U_{iso}) of each H atom set to 1.2 (1.5 for methyl groups).

The structure of **58** was refined with no other restraints, but for the structures of **56** and **57** convergence of the refinement required the use of restraints.   In the structure of **57** the THF molecules are disordered.   The two tetrahydrofuran molecules have been modelled as disordered over two positions. The occupancies of the disordered atoms were allowed to refine with isotropic atom treatment. Upon convergence, the occupancies were fixed before anisotropy was introduced into the model. The ADPs of the disordered atoms were constrained using the EADP card and their geometry was restrained using the SADI card.

5.7.2 Preparation of [(Cp^{4Me}Me$_2$Si)(Me$_3$Si)$_2$C]LaI(THF)$_2$ [56]

A dark red solution of [(Cp^{4Me}Me$_2$Si)(Me$_3$Si)$_2$C]K$_2$ (0.81g, 1.95 mmol) in THF (15 ml) was added, dropwise, to a slurry of LaI$_3$(THF)$_4$ (1.58g, 1.95 mmol) in THF (10 ml) at room temperature to give a pale yellow reaction mixture with a colourless precipitate. After stirring for 5 hours the reaction mixture was filtered and the solvent removed *in vacuo* from the filtrate to give a pale yellow foam, which was dissolved in toluene (ca. 10 ml) and a few drops of THF. Colourless crystals suitable for X-ray diffraction were grown from this solution at -24°C. Yield = 0.7 g, 47%. One molecule of coordinated THF was lost very readily when the crystals were placed under vacuum during preparation of the NMR sample and so all analyses relate to this desolvated compound [(Cp^{4Me}Me$_2$Si)(Me$_3$Si)$_2$C]LaI(THF), **56a**.

^{1}H NMR (300.13 MHz, d$_8$-THF, 21°C): δ 0.14 (s, 18H, SiMe$_3$), 0.56 (s, 6H, SiMe$_2$), 1.78 (m, 4H, THF), 2.10 (s, 6H, Cp*Me$_A$*), 2.14 (s, 6H, Cp*Me$_B$*), 3.62 (m, 4H, THF).

^{13}C{^{1}H} NMR (100.53 MHz, d$_8$-THF, 20.3°C): δ 3.97 ({Me$_3$Si}$_2$*C*La), 8.75 ({*Me$_3$*Si}$_2$CLa), 10.28 (Cp*Me$_2$*Si), 13.33 (Cp*Me$_A$*), 15.96 (Cp*Me$_B$*), 26.54 (THF), 68.39 (THF), 107.30 ({*C*}Cp^{4Me}), 129.96 ({*C*Me}Cp), 130.54 ({*C*Me}Cp).

Elemental analysis of crystals (%) calculated for C$_{26}$H$_{50}$ILaO$_2$Si$_3$: C 41.93, H 6.77; found: C 41.51, H 7.15.

5.7.3 Preparation of [(Cp^{4Me}Me$_2$Si)(Me$_3$Si)C{PMe$_2$(BH$_3$)}]SmI(THF)$_3$ [57]

To a cold (-78°C) slurry of SmI$_3$(THF)$_{3.5}$ (1.71 g, 2.18 mmol) in THF was added a dark red solution of [(Cp^{4Me}Me$_2$Si)(Me$_3$Si)C{PMe$_2$(BH$_3$)}]K$_2$ (25.29 ml, 2.18 mmol), prepared and used *in situ* as an 0.086 M solution in THF. The reaction mixture was allowed to warm to room temperature overnight with stirring. The reaction mixture was analysed using ^{31}P{^{1}H} and ^{11}B{^{1}H} NMR spectroscopy. The solvent was

removed *in vacuo* and the product was extracted into diethyl ether and filtered to remove KI. The red diethyl ether solution was concentrated to ca. 5 ml. On exposure to argon evaporation of some of the solvent gave a red microcrystalline solid. The solid was re-dissolved by adding ca. 3 ml of diethyl ether and large red crystals suitable for X-ray crystallography were grown from this solution at 3°C. The crystals were isolated by decanting off the mother liquor. Yield = 0.577 g, 32%.

^{1}H{^{11}B} NMR (300 MHz, C$_6$D$_6$, 23°C): δ -17.02 (s, 3H, BH$_3$), -0.50 (s, 6H, SiMe$_2$), 0.30 (s, 9H, SiMe$_3$), 0.90 (s, 6H, Cp*Me$_A$*), 1.44 (s, 6H, Cp*Me$_B$*), 1.57 (br unresolved, 18H, coordinated THF -C*H$_2$* and −PMe$_2$), 3.80 (br, 12H, coordinated THF -OC*H$_2$*).

^{13}C{^{1}H} NMR (176.06 MHz, C$_6$D$_6$, 23°C): δ -50.85 ([(Cp^{4Me}Me$_2$Si)(Me$_3$Si)*C*{PMe$_2$(BH$_3$)}]), 7.53 (Si*Me$_3$*), 11.62 ({*C*Me$_B$}*Cp^{4Me}*), 17.75 ({*C*Me$_A$}*Cp^{4Me}*), 20.63 (Si*Me$_2$*), 21.19 (P*Me$_2$*/thf), 25.85 (coordinated THF -*C*H$_2$-), 65.93 (coordinated THF -O*C*H$_2$-), 70.35 (P*Me$_2$*/thf), 107.53, 123.77, 124.77 (quaternary carbon atoms: ({*C*Me$_B$}*Cp^{4Me}*, {*C*Me$_A$}*Cp^{4Me}* and {*C*}*Cp^{4Me}*).

^{11}B{^{1}H} NMR (128.27 Hz, C$_6$D$_6$, 298K): δ -48.2 (br).

^{31}P{^{1}H} NMR (161.85 Hz, C$_6$D$_6$, 298K): δ -3.0 (br).

Elemental analysis of crystals (%) calculated for C$_{29}$H$_{57}$BIO$_3$PSi$_2$Sm: C 42.02, H 6.93; found C 41.87, H 7.04.

5.7.4   Preparation of [(Cp^{4Me}Me$_2$Si)(Me$_3$Si)C{PMe$_2$(BH$_3$)}]Ca(THF)$_2$ [58]

To a cold (-78°C) slurry of CaI$_2$ (0.752 g, 2.56 mmol) in THF (10 ml) was added a dark red solution of [(Cp^{4Me}Me$_2$Si)(Me$_3$Si)C{PMe$_2$(BH$_3$)}]K$_2$ (25.29 ml, 2.18 mmol; prepared and used *in situ* as an 0.086 M solution in THF). The reaction mixture was allowed to warm to room temperature overnight with stirring. The solvent was removed *in vacuo* and the product was extracted into diethyl ether and filtered to

remove KI. The colourless diethyl ether solution was concentrated to ca. 10 ml and cooled to -24 °C, colourless crystals were obtained. The crystals could not be manipulated rapidly enough to avoid loss of crystallinity due to solvent loss. The mother liquor was decanted and the colourless solid dissolved in ca. 8 ml of a 1:1 mixture of cold (0°C) toluene and diethyl ether. The solution was quickly filtered into a cooled (0°C) Schlenk flask and crystals suitable for X-ray diffraction were grown at -24 °C. Yield = 0.48 g, 36%.

^{1}H{^{11}B} NMR (400 MHz, C_6D_6, 23°C): δ 0.48 (s, 9H, SiMe$_3$), 0.67 (d, $^2J_{PH}$ = 10.1 Hz, 3H, -BH$_3$), 0.89 (s, 6H, SiMe$_2$), 1.28 (m, 8H, THF), 1.51 (d, $^2J_{PH}$ = 9.6 Hz, 6H, PMe$_2$), 2.09 (s, 6H, Cp*Me*), 2.59 (s, 6H, Cp*Me*), 2.14 (s, 6H, Cp*Me*$_B$) δ 3.62 (m, 4H, THF).

^{13}C{^{1}H} NMR (100 MHz, C_6D_6, 23°C): δ 7.79 (d, poorly resolved, quaternary carbon atom), 8.86 (Si*Me*$_3$), 9.46 (Si*Me*$_2$), 11.94 (Cp^{4Me}*Me*$_A$), 15.30 (Cp^{4Me}*Me*$_B$), 23.00 (d, J_{PC} = 37.2 Hz, P*C*H$_3$,), 25.41 (THF), 68.80 (THF), 118.85 ({*C*}Cp^{4Me}), 121.97 ({*C*Me}Cp^{4Me}), 127.52 ({*C*Me$_A$}Cp^{4Me}).

^{11}B{^{1}H} NMR (96.3 Hz, C_6D_6, 298K): δ -27.2 (d, J_{PB} = 97 Hz).

^{31}P{^{1}H} NMR (C_6D_6, 298K): δ -11.1 (poorly resolved q, J_{PB} = 97 Hz).

Elemental analysis of crystals (%) calculated for $C_{25}H_{51}BCaO_2PSi_2$: C 57.56, H 9.85; found C 57.21, H 9.85

5.8　　References

(1)　　Schumann, H.; Meese-Marktscheffel, J. A.; Esser, L. *Chem. Rev.* **1995**, *95*, 865.

(2)　　Zimmermann, M.; Anwander, R. *Chem. Rev.* **2010**, *110*, 6194.

(3)　　Arndt, S.; Beckerle, K.; Hultzsch, K. C.; Sinnema, P.-J.; Voth, P.; Spaniol, T. P.; Okuda, J. *J. Mol. Catal.* **2002**, *190*, 215.

(4)　　Van der Heijden, H.; Schaverien, C. J.; Orpen, A. G. *Organometallics* **1989**, *8*,

255

(5) Klooster, W. T.; Brammer, L.; Schaverien, C. J.; Budzelaar, P. H. M. *J. Am. Chem. Soc.* **1999**, *121*, 1381.

(6) Van der Heijden, H.; Pasman, P.; De Boer, E. J. M.; Schaverien, C. J.; Orpen, A. G. *Organometallics* **1989**, *8*, 1459.

(7) Hultzsch, K. C.; Voth, P.; Beckerle, K.; Spaniol, T. P.; Okuda, J. *Organometallics* **2000**, *19*, 228.

(8) Shapiro, P. J.; Bunel, E.; Schaefer, W. P.; Bercaw, J. E. *Organometallics* **1990**, *9*, 867.

(9) Shapiro, P. J.; Schaefer, W. P.; Labinger, J. A.; Bercaw, J. E.; Cotter, W. D. *J. Am. Chem. Soc.* **1994**, *116*, 4623.

(10) Arndt, S.; Voth, P.; Spaniol, T. P.; Okuda, J. *Organometallics* **2000**, *19*, 4690.

(11) Zhang, W. X.; Nishiura, M.; Hou, Z. *Chem. - A Eur. J.* **2007**, *13*, 4037.

(12) Nishiura, M.; Hou, Z.; Wakatsuki, Y.; Yamaki, T.; Miyamoto, T. *J. Am. Chem. Soc.* **2003**, *125*, 1184.

(13) Zhang, W. X.; Nishiura, M.; Mashiko, T.; Hou, Z. *Chem. - Eur. J.* **2008**, *14*, 2167.

(14) Hou, Z.; Koizumi, T.; Nishiura, M.; Wakatsuki, Y. *Organometallics* **2001**, *20*, 3323.

(15) Tardif, O.; Hou, Z.; Nishiura, M.; Koizumi, T.; Wakatsuki, Y. *Organometallics* **2001**, *20*, 4565.

(16) Chum, P. S.; Kruper, W. J.; Guest, M. J. *Adv. Mater.* **2000**, *12*, 1759.

(17) Braunschweig, H.; Breitling, F. M. *Coord. Chem. Rev.* **2006**, *250*, 2691.

(18) Shapiro, P. J.; Bunel, E.; Schaefer, W. P.; Bercaw, J. E. *Organometallics* **1990**, *9*, 867.

(19) Eaborn, C.; Hill, M. S.; Hitchcock, P. B.; Smith, J. D.; Zhang, S.; Ganicz, T. *Organometallics* **1999**, *18*, 2342.

(20) Ashcroft, N. W.; Mermin, N. D. *Solid state physics*; Harcourt College Publishers, **1976**.

(21) Funk, A.; Max. *Dissecting the theories of lanthanide magnetic resonance,*

Durham University, PhD Thesis, **2014**

(22)   Chalmers, K. H.; De Luca, E.; Hogg, N. H. M.; Kenwright, A. M.; Kuprov, I.; Parker, D.; Botta, M.; Ian Wilson, J.; Blamire, A. M. *Chem. - Eur. J.* **2010**, *16*, 134.

(23)   Cotton, S. *Lanthanide and Actinide Chemistry*; John Wiley & Sons, Ltd., **2007**.

(24)   Kaltsoyannis, N.; Scott, S. *The f elements*; Evans, J., Ed.; Oxford University Press: Oxford, 1999.

(25)   Friebolin, H. *Basic One- and Two-Dimensional NMR Spectroscopy*, 5th ed.; Wiley-VCH Verlag GmbH & Co. KGaA: Weinheim, **2011**.

(26)   Aspinall, H. C. *Chemistry of the f-block elements*; Gordon & Breach, **2001**.

(27)   Binnemans, K.; Görller-Walrand, C. *Chem. Phys. Lett.* **1995**, *245*, 75.

(28)   Bleaney, B. *J. Magn. Reson.* **1972**, *8*, 91.

(29)   Funk, A. M.; Finney, K.-L. N. A.; Harvey, P.; Kenwright, A. M.; Neil, E. R.; Rogers, N. J.; Kanthi Senanayake, P.; Parker, D. *Chem. Sci.* **2015**, *6*, 1655.

(30)   Visseaux, M.; Terrier, M.; Mortreux, A.; Roussel, P. *Eur. J. Inorg. Chem.* **2010**, *2010*, 2867.

(31)   Wang, B.; Nishiura, M.; Cheng, J.; Hou, Z.; Cotter, W. D.; Jones, C.; Kaltsoyannis, N.; Mountford, P.; Aldridge, S. *Dalton. Trans.* **2014**, *43*, 14215.

(32)   Bowman, L. J.; Izod, K.; Clegg, W.; Harrington, R. W. *Organometallics* **2006**, *25*, 2999.

(33)   Izod, K.; Wills, C.; Clegg, W.; Harrington, R. W. *Inorg. Chem.* **2007**, *46*, 4320.

(34)   Bonnet, F.; Visseaux, M.; Hafid, A.; Baudry-Barbier, D.; Kubicki, M. M.; Vigier, E. *Inorg. Chem. Commun.* **2007**, *10*, 690.

(35)   Izod, K.; Wills, C.; El-Hamruni, S.; Harrington, R. W.; Waddell, P. G.; Probert, M. R. *Organometallics* **2015**, *34*, 2406.

(36)   Izod, K.; Liddle, S. T.; Clegg, W. *Inorg. Chem.* **2003**, *43*, 214.

(37)   Dolomanov, O. V.; Bourhis, L. J.; Gildea, R. J.; Howard, J. A. K.; Puschmann, H. *J. Appl. Crystallogr.* **2009**, *42*, 339.

(38)   Sheldrick, G. M. *Acta Cryst. Sect. A.* **2007**, *A64*, 112.

(39)   Sheldrick,   G.   M.   *Acta   Cryst.   Sect.   A.*   **2015**,   *A71*,   3.

Appendix

X-ray crystallographic data, NMR spectra, details of calculation and output files from DFT calculations and NBO analyses are available as an electronic appendix organised by chapter.